Implementing Aspects of Quantum Information into the AdS/CFT Correspondence
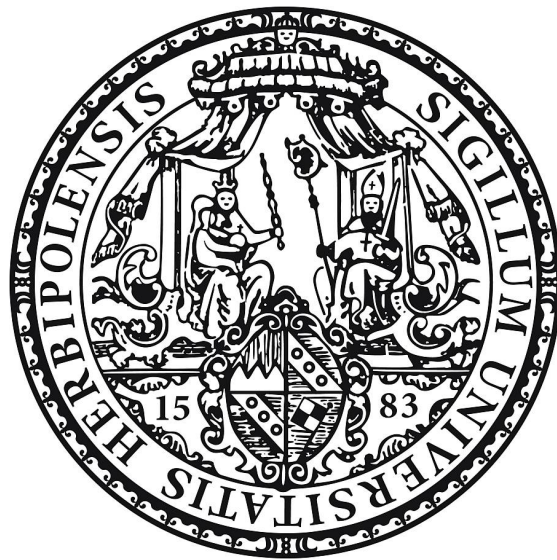
Dissertation zur Erlangung des
naturwissenschaftlichen Doktorgrades
der Julius-Maximilians-Universität Würzburg

vorgelegt von

Raimond Abt
geboren in Immenstadt i. Allgäu

Würzburg, 2019

Eingereicht am: 13.06.2019
bei der Fakultät für Physik und Astronomie

1. Gutachter(in):   Prof. Dr. Johanna Karen Erdmenger

2. Gutachter(in):   Prof. Dr. Thorsten Ohl

3. Gutachter(in):   Prof. Dr. Robert Graham Leigh
der Dissertation

Vorsitzende(r):   Prof. Dr. Karl Mannheim

1. Prüfer(in):   Prof. Dr. Johanna Karen Erdmenger

2. Prüfer(in):   Prof. Dr. Thorsten Ohl

3. Prüfer(in):   Prof. Dr. Bert Hecht
im Promotionskolloquium

Tag des Promotionskolloquiums: 20.09.2019
Doktorurkunde ausgehändigt am: ....

To my parents Christine and Karlheinz Abt,
my sister Franziska Abt,
and my godson Jonas Abt.

Abstract

In recent years many discoveries have been made that reveal a close relation between quantum information and geometry in the context of the AdS/CFT correspondence. In this duality between a conformal quantum field theory (CFT) and a theory of gravity on Anti-de Sitter spaces (AdS) quantum information quantities in CFT are associated with geometric objects in AdS. Subject of this thesis is the examination of this intriguing property of AdS/CFT. We study two central elements of quantum information: subregion complexity – which is a measure for the effort required to construct a given reduced state – and the modular Hamiltonian – which is given by the logarithm of a considered reduced state.

While a clear definition for subregion complexity in terms of unitary gates exists for discrete systems, a rigorous formulation for quantum field theories is not known. In AdS/CFT, subregion complexity is proposed to be related to certain codimension one regions on the AdS side. The main focus of this thesis lies on the examination of such candidates for gravitational duals of subregion complexity.

We introduce the concept of *topological complexity*, which considers subregion complexity to be given by the integral over the Ricci scalar of codimension one regions in AdS. The Gauss-Bonnet theorem provides very general expressions for the topological complexity of CFT_2 states dual to global AdS_3, BTZ black holes and conical defects. In particular, our calculations show that the topology of the considered codimension one bulk region plays an essential role for topological complexity.

Moreover, we study holographic subregion complexity (HSRC), which associates the volume of a particular codimension one bulk region with subregion complexity. We derive an explicit field theory expression for the HSRC of vacuum states. The formulation of HSRC in terms of field theory quantities may allow to investigate whether this bulk object indeed provides a concept of subregion complexity on the CFT side. In particular, if this turns out to be the case, our expression for HSRC may be seen as a field theory definition of subregion complexity. We extend our expression to states dual to BTZ black holes and conical defects.

A further focus of this thesis is the modular Hamiltonian of a family of states ρ_λ depending on a continuous parameter λ. Here λ may be associated with the energy density or the temperature, for instance. The importance of the modular Hamiltonian for quantum information is due to its contribution to relative entropy – one of the very few objects in quantum information with a rigorous definition for quantum field theories. The first order contribution in $\tilde{\lambda} = \lambda - \lambda_0$ of the modular Hamiltonian to the relative entropy between ρ_λ and a reference state ρ_{λ_0} is provided by the first law of entanglement. We study under which circumstances higher order contributions in $\tilde{\lambda}$ are to be expected. We show that for states reduced to two entangling regions A, B the modular Hamiltonian of at least one of these regions is expected to provide higher order contributions in $\tilde{\lambda}$ to the relative entropy if A and B saturate the Araki-Lieb inequality. The statement of the Araki-Lieb inequality is that the difference between the entanglement entropies of A and B is always smaller or equal to the entanglement entropy of the union of A and B. Regions for which this inequality is saturated are referred to as entanglement plateaux. In AdS/CFT the relation between geometry and quantum information

provides many examples for entanglement plateaux. We apply our result to several of them, including large intervals for states dual to BTZ black holes and annuli for states dual to black brane geometries.

The content of this thesis is based on research projects I was involved in during my time as a doctoral student under the supervision of Prof. Dr. J. Erdmenger at the Fakultät für Physik und Astronomie of the Julius-Maximilians-Universität Würzburg, starting in October 2016. The corresponding publications are:

[1] R. Abt, J. Erdmenger, H. Hinrichsen, C. M. Melby-Thompson, R. Meyer, C. Northe and I. A. Reyes, *Topological Complexity in AdS3/CFT2*, *Fortschr. Phys.* **66** (2018) 1800034, [`arXiv:1710.01327`].

[2] R. Abt, J. Erdmenger, M. Gerbershagen, C. M. Melby-Thompson and C. Northe, *Holographic Subregion Complexity from Kinematic Space*, *JHEP* **01** (2019) 012, [`arXiv:1805.10298`].

[3] R. Abt and J. Erdmenger, *Properties of Modular Hamiltonians on Entanglement Plateaux*, *JHEP* **11** (2018) 002, [`arXiv:1809.03516`].

Zusammenfassung

In den letzten Jahren wurden viele Entdeckungen gemacht, welche eine enge Beziehung zwischen Quanteninformation und Geometrie im Kontext der AdS/CFT-Korrespondenz aufzeigen. In dieser Dualität zwischen einer konformen Quantenfeldtheorie (CFT) und einer Gravitationstheorie auf Anti-de-Sitter-Räumen (AdS) werden Quanteninformationsgrößen der CFT mit geometrischen Objekten in AdS assoziiert. In der vorliegenden Arbeit wird dieser faszinierende Aspekt von AdS/CFT untersucht. Wir studieren zwei Objekte welche eine zentrale Rolle in der Quanteninformation spielen: Die Teilregionkomplexität (subregion complexity) – welche ein Maß für den nötigen Aufwand zur Konstruktion eines vorgegebenen reduzierten Zustandes ist – und den modularen Hamiltonoperator – welcher durch den Logarithmus eines reduzierten Zustandes gegeben ist.

Während eine klare Definition der Teilregionkomplexität mittels unitärer Gatter für diskrete Systeme angegeben werden kann, ist eine präzise Formulierung für Quantenfeldtheorien nicht bekannt. In der AdS/CFT-Korrespondenz wird angenommen, dass die Teilregionkomplexität mit bestimmten Regionen der Kodimension eins in AdS-Räumen in Beziehung stehen. Der Hauptfokus der vorliegenden Arbeit ist die Untersuchung derartiger Kandidaten für Gravitationsduale der Teilregionkomplexität.

Wir führen das Konzept der *topologischen Komplexität* (topological complexity) ein, welches das Integral über den Ricci-Skalar bestimmter Teilregionen von AdS-Räumen als das Gravitationsdual der Teilregionkomplexität ansieht. Der Satz von Gauss-Bonnet erlaubt es uns sehr allgemeine Ausdrücke für die Teilregionkomplexität von CFT_2-Zuständen mit globalem AdS_3, BTZ-Schwarzen-Löchern oder konischen Defekten als Gravitationsdual zu konstruieren. Unsere Berechnungen zeigen insbesondere, dass die Topologie der betrachteten Kodimension-Eins-Regionen eine große Rolle für die topologische Komplexität spielt.

Weiterhin befassen wir uns mit der holographischen Teilregionkomplexität (holographic subregion complexity, HSRC), welche annimmt, dass die Teilregionkomplexität durch das Volumen bestimmter Kodimension-Eins-Regionen in AdS-Räumen gegeben ist. Wir leiten einen expliziten Ausdruck für die HSRC von Vakuumzuständen in Größen der Feldtheorie her. Die Formulierung der HSRC in Feldtheoriegrößen könnte es ermöglichen zu untersuchen ob diese Größe tatsächlich als die Teilregionkomplexität der CFT interpretiert werden kann. Sollte sich dies bestätigen, kann unser Feldtheorieausdruck für HSRC als Definition für die Teilregionkomplexität der CFT angesehen werden. Wir verallgemeinern unseren Ausdruck für HSRC dahingehend, dass er auch für Zustände dual zu BTZ-Schwarzen-Löchern und konischen Defekten gültig ist.

Ein weiterer Fokus der vorliegenden Arbeit ist der modulare Hamiltonoperator einer Familie von Zuständen ρ_λ, welche von einem kontinuierlichen Parameter λ abhängen. Hierbei kann λ beispielsweise der Energiedichte oder der Temperatur entsprechen. Die Bedeutung des modularen Hamiltonoperator für die Quanteninformation ist auf seinen Beitrag zur relativen Entropie zurückzuführen – eine der wenigen Größen der Quanteninformation für welche eine formale Definition für Quantenfeldtheorien bekannt ist. Der Beitrag erster Ordnung in $\tilde\lambda = \lambda - \lambda_0$ des modularen Hamiltonoperators zur relativen Entropie zwischen ρ_λ und einem

Referenzzustand ρ_{λ_0} ist gegeben durch den ersten Hauptsatz der Verschränkung (first law of entanglement). Wir untersuchen unter welchen Umständen Beiträge höherer Ordnung in $\tilde{\lambda}$ zu erwarten sind. Wir zeigen, dass für Zustände die auf zwei Teilregionen A, B reduziert wurden in der Regel mindestens einer dieser Beiträge höherer Ordnung in $\tilde{\lambda}$ zur relativen Entropie liefert, wenn A und B die Araki-Lieb-Ungleichung saturieren. Die Araki-Lieb-Ungleichung besagt, dass die Differenz der Verschränkungsentropien von A und B stets kleiner oder gleich der Verschränkungsentropie der Vereinigung von A und B ist. Regionen für welche die Araki-Lieb-Ungleichung saturiert ist werden als Verschränkungsplateaus (entanglement plateaux) bezeichnet. In der AdS/CFT-Korrespondenz gibt es aufgrund der Beziehung zwischen Quanteninformation und Geometrie viele Beispiele für derartige Plateaus. Wir wenden unser Resultat auf einige dieser an. Unter anderem diskutieren wir große Intervalle für Zustände dual zu BTZ-Schwarzen-Löchern und Annuli für Zustände dual zu schwarzen Branen.

Der Inhalt der vorliegenden Arbeit basiert auf Projekten an denen ich während meiner Zeit als Doktorand unter der Aufsicht von Prof. Dr. J. K. Erdmenger an der Fakultät für Physik und Astronomie der Julius-Maximilians-Universität Würzburg seit Oktober 2016 beteiligt war. Die entsprechenden Veröffentlichungen sind:

[1] R. Abt, J. Erdmenger, H. Hinrichsen, C. M. Melby-Thompson, R. Meyer, C. Northe and I. A. Reyes, *Topological Complexity in AdS3/CFT2*, *Fortschr. Phys.* **66** (2018) 1800034, [`arXiv:1710.01327`].

[2] R. Abt, J. Erdmenger, M. Gerbershagen, C. M. Melby-Thompson and C. Northe, *Holographic Subregion Complexity from Kinematic Space*, *JHEP* **01** (2019) 012, [`arXiv:1805.10298`].

[3] R. Abt and J. Erdmenger, *Properties of Modular Hamiltonians on Entanglement Plateaux*, *JHEP* **11** (2018) 002, [`arXiv:1809.03516`].

Contents

Chapter 1

Introduction

The realization that the laws of nature may be formulated in the language of mathematics is one of the greatest achievements of mankind. Providing clear predictions for the behavior of physical systems that may be tested by experiments, this approach substantially shaped our understanding of the cosmos as well as our technological progress. Over the last centuries the mathematical models for physical systems became sufficiently advanced that they allowed the study of aspects of physics inaccessible to the experimental capabilities of their time. A seminal example for this impressive accomplishment of theoretical physics is the Higgs mechanism, whose theoretical postulation [4–6] (1964) outran the experimental discovery of the Higgs particle [7, 8] (2012) by several decades.

Also many conclusions of Einstein's theory of general relativity [9] were veryfied by experiments only a long time after their theoretical formulation. For instance, the gravitational waves postulated by Einstein [10, 11] (1916) were detected directly for the first time a century after their prediction [12, 13] (2015). This shows the great impact general relativity has to experimental physics even today, so many years after its formulation in theoretical physics. In fact, we presently find ourselves at the beginning of a new era of experimental research regarding general relativity, as many new experimental setups – such as LISA [14] or LIGO-India [15] – are currently in preparation. Thus, we may look forward to new exciting experimental results for general relativity in the future. As the most recent experimental accomplishment regarding general relativity, we mention the first image of a black hole [16–21], which was taken by the Event Horizon Telescope and presented to the public in April 2019.

In theoretical physics there are many cases in which several mathematical formulations for the behavior of a given physical system exist. This is a well established fact which can even be witnessed in very common fields such as classical mechanics. Here we have two very different but equivalent methods for describing the dynamics of a physical system: the Lagrange and the Hamilton formalism. Further well known examples include the formulation of quantum mechanics in position and momentum space, the Schrödinger, Heisenberg and interaction picture and the path integral and Hamilton formalism in quantum field theory. Usually the different mathematical formulations highlight different properties of the physical system under consideration. A certain aspect of the system may be naturally studied in one formulation, while it is particularly hard to access in another. The

Lagrange and Hamilton formalism provide a good example for such a situation: while the time evolution of observables is naturally provided by the canonical equations of motion in the Hamilton formalism, it cannot be studied that easily in the Lagrange formalism. On the other hand, the Lagrange formalism is ideal for the construction of conserved quantities, due to Noether's theorem.

The subject of this thesis is a further, however more advanced, example for a physical system that can be described mathematically in two different ways: the *AdS/CFT correspondence.* Proposed by Maldacena in 1997 [22], the AdS/CFT correspondence states a duality between a theory of gravity on asymptotic $(d+1)$-dimensional Anti-de Sitter space (AdS) and a conformal quantum field theory (CFT) in d dimensions ($\mathrm{AdS}_{d+1}/\mathrm{CFT}_d$). To be more precise, AdS/CFT suggests that these two theories actually describe the same physics, i.e. they are *dynamically equivalent.* This is a remarkable result, as it relates general relativity and quantum field theory in a very surprising way. These two pillars of modern physics describe two very different aspects of our reality and their unification is one of the most prominent unsolved problems of our time. The AdS/CFT correspondence states that some quantum field theories are actually equivalent to theories of gravity. We need to note however that even though AdS/CFT has passed many non-trivial tests (see e.g. [23, 24]), it is still a proposal for which no formal proof has been constructed so far. The interpretation of a CFT as a theory of gravity on AdS offers new ways for studying the CFT. Many aspects of the CFT which are particularly hard to grasp turn out to have a relatively easy access on the AdS side. Especially for the study of quantum information aspects of the CFT this strategy has proven to be very successful. In this thesis, we provide further results about quantum information in the context of AdS/CFT.

1.1   Quantum Information in Modern Physics

One of the most fundamental differences between classical and quantum physics is the concept of *entanglement.* Describing a new type of correlations with no classical analogue, entanglement was not easily accepted in the physics community in the early years of quantum mechanics. Most famously, Albert Einstein referred to it as *spooky action at a distance*[1] and considered it a powerful argument against quantum theory.[2] Later experiments however confirmed the existence of entanglement[3] which is today an integral part of modern physics.

Describing a certain type of correlations between different subsystems of a given quantum system, entanglement is most successfully studied in the context of quantum information.[4] This field is a generalization of classical information theory to quantum systems. In analogy to the classical case, the purpose of the notion of quantum information is to quantify diverse properties of the inner structure of a given quantum state, such as correlations or the information content. In particular,

---

[1]Einstein used this phrase in a letter to M. Born on March 3rd, 1947.

[2]For the context of the discussion about the counterintuitive properties of quantum systems we refer to the famous paper by Einstein, Podolski and Rosen (EPR) [25] from 1935.

[3]For a recent experiment we refer to [26].

[4]For an introduction to the subject see [27–31].

quantum information offers methods for comparing different states in context of these aspects. For this purpose several quantities were introduced which are meant to grasp different quantum information aspects of a system. For instance, the entanglement entropy (see e.g. [27–30, 32, 33]) is used to study the entanglement between a subsystem and its complement for pure states. It can be generalized to quantities like the (conditional) mutual information (see e.g. [27–30]) which capture general correlations between different subsystems. Moreover, concepts like the relative entropy (see e.g. [31, 34, 35]) or Fisher information (see e.g. [36]) allow to compare different states with each other. This method of comparing two states is closely related to the concept of hypothesis testing in statistics: for a system in a given state ρ_1 which is mistakenly assumed to be in a state ρ_0, it is examined how strongly our expectations deviate from the actual behavior of the system (see Section 3.3.3 for more details). An alternative approach for comparing two states provides complexity (see e.g. [37, 38]). Here the goal is to determine how hard it is to construct a state from a given reference state by applying only certain allowed quantum operations. Usually the reference state is taken to be very simple in the sense that it does not have any inner correlations. So in particular, complexity captures the inner structure of a state. We discuss complexity in more detail in Section 3.2.

Many of the quantities introduced for quantum information have their origin in classical information theory. The generalization of their classical counterparts to quantum systems is mostly done in a straightforward way, as long as the quantum system is discrete. An example for such a discrete system is given by a chain of atoms. By only considering their spin, for each atom two discrete settings (spin up, spin down) may be distinguished. Due to the similarity of this situation to bits in classical information theory, such systems are referred to as *quantum-bits* (q-bits). Even at this very simple example we see a clear difference between the classical and the quantum situation. Unlike classical bits, q-bits may not only be in one of the two possible states but generic superpositions of them are possible.

In recent years – in particular motivated by AdS/CFT – quantum information for quantum field theories (QFT) became a subject of intense study (see e.g. [35, 39–42]). The mathematical rigorous introduction of quantum information measures to QFTs however, is in general a very challenging task. In particular, measures of quantum information – such as entanglement entropy – tend to be UV divergent in QFTs (see e.g. [33, 35]). Nevertheless, the study of quantum information is essential for gaining a deeper understanding about the inner structure of Hilbert spaces in QFT. For instance, the algebraic structure in QFTs leads to the intriguing conclusion that QFT states are usually strongly entangled. To make this statement more accessible, we present an argument showing that the vacuum state $|0\rangle$ in QFTs is allways entangled. This is a direct conclusion of the Reeh-Schlieder theorem [43], as we now discuss.[5] The Reeh-Schlieder theorem states that given any open subset A of a Cauchy slice, the vacuum sector of a QFT can be generated by operators localized in a small neighborhood $\mathfrak{N}_A$ of A. This statement implies that the region $\mathfrak{N}_A$ is correlated – and therefore entangled – with

---

[5]The following discussion is motivated by [35].

any other space-time region. To see this we may consider an operator $\mathcal{O} \neq 0$ in the vacuum sector, localized in a region $\mathfrak{N}'$ far away from $\mathfrak{N}_A$ and with vanishing vacuum expectation value. Due to the Reeh-Schlieder theorem we can find an operator a localized in $\mathfrak{N}_A$ such that $\langle 0| \, a^\dagger \mathcal{O} a \, |0\rangle \neq 0$ holds. Since a is localized in $\mathfrak{N}_A$ and $\mathcal{O}$ in some other region $\mathfrak{N}'$ far away from $\mathfrak{N}_A$, we conclude that $\mathcal{O}$ and a commute. This allows us to deduce that the expectation value of the operator $a^\dagger a \mathcal{O}$ does not factorize, i.e.

$$\langle 0| \, a^\dagger a \mathcal{O} \, |0\rangle \neq \langle 0| \, a^\dagger a \, |0\rangle \, \langle 0| \, \mathcal{O} \, |0\rangle \,, \tag{1.1}$$

as $\mathcal{O}$ has a vanishing vacuum expectation value. Since $a^\dagger a$ and $\mathcal{O}$ are localized in $\mathfrak{N}_A$ and $\mathfrak{N}'$ respectively, we see that the vacuum state contains correlations between $\mathfrak{N}_A$ and $\mathfrak{N}'$ and is thus an entangled state.[6]

The above discussion demonstrates that correlations such as entanglement are a fundamental part of QFT states and therefore deserve a deeper analysis. In particular, the entanglement in QFT states tends to be so strong that it leads to UV divergences in the entanglement entropy (see e.g. [33,35]). In practice, these issues are approached by putting the QFT on a lattice for the computation of quantum information quantities – such as entanglement entropy (see Section 3.1.4).

A further reason for the study of quantum information for QFTs is its role in general relativity. The formulation of a quantum theory for gravity is one of the most prominent unsolved problems of modern physics whose importance for understanding the nature of our reality cannot be overstated. Quantum information is a very powerful tool for establishing connections between a QFT and the theory of general relativity describing the space-time it is defined on. In particular in the presence of a horizon this is an evident observation. A horizon naturally separates space-time into two regions, which immediately leads to the question about the quantum correlations between the two regions (see e.g. [44,45]). We stress that a horizon not only plays a role for exotic objects like black holes but also appears for very simple configurations. One of the most prominent examples for such a situation is the space-time seen by a constantly accelerating observer [46]. As we depict in Figure 1.1, an observer accelerating in x^1 direction in flat Minkowski space is restricted to the so-called *Rindler wedge* [47], i.e. the region with $x^1 \geq |x^0|$, where x^0 is the time coordinate. Consequently, the observer is separated from the rest of space-time by a horizon at $x^1 = |x^0|$ known as the *Rindler horizon*. This example shows that even in very simple geometries – like flat space-time – situations may be considered where an observer cannot see all of space-time but is restricted to a subregion. We emphasize that this restriction is not introduced artificially by adding some kind of barrier by hand to the system but emerges very naturally from basic concepts of general relativity. Due to the isolation from the rest of space-time, the accelerating observer experiences the state of the system as thermal [46].[7] This observation establishes the physical importance of quantum information. We see

---

[6]We note that in this motivation for entanglement in the vacuum state we ignored some mathematical caveats. For instance, it is not possible to generate the full vacuum sector out of $\mathfrak{N}_A$ but only a dense subset. For a more detailed discussion of the subject, we refer to [35].

[7]For recent reviews of this setup we refer to [30,35]. See also [45].
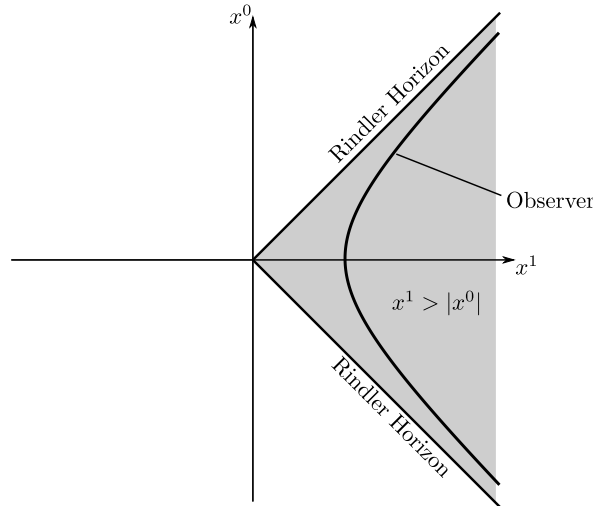
Figure 1.1: A constantly accelerating observer in Minkowski space. Due to their acceleration in x^1 direction, the observer is restricted to the Rindler wedge (grey) $x^1 > |x^0|$. All events outside that region are inaccessible for them. Thus the observer sees a horizon – the Rindler horizon – at the boundary of the Rindler wedge, $x^1 = |x^0|$.

that it is not just an information theoretic construct for quantifying correlations but provides a deeper understanding for the origins of observable aspects of the system, such as temperature.

So far we have only discussed entanglement in order to clarify the role of quantum information in QFTs. However, the study of entanglement is not sufficient for understanding the full quantum information content of a given state. The aspect of quantum information we focus on in this thesis is complexity (see e.g. [37, 38]). For discrete systems, the basic idea behind complexity is very easily understood. We consider a reference state $|\psi_r\rangle$ and a set of unitary operations which are referred to as gates. The complexity of a given target state $|\psi_t\rangle$ is the minimal number of gates that needs to be applied to $|\psi_r\rangle$ in order to approximate $|\psi_t\rangle$ up to a given tolerance. The generalization of complexity to QFTs however is not very well understood and a subject of current research (see e.g. [48–51]). The reason for the growing interest in complexity, especially in the AdS/CFT community (see e.g. [52–55]), can be traced back to the work of Susskind and his collaborators [56–59]. Susskind considered the eternal two-sided AdS black hole and argued that the effort it takes to send a signal along an Einstein-Rosen bridge from one side of the black hole to the other may be associated with complexity. In the context of AdS/CFT this led him to the conclusion that the growth of the Einstein-Rosen bridge in time is related to the complexity of the dual CFT state. This example was also used to justify the importance of complexity for field theories (see e.g. [57]): the two sided eternal AdS black hole is dual to the thermofield double state of two identical CFTs [60, 61]. This state reaches thermal equilibrium very fast, so that many aspects of the state stop evolving in time. In

particular, the evolution of entanglement entropy stagnates [62]. Therefore, a new quantity is required to study the evolution of quantum information aspects of the state beyond thermal equilibrium. Complexity turns out to be a good candidate for such a quantity, as it keeps evolving in time, even after thermal equilibrium has been reached [57, 58]. So we see that complexity is a measure for quantum information which grasps aspects of a given state that cannot be studied solely by considering entanglement entropy.

The AdS/CFT correspondence provides a distinct approach towards a formal definition of complexity for QFTs: instead of working directly with the CFT, possible candidates for complexity can be constructed on the AdS side. We briefly review the most popular of these candidates in Section 3.2.3. In this thesis a proposal by Alishahiha [63] for the dual description of the complexity of reduced CFT states on the AdS side is studied in great detail. Alishahiha's proposal relates the complexity of reduced states – the so-called *subregion complexity* – to the volumes of certain codimension one regions on the AdS side.

We contribute the following two new insights to the study of complexity in the context of AdS/CFT:

1. In Chapter 4 we present a novel proposal for a dual of complexity on the AdS side in AdS_3/CFT_2 which my collaborators and I published in [1]. This proposal reveals a clear relation between complexity on the CFT side and certain topological aspects of the gravity dual. Moreover, for the examples considered in this thesis it differs from Alishahiha's proposal only by a proportionality factor and thus establishes a relation between topology and this proposal as well.

2. We investigate Alishahiha's proposal for subregion complexity in Chapter 5. This chapter is based on results my collaborators and I published in [1] and [2]. We construct an explicit CFT expression for Alishahiha's proposal for vacuum states. This provides new insights to the meaning of Alishahiha's proposal on the CFT side and thus is an important first step towards testing whether the proposed AdS quantity is actually a good measure for complexity.

Besides complexity, we study a further quantum information object in this thesis that currently gains a lot of attention (see e.g. [41, 64–72]), the *modular Hamiltonian* [73]. For a given state ρ, [8] the modular Hamiltonian K is defined via

$$\rho = \frac{e^{-K}}{\text{tr}(e^{-K})} \,. \tag{1.2}$$

In particular, we examine its contribution to the relative entropy for a family of states depending on a continuous parameter λ. The relative entropy (see Section 3.3.3) is of particular interest for QFTs, as it is one of the very few quantum information quantities for which a rigorous definition for QFTs is known.[9] The modular Hamiltonian plays a crucial role in computing the relative entropy for

---

[8]Note that we treat the terms "state" and "density matrix" as synonymous in this thesis.

[9]See e.g. [34] and [35] for a review.
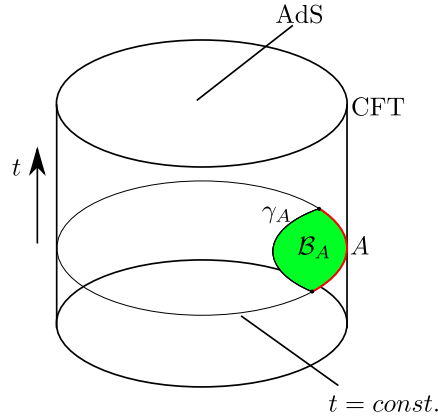
Figure 1.2: The AdS/CFT correspondence. The AdS/CFT correspondence states a duality between a theory of gravity on asymptotic AdS space and a conformal field theory (CFT) residing on the conformal boundary of this space. The Ryu-Takayanagi proposal relates the entanglement entropy of a CFT region A on a constant time slice with a surface γ_A in AdS, homologous to A. In the geometries we consider in this thesis, γ_A lies in the same constant time slice as A. The volume of the region $\mathcal{B}_A$ enclosed by A and γ_A (green) is conjectured to be a measure for the complexity of the reduced CFT state on A.

explicit examples. However, despite intense investigation it was only possible to construct an explicit expression for the modular Hamiltonian in a few cases (see e.g. [74–78]), some of which we present in Section 3.3.2. This makes the modular Hamiltonian a challenging object to work with.

In Chapter 6 we present an observation I published in [3] regarding the λ-dependence of the contribution of K to relative entropy. In particular, this observation establishes an intriguing relation between the modular Hamiltonian and entanglement entropy. We note that even though my result regarding modular Hamiltonians may be applied to many examples in AdS/CFT, it is not restricted to such situations but holds for any quantum theory.

1.2 Application of AdS/CFT to Quantum Information

The AdS/CFT correspondence states a duality between a theory of gravity on asymptotic AdS space and a conformal field theory. Here the conformal field theory is considered to be defined on the conformal boundary of the AdS space (see Figure 1.2). In this picture we find AdS/CFT to describe a system on asymptotic AdS whose physical content is also contained on its boundary. This makes AdS/CFT an explicit example for the holographic principle [79–81]. Already at this point we can see that information theory appears in an natural way in AdS/CFT. Thus it should not be surprising that AdS/CFT provides a very elegant approach towards quantum information.

The attention of the AdS/CFT community was drawn towards quantum information by a celebrated paper by Ryu and Takayanagi [82]. In this paper the authors argue that the entanglement entropy of a given subregion A on a constant time slice of the CFT corresponds to the area of the minimal surface on the AdS side, homologous to A. In this picture, A is seen as a subset of the conformal boundary of AdS. This proposal established a clear relation between the quantum information content of the CFT and geometric aspects of the gravity dual. This intruiging realization was further explored in the following years (see e.g. [83–86]). In particular, in [87, 88] it was argued that the connectedness of space-time on the AdS side is intimately related to entanglement on the CFT side. Moreover, in [89] it was even shown that Einstein's equations may be derived from entanglement to linear order. The proposal by Ryu and Takayanagi is also related to work associating the reconstruction of field excitations in AdS on the CFT side with quantum error correcting codes [39, 90, 91]. These concepts are of particular interest for discrete versions of AdS/CFT involving tensor networks [92, 93].

In AdS$_3$/CFT$_2$ the Ryu-Takayanagi formula provides an exceptionally rigorous approach for the study of the relation between entanglement and geometry. Here it identifies the entanglement entropy of a given interval A on a constant time slice of the CFT with the length of the geodesic γ_A in AdS$_3$ lying on the same constant time slice and ending on the conformal boundary at the endpoints of A (see Figure 1.2). This leads to a one-to-one correspondence between intervals A on the CFT side and the corresponding geodesics γ_A in AdS$_3$. Therefore, the space $\mathcal{K}$ of all these geodesics (intervals) is a valuable auxiliary construction which can be interpreted both from the AdS side and the CFT side. The space $\mathcal{K}$ is known as *kinematic space* and has been established in AdS/CFT by Czech and his collaborators in [94–97]. The value of kinematic space lies in the fact that it offers a systematic way for expressing geometric quantities on the AdS side in terms of entanglement entropy of the CFT and therefore reveals the immense depth of the relation between entanglement and geometry. For instance, an early version of the kinematic space formalism was used to derive an integral expression over entanglement entropies for the length of curves on the constant time slice of the AdS side [94]. The results we present in Chapter 5 may be seen as an extension of this method. We show how the kinematic space formalism can be applied to express the volume of an arbitrary codimension-one surface lying in the constant time slice of AdS$_3$ as an integral over entanglement entropies. The fact that it is possible to express such volumes in terms of entanglement entropies is of particular importance for the concept of *holographic subregion complexity (HSRC)* introduced by Alishahiha [63]. As we depict in Figure 1.2, HSRC is given by the volume of the codimension one region $\mathcal{B}_A$ enclosed by γ_A and A. This volume is proposed to be a measure for the subregion complexity of the reduced state on A. Our formulation of volumes in terms of entanglement entropies provides a field theory expression for vol($\mathcal{B}_A$) and therefore for HSRC. The knowledge about the field theory dual of HSRC is of particular importance for investigating whether vol($\mathcal{B}_A$) actually encodes subregion complexity.

1.3 Outline of this Thesis

The main results of this thesis are based on [1–3] and presented in Chapters 4, 5 and 6. In Chapter 4 we discuss topological complexity, which associates the integral over the Ricci scalar of $\mathcal{B}_A$ (see Figure 1.2) with the subregion complexity of the corresponding entangling interval A. We compute the topological complexity for examples involving global AdS$_3$, BTZ black holes and conical defects. For these geometries we find that the topology of $\mathcal{B}_A$ and A is of integral importance for topological complexity. The focus of Chapter 5 is the construction of a field theory expression for HSRC in AdS$_3$/CFT$_2$. We derive a formulation of HSRC in terms of entanglement entropies for CFT vacuum states using the kinematic space formalism. Moreover, we generalize this expression to states dual to BTZ black holes and conical defects. Our results regarding modular Hamiltonians are presented in Chapter 6. We consider a one-parameter family of states reduced to two entangling regions A, B for which the Araki-Lieb inequality is saturated (see (1.3) below). For this setup we argue that the relative entropy of at least one of the regions A, B is expected to contain contributions of the modular Hamiltonian that are of quadratic or higher order in the parameter of the family of states.

The purpose of the preceding Chapters 2 and 3 is to establish the theoretical background required for understanding these results. In Chapter 2 we provide a brief introduction to AdS/CFT, including a review of conformal field theories, Anti-de Sitter spaces and Maldacena's original argument for AdS$_5$/CFT$_4$ in Sections 2.1.1, 2.1.2 and 2.2, respectively. Moreover, we discuss AdS$_3$/CFT$_2$, which is of particular importance for this thesis, in Section 2.3 and present further aspects of AdS/CFT in Sections 2.4 and 2.5 which establish how AdS/CFT is applied in practice.

The focus of Chapter 3 is quantum information and the way it is handled in the context of AdS/CFT. The quantum information concepts we require for this thesis are entanglement entropy, complexity and modular Hamiltonians, which we introduce in Sections 3.1, 3.2 and 3.3, respectively.

Even though we discuss many of the physical concepts this thesis is based on in Chapters 2 and 3, some preliminary knowledge about quantum information, quantum field theories, general relativity and differential geometry is required. For an introduction to quantum information we refer to [27–29,98]. Standard textbooks regarding quantum field theory are [99–101]. Reviews of general relativity and differential geometry can be found in [102–105]. Moreover, Maldacena's motivation for AdS$_5$/CFT$_4$, as presented in Section 2.2, presumes some basic knowledge about string theory, which is provided by e.g. [106–112].

Chapter 4: Topological Complexity

In [1] Johanna Erdmenger, Haye Hinrichsen, Charles M. Melby-Thompson, René Meyer, Christian Northe, Ignacio A. Reyes and I introduced the concept of *topological complexity* for AdS$_3$/CFT$_2$. This is a new proposal for a gravity dual of the subregion complexity of a reduced state on a subregion A on the CFT side. Just as Alishahiha's HSRC [63], we consider the region $\mathcal{B}_A$ enclosed by A and γ_A (see Figure 1.2). However, instead of the volume vol($\mathcal{B}_A$), we propose the integral

over $\mathcal{B}_A$ of the Ricci scalar of the considered constant time slice to correspond to complexity. The advantage of this approach is the fact that this integral is dimensionless by construction; a property which it shares with complexity. In the case of HSRC an additional scaling factor needs to be introduced by hand in order to obtain dimensionlessness. Moreover, we can use the Gauss-Bonnet theorem to show that the topology of A and $\mathcal{B}_A$ play a crucial role for our proposal (see Section 4.1). This justifies the name "topological complexity". This dependence on topology allows us to formulate a closed expression for the topological complexity of a generic region A in the case where the gravity dual has the geometry of global AdS$_3$ or the BTZ black hole. If A is not just a single interval but the union of several intervals, γ_A assumes different phases depending on the position of the intervals relative to each other. When γ_A undergoes a phase transition, the topology of $\mathcal{B}_A$ changes, leading to discrete jumps in topological complexity. In Section 4.2 we compute topological complexity for the geometries of global AdS$_3$, BTZ black holes and conical defects. In all these cases, topological complexity and HSRC differ only by a scaling factor. Therefore, we conclude that the topology of $\mathcal{B}_A$ and A are also essential for HSRC in these geometries.

Chapter 5: Holographic Subregion Complexity from Kinematic Space

In addition to topological complexity, my collaborators and I also introduced a method for expressing volumes of codimension one regions $\mathcal{Q}$ in AdS$_3$ lying on a constant time slice in terms of entanglement entropy in [1]. This method was discussed in detail and further developed in [2] by Johanna Erdmenger, Marius Gerbershagen, Charles M. Melby-Thompson, Christian Northe and me. We use the kinematic space formalism – which we introduce in Section 5.1 – to express the volume of $\mathcal{Q}$ as an integral over the length of geodesics. We prove the validity of this expression in Section 5.2. The Ryu-Takayanagi formula allows us interpret the appearing lengths as entanglement entropies and thus provides a CFT formulation for vol($\mathcal{Q}$). By setting $\mathcal{Q} = \mathcal{B}_A$, this result offers a CFT construction of HSRC, which we discuss in great detail in Section 5.3. We generalize our findings to the geometries of BTZ black holes and conical defects in Section 5.4. The CFT formulation of HSRC is a very important step towards a CFT interpretation of HSRC. In Section 5.5 we discuss the conclusions to which we come for the role of HSRC on the CFT side. In particular, we examine what lessons can be learned if HSRC is actually a measure for complexity – as conjectured.

Chapter 6: Modular Hamiltonians on Entanglement Plateaux

In [3] Johanna Erdmenger and I published a result regarding the modular Hamiltonians of two reduced states on regions A, B for which the Araki-Lieb inequality [113] is saturated, i.e.

$$S(AB) = |S(A) - S(B)|, \qquad (1.3)$$

where S is the entanglement entropy of the respective regions. Regions which satisfy (1.3) are referred to as *entanglement plateaux* [114] (see Section 6.1). We consider a one-parameter family of states ρ_λ on an entanglement plateau, i.e. we

assume the reduced states ρ_λ^A, ρ_λ^B, ρ_λ^{AB} to satisfy (1.3) for all values of the parameter λ. Here λ may be chosen to be the energy density or the temperature of ρ_λ, for instance. Moreover, we assume the entanglement plateau to be stable under variations of the size of A and B that keep AB invariant. For this setup, we study the λ-dependence of the object $\Delta \langle K_0 \rangle (A, \lambda)$ (6.1), which is the contribution of the modular Hamiltonian $K_0(A)$ of a reference state $\rho_{\lambda_0}^A$ to the relative entropy of ρ_λ^A and $\rho_{\lambda_0}^A$. In particular, we are interested in the case where $\Delta \langle K_0 \rangle (A, \lambda)$ is linear in $\tilde{\lambda} = \lambda - \lambda_0$. In this situation, the first law of entanglement [115] allows to express $\Delta \langle K_0 \rangle (A, \lambda)$ in terms of entanglement entropy without explicit knowledge of the modular Hamiltonian $K_0(A)$ (see Section 6.2). We show that on entanglement plateaux, $\Delta \langle K_0 \rangle$ takes this simple form only in special cases. The statement of our result, which we present and prove in Section 6.3, goes as follows. If A and B form an entanglement plateau which is stable under variations of the size of A and B that keep AB invariant and $\Delta \langle K_0 \rangle$ is linear in $\tilde{\lambda}$ for A, B and variations of their size, then $\partial_\lambda^2 S$ is invariant under variations of the size of A and B.

This result is of particular interest in the context of the first law of entanglement: the first law states a relation between entanglement and the first order contribution in $\tilde{\lambda}$ to $\Delta \langle K_0 \rangle$. We establish a relation between higher order contributions in $\tilde{\lambda}$ and entanglement entropy.

Entanglement plateaux are very common in AdS/CFT. This allows us to apply our result to several examples from AdS/CFT in Section 6.4. These include disjoint intervals for thermal states dual to black string geometries and large intervals for states dual to BTZ black holes. We note that our result is not restricted to holographic situations but holds for any quantum system.

Chapter 2

AdS/CFT Correspondence

We start our discussion by reviewing the aspects of the AdS/CFT correspondence relevant for this thesis.[1] The AdS/CFT correspondence, which we also refer to as simply AdS/CFT in this thesis, is a conjectured duality between a conformal quantum field theory (CFT) and a theory of gravity involving asymptotic Anti-de Sitter spaces (AdS). We note that the theory of gravity in general not only considers Anti-de Sitter spaces but also an additional compact manifold $\mathcal{M}$. So the geometries we are working with on the gravity side take the form AdS $\times \mathcal{M}$.

The fields in a CFT transform covariantly under suitable representations of conformal transformations, i.e. local rescalings of space-time. This provides the theory with a very powerful algebraic structure for observables which allows to derive many general expressions for expectation values simply from the conformal symmetry without explicit path integral computations.

Anti-de Sitter spaces are solutions of the vacuum Einstein equations for a negative cosmological constant. The hyperbolic structure of AdS allows light rays to reach radial infinity at finite times and thus provides the concept of a conformal boundary. The boundary has codimension one and is considered to be the domain of the dual CFT (see Figure 1.2).

Throughout this thesis we use the terms AdS side, AdS, gravity side, gravity dual, gravitational dual, bulk (dual) and holographic (dual) for references regarding the theory of gravity on AdS. For the conformal field theory the terms field theory side, field theory dual, CFT (side), CFT dual or boundary are used.

We may distinguish three different versions of the theory of gravity involving asymptotic AdS, depending on the considered form of AdS/CFT. In its *strongest form*, the gravity dual is considered to be a theory of quantum strings. Moreover, it may also be taken to be a classical string theory, which is referred to as the *strong form* of AdS/CFT. The *weak form* of AdS/CFT – on which we focus here – considers a classical theory of supergravity (SUGRA) for point-like particles as dual of the CFT. Many non-trivial tests have been performed for the weak form of AdS/CFT (see e.g. [23, 24]), which provide strong evidence for the validity of the AdS/CFT correspondence.

$\mathrm{AdS}_{d+1}/\mathrm{CFT}_d$ was originally introduced by J. Maldacena [22] as a duality between a CFT in d space-time dimensions (CFT_d) and a theory of gravity involving

---

[1]Reviews of AdS/CFT can also be found in [106, 109, 110, 116–119].

$(d + 1)$-dimensional asymptotic AdS spaces (AdS_{d+1}). The best understood example is the case $d = 4$, i.e. $\text{AdS}_5/\text{CFT}_4$, which is the main focus of [22]. An important property of $\text{AdS}_{d+1}/\text{CFT}_d$ is the fact that the conformal field theory is defined on a space-time which has one spatial dimension less than the corresponding AdS space. This allows the previously mentioned association of the conformal boundary of AdS_{d+1} with the domain of the CFT_d.

We provide an introduction to the foundations and basic concepts necessary for AdS/CFT in Section 2.1. Moreover, we present Maldacena's original motivation for $\text{AdS}_5/\text{CFT}_4$ in Section 2.2. In Section 2.3 we briefly review $\text{AdS}_3/\text{CFT}_2$, which is the example we work with the most in this thesis. The remaining two sections (i.e. Sections 2.4 and 2.5) focus on the application of AdS/CFT to explicit computations.

2.1 Foundations of AdS/CFT

In this section we review the most important aspects of conformal field theories and Anti-de Sitter spaces. Since AdS/CFT is a conjecture for a duality between a conformal field theory and a theory of gravity on asymptotic AdS spaces, these two subjects may be seen as the foundation necessary to properly formulate AdS/CFT.

2.1.1 Conformal Field Theories (CFT)

We begin by giving an introduction to CFTs. Since the AdS/CFT correspondence states a duality between a theory of gravity and a CFT, some basic knowledge about CFTs is required in order to understand the actual statement of AdS/CFT. However, the main focus of this thesis is the theory of gravity in AdS/CFT. Therefore, we do not provide an extended discussion of CFTs in this section but just present the basic aspects of the field. There is a vast amount of literature where CFTs are discussed in great detail. In particular, we recommend [109, 110, 120–122].

A CFT is by definition a field theory that is invariant under conformal transformations. In simple terms, a conformal transformation is a local rescaling of the space the field theory is defined on. In particular, this rescaling leaves angles invariant. A field theory with a conformal symmetry therefore has no natural length scale associated with it. Moreover, the conformal symmetry provides the theory with a very powerful algebraic structure. In particular for two-dimensional CFTs this structure may be used to obtain many non-trivial results for CFTs without even specifying a Lagrangian. The introduction to CFTs presented in this section is based on [109, 120–122].

Conformal Transformations

In the following we introduce the concept of conformal transformations. Note that we only discuss conformal transformations for flat space. However, the concept can be generalized to curved spaces. Consider the d-dimensional Minkowski space

$\mathbb{R}^{d-1,1}$ with metric

$$\eta = \text{diag}(-1, 1, \dots, 1).\tag{2.1}$$

A conformal transformation $x^\mu \longmapsto y^\mu$ of $\mathbb{R}^{d-1,1}$ leaves the metric invariant, up to a local scaling factor $\Omega(x) > 0$,

$$\eta_{\lambda\sigma} \frac{\partial y^\lambda}{\partial x^\mu} \frac{\partial y^\sigma}{\partial x^\nu} = \Omega(x)\eta_{\mu\nu}.\tag{2.2}$$

Evidently, this definition in particular includes Poincaré transformations, for which $\Omega(x) = 1$ holds.

In order to make the concept of conformal transformations more accessible, we now consider an infinitesimal conformal transformation

$$x^\mu \longmapsto x^\mu + v^\mu(x).\tag{2.3}$$

As we show below, this allows us to identify certain types of conformal transformations and in particular determine their generators. By doing so we are able to determine the conformal group, i.e. the group of all invertible globally defined finite conformal transformations.

We now derive several equations v^μ has to satisfy in order to correspond to an infinitesimal conformal transformation. Applying (2.3) to (2.2) and expanding to first order in v^μ, we find

$$\partial_\mu v_\nu + \partial_\nu v_\mu = s(x)\eta_{\mu\nu},\tag{2.4}$$

where $s(x) = \Omega(x) - 1$. Contracting (2.4) with $\eta^{\mu\nu}$ leads to

$$s(x) = \frac{2}{d}\partial_\lambda v^\lambda.\tag{2.5}$$

Therefore, in order for (2.3) to be an infinitesimal conformal transformation, v^μ is required to satisfy the equation

$$\partial_\mu v_\nu + \partial_\nu v_\mu = \frac{2}{d}\partial_\lambda v^\lambda \eta_{\mu\nu}.\tag{2.6}$$

From (2.6) the relations

$$\left(\eta_{\mu\nu}\partial^\sigma \partial_\sigma + (d-2)\partial_\mu \partial_\nu\right)\partial_\lambda v^\lambda = 0\tag{2.7}$$

$$2\partial_\mu \partial_\nu v_\rho = \frac{2}{d}\left(\eta_{\rho\mu}\partial_\nu + \eta_{\rho\nu}\partial_\mu - \eta_{\mu\nu}\partial_\rho\right)\partial_\lambda v^\lambda\tag{2.8}$$

may be derived (see e.g. [121]). Here we see that the case of $d = 2$ is special, since (2.7) simplifies to $\partial_\sigma \partial^\sigma \partial_\lambda v^\lambda = 0$. Therefore, we need to treat the cases $d > 2$ and $d = 2$ separately in our analysis of CFTs.

Conformal Transformations for $d > 2$

We may now deduce the general expression for v^μ for $d > 0$ by studying (2.7) and (2.8). By contracting (2.7) with $\eta^{\mu\nu}$, we find

$$\partial_\sigma \partial^\sigma \partial_\lambda v^\lambda = 0.\tag{2.9}$$

Applying this result to (2.7) leads to

$$\partial_\mu \partial_\nu \partial_\lambda v^\lambda = 0 \,, \tag{2.10}$$

i.e. $\partial_\lambda v^\lambda$ is at most linear in x^μ,

$$\partial_\lambda v^\lambda = A + B_\mu x^\mu \,, \tag{2.11}$$

where A and B_μ are constant. By inserting this result into (2.8) we find that v^μ is at most quadratic in x^μ,

$$v_\mu = a_\mu + b_{\mu\nu} x^\nu + c_{\mu\nu\rho} x^\nu x^\rho \,. \tag{2.12}$$

Here a_μ, $b_{\mu\nu}$ and $c_{\mu\nu\rho} = c_{\mu\rho\nu}$ are constant. We can determine the form of the coefficients $b_{\mu\nu}$ and $c_{\mu\nu\rho}$ by inserting (2.12) into (2.6) and (2.8) and perform a coefficient comparison. This allows us to conclude that $b_{\mu\nu}$ and $c_{\mu\nu\rho}$ are of the form

$$b_{\mu\nu} = \alpha \eta_{\mu\nu} + m_{\mu\nu} \,, \quad c_{\mu\nu\rho} = \eta_{\mu\rho} b_\nu + \eta_{\mu\nu} b_\rho - \eta_{\nu\rho} b_\mu \,, \tag{2.13}$$

where the constant coefficients α, b_μ and $m_{\mu\nu} = -m_{\nu\mu}$ may be chosen arbitrarily. By applying (2.13) to (2.3) we are now able to write down the general form of an infinitesimal conformal transformation,

$$x^\mu \longmapsto (1+\alpha)x^\mu + a^\mu + m^\mu{}_\nu x^\nu + 2b_\lambda x^\lambda x^\mu - x_\lambda x^\lambda b^\mu \,. \tag{2.14}$$

This result now allows us to classify the conformal transformations and the commutation relations of their respective generators.

Scale Transformations (D). From the first term in (2.14) it is easy to see that the parameter α corresponds to an infinitesimal rescaling of x^μ. The corresponding generator is denoted by D.

Poincaré Transformations (P_μ, $J_{\mu\nu}$). The terms a^μ and $m^\mu{}_\nu x^\nu$ in (2.14) correspond to infinitesimal translations and Lorentz transformations, respectively. We denote their generators by P_μ and $J_{\mu\nu}$, respectively.

Special Conformal Transformations (K_μ). The remaining terms in (2.14) – proportional to b^μ – are referred to as *special conformal transformation*. The corresponding generator is called K_μ. The finite version of a special conformal transformation,

$$x^\mu \longmapsto y^\mu = \frac{x^\mu - x_\lambda x^\lambda b^\mu}{1 - 2b_\lambda x^\lambda + b_\lambda b^\lambda x_\sigma x^\sigma} \,, \tag{2.15}$$

may be interpreted as a combination of inversions of x^μ and a shift by b^μ. This is evident by considering the relation

$$\frac{y^\mu}{y_\lambda y^\lambda} = \frac{x^\mu}{x_\lambda x^\lambda} - b^\mu \,, \tag{2.16}$$

which is an immediate consequence of (2.15).

The commutation relations of the generators D, P_μ, $J_{\mu\nu}$, K_μ are given by

$$
\begin{aligned}
&[D, P_\mu] = iP_\mu \,, \quad [D, J_{\mu\nu}] = 0 \,, \quad [D, K_\mu] = -iK_\mu \,, \\
&[P_\mu, P_\nu] = 0 \,, \quad [P_\mu, J_{\alpha\beta}] = i\big(\eta_{\mu\alpha}P_\beta - \eta_{\mu\beta}P_\alpha\big) \,, \\
&[P_\mu, K_\nu] = -2i\big(\eta_{\mu\nu}D + J_{\mu\nu}\big) \\
&[J_{\mu\nu}, J_{\alpha\beta}] = i\big(\eta_{\mu\beta}J_{\nu\alpha} + \eta_{\nu\alpha}J_{\mu\beta} - \eta_{\mu\alpha}J_{\nu\beta} - \eta_{\nu\beta}J_{\mu\alpha}\big) \,, \\
&[J_{\mu\nu}, K_\alpha] = -i\big(\eta_{\mu\alpha}K_\nu - \eta_{\nu\alpha}K_\mu\big) \,, \quad [K_\mu, K_\nu] = 0 \,.
\end{aligned}
\tag{2.17}
$$

We note that the special conformal transformations are not globally defined since the x^μ with

$$
1 - 2b_\lambda x^\lambda + b_\lambda b^\lambda x_\sigma x^\sigma = 0
\tag{2.18}
$$

are mapped to infinity via (2.15). In order to establish (2.15) globally, we have to perform a conformal compactification of $\mathbb{R}^{d-1,1}$ (see [121] for more details).

Conformal Group for $d > 2$

Having established the commutation relations (2.17), we may now motivate the form of the conformal group for $d > 2$. The conformal group turns out to be $SO(d, 2)$ as may be seen as follows. We arrange the generators D, P_μ, $J_{\mu\nu}$, K_μ in a matrix $\bar{J}_{UV}$ with $U, V = 0, 1, \ldots, d+1$ via

$$
\bar{J}_{\mu\nu} = J_{\mu\nu} \,, \quad \bar{J}_{d\mu} = \frac{1}{2}(P_\mu + K_\mu) \,, \quad \bar{J}_{(d+1)\mu} = \frac{1}{2}(P_\mu - K_\mu) \,, \quad \bar{J}_{(d+1)d} = D \,,
\tag{2.19}
$$

where $\mu, \nu = 0, 1, \ldots, d-1$ and $\bar{J}_{UV} = -\bar{J}_{VU}$. This allows us to write the commutation relations (2.17) as

$$
[\bar{J}_{UV}, \bar{J}_{AB}] = i\big(\bar{\eta}_{UB}\bar{J}_{VA} + \bar{\eta}_{VA}\bar{J}_{UB} - \bar{\eta}_{UA}\bar{J}_{VB} - \bar{\eta}_{VB}\bar{J}_{UA}\big) \,,
\tag{2.20}
$$

were $\bar{\eta}_{UV}$ is defined to be the metric of $\mathbb{R}^{d,2}$,

$$
\bar{\eta} = \mathrm{diag}(-1, 1, \ldots, 1, -1) \,.
\tag{2.21}
$$

The commutation relations (2.20) are associated with the Lie algebra $\mathfrak{so}(d, 2)$ of $SO(d, 2)$. Thus, we conclude that the conformal group for $d > 2$ is $SO(d, 2)$.

We note that the above discussion of conformal transformations may be performed analogously in Euclidean signature, i.e. when the Minkowski metric $\eta_{\mu\nu}$ is replaced by the Euclidean $\delta_{\mu\nu}$. In particular, in this case the conformal group is $SO(d+1, 1)$.

Conformal Transformations for $d = 2$

The equation (2.6) describing infinitesimal conformal transformations takes the form

$$
\partial_\mu v_\nu + \partial_\nu v_\mu = \partial_\lambda v^\lambda \eta_{\mu\nu}
\tag{2.22}
$$

for $d = 2$. For our discussion of two-dimensional CFTs we consider Euclidean signature, i.e. we replace $\eta_{\mu\nu}$ by $\delta_{\mu\nu}$. This allows us to uncover an intriguing relation between conformal transformations and holomorphic functions. From (2.22) in Euclidean signature we obtain

$$\partial_0 v_0 = \partial_1 v_1 \quad \text{and} \quad \partial_0 v_1 = -\partial_1 v_0 \,. \tag{2.23}$$

These are the well-known Cauchy-Riemann equations. We may use these equations to identify conformal transformations with holomorphic functions. For this purpose, we introduce complex variables and functions together with their complex conjugates,

$$\begin{aligned} z &= x^0 + ix^1 \,, & v &= v^0 + iv^1 \,, \\ \bar{z} &= x^0 - ix^1 \,, & \bar{v} &= v^0 - iv^1 \,. \end{aligned} \tag{2.24}$$

The Cauchy-Riemann equations (2.23) now imply that v and therefore

$$z \longmapsto w = f(z) \,, \tag{2.25}$$

where $f(z) = z + v(z)$, are holomorphic in some open set. Since (2.25) corresponds to the conformal transformation $x^\mu \longmapsto y^\mu$ – where $w = y^0 + iy^1$ – in complex variables, we conclude that every holomorphic function f induces an infinitesimal conformal transformation. In particular, a given f transforms the metric as

$$ds^2 = \delta_{\mu\nu} dy^\mu dy^\nu = dw d\bar{w} = \frac{\partial f}{\partial z} \frac{\partial \bar{f}}{\partial \bar{z}} dz d\bar{z} \,. \tag{2.26}$$

We now derive the general expression for an infinitesimal conformal transformation, similar to the expression (2.14) for $d > 2$. Note that even though f is holomorphic on some open set, we allow it to have isolated singularities on $\mathbb{C}$, i.e. f is considered to be meromorphic. Therefore, we may use the Laurent expansion of v and $\bar{v}$ to obtain the general form of an infinitesimal conformal transformation,

$$z \longmapsto w = z + \sum_{n \in \mathbb{Z}} v_n(-z^{n+1}) \,, \quad \bar{z} \longmapsto \bar{w} = \bar{z} + \sum_{n \in \mathbb{Z}} \bar{v}_n(-\bar{z}^{n+1}) \,. \tag{2.27}$$

The parameters $v_n, \bar{v}_n$ are complex constants. From (2.27) we see that the structure of infinitesimal conformal transformations in two dimensions fundamentally differs from the higher-dimensional case, as it involves infinitely many terms – unlike its higher dimensional counterpart (2.14). The resulting generator algebra of infinitesimal conformal transformations is infinite dimensional. The generators l_n, $\bar{l}_n$ associated with the $v_n, \bar{v}_n$ term in (2.27) obey the commutation relations

$$[l_m, l_n] = (m - n)l_{m+n} \,, \tag{2.28}$$

$$[\bar{l}_m, \bar{l}_n] = (m - n)\bar{l}_{m+n} \,, \tag{2.29}$$

$$[l_m, \bar{l}_n] = 0 \,. \tag{2.30}$$

The relations (2.28) and (2.29) each define one copy of the so-called *Witt algebra*, while (2.30) implies that these two copies commute. Consequently, the two copies

of the Witt algebra are independent from each other, which allows us to treat z and $\bar{z}$ as two independent variables.

We now restrict our analysis to z, i.e. the copy of the Witt algebra generated by the l_n, $n \in \mathbb{Z}$. Of course, the same discussion may be performed for $\bar{z}$ as well. As for $d > 2$, it is necessary to conformally compactify the complex plane in order to globally define the conformal transformations. We do that by adding a point at infinity to the complex plane,

$$\mathbb{C} \longrightarrow S^2 \simeq \mathbb{C} \cup \{\infty\}\,, \tag{2.31}$$

turning $\mathbb{C}$ into the Riemann sphere. However, even on the Riemann sphere only l_{-1}, l_0 and l_1 are globally defined. All other l_n have a singularity either at $z = 0$ or $z = \infty$. [2] So we conclude that conformal transformations on the Riemann sphere that are globally defined are generated only by l_{-1}, l_0 and l_1. In particular, these conformal transformations may be seen as the two-dimensional analogue of the transformations (2.14) obtained for $d > 2$. For instance, l_{-1} generates translations

$$z \longmapsto z + b\,, \tag{2.32}$$

where $b \in \mathbb{C}$ is constant. Moreover, l_0 generates scale transformations of the form

$$z \longmapsto az\,, \tag{2.33}$$

for constant $a \in \mathbb{C}$ and may be combined with $\bar{l}_0$ to the generators of two-dimensional scale transformations $(l_0 + \bar{l}_0)$ and rotations $(l_0 - \bar{l}_0)$. The latter are the Euclidean analogue of the Lorentz transformations we encountered for $d > 0$. The remaining generator l_1 corresponds to special conformal transformations

$$z \longmapsto \frac{z}{ez + 1}\,, \tag{2.34}$$

where $e \in \mathbb{C}$ is constant. We refer to [120–122] for more details regarding l_{-1}, l_0, l_1.

Conformal Group for $d = 2$

From our above discussion of global conformal transformations we may now derive the conformal group for $d = 2$. The transformations (2.32), (2.33), (2.34) generated by l_{-1}, l_0 and l_1 allow us to deduce that a general global conformal transformation is of the form

$$z \longmapsto \frac{az + b}{ez + d}\,, \tag{2.35}$$

where $a, b, e, d \in \mathbb{C}$ are constant. The transformations (2.35) are referred to as *Möbius transformations*. The corresponding group is the *Möbius group* $SL(2, \mathbb{C})/\mathbb{Z}_2$, where the quotient w.r.t. $\mathbb{Z}_2$ is due to the fact that a, b, e, d and $-a, -b, -e, -d$ correspond to the same Möbius transformation.

---

[2] See e.g. [121, 122] for more details.

Virasoro Algebra and Central Charge

In two-dimensional conformally invariant quantum field theories it can be shown that the Witt algebra (2.28) needs to be modified by a central extension. To be more precise, a quantum CFT does not carry a representation of the Witt algebra but the so-called *Virasoro algebra*,[3]

$$[L_m, L_n] = (m-n)L_{m+n} + \frac{c}{12}(m^3 - m)\delta_{m+n,0}\,, \qquad (2.36)$$

where $n, m \in \mathbb{Z}$. The parameter c is the so-called central charge.

The emergence of the Virasoro algebra in a conformal quantum field theory may be motivated by considering a Laurent expansion of the energy momentum tensor in operator modes. From the operator product of the energy momentum tensor with itself it can be deduced that these operator modes obey the commutation relations (2.36). In this procedure, the central charge c appears as a coefficient in the operator product of the energy momentum tensor with itself (see [122]). So every conformal quantum field theory determines a representation of the Virasoro algebra (2.36).

We note that the operators L_{-1}, L_0 and L_1 obey the same commutation relations as l_{-1}, l_0 and l_1 (see (2.28) and (2.36)). Therefore, they are the generators of globally defined conformal transformations.

(Quasi-)Primary Fields

In conformal field theories (of any dimension d) there exists a distinct class of fields ϕ, so-called *quasi-primary fields*. From these fields, all other fields of the theory can be obtained by repeatedly acting with P_μ on ϕ. The resulting fields are referred to as *conformal descendants*. Quasi-primary fields are defined via their behavior under infinitesimal conformal transformations,

$$\begin{aligned}
[D, \phi(x)] &= -i\big(x^\lambda\partial_\lambda + \Delta\big)\phi(x) \\
[P_\mu, \phi(x)] &= -i\partial_\mu\phi(x) \\
[J_{\mu\nu}, \phi(x)] &= i\big(x_\mu\partial_\nu - x_\nu\partial_\mu\big)\phi(x) + \mathcal{J}_{\mu\nu}\phi(x) \\
[K_\mu, \phi(x)] &= \Big(-i\big(2x_\mu\Delta + 2x_\mu x^\lambda\partial_\lambda - x_\lambda x^\lambda\partial_\mu\big) - x^\nu\mathcal{J}_{\mu\nu}\Big)\phi(x)\,,
\end{aligned} \qquad (2.37)$$

where $\mathcal{J}_{\mu\nu}$ corresponds to a finite-dimensional representation of the Lorentz group which determines the spin of ϕ. Moreover, Δ is the scaling dimension of ϕ. The relations (2.37) allow us to determine the behavior of ϕ under a conformal transformation $x^\mu \longmapsto y^\mu$. For instance, if ϕ is a scalar (spin=0) field, it follows

$$\phi(x) \longmapsto \phi'(y) = \left|\frac{\partial y}{\partial x}\right|^{-\Delta/d}\phi(x)\,, \qquad (2.38)$$

where $|\partial y/\partial x|$ denotes the Jacobian of the transformation $x^\mu \longmapsto y^\mu$.

_____

[3]We present the Virasoro algebra for z here. In analogy to the two copies of the Witt algebra (2.28), (2.29), there is a further copy of the Virasoro algebra in quantum CFTs, corresponding to $\bar{z}$.

In the CFT formalism with complex variables $z, \bar{z}$, introduced above for $d = 2$, quasi-primary fields transform as

$$\phi(z, \bar{z}) \longmapsto \phi'(w, \bar{w}) = \left(\frac{\partial f}{\partial z}\right)^{-h} \left(\frac{\partial \bar{f}}{\partial \bar{z}}\right)^{-\bar{h}} \phi(z, \bar{z}). \qquad (2.39)$$

Here $f(z)$ is the holomorphic function associated with the conformal transformation $z \longmapsto w = f(z)$. The transformation $z \longmapsto w$ is assumed to be globally defined, i.e. generated by L_{-1}, L_0, L_1. The parameters $(h, \bar{h})$ are referred to as the conformal dimension of ϕ. We emphasize that h and $\bar{h}$ are real valued. In particular, $\bar{h}$ is not the complex conjugate of h. A field with conformal dimension $(h, \bar{h})$ has scaling dimension $\Delta = h + \bar{h}$ and spin $h - \bar{h}$. If (2.39) also holds for local conformal transformations, i.e. transformations generated by the L_n with $n \neq -1, 0, 1$, ϕ is called *primary*. Evidently, all primary field are quasi-primary fields as well.

Note that in AdS/CFT it is common practice to drop the term "quasi" for quasi-primari fields and simply refer to them as "primary fields". We adopt this convention for the rest of this thesis. In particular for $d = 2$ it is important to keep this convention in mind, since the term "primary" usually refers to a special class of quasi-primary fields, as pointed out above. Moreover, the scaling dimension Δ is often referred to as the conformal dimension.[4] This notation is used in this thesis as well.

$\mathcal{N} = 4$ $SU(N)$ **Super Yang-Mills Theory**

We conclude our review of conformal field theories by presenting an explicit example for such a theory. The example we consider is the Super Yang-Mills (SYM) gauge theory with gauge group $SU(N)$ and $\mathcal{N} = 4$ supersymmetry generators in $d = 4$ dimensions. Note that there are much simpler examples for CFTs – such as the free boson. However, $\mathcal{N} = 4$ $SU(N)$ SYM plays a distinct role for the $\text{AdS}_5/\text{CFT}_4$ correspondence (see Section 2.2), which is why we present this particular CFT. Since we do not work with this theory in this thesis but just need it to properly formulate $\text{AdS}_5/\text{CFT}_4$ in Section 2.2, we restrict our review to presenting the corresponding Lagrangian $\mathcal{L}_{\mathcal{N}=4}$ and the field content.

The Lagrangian of $\mathcal{N} = 4$ $SU(N)$ SYM is given by (see e.g. [109, 123])

$$\begin{aligned} \mathcal{L}_{\mathcal{N}=4} = \text{tr} \Bigg(&-\frac{1}{2g_{YM}^2} F_{\mu\nu} F^{\mu\nu} - i\bar{\lambda}^a \bar{\sigma}^\mu D_\mu \lambda_a - \sum_{i=1}^{6} D_\mu \phi^i D^\mu \phi^i \\ &+ g_{YM} \sum_{a,b=1}^{4} \sum_{i=1}^{6} C^{ab}{}_i \lambda_a [\phi^i, \lambda_b] + g_{YM} \sum_{a,b=1}^{4} \sum_{i=1}^{6} \bar{C}_{abi} \bar{\lambda}^a [\phi^i, \bar{\lambda}^b] \\ &+ \frac{g_{YM}^2}{2} \sum_{i,j=1}^{6} [\phi^i, \phi^j]^2 \Bigg), \end{aligned} \qquad (2.40)$$

---

[4]Note that the term "conformal dimension" usually refers to $(h, \bar{h})$ for $d = 2$.

where g_{YM} is the coupling constant, D_μ is the covariant derivative, $C^{ab}{}_i$ are Clebsch-Gordan coefficients. Moreover, $\bar{\sigma}^\mu$ is given by $\bar{\sigma}^0 = -\mathbb{1}$ and $\bar{\sigma}^r = -\sigma^r$, $r = 1, 2, 3$, where σ^r is the r-th Pauli matrix. The fields contained in $\mathcal{L}_{\mathcal{N}=4}$ are the gauge field A_μ with field strength $F_{\mu\nu}$, four Weyl fermions λ_α^a, $a = 1, 2, 3, 4$, $\alpha = 1, 2$ and six real scalars ϕ^i, $i = 1, 2, \ldots, 6$. Regarding the $SU(4)_R$ R-symmetry of the theory, the fields transform as follows. The gauge field A_μ transforms as **1** (singlet), the Weyl fermions λ_α^a as **4** (fundamental) and the six scalar fields ϕ^i as **6** (antisymmetric).

2.1.2 Anti-de Sitter Spaces (AdS)

The concept of Anti-de Sitter spaces is very well established in general relativity and discussed extensively in the literature (e.g. [109, 110, 116, 117, 119]). The introduction we present here is based on [109].

Anti-de Sitter spaces play a distinct role in general relativity as they come with a maximal number of symmetries. In fact, the symmetries of D-dimensional AdS_D allow to locally determine it by the space-time dimension D and the value of the Ricci scalar $\mathcal{R}$. In the following, we first introduce AdS_D as a space-time with a maximal amount of symmetries and second present an explicit construction of AdS_D as a submanifold of $\mathbb{R}^{D-1,2}$. Moreover, we present several sets of coordinates and discuss the concept of the conformal boundary for AdS_D.

Maximally Symmetric Spaces

We now introduce AdS_D as a space with a maximal number of symmetries. To be more precise, we define AdS_D to be a space for which the number of independent coordinate transformations that keep its metric invariant is maximal, i.e. we demand that there is no D-dimensional metric with more of such coordinate transformations.

We begin our construction of AdS_D by examining what coordinate transformations keep a given D-dimensional metric

$$ds^2 = g_{MN}(x)dx^M dx^N \tag{2.41}$$

invariant. For this purpose we apply an infinitesimal coordinate transformation

$$x^M \longmapsto y^M = x^M + V^M(x), \tag{2.42}$$

where $V^M(x)$ is a given vector field, to (2.41). By demanding this coordinate transformation to keep ds^2 invariant, we find

$$g_{MN}(x) = g_{PR}(y)\frac{\partial y^P}{\partial x^M}\frac{\partial y^R}{\partial x^N} \sim g_{MN}(x) + \nabla_M V_N + \nabla_N V_M, \tag{2.43}$$

where we have expanded to leading order in V^M and ∇_M is the covariant derivative w.r.t. $\partial/\partial x^M$. From (2.43) we deduce that the vector field V^M is required to satisfy the *Killing equation*

$$\nabla_M V_N + \nabla_N V_M = 0. \tag{2.44}$$

The solutions of the Killing equation are called *Killing vector fields* or simply *Killing vectors*.

For a D-dimensional manifold there are at most $D(D+1)/2$ linearly independent Killing vector fields. Consequently, the number of independent coordinate transformations keeping ds^2 invariant is bounded by $D(D+1)/2$. Spaces with exactly $D(D+1)/2$ linearly independent Killing vectors are called *maximally symmetric*.

We define AdS_D to be such a maximally symmetric space. However, this property is not sufficient to locally determine the AdS_D geometry. For instance, $(D = d + 1)$-dimensional Minkowski space $\mathbb{R}^{d,1}$ is maximally symmetric as well. This may be seen by counting the number of symmetries of $\mathbb{R}^{d,1}$: as it is well known, $\mathbb{R}^{d,1}$ is invariant under Poincaré transformations, i.e. $d + 1$ translations and $(d + 1)d/2$ Lorentz transformations, which add up to

$$\frac{(d + 1)(d + 2)}{2} = \frac{D(D + 1)}{2} \tag{2.45}$$

transformations and consequently lead to $D(D+1)/2$ linearly independent Killing vectors, as required for a maximally symmetric space.

The additional property which – together with maximal symmetry and dimension D – determines AdS_D is the value of the Ricci scalar $\mathcal{R}$. This is due to the fact that maximally symmetric spaces can be classified by their dimension D and their Ricci scalar $\mathcal{R}$. [5] In particular, the Ricci scalar of a maximally symmetric space is constant.

This classification via $\mathcal{R}$ allows us to distinguish three different types of maximally symmetric spaces: spaces with $\mathcal{R} = 0$, $\mathcal{R} > 0$ and $\mathcal{R} < 0$. The first ($\mathcal{R} = 0$) is obviously given by $\mathbb{R}^{d,1}$. Spaces in the second class ($\mathcal{R} > 0$) are called *de Sitter spaces*. The spaces we are interested in, i.e. *Anti-de Sitter spaces*, correspond to the third class ($\mathcal{R} < 0$).

We may introduce a length scale $L > 0$ for an AdS_D with given Ricci scalar $\mathcal{R}_{\mathrm{AdS}_D}$ via

$$\mathcal{R}_{\mathrm{AdS}_D} = -\frac{D(D - 1)}{L^2} \, . \tag{2.46}$$

The length scale L is known as *AdS radius*. The above discussion of maximally symmetric spaces allows us to introduce Anti-de Sitter spaces in the following way.

> The D-dimensional Anti-de Sitter space AdS_D with AdS radius L is a maximally symmetric space with Ricci scalar $\mathcal{R}_{\mathrm{AdS}_D} = -D(D-1)/L^2$.

---

[5]Note that in order to classify a maximally symmetric space it is also necessary to state whether the considered manifold is Riemannian or Lorentzian. Since we are working exclusively with Lorentzian space-times here, we drop this additional property.

We conclude our discussion of maximally symmetric spaces by noting that their symmetry leads to a Riemann tensor of the form

$$\mathcal{R}_{MNPR} = \frac{\mathcal{R}}{D(D-1)}\left(g_{NR}g_{MP} - g_{NP}g_{MR}\right).$$

$$(2.47)$$

In particular, they are solutions to Einstein's field equations in the vacuum

$$\mathcal{R}_{MN} - \frac{1}{2}\mathcal{R}g_{MN} + \Lambda g_{MN} = 0,$$

$$(2.48)$$

for the value

$$\Lambda = \frac{D-2}{2D}\mathcal{R}$$

$$(2.49)$$

of the cosmological constant Λ. This particularly implies that Anti-de Sitter spaces have a negative cosmological constant, as may be seen by considering (2.46).

Construction of Anti-de Sitter Spaces

The introduction of AdS_D presented above, though very elegant, does not provide any explicit coordinate representation for the metric of AdS_D. A coordinate representation may be obtained by introducing AdS_D as a submanifold of a surrounding space whose metric may be pulled back to AdS_D. We now present such a construction for AdS_D, where we consider the surrounding space to be $((D-1)+2)$-dimensional Minkowski space $\mathbb{R}^{D-1,2}$. We introduce the notation $D = d + 1$ for the space-time dimensions, since this is the convention most commonly used in AdS/CFT.

The $(d+2)$-dimensional Minkowski space $\mathbb{R}^{d,2}$ comes with the metric

$$ds_{d,2}^2 = \bar{\eta}_{UV}dX^U dX^V = -\left(dX^0\right)^2 + \sum_{i=1}^{d}\left(dX^i\right)^2 - \left(dX^{d+1}\right)^2.$$

$$(2.50)$$

We may identify the $(d+1)$-dimensional Anti-de Sitter space with AdS radius L with the submanifold of $\mathbb{R}^{d,2}$ given by

$$\bar{\eta}_{UV}X^U X^V = -L^2.$$

$$(2.51)$$

We depict this construction of AdS_{d+1} in Figure 2.1 for $d = 1$.

In order to verify that the submanifold defined by (2.51) is in agreement with the introduction of AdS_{d+1} presented below (2.46), we need to show that it is maximally symmetric and has the correct Ricci scalar (2.46). We postpone the latter to the following section where we present explicit coordinates for AdS_{d+1}. Given these coordinates, the verification of (2.46) may be performed straightforwardly.

The fact that the hypersurface (2.51) is maximally symmetric is a consequence of the evident fact that (2.51) is invariant under $O(d, 2)$. This group has $(d+1)(d+2)/2$ generators which leads to the same number of linearly independent Killing vectors, i.e. the maximal number of Killing vectors a $(d + 1)$-dimensional space can have. This shows that (2.51) indeed defines a maximally symmetric space.
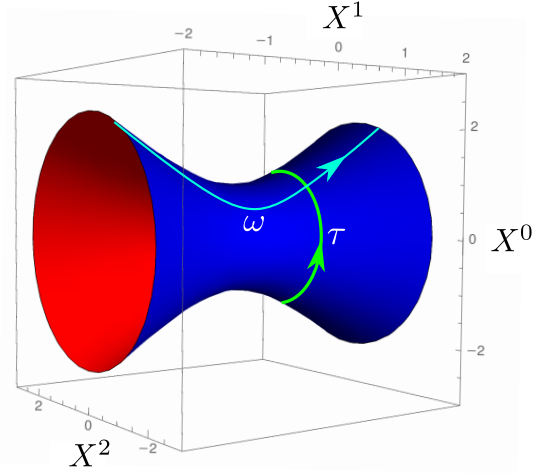
Figure 2.1: AdS$_2$ embedded into $\mathbb{R}^{1,2}$. We depict the submanifold (2.51) of $\mathbb{R}^{1,2}$ corresponding to AdS$_2$. The coordinates ω (cyan) and τ (green) are given by (2.52). Note that for AdS$_2$ we have $S^0 = \{-1, 1\}$. This subtlety is dealt with by considering $\omega \in \mathbb{R}$ instead of $\omega > 0$.

Coordinates for AdS

Using the definition (2.51) of AdS$_{d+1}$ as hypersurface of $\mathbb{R}^{d,2}$, we may now introduce various sets of coordinates for AdS$_{d+1}$. We start by constructing the so-called *global coordinates* of AdS$_{d+1}$ by considering (X^0, X^{d+1}) and $(X^1, \cdots, X^d)$ (see (2.50)) in spherical coordinates respectively,

$$
\begin{aligned}
X^0 &= \tilde{w} \cos(\tau) \, , \\
X^{d+1} &= \tilde{w} \sin(\tau) \, , \\
X^i &= L \sinh(\omega)\Omega^i \quad \text{for} \quad i = 1, \cdots, d \, .
\end{aligned} \tag{2.52}
$$

Here, we have written the radial coordinate of $(X^1, \cdots, X^d)$ w.l.o.g. as $L \sinh(\omega)$ for $\omega > 0$. The coordinates Ω^i parametrize the sphere S^{d-1}, i.e. they satisfy

$$
\sum_{i=1}^{d} (\Omega^i)^2 = 1 \, . \tag{2.53}
$$

Moreover, we have $\tau \sim \tau + 2\pi$ and $\tilde{w} > 0$. By inserting (2.52) into (2.51) we obtain

$$
\tilde{w} = L \cosh(\omega) \, . \tag{2.54}
$$

We depict the coordinates (τ, ω, Ω^i) in Figure 2.1 for $d = 1$. Using (τ, ω, Ω^i) to pull the metric (2.50) back to the hypersurface defined via (2.51), we obtain the metric of AdS$_{d+1}$ in global coordinates,

$$
ds^2_{\text{AdS}} = L^2 \big(- \cosh^2(\omega) d\tau^2 + d\omega^2 + \sinh^2(\omega) d\Omega^2_{d-1} \big) \, , \tag{2.55}
$$

where $d\Omega^2_{d-1}$ is the standard metric for S^{d-1}. Note that we have used

$$
\sum_i \Omega^i d\Omega^i = \frac{1}{2} d\Big[\sum_i (\Omega^i)^2 \Big] = \frac{1}{2} d1 = 0 \tag{2.56}
$$

in the derivation of (2.55).

Given the metric (2.55), the corresponding Ricci scalar may be straightforwardly computed. It agrees with (2.46). This confirms that the hypersurface (2.51) – which is already known to be maximally symmetric (see discussion below (2.51)) – is indeed AdS_{d+1} with AdS radius L.

As can be seen in Figure 2.1, the time coordinate τ is periodic. This leads to closed time-like curves. Thus, in order to maintain causality, the time coordinate needs to be unwrapped by considering $\tau \in \mathbb{R}$ instead of $\tau \in [0, 2\pi]$. The resulting manifold is the universal covering of AdS_{d+1}.

We may introduce an alternative version of the global coordinates (2.55) by using the coordinate $\tilde{r} = L \sinh(\omega) > 0$ instead of ω. This leads to

$$ds^2_{\text{AdS}} = -\left(1 + \frac{\tilde{r}^2}{L^2}\right) d\tilde{t}^2 + \frac{1}{1 + \frac{\tilde{r}^2}{L^2}} d\tilde{r}^2 + \tilde{r}^2 d\Omega^2_{d-1}, \tag{2.57}$$

where $\tilde{t} = L\tau$. Moreover, by introducing the coordinate $\theta \in [0, \pi/2)$ via $\tan(\theta) = \sinh(\omega)$, we can bring the metric (2.55) into the form

$$ds^2_{\text{AdS}} = \frac{L^2}{\cos^2(\theta)} \left(-d\tau^2 + d\theta^2 + \sin^2(\theta) d\Omega^2_{d-1}\right). \tag{2.58}$$

Another set of coordinates that we use in this thesis are the *Poincaré patch coordinates*

$$t \in \mathbb{R}, \quad \vec{x} = (x^1, \cdots, x^{d-1}) \in \mathbb{R}^{d-1}, \quad r > 0, \tag{2.59}$$

which parametrize AdS_{d+1} via

$$\begin{aligned}
X^0 &= \frac{L^2}{2r}\left(1 + \frac{r^2}{L^4}\left(\vec{x}^2 - t^2 + L^2\right)\right) \\
X^i &= \frac{rx^i}{L} \quad \text{for} \quad i = 1, \cdots, d-1, \\
X^d &= \frac{L^2}{2r}\left(1 + \frac{r^2}{L^4}\left(\vec{x}^2 - t^2 - L^2\right)\right) \\
X^{d+1} &= \frac{rt}{L}.
\end{aligned} \tag{2.60}$$

Since $0 < r = X^0 - X^d$, these coordinates only cover the part of the hypersurface (2.51) where $X^0 - X^d > 0$ holds, i.e. half of AdS_{d+1}. This part of AdS_{d+1} is referred to as *Poincaré patch*.

The metric of the Poincaré patch is given by

$$ds^2_{\text{PP}} = \frac{r^2}{L^2}\eta_{\mu\nu}dx^\mu dx^\nu + \frac{L^2}{r^2}dr^2 = \frac{L^2}{z^2}\left(\eta_{\mu\nu}dx^\mu dx^\nu + dz^2\right), \tag{2.61}$$

where $x^0 = t$ and $z = L^2/r$. This metric has a coordinate singularity at $r = 0$ ($z = 0$).
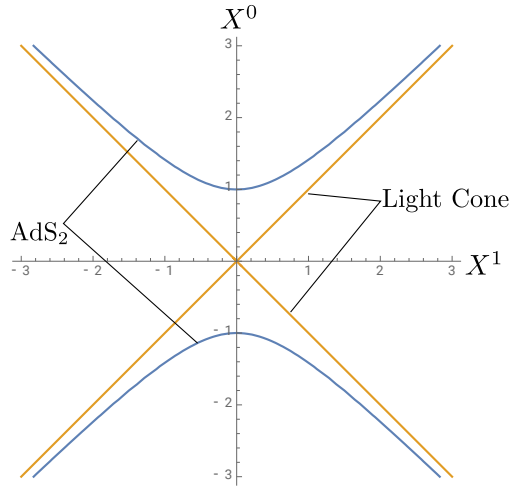
Figure 2.2: The $X^2 = 0$ slice of $\mathbb{R}^{1,2}$. It is evident that AdS_2 (blue) approaches the light cone (orange) for large absolute values of X^1, or equivalently large absolute values of ω (see Figure 2.1). This motivates the definition of the conformal boundary of AdS_2 as the set of all light rays in $\mathbb{R}^{1,2}$ (2.63).

The Conformal Boundary of AdS

Remarkably, the Anti-de Sitter space turns out to have a boundary. We motivate this by the following physical argument. Consider the AdS_{d+1} metric in the form (2.58). The coordinate $\theta \in [0, \pi/2)$ takes the role of a radial direction. By using the time coordinate τ to parametrize a light ray γ pointing radially outwards (see e.g. [117]),

$$\gamma(\tau) = \big(\gamma_\tau(\tau), \gamma_\theta(\tau)\big) = (\tau, \tau), \tag{2.62}$$

where we dropped the angular coordinates corresponding to S^{d-1}, we see that the light ray approaches $\theta = \pi/2$ at $\tau = \pi/2$. So from a physical point of view, AdS_{d+1} has a boundary at $\theta = \pi/2$ that can be reached in finite time. However, this boundary may not be interpreted as the boundary of a manifold in the conventional sense, as the metric (2.58) diverges for $\theta \longrightarrow \pi/2$. All points in AdS_{d+1} are interior points, which is evident by considering the original construction of AdS_{d+1} as a hypersurface of $\mathbb{R}^{d,2}$ (2.51). Moreover, in Figure 2.1 we see that AdS_{d+1} is a hypersurface that expands infinitely, which gives further support to the fact that AdS_{d+1} has no boundary in the conventional sense. The boundary at $\theta = \pi/2$ in AdS_{d+1} is a *conformal boundary*, i.e. it is an equivalence class of d-dimensional Lorentzian manifolds that are related to each other via conformal transformations.

We may motivate a formal definition for the conformal boundary by considering the AdS_{d+1} metric in the coordinates (2.55). As depicted in Figure 2.2, AdS_{d+1} approaches the light cone $\bar{\eta}_{UV} X^U X^V = 0$ of the surrounding $\mathbb{R}^{d,2}$ for large ω. Therefore, the conformal boundary $\partial \mathrm{AdS}_{d+1}$ of AdS_{d+1} is defined to be the set of all light rays,

$$\partial \mathrm{AdS}_{d+1} = \{[X] | X \in \mathbb{R}^{d,2}, X \neq 0, \bar{\eta}_{UV} X^U X^V = 0\}, \tag{2.63}$$

where $X' \in [X]$ iff $X' = aX$ for some $a \in \mathbb{R}$. We can make this definition of $\partial \text{AdS}_{d+1}$ more accessible by considering a representative X with

$$\sum_{i=1}^{d} \left(X^i\right)^2 = 1 \tag{2.64}$$

for each equivalence class $[X] \in \partial \text{AdS}_{d+1}$. From (2.63) it follows that X satisfies

$$\left(X^0\right)^2 + \left(X^{d+1}\right)^2 = 1 \tag{2.65}$$

and therefore conclude, by associating each $[X] \in \partial \text{AdS}_{d+1}$ with its representative X,

$$\partial \text{AdS}_{d+1} = \left(S^1 \times S^{d-1}\right)/\mathbb{Z}_2. \tag{2.66}$$

The division by $\mathbb{Z}_2$ is due to the fact that X and $-X$ are both representatives with the property (2.64) that belong to the same equivalence class, i.e. $[X] = [-X]$.

The conformal boundary of AdS_{d+1} may be interpreted as a conformal compactification of d-dimensional Minkowski space.[6] To see this explicitly, we now construct the metric of $\partial \text{AdS}_{d+1}$ by using the coordinates (2.58). For this purpose, we multiply the metric (2.58) by a positive smooth function $G(\tau, \theta, \alpha^i)$ – where the α^i parametrize S^{d-1} – that keeps $G ds^2_{\text{AdS}}$ finite in the limit $\theta \longrightarrow \pi/2$. Such a function G is called *defining function*. This procedure leads to a boundary metric of the form

$$\begin{aligned} ds^2_{\partial \text{AdS}} &= \lim_{\theta \to \pi/2} \frac{L^2 G(\tau, \theta, \alpha^i)}{\cos^2(\theta)}\left(-d\tau^2 + \sin^2(\theta)d\Omega^2_{d-1}\right) \\ &= \Omega(\tau, \alpha^i)\left(-d\tau^2 + d\Omega^2_{d-1}\right), \end{aligned} \tag{2.67}$$

where $\Omega(\tau, \alpha^i)$ is some smooth positive function. The metric (2.67) is a conformal compactification of $\mathbb{R}^{d-1,1}$.[7] We see that the metric of $\partial \text{AdS}_{d+1}$ is defined only up to conformal equivalence, since the prefactor $\Omega(\tau, \alpha^i)$ in (2.67) is not unique. As $\partial \text{AdS}_{d+1}$ is a conformal boundary, this result was to be expected.

The above method of obtaining a metric for the boundary by multiplying ds^2_{AdS} with a defining function also works in other coordinates. In Poincaré patch coordinates (2.61) for instance, the boundary is located at $r = \infty$. So we need to multiply ds^2_{PP} by a defining function $G_{\text{PP}}(x^\mu, r)$ that keeps the metric finite for $r \longrightarrow \infty$. This leads to

$$ds^2_{\partial \text{AdS}} = \lim_{r \to \infty} G_{\text{PP}}(x^\mu, r)\frac{r^2}{L^2}\eta_{\mu\nu}dx^\mu dx^\nu = \Omega_{\text{PP}}(x^\mu)\eta_{\mu\nu}dx^\mu dx^\nu, \tag{2.68}$$

where $\Omega_{\text{PP}}(x^\mu)$ is a smooth positive function. So in Poincaré patch coordinates we see that the metric of $\partial \text{AdS}_{d+1}$ is conformally equivalent to $\mathbb{R}^{d-1,1}$ and may therefore be conformally transformed to a conformal compactification of $\mathbb{R}^{d-1,1}$ to get in touch with the boundary constructed from global coordinates (2.67).

---

[6]For more details see e.g. [109].

[7]We note that (2.67) is strictly speaking a conformally compactified extension of Minkowski space. We do not discuss this subtlety here but refer to [110] instead.

2.2 AdS$_5$/CFT$_4$ Correspondence

We now present the original version of AdS/CFT introduced by Maldacena in [22]. In this paper, Maldacena conjectured a duality between $\mathcal{N} = 4$ Super Yang-Mills theory with gauge group $SU(N)$ in four space-time dimensions (2.40) and a theory of gravity on AdS$_5 \times S^5$, i.e. AdS$_5$/CFT$_4$. For the motivation of AdS$_5$/CFT$_4$ presented in this section, some basic knowledge of string theory is required. We refer to [106–112] for an introduction to the subject. The review of the basic concepts of AdS$_5$/CFT$_4$ we present here is a combination of the discussions of the subject provided in [106, 109, 110]. Further introductions to AdS$_5$/CFT$_4$ can be found in [116–119].

2.2.1 Three Forms of AdS$_5$/CFT$_4$

Strongest Form. We begin by presenting the explicit statement of AdS$_5$/CFT$_4$ in its strongest form.

> The $\mathcal{N} = 4$ Super Yang-Mills (SYM) $SU(N)$ gauge theory (2.40) is
>
> $$\textit{dynamically equivalent} \tag{2.69}$$
>
> to type IIB string theory (ST) on AdS$_5 \times S^5$ with N units of $F_{(5)}$ flux on S^5.

In this proposed duality the coupling constant g_{YM} of the SYM theory is related to the string coupling g_s, the string length $l_s = \sqrt{\alpha'}$ and the AdS radius L via

$$g_{YM}^2 = 2\pi g_s \quad \text{and} \quad 2g_{YM}^2 N = \frac{L^4}{\alpha'^2}. \tag{2.70}$$

As pointed out in Section 2.1.1, $\mathcal{N} = 4$ SYM is a conformal field theory. Therefore we see that the AdS/CFT correspondence states that a certain quantum string theory on AdS$_5 \times S^5$ may be understood as a conformal QFT.

Though very intriguing, this statement is hard to test since very little is known about the full quantum version of string theory on curved space-time backgrounds. Therefore, two further forms of AdS/CFT with more accessible gravity duals may be considered. These two forms – which are implications of the strongest form (2.69) – are referred to as strong and weak form of AdS/CFT.

Strong Form. In its strong form, AdS/CFT states that (2.69) holds in the so-called *'t Hooft* or *large N limit*, where we take $N \longrightarrow \infty$ for fixed 't Hooft coupling $\lambda_H = g_{YM}^2 N$. In this limit $\mathcal{N} = 4$ SYM becomes an effective theory with coupling constant λ_H [124].[8] By considering the relation (2.70) we see that in this

---

[8] We do not discuss the large N limit in detail here as this is unnecessary for the content of this thesis. Reviews of this subject may be found in e.g. [106, 109, 110, 116]. We note however that this limit may also be taken in other $SU(N)$ Yang-Mills theories. For the versions of AdS/CFT studied in this thesis, the corresponding CFT is always considered in the large N limit.

Form of $\mathrm{AdS}_5/\mathrm{CFT}_4$	CFT side: $\mathcal{N} = 4$ SYM $SU(N)$ gauge theory	AdS side: IIB theory on $\mathrm{AdS}_5 \times S^5$
Strongest	any N and λ_H	Quantum ST for any g_s and α'/L^2
Strong	$N \to \infty$ for fixed λ_H	Classical ST with $g_s \to 0$ for $\alpha'/L^2 > 0$
Weak	$N \to \infty$ for large λ_H	Classical SUGRA with $g_s \to 0$ and $\alpha'/L^2 \to 0$

Table 2.1: The three forms of $\mathrm{AdS}_5/\mathrm{CFT}_4$. Depending on the choice of N and $\lambda_H = g_{YM}^2 N$, $\mathrm{AdS}_5/\mathrm{CFT}_4$ proposes a duality between $\mathcal{N} = 4$ SYM and a IIB theory on $\mathrm{AdS}_5 \times S^5$. The free parameters on the AdS side are related to the ones on the CFT side via (2.70).

limit the string coupling g_s becomes very small and L^4/α'^2 stays finite. In particular, the quantum string theory on $\mathrm{AdS}_5 \times S^5$ reduces to a classical string theory. Consequently, the strong form of AdS/CFT states a duality between a conformal field theory and a classical string theory.

Weak Form. If we – in addition to the 't Hooft limit of the strong form – consider λ_H to be large, we recover the weak form of AdS/CFT. In this form we find the string length $l_s = \sqrt{\alpha'}$ to be very small compared to the AdS radius L, as can be seen from (2.70). Consequently, the strings are approximated to be point particles. This means that the type IIB string theory is reduced to classical type IIB supergravity. Therefore, the weak form of AdS/CFT states that a certain conformal field theory with strong 't Hooft coupling is dual to a classical theory of supergravity.

We list the strongest, strong and weak form of AdS/CFT discussed above in Table 2.1. In this thesis we focus on the weak form of AdS/CFT, for which we present a motivation in Section 2.2.3.

2.2.2 Dp-Branes

The motivation for $\mathrm{AdS}_5/\mathrm{CFT}_4$ is based on superstring theory, where a certain low energy limit is considered for a stack of N $D3$-branes. This limit allows to derive both the AdS side and the CFT side from the dynamics of this setup. In order to make the motivation of $\mathrm{AdS}_5/\mathrm{CFT}_4$ more accessible, we now discuss the concept of Dp-branes.[9] They are non-perturbative extended objects of dimension $p+1$ which interact with strings. For low energies, depending on the strength of the string coupling, a stack of N branes may be viewed from two different perspectives, the *open* (weak coupling) and the *closed string picture* (strong coupling).

The open string picture considers Dp-branes to be $(p+1)$-dimensional Lorentzian hypersurfaces on which open strings end while in the closed string picture they are

---

[9]The following introduction to Dp-branes is based on [106–112].

interpreted as very massive objects that curve the ten-dimensional space-time in which they are embedded.

In the Maldacena argument (Section 2.2.3) the open string picture motivates the CFT side, while the closed string picture gives the AdS side of AdS/CFT.

Dp-Branes as Hypersurfaces (Open String Picture)

We now discuss the open string picture, where *Dp*-branes are seen as hypersurfaces on which open strings end.

Consider an open string $X^M(\tau, \sigma)$ $(M = 0, \ldots, 9)$ in ten-dimensional space-time, parametrized by the worldsheet coordinates τ and σ, where τ refers to the time and σ to the space direction. Since a string is an extended object, we may impose boundary conditions for the endpoints $\sigma = 0, \pi$ of the string for every direction, i.e. every M. We distinguish between *Neumann*

$$\partial_\sigma X^\mu(\tau, \sigma)|_{\sigma=0} = \partial_\sigma X^\mu(\tau, \sigma)|_{\sigma=\pi} = 0 \,, \tag{2.71}$$

for $\mu = 0, \ldots, p$, and *Dirichlet boundary conditions*,

$$X^i(\tau, 0) = X^i(\tau, \pi) = 0 \,, \tag{2.72}$$

for $i = p + 1, \ldots, 9$. The conditions (2.71) and (2.72) imply that the endpoints of the string can move freely in the x^μ directions but are fixed along the x^i coordinates of space-time. As we depict on the l.h.s. of Figure 2.3, this suggests that the string is attached to a *Dp*-brane, i.e. a $(p+1)$-dimensional hypersurface, located at $x^i = 0$ and expanding along the directions x^μ.

A more detailed analysis (see e.g. [106,107,111,112]) reveals that *Dp*-branes are not just a mathematical construction to impose boundary conditions but actual physical objects with energy and charge. In particular, *Dp*-branes are dynamical and interact with closed strings. In this picture, the excitations of the *Dp*-branes are given by the dynamics of the attached open strings (see Figure 2.3). These excitations include fluctuations of the brane in the x^i directions, i.e. transverse to the brane. To examine these deformations of the brane we use the worldsheet coordinates ξ^μ to parametrize the brane via

$$\left(\xi^0, \ldots, \xi^p\right) \longmapsto \left(x^0(\xi^\mu), \ldots x^p(\xi^\mu), \Phi^{p+1}(\xi^\mu), \ldots, \Phi^9(\xi^\mu)\right). \tag{2.73}$$

The $9 - p$ functions Φ^i correspond to the transverse fluctuations, as we depict on the r.h.s. of Figure 2.3. The low energy effective action for one *Dp*-brane is given by

$$\mathcal{S}_{open} = -\tau_p \int d^{p+1}\xi \, e^{-\phi} \sqrt{-\det\left(\mathcal{P}[g] + \mathcal{P}[B] + 2\pi\alpha' F\right)} + \mathcal{S}_{WZ} \,, \tag{2.74}$$

where the first term is known as the *Dirac-Born-Infeld (DBI) action* $\mathcal{S}_{\mathrm{DBI}}$ and $\mathcal{S}_{WZ}$ is the *Wess-Zumino action*

$$\mathcal{S}_{WZ} = \frac{\tau_p}{g_s} \int \sum_q \mathcal{P}[C_{(q+1)}] \wedge e^{\mathcal{P}[B]+2\pi\alpha' F} \,. \tag{2.75}$$
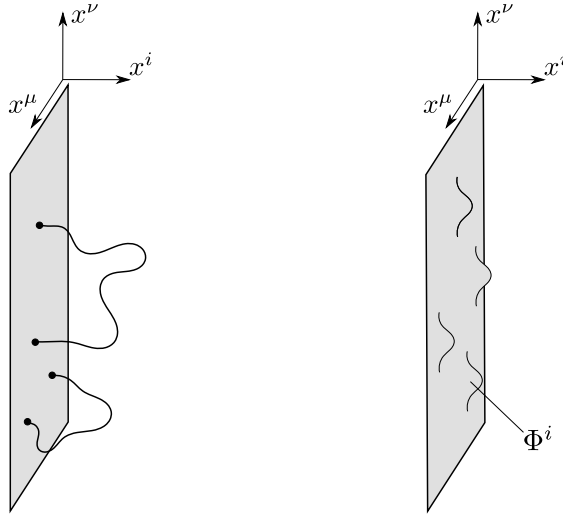
Figure 2.3: Dp-branes in the open string picture. By imposing Neumann (2.71) and Dirichlet (2.72) boundary conditions for open strings we introduce a Dp-brane on which open strings end (l.h.s.). These Dp-branes are dynamical objects themselves. The excitations of the branes may be viewed as the dynamics of the attached strings. These excitations include deformations of the shape of the brane (r.h.s.), which may be parametrized by Φ^i, $i = p + 1, \ldots, 9$ (see (2.73)).

In (2.74) τ_p is given by

$$\tau_p = (2\pi)^{-p}\alpha'^{-(p+1)/2} , \qquad (2.76)$$

and

$$\mathcal{P}[g]_{\mu\nu} = \frac{\partial x^\lambda}{\partial \xi^\mu}\frac{\partial x^\sigma}{\partial \xi^\nu}g_{\lambda\sigma} + \frac{\partial \Phi^i}{\partial \xi^\mu}\frac{\partial x^\sigma}{\partial \xi^\nu}g_{i\sigma} + \frac{\partial x^\lambda}{\partial \xi^\mu}\frac{\partial \Phi^j}{\partial \xi^\nu}g_{\lambda j} + \frac{\partial \Phi^i}{\partial \xi^\mu}\frac{\partial \Phi^j}{\partial \xi^\nu}g_{ij} \qquad (2.77)$$

is the pull-back of the ten-dimensional metric g_{MN} of the surrounding space-time to the brane. The pull-back $\mathcal{P}[B]_{\mu\nu}$ of the Kalb-Ramond field B_{MN} is defined in an analogous way. Moreover, ϕ is the dilaton and $F_{\mu\nu}$ is the field strength of a $U(1)$ gauge field residing on the brane. In the Wess-Zumino action (2.75) g_s is the string coupling, $\mathcal{P}[C_{(q+1)}]$ is the pull-back of the Ramond-Ramond (R-R) $(q + 1)$-form $C_{(q+1)}$ and the exponential of the two-form $\mathcal{P}[B] + 2\pi\alpha'F$ is defined via the wedge product.

The action (2.74) only contains massless fields, which is a consequence of the of the fact that we only consider low energies. We note that the full action describing the dynamics of a Dp-brane also contains a term for the fermionic excitations of the brane. We do not discuss this term here, which is why we do not include it in $\mathcal{S}_{open}$.

To make the DBI action more accessible we consider the special case $e^\phi = g_s = const.$, $F = 0$ and $B = 0$,

$$\mathcal{S}_{\text{DBI}} = -\frac{\tau_p}{g_s}\int d^{p+1}\xi\sqrt{-\det\left(\mathcal{P}[g]\right)} . \qquad (2.78)$$
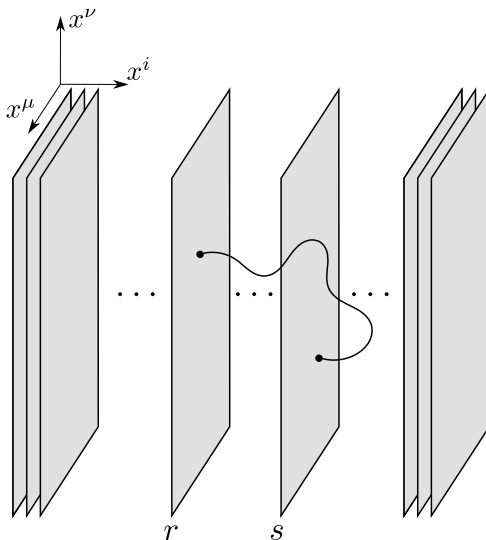
Figure 2.4: A stack of N coincident Dp-branes. When we consider N branes instead of just one, open strings can be attached to two different branes. Here we depict a string stretching from the r-th to the s-th brane. Such a string is labeled by a Chan-Paton factor λ_{rs}. We need to emphasize that the Dp-branes in this graphic coincide, i.e. they all lie on top of each other. The spatial distance of the branes is only introduced here to facilitate the graphical representation of the setup.

We see that in this simple situation the DBI action reduces to the area of the Dp-brane. Consequently, the corresponding equations of motion imply that Dp-branes are minimal surfaces. The prefactor τ_p/g_s in (2.78) may be interpreted as the tension of the brane.

Since the field F in $\mathcal{S}_{open}$ (2.74) can be interpreted as a $U(1)$ gauge field, $\mathcal{S}_{open}$ describes a $U(1)$ gauge theory that is defined on the Dp-brane. It is possible to extend this concept to introduce $U(N)$ gauge theories for generic N by considering a stack of N coincident Dp-branes instead of just one. As we depict in Figure 2.4, a stack of N branes introduces an additional pair of indices $r, s = 1, \ldots, N$ to open strings in a natural way: the indices refer to the branes the two endpoints of the string are attached to. In practice, these indices appear in form of so-called *Chan-Paton factors* λ_{rs} which label an oriented string stretching from the r-th to the s-th Dp-brane. The $N \times N$ matrix with entries λ_{rs} is an element of the Lie algebra $\mathfrak{u}(N)$. This is how the gauge group $U(N)$ emerges for a stack of N branes. The fields on the branes then carry representations of $U(N)$, i.e.

$$\Phi^i = \Phi^{ia}T^a\,, \quad A_\mu = A_\mu^a T^a\,, \tag{2.79}$$

where A_μ is the gauge field corresponding to $F_{\mu\nu}$ and T^a are the generators of $U(N)$. Consequently, Φ^i and A_μ are fields in the adjoint representation of $U(N)$. The action $\mathcal{S}_{open}$ for the stack of Dp-branes is an adapted version of (2.74). For instance, it includes traces to ensure gauge invariance. By taking the appropriate

limits, the field theory described by $\mathcal{S}_{open}$ for a stack of $D3$ branes motivates the CFT side of $\mathrm{AdS}_5/\mathrm{CFT}_4$, as we explain in Section 2.2.3.

In addition to the effective action (2.74), we need to include the action $\mathcal{S}_{closed}$ of closed strings propagating through space-time. This is necessary in order to obtain a complete description of Dp-branes as dynamical objects embedded in a ten-dimensional space-time. The closed string action is given by

$$\mathcal{S}_{closed} = \frac{1}{(2\pi)^7\alpha'^4} \int d^{10}x\sqrt{-\det(g)}\Big(e^{-2\phi}\mathcal{R} + \cdots\Big), \qquad (2.80)$$

where the dots refer to terms including fields like the dilaton or the Kalb-Ramond field. Note that these fields, as well as the metric g_{MN}, also appear in $\mathcal{S}_{open}$ (2.74). Therefore, the Dp-branes and closed strings interact with each other. The action describing both branes and closed strings is given by

$$\mathcal{S} = \mathcal{S}_{open} + \mathcal{S}_{closed}\,. \qquad (2.81)$$

Dp-Branes as Massive Objects (Closed String Picture)

In the previous section we pointed out that closed strings couple to Dp-branes. When this coupling becomes very strong, Dp-branes may be interpreted as very massive objects that curve the surrounding space-time, so-called *extremal p-branes*.

This perspective is referred to as closed string picture.[10] In the Maldacena argument the closed string picture provides the AdS side of AdS/CFT. p-branes are very massive $(p+1)$-dimensional objects which usually come with a curvature singularity and a horizon. If the position of the horizon and the singularity coincide, the branes are referred to as extremal, which is the situation we consider here. Since it is not known how a full quantum field theory describing this setup can be constructed, it is common to restrict further discussions to the classical limit, i.e. Dp-branes are introduced as classical solutions of type II supergravity. This provides the weak form of AdS/CFT (see Table 2.1).

The solutions of type II SUGRA associated with Dp-branes are of the form [125–127]

$$ds^2_{Dp} = g_{DpMN}dx^M dx^N = \frac{1}{\sqrt{H_p(r)}}\eta_{\mu\nu}dx^\mu dx^\nu + \sqrt{H_p(r)}\delta_{ij}dy^i dy^j\,, \qquad (2.82)$$

$$e^\phi = g_s H_p(r)^{(3-p)/4}\,, \qquad (2.83)$$

$$C_{(p+1)} = \big(H_p(r)^{-1} - 1\big)dx^0 \wedge \cdots \wedge dx^p\,, \qquad (2.84)$$

$$B_{MN} = 0\,, \qquad (2.85)$$

where

$$H_p(r) = 1 + \left(\frac{L_p}{r}\right)^{7-p} \quad \text{and} \quad r^2 = \sum_i \big(y^i\big)^2\,. \qquad (2.86)$$

The Greek indices μ, ν run over $0, \ldots, p$ and denote the coordinates parallel to the brane. Moreover, we have $i = p+1, \ldots, 9$ and the coordinates y^i correspond to the directions transverse to the brane.

---

[10]The following introduction to the closed string picture is based on [109, 110].

The extremal p-brane solutions of supergravity (2.82) are a special case of a certain class of geometries with a curvature singularity surrounded by a horizon. They correspond to the situation when the positions of the singularity and the horizon coincide. In the coordinates chosen in (2.82) the horizon/singularity is located at $r = 0$, as may be deduced from the behavior of the Ricci scalar

$$\mathcal{R}_{Dp} = \frac{(p-7)^2(3-p)(1+p)}{4r^2\sqrt{(1+(L/r)^{7-p})}(1+(r/L)^{7-p})^2} \tag{2.87}$$

in the limit $r \longrightarrow 0$. Note that for $p = 3$ the geometry is well behaved at $r = 0$. We discuss this case in greater detail in Section 2.2.3.

Starting from the explicit form (2.82) – (2.86) of the supergravity solution, we may now discuss when this is a valid approximation for string theory. One very intuitive criterion is that the string length needs to be very small compared to a typical length of space-time. Since the only length scale in (2.82) is L_p, this implies $\sqrt{\alpha'} \ll L_p$. In addition, the space-time curvature is required to be very small compared to the string scale. In (2.87) we see that for $p \neq 3$ there is a singularity at $r = 0$, so in these cases the supergravity solution is only valid in a region sufficiently far away from $r = 0$. Moreover, the effective string coupling e^ϕ needs to be small for the supergravity approximation since string loop corrections may not be ignored otherwise. From (2.83) we see that e^ϕ diverges at $r = 0$ for $p < 3$ which gives further support to the statement that the supergravity approximation is not valid for $p < 3$ at $r = 0$.

For $p = 3$ the Ricci scalar vanishes and $e^\phi = g_s$ is constant (see (2.87) and (2.83)). So we find the supergravity approximation to be valid at any point for $p = 3$ if we choose $g_s < 1$ and $\sqrt{\alpha'} \ll L_3$. We further discuss the $p = 3$ case in Section 2.2.3, where we use it to recover the AdS side of AdS/CFT from the closed string picture.

We may associate the supergravity solution (2.82) – (2.86) in the closed string picture with a stack of N Dp-branes in the open string picture via the relation

$$L_p^{7-p} = (4\pi)^{(5-p)/2}\Gamma\left(\frac{7-p}{2}\right)g_s N \alpha'^{(7-p)/2} \tag{2.88}$$

between L_p (2.86) and N. This relation is obtained as follows (see e.g. [109]). Consider the R-R charge Q, which – in terms of N – is given by

$$Q = \frac{N}{(2\pi)^p \alpha'^{(p+1)/2} g_s}. \tag{2.89}$$

In the supergravity solution (2.82) – (2.86), Q may be computed via the R-R flux through the $(8-p)$-sphere surrounding the singularity at $r = 0$, as we visualize in Figure 2.5, i.e.

$$Q = \frac{1}{2\kappa_{10}^2}\int_{S^{8-p}} *F_{(p+2)}, \tag{2.90}$$

where

$$F_{(p+2)} = dC_{(p+1)} = \frac{(7-p)L_p^{7-p}}{r^{8-p}H_p^2(r)}dr \wedge dx^0 \wedge \cdots \wedge dx^p, \tag{2.91}$$
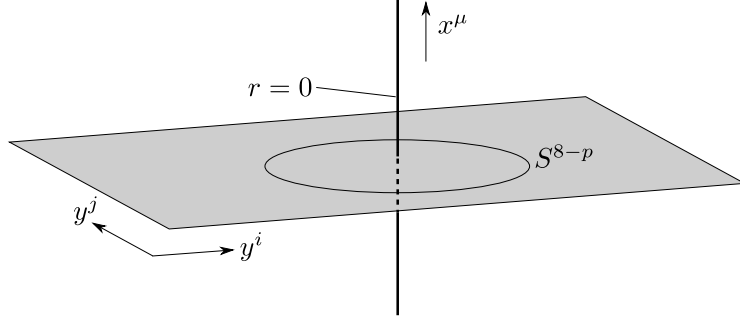
Figure 2.5: The R-R charge of the *Dp*-brane geometry. The *Dp*-brane metric is given by (2.82). In analogy to the electric charge of a point particle, the R-R charge of the *Dp*-brane may be determined by the flux through the $(8 - p)$-sphere around $r = 0$.

and $2\kappa_{10}^2 = (2\pi)^7 \alpha'^4 g_s^2$. The Hodge dual of $F_{(p+2)}$ is given by

$$
\begin{aligned}
*F_{(p+2)} =& \frac{(7-p)L_p^{7-p}}{r^{8-p}H_p^2(r)} \frac{\sqrt{-\det(g_{Dp})}}{(8-p)!} \\
& \times g_{Dp}^{rN_1} g_{Dp}^{0N_2} \cdots g_{Dp}^{pN_{p+2}} \epsilon_{M_1 \cdots M_{8-p} N_1 \cdots N_{p+2}} dx^{M_1} \wedge \cdots \wedge dx^{M_{8-p}} \\
=& (7-p)L_p^{7-p}\omega_{S^{8-p}} ,
\end{aligned}
\tag{2.92}
$$

where $\omega_{S^{8-p}}$ is the standard volume form of S^{8-p}. By comparing (2.89) with (2.90) we obtain (2.88). So we see that a stack of N Dp-branes in the open string picture may be interpreted in the closed string picture as a supergravity solution of the form (2.82) – (2.86) with L_p given by (2.88).

2.2.3   The Maldacena Argument

We now review Maldacena's original motivation [22] for the weak form of $\text{AdS}_5/\text{CFT}_4$ (see Table 2.1). [11] The basis of Maldacena's argument are the two pictures for a stack of N $D3$-branes discussed in Section 2.2.2. When we only consider low energies and reduce the strings to point particles, i.e. $\alpha' \longrightarrow 0$, we obtain the CFT side from the open and the AdS side from the closed string picture. Since both pictures describe the same physical object, we conclude that the AdS side and the CFT side describe the same physics and therefore recover $\text{AdS}_5/\text{CFT}_4$.

   We begin our review of this motivation for $\text{AdS}_5/\text{CFT}_4$ by presenting the exact limits we consider. First, we only work with low energies, i.e. $E \ll 1/\sqrt{\alpha'}$ to avoid any stringy excitations. Second, we take the point-particle limit

$$
\alpha' \longrightarrow 0 , \quad \text{for fixed} \quad \frac{r}{\alpha'} ,
\tag{2.93}
$$

where r is any length scale. This limit is known as the *Maldacena limit*. By keeping r/α' fixed we ensure that the expectation values of the theory stay fixed for $\alpha' \longrightarrow 0$, as we show below.

---

[11]This section is based on [106, 109, 110].

By applying these two limits we recover the CFT side from the open string picture and the AdS side from the closed string picture.

Open String Picture (CFT Side)

We first consider the stack of N $D3$-branes in the open string picture. As already pointed out at the beginning of Section 2.2.2, this picture is only reliable if the coupling between open and closed strings is weak. For a stack of N $D3$-branes this coupling is effectively given by $g_s N$. So we implicitly assume $g_s N \ll 1$ in this section. We mentioned in Section 2.2.2 that for low energies the action for the fields in the open string picture is a sum of two terms (2.81). A term $\mathcal{S}_{open}$ (2.74) describing a $U(N)$ gauge theory on the branes and a term $\mathcal{S}_{closed}$ (2.80) corresponding to the closed string modes propagating through ten-dimensional space-time. By construction of $\mathcal{S}_{open}$, the excitations of the branes couple to the closed strings.

To obtain the CFT side from this setup we consider the rescalings

$$ e^\phi = g_s e^{\kappa_{10}\tilde{\phi}}, \quad \Phi^i = 2\pi\alpha'\phi^i, \quad g_{MN} = \eta_{MN} + \kappa_{10} h_{MN}, \qquad (2.94) $$

where $2\kappa_{10}^2 = (2\pi)^7 \alpha'^4 g_s^2$, which ensure the canonical normalization of the fields. Note that the redefinition of the metric g_{MN} implies that we only consider small excitations of space-time, which is in agreement with the low energy limit.

By taking the Maldacena limit (2.93) we ensure that the expectation values of the theory are fixed for $\alpha' \longrightarrow 0$. To see this we consider the following example: we add an additional $D3$-brane parallel to the stack of N branes at $x^9 = r$. In the low energy limit – where only massless modes are considered – this implies that the corresponding gauge group $U(N+1)$ is broken to $U(N) \times U(1)$ and ϕ^9 has the vacuum expectation value $\langle \phi^9 \rangle = r/(2\pi\alpha')$. In the Maldacena limit $\alpha' \longrightarrow 0$ for r/α' fixed, this vacuum expectation value does not change.

We now apply the Maldacena limit to $\mathcal{S}_{open}$ (2.74). Since a detailed discussion for a stack of N $D3$-branes for generic N would exceed the requirements for this thesis, we restrict our discussion to the bosonic part of just one $D3$-brane with vanishing Kalb-Ramond field. Moreover, we ignore the contribution of the Wess-Zumino action $\mathcal{S}_{WZ}$. Considering these simplifications, $\mathcal{S}_{open}$ takes the form

$$ \mathcal{S}_{open} = -\frac{1}{(2\pi)^3 \alpha'^2} \int d^4x\, e^{-\phi} \sqrt{-\det\left(\mathcal{P}[g] + 2\pi\alpha' F\right)}. \qquad (2.95) $$

Here we used (2.76) for $p = 3$ and chose the x^μ space-time coordinates as worldsheet coordinates, i.e. $x^\mu = \xi^\mu$. By applying (2.94) to (2.95) and expanding in α', we find

$$ \mathcal{S}_{open} = -\frac{1}{2\pi g_s} \int d^4x \left(\frac{1}{4} F_{\mu\nu} F^{\mu\nu} + \frac{1}{2} \eta^{\mu\nu} \delta_{ij} \partial_\mu \phi^i \partial_\nu \phi^j + \mathcal{O}(\alpha')\right). \qquad (2.96) $$

So we recover the typical terms expected in the action of a $U(1)$ gauge theory. It is possible to generalize this discussion to a stack of N $D3$-branes. By doing so we find that in the limit $\alpha' \longrightarrow 0$, $\mathcal{S}_{open}$ becomes the action of $\mathcal{N} = 4$ SYM with

gauge group $SU(N)$ (see (2.40)), i.e. the CFT side.[12] In particular, the coupling constant g_{YM} turns out to be

$$g_{YM}^2 = 2\pi g_s \, . \tag{2.97}$$

Having established the derivation of the CFT side from $\mathcal{S}_{open}$, we now discuss the remaining part $\mathcal{S}_{closed}$ of the action (2.81). By applying (2.94) to the expression (2.80) for $\mathcal{S}_{closed}$ we obtain

$$\mathcal{S}_{closed} = -\frac{1}{2}\int d^{10}x\Big((\partial h)^2 + \cdots + \mathcal{O}(\kappa_{10})\Big)\, . \tag{2.98}$$

Here $(\partial h)^2$ refers to the leading order contribution of $\sqrt{-\det(g)}\mathcal{R}$ in κ_{10}. It turns out to be the action describing free gravitons in ten-dimensional Minkowski space. The dots in (2.98) refer to the leading order contributions of the other terms in (2.80). They correspond to fields defined on ten-dimensional Minkowski space as well. In total, $\mathcal{S}_{closed}$ turns out to be the action for type IIB supergravity on $\mathbb{R}^{9,1}$.

Summing up the results of this section, we find that the action (2.81) for the open string picture contains the action $\mathcal{S}_{\mathcal{N}=4}$ of $\mathcal{N} = 4$ SYM $SU(N)$ and the action $\mathcal{S}_{\text{IIB}}$ of type IIB SUGRA. The coupling terms between $\mathcal{S}_{\mathcal{N}=4}$ and $\mathcal{S}_{\text{IIB}}$ – provided by $\mathcal{S}_{open}$ (2.74) – turn out to be of order α'^2 and may therefore be ignored in the limit $\alpha' \longrightarrow 0$. Consequently, the resulting action describes a $\mathcal{N} = 4$ SYM theory and a theory of supergravity which completely decouple from each other,

$$\mathcal{S}_{open} + \mathcal{S}_{closed} \longrightarrow \mathcal{S}_{\mathcal{N}=4} + \mathcal{S}_{IIB} \, . \tag{2.99}$$

Closed String Picture (AdS Side)

The AdS side may be obtained from the closed string picture of a stack of N $D3$-branes in the following way. In contrast to the open string picture, we first consider the Maldacena limit (2.93) here and afterwards take the low energy limit. By performing the limit $\alpha' \longrightarrow 0$ we in particular impose $\sqrt{\alpha'} \ll L_3$. In this situation the classical supergravity limit is a good approximation if we in addition choose $g_s < 1$, as discussed in Section 2.2.2. From (2.82) – (2.86) we obtain

$$ds_{D3}^2 = \frac{1}{\sqrt{H_3(r)}}\eta_{\mu\nu}dx^\mu dx^\nu + \sqrt{H_3(r)}\big(dr^2 + r^2 d\Omega_5\big)\, , \tag{2.100}$$

$$e^\phi = g_s = const. \, , \tag{2.101}$$

$$C_{(4)} = \big(H_3(r)^{-1} - 1\big)dx^0 \wedge \cdots \wedge dx^3 \, , \tag{2.102}$$

$$B_{MN} = 0 \, , \tag{2.103}$$

where

$$H_3(r) = 1 + \left(\frac{L_3}{r}\right)^4 \, . \tag{2.104}$$

---

[12]Note that in Section 2.2.2 we stated that a stack of N Dp-branes provides a $U(N)$ gauge theory. The reason why we only consider a $SU(N)$ gauge symmetry here is due to the fact that the $U(N)$ gauge theory contains decoupling $U(1)$ degrees of freedom. In AdS/CFT only the remaining $SU(N)$ degrees of freedom are considered. For more details we refer to [110].
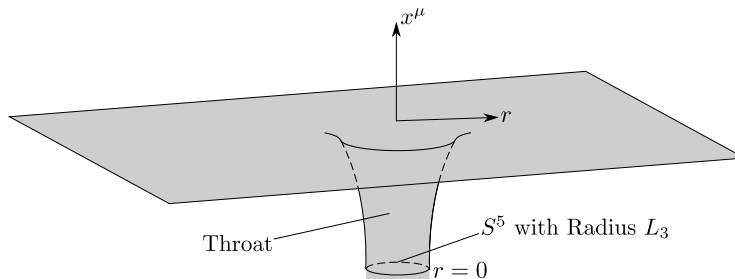
Figure 2.6: The geometry induced by a stack of N $D3$-branes. (This figure is inspired by a similar graphic in [106].) By considering the metric (2.100) it is easy to see that the radius of the S^5 sphere surrounding $r = 0$ asymptotes to $L_3 > 0$ in the limit $r \longrightarrow 0$. So the geometry may be interpreted as a throat.

Note that we have used spherical coordinates for the directions transverse to the brane. These transverse coordinates form the geometry of a throat, since the S^5 sphere surrounding the horizon at $r = 0$ has a finite radius L_3, as depicted in Figure 2.6.

The deeper an object is located in the throat, the more it is red-shifted, as we now discuss. For an observer at infinity an object with energy E_r located at a finite r has a red-shifted energy

$$E = H_3^{-1/4}(r)E_r \,. \tag{2.105}$$

So the energy E measured at $r = \infty$ decreases the closer the object is moved to the horizon at $r = 0$. We may consider objects at $r = 0$ with arbitrary energy E – which is the energy measured in the field theory – by keeping $\sqrt{\alpha'}E_r$ fixed while taking the Maldacena limit, i.e. $\alpha' \longrightarrow 0$ for r/α' fixed. This is easy to be seen by approximating

$$H_3(r) \sim \frac{L_3^4}{r^4} \tag{2.106}$$

for $r \ll L_3$ and inserting (2.88) for $p = 3$ into (2.105).

The next essential step is to take the low energy limit. We may distinguish two different types of excitations that have low energy for an observer at infinity: massless modes with very large wave-lengths propagating through space-time far away from the throat, and excitations located very close to $r = 0$ which have low energy due to the red-shift (2.105). We depict these two types in Figure 2.7.

By taking the low energy limit, these two types of low energy excitations are decoupled from each other. This may be seen as follows: We choose the wave-lengths of the massless excitations far away from the horizon to be much larger than the radius L_3 of the S^5 sphere surrounding it. Consequently, the length scale L_3 of the horizon cannot be approached by the considered low-energy particles. Moreover, the horizon has an infinite radial distance from any other point on the geometry. Therefore, the excitations very close to $r = 0$ are trapped inside the throat.
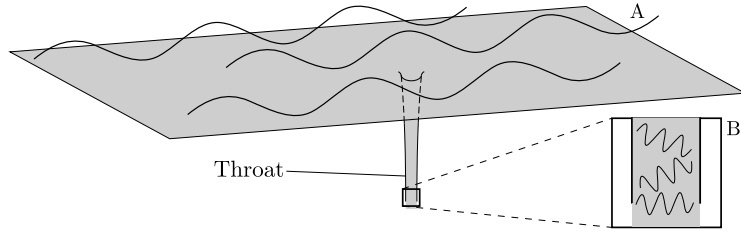
Figure 2.7: The two types of low energies in the brane geometry (2.100). We can distinguish two types of excitations that have low energy E for an observer at infinity. Excitations with long wave-lengths far away from the throat (A) and excitations that are trapped inside the throat (B). The latter are red-shifted for an observer at infinity. In the low energy limit these two types decouple.

In this decoupling limit, the massless large-wave-length modes form IIB supergravity on flat ten-dimensional Minkowski space, since the metric (2.100) is asymptotically flat for $r \gg L_3$. For the excitations near $r = 0$ we may apply (2.106). This allows us to recover the metric of $AdS_5 \times S^5$ from (2.100) by identifying L_3 with the AdS radius L (see (2.61) for the AdS part of the metric),

$$ds_{D3}^2 \sim \frac{r^2}{L^2}\eta_{\mu\nu}dx^\mu dx^\nu + \frac{L^2}{r^2}dr^2 + L^2 d\Omega_5^2 \,. \tag{2.107}$$

So we find the near horizon excitations to describe a theory of supergravity on $AdS_5 \times S^5$, which is the AdS side of AdS/CFT (2.69).

Furthermore, we recover a relation between the AdS radius and the parameters N, g_s and α' by setting $L_3 = L$ in (2.88) for $p = 3$,

$$4\pi g_s N = \frac{L^4}{\alpha'^2} \,. \tag{2.108}$$

This relation implies that the limit $\alpha' \longrightarrow 0$ – which is necessary for the classical supergravity approximation to be reliable – is consistent only when $g_s N \gg 1$. This is in agreement with the statement made at the beginning of Section 2.2.2: the coupling between open and closed strings (which is given by $g_s N$) has to be strong in order for the interpretation of branes as massive objects to be trusted.

As a final comment we mention that since the radius of the S^5 sphere in (2.107) is equal to the AdS radius L, we find the Ricci scalar of the sphere to be

$$\mathcal{R}_{S^5} = \frac{20}{L^2} = -\mathcal{R}_{\text{AdS}_5} \,, \tag{2.109}$$

where the second equality is a consequence of (2.46). So we find the Ricci scalar of (2.107) to vanish, which is in agreement with (2.87) for $p = 3$. Therefore, the divergence of the metric (2.107) at $r = 0$ is merely due to a coordinate singularity. We can avoid this singularity by using global coordinates – e.g. (2.57) – for the AdS part of the metric instead of Poincaré patch coordinates (2.61).
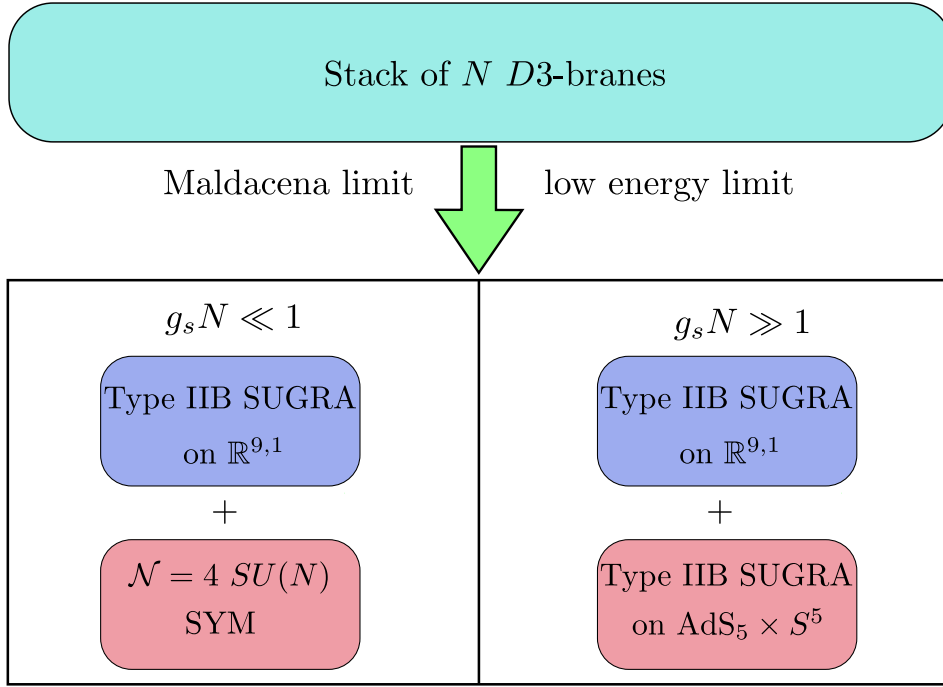
Figure 2.8: A visualization of the Maldacena argument. We start with a stack of N $D3$-branes. By taking the low energy and the Maldacena limit we recover in the open string picture ($g_s N \ll 1$) type IIB supergravity on $\mathbb{R}^{9,1}$ and the $\mathcal{N} = 4$ SYM theory with gauge group $SU(N)$. In the closed string picture ($g_s N \gg 1$) we obtain type IIB supergravity on $\mathbb{R}^{9,1}$ and type IIB supergravity on AdS$_5 \times S^5$. Since in both pictures a type IIB supergravity on $\mathbb{R}^{9,1}$ is present that decouples from the rest of the theory we may conclude that the $\mathcal{N} = 4$ SYM theory is dynamically equivalent to type IIB supergravity on AdS$_5 \times S^5$.

Combining the Open and Closed String Picture

Combining the CFT and AdS side derived from the open and closed string picture respectively, we may now to motivate AdS$_5$/CFT$_4$. In the open string picture we saw that by considering the low energy and Maldacena limits, the action (2.81) for $D3$-branes decouples into the action of $\mathcal{N} = 4$ $SU(N)$ SYM (2.40) and the action for type IIB supergravity on $\mathbb{R}^{9,1}$. In the closed string picture on the other hand, we found that in the low energy and Maldacena limits the theory describes two different types of excitations that decouple from each other, type IIB supergravity modes on AdS$_5 \times S^5$ and $\mathbb{R}^{9,1}$.

So we see that in both the open and the closed string picture the theory of type IIB supergravity on $\mathbb{R}^{9,1}$ is present and decouples from the rest the theory. Since both pictures describe the same physical situation, we may conclude that the remaining parts, i.e. $\mathcal{N} = 4$ $SU(N)$ SYM and type IIB supergravity on AdS$_5 \times S^5$, describe the same physics as well – which is the statement of AdS$_5$/CFT$_4$. We depict this train of thought in Figure 2.8. In particular, by combining the formula (2.97) for the coupling constant g_{YM} with the relation between the string coupling g_s and the AdS radius (2.108), we recover the relation (2.70) between the free

parameters of the AdS and CFT side.

A point to note is that the open string picture is only reliable for $g_s N \ll 1$, while the closed string picture requires $g_s N \gg 1$, as we discuss in the corresponding sections. The above conclusion that $\mathcal{N} = 4$ $SU(N)$ SYM is dual to type IIB on $AdS_5 \times S^5$ does not consider this subtlety and is therefore just a motivation for AdS_5/CFT_4, not a formal proof.

2.3 AdS$_3$/CFT$_2$ Correspondence

In this section we review the AdS$_3$/CFT$_2$ correspondence, which is of particular importance for this thesis as most of our results concern this setup.

Similar to AdS$_5$/CFT$_4$ (see Section 2.2), the AdS$_3$/CFT$_2$ correspondence may be motivated by a particular configuration of D-branes. However, unlike in the AdS$_5$/CFT$_4$ case, these branes are not embedded in ten-dimensional Minkowski space $\mathbb{R}^{9,1}$ but in

$$\mathbb{R}^{4,1} \times S^1 \times T^4 \,, \tag{2.110}$$

where T^4 is the four-torus. The following motivation of AdS$_3$/CFT$_2$ is taken from [109]. Further reviews can be found in [22, 110, 128–130]. The brane configuration we consider here consists of N_1 $D1$-branes wrapping the S^1 in (2.110) and N_5 $D5$-branes wrapping $S^1 \times T^4$. We depict this setup together with the coordinates we use in Table 2.2.

Geometry	$\mathbb{R}^{4,1}$					S^1	T^4			
Coordinates	x^0	x^1	x^2	x^3	x^4	x^5	x^6	x^7	x^8	x^9
$D1$	$\times$	$\cdot$	$\cdot$	$\cdot$	$\cdot$	$\times$	$\cdot$	$\cdot$	$\cdot$	$\cdot$
$D5$	$\times$	$\cdot$	$\cdot$	$\cdot$	$\cdot$	$\times$	$\times$	$\times$	$\times$	$\times$

Table 2.2: Embedding of the $D1$ and $D5$ branes. The brane configuration motivating AdS$_3$/CFT$_2$ considers N_1 $D1$-branes wrapping the S^1 in x^5 direction and N_5 $D5$-branes wrapping the $S^1 \times T^4$ along $x^5, \ldots, x^9$.

The low energy dynamics of this configuration – which provides the CFT side – is located at the $(1+1)$-dimensional intersection of the $D1$ and $D5$-branes. Note that we assume the characteristic length scales of T^4 to be small compared to S^1. In order to motivate the corresponding gravity dual, we consider the IIB supergravity solution of the $D1/D5$ system – analogous to the derivation of $AdS_5 \times S^5$ in AdS$_5$/CFT$_4$ (see Section 2.2). The metric of this solution – in Euclidean signature – is given by

$$\frac{1}{\sqrt{H_1(r)H_5(r)}}\left((dx^0)^2 + (dx^5)^2\right) + \sqrt{H_1(r)H_5(r)}\delta_{ij}dx^i dx^j + \sqrt{\frac{H_1(r)}{H_5(r)}}ds_{T^4}^2 \,, \tag{2.111}$$

where $i, j = 1, \ldots, 4$, $ds_{T^4}^2$ is the metric of the four-torus T^4 and

$$H_1(r) = 1 + \frac{Q_1}{r^2} \,, \quad H_5(r) = 1 + \frac{Q_5}{r^2} \quad \text{with} \quad r^2 = \sum_{i=1}^{4}(x^i)^2 \,. \tag{2.112}$$

Moreover, we have

$$Q_1 = \frac{(2\pi)^4 g_s N_1 \alpha'^3}{V_4} \quad \text{and} \quad Q_5 = g_s N_5 \alpha' \,, \tag{2.113}$$

where V_4 is the volume of T^4. Just as for AdS_5/CFT_4 (see Section 2.2) we take the Maldacena limit $\alpha' \longrightarrow 0$ for r/α' fixed. We obtain the geometry

$$\frac{r^2}{L^2}\big((dx^0)^2 + (dx^5)^2\big) + \frac{L^2}{r^2}dr^2 + L^2 d\Omega_3 + \sqrt{\frac{Q_1}{Q_5}}ds_{T^4}^2 \tag{2.114}$$

of $AdS_3 \times S^3 \times T^4$ (in Euclidean signature) on which the gravity dual of the CFT is defined. Note that we chose spherical coordinates for the directions x^i, $i = 1, \dots, 4$. The AdS radius L is given by

$$L^4 = Q_1 Q_5 \,. \tag{2.115}$$

The metric (2.114) contains the Poincaré patch of AdS_3 (2.61), which may be extended to global AdS_3 (2.57), [13]

$$ds_{\text{AdS}}^2 = -\Big(1 + \frac{\tilde{r}^2}{L^2}\Big)d\tilde{t}^2 + \frac{1}{1 + \frac{\tilde{r}^2}{L^2}}d\tilde{r}^2 + \tilde{r}^2 d\phi^2 \,, \tag{2.116}$$

where $\phi \sim \phi + 2\pi$. The CFT is defined on the conformal boundary of AdS_3, whose constant time slice is given by a circle (see (2.67) for $d = 2$). Moreover, the central charge c of the CFT is related to Newton's constant G_3 in 3 dimensions and the AdS radius via the formula

$$c = \frac{3L}{2G_3} \,, \tag{2.117}$$

which was derived by Brown and Henneaux [132].

2.4 Dictionary

In order to make practical use of AdS/CFT, a one-to-one correspondence between field theory and gravity quantities is required. To be more precise, we need to know how a given field theory quantity is represented on the gravity side, i.e. what is its gravitational dual. This one-to-one correspondence between field theory and gravity quantities is referred to as the *dictionary*.

The dictionary allows to perform field theory calculations on the gravity side and therefore provides many non-trivial tests of AdS/CFT. As an explicit example for an entry of the dictionary, we mention the duality between chiral primary operators (CFT side) and certain fluctuations of the metric and the R-R five form (AdS side) in AdS_5/CFT_4 [23]. A further entry of the dictionary is the Ryu-Takayanagi formula, which relates entanglement entropies (CFT side) to minimal surfaces (AdS side) [82]. We discuss the Ryu-Takayanagi formula in Section 3.1.6.

---

[13]We note that the x^5 direction in (2.114) parametrizes S^1 (see Table 2.2). The corresponding direction for the Poincaré patch (2.61) however, is non-compact. Therefore, following the construction presented in this section, we may obtain (2.116) only locally. As pointed out in [129], in order to obtain (2.116) globally, a rotating version of the $D1$-$D5$ brane configuration is required (see e.g. [131]).

2.4.1 Field-Operator Map

A very concrete realization of the dictionary is the *field-operator map* [133,134]. It relates bulk fields with boundary operators via the asymptotic behavior of the bulk fields at the conformal boundary of AdS_{d+1}. In particular, the field operator map makes the statement that the considered field theory is defined on the boundary of the respective AdS_{d+1} space, more explicit. Moreover, the field-operator map provides an explicit expression for n-point functions of boundary operators in terms of bulk quantities.

Kaluza-Klein Reduction

The field operator map associates fields on AdS_{d+1} with operators on the CFT side. However, in AdS/CFT we usually consider a theory of gravity on $\mathrm{AdS}_{d+1} \times \mathcal{M}$ – where $\mathcal{M}$ is a compact manifold – to be dual to a conformal field theory. For instance, the additional manifold $\mathcal{M}$ is S^5 in $\mathrm{AdS}_5/\mathrm{CFT}_4$ (see Section 2.2) and $S^3 \times T^4$ in $\mathrm{AdS}_3/\mathrm{CFT}_2$ (see Section 2.3). In order to understand the field operator map, we first need to examine how the fields on the gravity side, which are defined on $\mathrm{AdS}_{d+1} \times \mathcal{M}$, are related to the AdS_{d+1} fields dual to CFT operators.

The fields on AdS_{d+1} are obtained by considering a mode expansion in the harmonic functions on $\mathcal{M}$, i.e. a *Kaluza-Klein reduction* [135]. By this procedure, from each field on $\mathrm{AdS}_{d+1} \times \mathcal{M}$ an infinite tower of fields on AdS_{d+1} is obtained. Each of these fields corresponds to one mode on $\mathcal{M}$. Since $\mathcal{M}$ is compact, the spectrum of these modes is discrete.

To see how the Kaluza-Klein reduction works in practice, we perfom it for a massless scalar field $\Phi(x^M, \theta^i)$ on $\mathrm{AdS}_5 \times S^5$. [14] Here, we use x^M, $M = 0, \ldots, 5$ and θ^i, $i = 1, \ldots, 5$ to parametrize AdS_5 and S^5 respectively. The equation of motion for Φ is given by the Klein-Gordon equation on $\mathrm{AdS}_5 \times S^5$,

$$\nabla^2_{\mathrm{AdS}_5 \times S^5} \Phi(x^M, \theta^i) = 0\,, \tag{2.118}$$

where $\nabla^2_{\mathrm{AdS}_5 \times S^5}$ is the d'Alembert operator of $\mathrm{AdS}_5 \times S^5$. It is easy to see that the d'Alembert operator on $\mathrm{AdS}_5 \times S^5$ is given by the sum of the respective operators on AdS_5 and S^5, i.e.

$$\nabla^2_{\mathrm{AdS}_5 \times S^5} = \nabla^2_{\mathrm{AdS}_5} + \nabla^2_{S^5}\,. \tag{2.119}$$

Therefore, (2.118) may be solved by the mode expansion

$$\Phi(x^M, \theta^i) = \sum_l \varphi_l(x^M) Y^l(\theta^i)\,, \tag{2.120}$$

where the φ_l, $l \in \mathbb{N}_0$, are scalar fields on AdS_5 and the Y^l are the spherical harmonics on S^5 satisfying the equation

$$\nabla^2_{S^5} Y^l = -\frac{l(l+4)}{L^2} Y^l\,. \tag{2.121}$$

---

[14]The following discussion is based on [116].

Here the L^2 in the denominator comes from the fact that the S^5 sphere in $\text{AdS}_5 \times S^5$ has radius L (see (2.107)). By inserting the mode expansion (2.120) together with (2.119) and (2.121) into (2.118), we find the equation of motion for each φ_l,

$$\nabla^2_{\text{AdS}_5}\varphi_l - m_l^2\varphi_l = 0\,, \tag{2.122}$$

where

$$m_l^2 = \frac{l(l+4)}{L^2}\,. \tag{2.123}$$

The equation (2.122) is the Klein-Gordon equation for a scalar field of mass m_l on AdS_5.

So we see that the Kaluza-Klein reduction of a single scalar field Φ on $\text{AdS}_5 \times S^5$ provides an entire tower of massive scalar fields φ_l on AdS_5. Each of these fields may now be associated with a particular operator on the CFT side. As we show below, the mass m_l (2.123) governs the asymptotic behavior of φ_l at the conformal boundary and is related to the conformal dimension of the dual CFT operator. Note that m_l is completely determined by the eigenvalues of $\nabla^2_{S^5}$ (2.121). Following the above arguments for the derivation of the mass spectrum m_l, it is easy to see that the same procedure may be performed in the general case of $\text{AdS}_{d+1} \times \mathcal{M}$. Evidently, the mass spectrum of the resulting scalar fields on AdS_{d+1} is determined by the eigenvalues of $\nabla^2_{\mathcal{M}}$. Since the masses of the bulk fields determine the conformal dimension of the dual operators, we see that the operator spectrum on the CFT side is encoded in the shape of $\mathcal{M}$ on the gravity side.

A Toy Model: Scalar Fields Dual to Primary Operators

In order to explain the basic concept of the field-operator map, we consider the following toy model,[15] which is taken from [109]. [16] Consider a scalar field φ of mass m in AdS_{d+1} – obtained by a Kaluza-Klein reduction – with a primary operator $\mathcal{O}$ as CFT_d dual. The conformal dimension of $\mathcal{O}$ is denoted as Δ. The action on AdS_{d+1} for φ is given by

$$\mathcal{S}_{\text{AdS}}[\varphi] = -\frac{C}{2}\int dz d^d x \sqrt{\det(g_{\text{PP}})}\big(g_{\text{PP}}^{MN}\partial_M\varphi\partial_N\varphi + m^2\varphi^2\big)\,, \tag{2.124}$$

where g_{PP} is the AdS_{d+1} metric in Poincaré patch coordinates (2.61) and C is a constant proportional to N^2. Note that we work in Euclidean signature here, i.e. we replace $\eta_{\mu\nu}$ by $\delta_{\mu\nu}$ in (2.61).

We now present how the asymptotic behavior (i.e. $z \longrightarrow 0$) of the solutions of the equation of motion corresponding to (2.124) is related to the conformal dimension Δ of $\mathcal{O}$ via the field operator map. The equation of motion for φ is given by

$$z^2\partial_z^2\varphi - (d-1)z\partial_z\varphi + z^2\delta^{\mu\nu}\partial_\mu\partial_\nu\varphi - m^2 L^2\varphi = 0\,, \tag{2.125}$$

---

[15]For more explicit examples, we refer to [23].
[16]Note that this example is also discussed in [110, 116], where more details are provided.

which follows from (2.124) and is in agreement with (2.122). By making the plane wave ansatz $\varphi(z, x) = \exp(ip_\mu x^\mu)\varphi_p(z)$, we find

$$z^2 \partial_z^2 \varphi_p - (d-1)z\partial_z \varphi_p - (z^2 p^2 + m^2 L^2)\varphi_p = 0, \qquad (2.126)$$

where $p^2 = \delta^{\mu\nu}p_\mu p_\nu$. The two independent solutions of (2.126) have a near boundary behavior of the form

$$\varphi_p \sim z^{\Delta_\pm}, \qquad (2.127)$$

where

$$\Delta_\pm = \frac{d}{2} \pm \sqrt{\frac{d^2}{4} + m^2 L^2}, \qquad (2.128)$$

i.e.

$$\Delta_\pm(\Delta_\pm - d) = m^2 L^2. \qquad (2.129)$$

Thus, we find that $\varphi(z, x)$ has the asymptotic behavior

$$\varphi(z, x) \sim \varphi_{(0)}(x)z^{\Delta_-} + \varphi_{(+)}(x)z^{\Delta_+} + \cdots \qquad (2.130)$$

near the conformal boundary at $z = 0$.

If the conformal dimension Δ of the operator $\mathcal{O}$ dual to φ satisfies $\Delta \geq d/2$, the relation between m and Δ is given by $\Delta = \Delta_+$ via (2.128). The corresponding prefactor $\varphi_{(+)}(x)$ in the series (2.130) of φ is then associated with the vacuum expectation value of $\mathcal{O}$. Moreover, (2.128) implies

$$\Delta_- = d - \Delta. \qquad (2.131)$$

The prefactor $\varphi_{(0)}$ corresponding to Δ_- in (2.130) is interpreted as a source of $\mathcal{O}$.

We note that the above procedure may also be performed for primary operators with conformal dimension $d/2 - 1 \leq \Delta < d/2$ if the interpretation of $\varphi_{(0)}$ and $\varphi_{(+)}$ as vacuum expectation value and source is interchanged. For more details we refer to [109].

This example shows nicely that it is appropriate to consider the CFT to be defined on the conformal boundary: the asymptotic behavior of fields in the bulk encode properties of the corresponding operator duals in the CFT.

2.4.2 Generating Functionals

The field-operator map allows to construct a bulk expression for the generating functional of connected Green's functions for a given operator $\mathcal{O}$ [133, 134]. This very powerful property of AdS/CFT provides a method for computing generic n-point functions of $\mathcal{O}$ from the gravity side.

To see how this construction of the gravity dual of the generating functional works, we consider once more the toy model of a scalar field φ in AdS_{d+1} corresponding to a primary CFT_d operator $\mathcal{O}$ with conformal dimension Δ (see Section 2.4.1). The following discussion is taken from [109]. The generating functional

$W[\varphi_{(0)}]$ for connected Green's functions of $\mathcal{O}$ may be introduced by adding a source term to the action $\mathcal{S}_{\text{CFT}}$ describing the dynamics of the CFT,

$$\mathcal{S}_{\text{CFT}} \longrightarrow \mathcal{S}'_{\text{CFT}} = \mathcal{S}_{\text{CFT}} - \int d^d x \varphi_{(0)}(x)\mathcal{O}(x) \,, \tag{2.132}$$

where $\varphi_{(0)}$ is the source of $\mathcal{O}$. The partition function $Z[\varphi_{(0)}]$ for $\mathcal{S}'_{\text{CFT}}$ in euclidean signature is then given by

$$Z[\varphi_{(0)}] = e^{-W[\varphi_{(0)}]} = \left\langle \exp\left(\int d^d x \varphi_{(0)}(x)\mathcal{O}(x) \right) \right\rangle_{\text{CFT}} \,, \tag{2.133}$$

which in particular defines the generating functional for connected Green's functions $W[\varphi_{(0)}]$.

The relation between $W[\varphi_{(0)}]$ and the gravity dual φ of $\mathcal{O}$ is introduced as follows. We associate the source $\varphi_{(0)}$ in (2.132) with the prefactor of the $z^{d-\Delta}$ term in the series expansion of the field φ (2.130), i.e.

$$\varphi_{(0)}(x) = \lim_{z \to 0} \varphi(z,x) z^{\Delta - d} \,. \tag{2.134}$$

With this identification, the bulk formulation of $W[\varphi_{(0)}]$ is given by [133, 134]

$$W[\varphi_{(0)}] = \mathcal{S}_{\text{AdS}}[\varphi] \Big|_{\lim_{z \to 0} \varphi(z,x) z^{\Delta - d} = \varphi_{(0)}(x)} \,, \tag{2.135}$$

i.e. the generating functional $W[\varphi_{(0)}]$ corresponds to the bulk action (2.124) evaluated at the solution φ of the respective equation of motion (2.125). Therefore, connected correlation functions $\langle \mathcal{O}(x_1)\mathcal{O}(x_2)\cdots\mathcal{O}(x_n) \rangle$ may be obtained by a bulk calculation via

$$\langle \mathcal{O}(x_1)\mathcal{O}(x_2)\cdots\mathcal{O}(x_n) \rangle = -\frac{\delta^n W}{\delta\varphi_{(0)}(x_1)\delta\varphi_{(0)}(x_2)\cdots\delta\varphi_{(0)}(x_n)}\Big|_{\varphi_{(0)}=0} \tag{2.136}$$

and the identification (2.135) of $W[\varphi_{(0)}]$ with the on-shell action (2.124) on the gravity side.

This approach for one operator $\mathcal{O}$ may be straightforwardly generalized to more complicated setups, such as several operators $\mathcal{O}_i$ $i = 1, 2, \dots$. The action $\mathcal{S}_{\text{AdS}}$ on the gravity side then describes the dynamics of the duals φ^i of the operators $\mathcal{O}_i$.

The association of the generating functional W of connected Green's functions with the on-shell action $\mathcal{S}_{\text{AdS}}$ is a central result of AdS/CFT. It offers a precise formulation of the AdS/CFT correspondence for operators and provides a clear procedure for how to apply AdS/CFT for computing correlation functions.

2.5 Generalizations of AdS/CFT

We conclude our introduction to AdS/CFT by reviewing how CFT states may be treated on the gravity side. So far we have restricted our discussion to the

situation where the bulk geometry is pure AdS_{d+1}. This geometry is associated with the vacuum state of the CFT. Considering the statements made in Section 2.4.2 this is evident. Bulk geometries different from pure AdS_{d+1} may be used as gravity duals for other CFT states.[17] The considered geometries are asymptotic AdS_{d+1} spaces ($AAdS_{d+1}$), i.e. a geometries which asymptote to AdS_{d+1} when – for instance – a suitable radial coordinate is taken to infinity. This emergence of AdS_{d+1} is necessary in order to ensure the existence of a conformal boundary, where the CFT is defined on.

2.5.1 Thermal States in AdS/CFT

Black holes in AdS_{d+1} are an example for asymptotic AdS_{d+1} spaces that has been studied extensively in the literature [61, 136–138]. These geometries are the holographic duals of thermal states on the field theory side [136]. The study of thermal CFT states in AdS/CFT is a very vast field that requires some discussion of thermal states in field theories in order to work with it properly. For instance, we need to distinguish between the case of Lorentzian and Euclidean signature of the metric. In the latter, the time direction is compactified to a circle, i.e. made periodic. The circumference of this circle is then associated with the temperature of the field theory side. The introduction of this additional length scale, i.e. the circumference, leads to non-trivial effects in the bulk, such as the Hawking-Page phase transition [136,139]. As we do not require a detailed knowledge of the aspects of thermal states in AdS/CFT for this thesis, we do not present an extended review of the subject here but refer to [109]. Instead, we restrict ourselves to discussing the black $D3$-brane geometry in the context of AdS_5/CFT_4 in order to give a motivation for the association of thermal states on the boundary with black holes in the bulk.[18]

The Metric of Black $D3$-Branes

Black $D3$-branes [127, 140] are a generalization of the extremal $D3$-branes considered in the motivation of the gravity side of AdS_5/CFT_4 (see Section 2.2). Employing the same near horizon limit to the black $D3$-brane geometry as in Section 2.2 for the extremal $D3$-branes leads to the metric

$$ds^2_{\text{BB}} = \frac{r^2}{L^2}\Big(-\big(1 - r_h^4/r^4\big)dt^2 + d\vec{x}_3^2 \Big) + \frac{L^2}{r^2}\frac{1}{1 - r_h^4/r^4}dr^2 + L^2 d\Omega_5^2\,, \qquad (2.137)$$

where $r_h < r$ and $d\vec{x}_3^2$ corresponds to the three spatial directions along which the black brane expands. The final term in (2.137) corresponds to a five-sphere of radius L, just as for the vacuum case (see (2.107)). The remaining terms in (2.137) form the metric of an asymptotic AdS_5 space in Poincaré patch coordinates (2.61), as may be easily seen by considering the limit $r \gg r_h$ and comparing (2.137) with (2.61). Therefore, the bulk geometry (2.137) corresponds to a CFT_4 state defined on $(3+1)$-dimensional Minkowski space, as this is the conformal boundary for the

---

[17]For a discussion of this subject, we refer to [118].
[18]The following discussion is motivated by [109]. See also [110].

Poincaré patch (2.68). In the following discussion we focus on the AAdS$_5$ part of (2.137),

$$ds^2_{\text{AAdS}} = \frac{r^2}{L^2}\Big(-\big(1 - r_h^4/r^4\big)dt^2 + d\vec{x}_3^2\Big) + \frac{L^2}{r^2}\frac{1}{1 - r_h^4/r^4}dr^2\,, \tag{2.138}$$

as the fields defined on the geometry (2.137) may be reduced to fields on (2.138) via a Kaluza-Klein reduction (see Section 2.4.1). We see that (2.138) has an event horizon at $r = r_h$. Thus we may interpret (2.138) as an extended version of a black hole, expanding along the three spatial directions corresponding to $d\vec{x}_3^2$.

Thermal States Dual to Black $D3$-Branes

We now present a simple argument that motivates the identification of the black $D3$-brane geometry (2.137) in the bulk with a thermal state on the boundary. For this we consider (2.138) for imaginary times, i.e. $t = it_E$, in order to establish Euclidean signature for (2.138),

$$ds^2_{\text{AAdS}} = \frac{L^2}{z^2}\Big(\big(1 - z^4/z_h^4\big)dt_E^2 + d\vec{x}_3^2 + \frac{1}{1 - z^4/z_h^4}dz^2\Big)\,. \tag{2.139}$$

Here we have performed the coordinate transformation $r = L^2/z$, which brings the conformal boundary to $z = 0$ and the horizon to $z = z_h = L^2/r_h$.

The strategy for motivating the association of the black brane with a thermal CFT state goes as follows. We show that the time direction t_E has to be periodic in order to guarantee that the metric (2.139) is regular at the horizon. This periodicity in the bulk is then also present at the boundary. Consequently, we find that in Euclidean signature the CFT has a periodic time direction. Since such periodic times are associated with thermal states in field theories, this completes our motivation for the interpretation of the black $D3$-brane geometry as gravity dual of a thermal state.

The motivation for the periodicity of t_E in (2.139) goes as follows. By performing the coordinate transformation

$$z = z_h\Big(1 - \frac{\varrho^2}{L^2}\Big)\,, \tag{2.140}$$

where $0 < \varrho < L$, we obtain

$$\begin{aligned} ds^2_{\text{AAdS}} =& \frac{L^2}{z_h^2}\frac{1 - \big(1 - \varrho^2/L^2\big)^4}{\big(1 - \varrho^2/L^2\big)^2}dt_E^2 + \frac{L^2}{z_h^2}\frac{1}{\big(1 - \varrho^2/L^2\big)}d\vec{x}_3^2 \\ &+ \frac{4\varrho^2/L^2}{\big(1 - \varrho^2/L^2\big)^2\big(1 - \big(1 - \varrho^2/L^2\big)^4\big)}d\varrho^2 \end{aligned} \tag{2.141}$$

from (2.139). Close to the horizon, i.e. $\varrho \ll L$, (2.141) asymptotes to

$$\frac{4\varrho^2}{z_h^2}dt_E^2 + \frac{L^2}{z_h^2}d\vec{x}_3^2 + d\varrho^2\,. \tag{2.142}$$

From this result we may now deduce that the coordinate t_E is required to be periodic in order to avoid a conical singularity at the horizon, $\varrho = 0$. By considering the coordinate transformation

$$t_E = z_h \vartheta / 2 \,, \tag{2.143}$$

we find that the metric on the $\varrho\vartheta$-plane of (2.142) is given by

$$d\varrho^2 + \varrho^2 d\vartheta^2 \,. \tag{2.144}$$

Evidently, this is the metric of $\mathbb{R}^2$ in polar coordinates. Consequently, we have to make ϑ 2π-periodic in order to avoid a conical singularity at $\varrho = 0$. Using (2.143) we obtain the wanted periodicity of t_E,

$$t_E \sim t_E + \pi z_h \,. \tag{2.145}$$

This periodicity of the time coordinate t_E allows us to conclude that the dual CFT state is thermal, as we now show. The relation (2.145) in the bulk implies that the CFT side has the same periodicity. This is an evident conclusion, as the CFT is defined on the conformal boundary of the bulk. It is a well known fact that in field theories periodic times in Euclidean signature may be used to describe thermal states. A periodicity of the form

$$t_E \sim t_E + \beta \tag{2.146}$$

is associated with a thermal state of temperature $T = 1/\beta$, where we have set the Boltzmann constant to one, $k_B = 1$. This completes our justification of the association of (2.137) with a thermal CFT state. Comparing (2.145) with (2.146) shows that the inverse temperature β on the CFT side is given by

$$\beta = \pi z_h \,. \tag{2.147}$$

We note that the above argumentation for the association of thermal states with black brane geometries may be generalized to further examples of black holes. This justifies the interpretation of other types of black holes as thermal states. For a review of this generalization we refer to [116].

2.5.2 Excited States in AdS$_3$/CFT$_2$

In this section we introduce two types of asymptotic AdS$_3$ geometries which we use extensively in this thesis. These geometries are the Bañados-Teitelboim-Zanelli (BTZ) black hole [141, 142] and the conical defect [143, 144].

BTZ Black Hole

The BTZ black hole is the asymptotic AdS black hole in $2 + 1$ dimensions. Its metric is given by [141]

$$ds^2_{\mathrm{BTZ}} = -\frac{\tilde{r}^2 - \tilde{r}_h^2}{L^2} d\tilde{t}^2 + \frac{L^2}{\tilde{r}^2 - \tilde{r}_h^2} d\tilde{r}^2 + \tilde{r}^2 d\phi^2 \,, \tag{2.148}$$
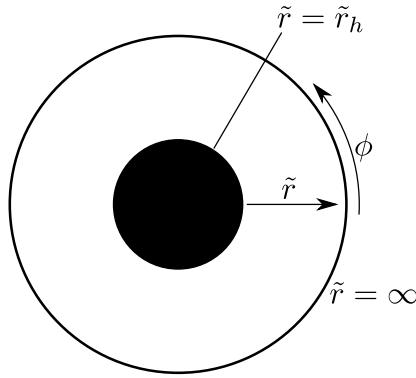
Figure 2.9: A constant time slice of the BTZ black hole. The metric of the BTZ black hole in terms of the coordinates $\tilde{r}$, ϕ and $\tilde{t}$ is given by (2.148). The geometry has an horizon at $\tilde{r} = \tilde{r}_h$. The conformal boundary – on which the dual CFT is defined – is located at $\tilde{r} = \infty$.

where $\tilde{t} \in \mathbb{R}$, $0 < \tilde{r}_h < \tilde{r}$ and $\phi \sim \phi + 2\pi$. Moreover, $\tilde{r}_h$ is the horizon of the black hole. It is related to the mass of the black hole via [141]

$$\tilde{r}_h = \sqrt{8 G_3 M L}\,. \tag{2.149}$$

In Figure 2.9 we depict a visualization of a constant time slice of the BTZ black hole which we use extensively in this thesis. By considering $\tilde{r} \gg \tilde{r}_h$ we find

$$ds^2_{\text{BTZ}} \sim -\frac{\tilde{r}^2}{L^2} d\tilde{t}^2 + \frac{L^2}{\tilde{r}^2} d\tilde{r}^2 + \tilde{r}^2 d\phi^2\,, \tag{2.150}$$

which agrees with the AdS$_3$ metric (2.116) for $\tilde{r} \gg L$. Thus, the BTZ black hole is an asymptotic AdS space, which allows us to consider it in the context of AdS/CFT.

We note that the coordinates (2.148) may also be considered for $\tilde{r} < \tilde{r}_h$. By doing so, we see that the BTZ black hole does not have a metric singularity at $\tilde{r} = 0$, unlike other types of black holes. However, $\tilde{r} = 0$ is still a region in the geometry that is not well behaved, since the Hausdorff manifold structure vanishes there. We do not require these aspects of the BTZ black hole, as our analysis will focus on the exterior of the black hole, i.e. $\tilde{r} > \tilde{r}_h$. Therefore we do not discuss them here and refer to [142] instead.

The BTZ black hole may be constructed as a quotient of the Poincaré patch (2.61) [142]. We present the quotienting procedure providing the BTZ black hole in Section 5.4.2 as an intermediate step in the construction of the kinematic space of the BTZ black hole.

In the context of AdS/CFT, the BTZ black hole corresponds to a thermal state of the CFT. As the conformal boundary of the BTZ geometry is a cylinder, the constant time slices of the CFT are circles. The relation between the inverse temperature β on the field theory side and the horizon radius is given by [137]

$$\frac{\tilde{r}_h}{L} = \frac{2\pi \ell_{CFT}}{\beta}\,, \tag{2.151}$$

where ℓ_{CFT} is the radius of the circle corresponding to a constant time slice on the CFT side.

Conical Defects

The conical defect is a further asymptotic AdS$_3$ space of particular importance for this thesis. In the context of AdS/CFT conical defects are associated with primary excitations on the field theory side [131, 145].[19] The corresponding metric is given by (see e.g. [145])

$$ds^2_{\text{CD}} = -\Big(\frac{\tilde{r}^2}{L^2} + \hat{N}^{-2}\Big)d\tilde{t}^2 + \frac{1}{\frac{\tilde{r}^2}{L^2} + \hat{N}^{-2}}d\tilde{r}^2 + \tilde{r}^2 d\phi^2\,, \qquad (2.152)$$

where $\tilde{t} \in \mathbb{R}$, $\phi \sim \phi + 2\pi$, $\tilde{r} > 0$ and $1 < \hat{N} < \infty$. In analogy to (2.150) we see that (2.152) asymptotes to global AdS$_3$ (2.116) for $\tilde{r}^2/L^2 \gg 1/\hat{N}^2$. The name "conical defect" originates from the fact that the metric (2.152) may be obtained from a slice of global AdS$_3$ with angular size $2\pi/\hat{N}$ (see e.g. [146]). By identifying the edges of the slice with each other, the geometry (2.152) is exposed to have a conical singularity at $\tilde{r} = 0$. We discuss this construction in greater detail in Section 5.4.1, where we use it to construct the kinematic space of the conical defect. Since there is no horizon surrounding it, the singularity of the conical defect is naked. We note however that by taking quantum corrections into account, the geometry develops a horizon surrounding the conical singularity in the semiclassical approximation [149].

From the physical point of view, the conical defect may be interpreted as a static particle of mass

$$M_{\text{CD}} = \frac{\hat{N} - 1}{4G_3\hat{N}}\,. \qquad (2.153)$$

This is due to the fact the (2.152) is not a solution of the vacuum Einstein equations but comes with a point-like source at $\tilde{r} = 0$ [144] (see also [150]).

Furthermore, we note that conical defects may be seen as extension of the BTZ metric (2.148) to negative masses M (2.149) via the identification [141]

$$\hat{N}^2 = \frac{1}{8G_3|M|}\,. \qquad (2.154)$$

This observation plays a crucial role in Section 4.2.2, where we study the behavior of topological complexity as a function of $8G_3M \in [-1, \infty)$.

---

[19]Reviews of the conical defect in the context of AdS/CFT can be found in [146–148].

Chapter 3

Quantum Information in AdS/CFT

One aspect of AdS/CFT that was studied intensively in recent years is its relation to quantum information. The field of quantum information focuses on the question how the structure of a quantum system encodes the information about its specific state. For an introduction to quantum information we refer to [27–29, 98]. Many quantities, such as entanglement entropy, (conditional) mutual information, relative entropy and complexity were defined in order to make the concept of the information of a system more accessible.

In discrete quantum systems, such as spin-chains, these quantities are mostly well understood. However, their generalization to quantum field theories has proven to be a challenging task as the corresponding calculations are in general very involved. The AdS/CFT correspondence allows to study the quantum information aspects of the boundary field theory from the gravity side. The conclusions drawn from this approach suggest a close relation between the geometry of the bulk and quantum information on the boundary.

The most prominent example for this relation is the seminal Ryu-Takayanagi (RT) proposal [82] which relates entanglement entropy to the area of extremal surfaces in the bulk. The RT proposal was the starting point for further approaches relating quantum information and geometry. For instance, in [89] it was shown that entanglement entropy may be used to derive Einstein's field equations to linear order. Furthermore, complexity was suggested to be related to bulk volumes or the action corresponding to a certain bulk region [57–59, 63] (see Section 3.2.3 for more details). Other concepts of quantum information that were studied in the context of AdS/CFT are entanglement of purification [151, 152], quantum error correcting codes [90], the Fisher information metric [40, 153] and fidelity susceptibility [154–156].

In this thesis we make extensive use of entanglement entropy, which is why we review this concept in Section 3.1, including its formulation in field theories and AdS/CFT. In particular, we require the RT formula for entanglement entropy for formulating our results for complexity, which we present in the following chapters. We provide an introduction to complexity and the bulk quantities proposed to be holographic duals for it in Section 3.2. Furthermore, we review the modular

Hamiltonian, which is essentially the logarithm of a given density matrix, in Section 3.3. This object is further studied in Chapter 6.

3.1 Entanglement Entropy

Entanglement describes non-classical correlations between two subsystems A and B belonging to the same total system Σ. [1] The pure states of such a system are considered to be the normalized vectors in a Hilbert space that is the tensor product of the Hilbert spaces corresponding to the subsystems A and B,

$$\mathcal{H}_\Sigma = \mathcal{H}_A \otimes \mathcal{H}_B \,. \tag{3.1}$$

Formally, a pure state $|\Psi\rangle_\Sigma \in \mathcal{H}_\Sigma$ is referred to as entangled if it does not factorize, i.e. if it is not possible to write it in the form

$$|\Psi\rangle_\Sigma = |\psi_1\rangle_A \otimes |\psi_2\rangle_B \,, \tag{3.2}$$

where $|\psi_1\rangle_A \in \mathcal{H}_A$ and $|\psi_2\rangle_B \in \mathcal{H}_B$. In practice, this definition implies that the results of independent measurements on both subsystems of an entangled state are correlated. To be more precise, there are observables of the form $\mathscr{A} \otimes \mathscr{B}$ whose expectation values do not factorize,

$$\langle \mathscr{A} \otimes \mathscr{B} \rangle_\Sigma \neq \langle \mathscr{A} \rangle_A \langle \mathscr{B} \rangle_B \,. \tag{3.3}$$

This is easy to see since a factorization of the expectation value for all observables of the form $\mathscr{A} \otimes \mathscr{B}$ obviously requires $|\Psi\rangle_\Sigma$ to be of the form (3.2).

The definition of entanglement may be generalized to mixed states ρ^Σ in the following way. A mixed state is referred to as entangled when it is not a classical ensemble of factorizing states, i.e. when it is not of the form

$$\rho^\Sigma = \sum_i p_i \; \rho_i^A \otimes \rho_i^B \,, \tag{3.4}$$

where $0 \leq p_i \leq 1$ with $\sum_i p_i = 1$ and $\rho_i^{A,B}$ are states on A and B respectively.

Entanglement is of fundamental importance for many physical concepts. As an example for a very well known system, where entanglement is present, we may consider the hydrogen atom. An electron which is bounded to a proton to form a hydrogen atom is quantum-mechanically described as a state where it is most likely to observe the electron very close to the proton. This means that the expected positions of the proton and the electron are correlated. So the state describing the hydrogen atom is an entangled state for the two subsystems corresponding to the electron and the proton.

---

[1]For reviews regarding entanglement we refer to [27–29, 32].

3.1.1 Definition of Entanglement Entropy

Entanglement entropy is a quantity introduced to quantify the amount of entanglement between the subsystems A and B. [2] From the definition of entanglement for pure states in the paragraph of (3.2) it is easy to see that the reduced state corresponding to the subsystem A

$$\rho^A = \operatorname{tr}_B \left(\left. |\Psi\rangle \langle\Psi| \right|_\Sigma \right) \tag{3.5}$$

is not pure, i.e. mixed, iff $|\Psi\rangle_\Sigma$ is entangled. Here tr_B refers to the partial trace over the subsystem B. The idea behind entanglement entropy is to quantify how mixed ρ^A is. To be more precise, entanglement entropy measures the amount of information required to describe ρ^A. The von Neumann entropy is known to be a measure for the information contained in a state. Thus it is reasonable to define the entanglement entropy $S(A)$ of a state w.r.t. the subsystem A as the von Neumann entropy of the reduced state ρ^A,

$$S(A) = - \operatorname{tr}_A \left(\rho^A \log \left(\rho^A \right) \right). \tag{3.6}$$

In particular, we see that for a disentangled pure state (3.2) the entanglement entropy vanishes, which is a reasonable property a measure for entanglement should have. This definition also applies to mixed states ρ^Σ. However, we need to stress that for mixed states the entanglement entropy does not only measure the entanglement of the state but also takes the mixedness of ρ^Σ into account. For instance, a disentangled state of the form

$$\rho^\Sigma = \sum_i p_i \left. |\psi_i\rangle \langle\psi_i| \right|_A \otimes \left. |\psi_i\rangle \langle\psi_i| \right|_B , \tag{3.7}$$

where $0 \leq p_i \leq 1$, $\sum_i p_i = 1$ and $\langle\psi_i | \psi_j\rangle_{A,B} = \delta_{ij}$, has the entanglement entropy

$$S(A) = - \sum_i p_i \log p_i , \tag{3.8}$$

which is the von Neumann entropy of ρ^Σ. So even though the state ρ^Σ corresponds to a classical ensemble of disentangled states $|\psi_i\rangle_A \otimes |\psi_i\rangle_B$, its entanglement entropy is not zero.

3.1.2 Properties of Entanglement Entropy

We list some of the most important properties of entanglement entropy which are particularly relevant for this thesis.

   Non-Negativity. Entanglement entropy is known to be a non-negative quantity,

$$S(A) \geq 0 , \tag{3.9}$$

---

[2]Reviews of entanglement entropy are [27–30, 32, 33].

where $S(A) = 0$ holds iff the reduced state ρ^A is pure.

Araki-Lieb Inequality. [113] For any state on a Hilbert space $\mathcal{H}_\Sigma = \mathcal{H}_A \otimes \mathcal{H}_B$ the Araki-Lieb inequality,

$$S(\Sigma) \geq |S(A) - S(B)|, \tag{3.10}$$

holds.[3]

Symmetry for Pure States. Consider a pure state $|\Psi\rangle_\Sigma$ on the Hilbert space $\mathcal{H}_\Sigma = \mathcal{H}_A \otimes \mathcal{H}_B$. Then the entanglement entropies of the subsystems A and B are equal, i.e.

$$S(A) = S(B). \tag{3.11}$$

This is an immediate consequence of the Araki-Lieb inequality (3.10) and the fact that the entanglement entropy is zero for pure states.

(Strong) Subadditivity. [158,159] For three independent subsystems A, B, C of a quantum system, the strong subadditivity of entanglement entropy states

$$S(AC) + S(BC) \geq S(ABC) + S(C). \tag{3.12}$$

In particular, we recover the subadditivity of entanglement entropy,

$$S(A) + S(B) \geq S(AB), \tag{3.13}$$

from (3.12) by setting $C = \emptyset$. Moreover, if the state on AB factorizes, i.e. $\rho^{AB} = \rho^A \otimes \rho^B$, we find the above inequality to be saturated,

$$S(AB) = S(A) + S(B), \tag{3.14}$$

as may be easily deduced from the definition of entanglement entropy (3.6).

3.1.3   (Conditional) Mutual Information

Entanglement entropy is the starting point for many other quantum information quantities. In particular, it may be used to introduce two new measures for information shared by different subsystems, the *mutual information* (see e.g. [27–29]) and its generalization, the *conditional mutual information* (see e.g. [28]). We require the concept of conditional mutual information in Chapter 5 in order to provide a physical interpretation for the volume form of kinematic space. Therefore, we review (conditional) mutual information here.

Mutual Information

Given two subsystems A, B of a quantum system, the mutual information between these two systems is given by

$$I(A : B) = S(A) + S(B) - S(AB). \tag{3.15}$$

---

[3]In [157] a proof of the Araki-Lieb inequality in the context of AdS/CFT was presented.
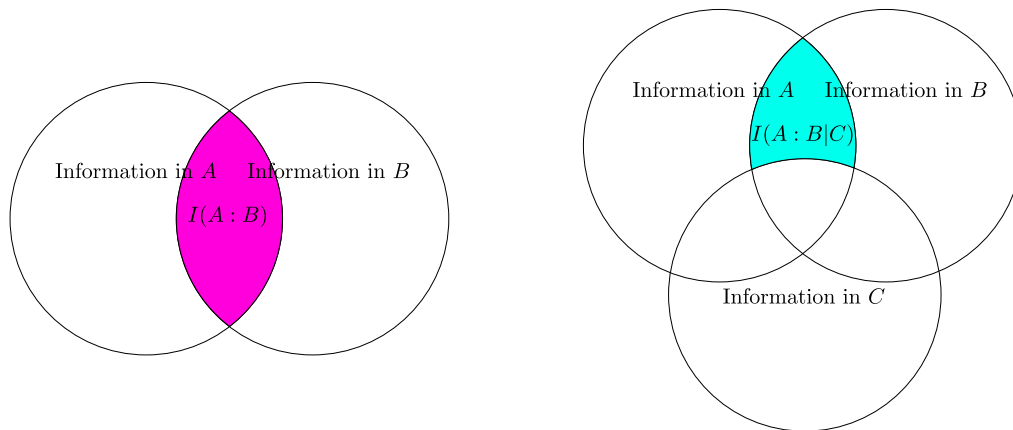
Figure 3.1: Interpretation of (conditional) mutual information. On the l.h.s. we depict the interpretation of mutual information (3.15). Given two subsystems A, B, $I(A : B)$ is a measure for the information that is stored in both A and B. For the conditional mutual information (3.18) we introduce an additional subsystem C. $I(A : B|C)$ gives the amount of information that is contained in both A and B, but not in C (r.h.s.).

Due to the subadditivity of the entanglement entropy (3.13), the mutual information is non-negative,

$$I(A : B) \geq 0 \,. \tag{3.16}$$

The mutual information may be interpreted as the ammount of information shared by A and B or the correlations between A and B (see e.g. [27, 28]). This can be motivated as follows. In Section 3.1.1 we established that entanglement entropy $S(A)$ quantifies the information contained in A. We may identify two classes of information contained in A: information that is contained in A and not in B and information that is contained in A and B. In an analogous way we find that $S(B)$ describes the information contained exclusively in B and the information contained in A and B. Moreover, $S(AB)$ gives the information contained exclusively in A and B, respectively and the information contained in both A and B. Applying this interpretation of $S(A)$, $S(B)$ and $S(AB)$ as sums of amounts of information, it is easy to see that (3.15) gives the information contained in A and B. We present a visualization of this interpretation in Figure 3.1.

Evidently, the information shared by A and B corresponds to correlations between the two subsystems. As a consistency check of this interpretation, we note that the mutual information of a state of the form $\rho^A \otimes \rho^B$ vanishes. Since there are no correlations between A and B in such a state, this agrees with the interpretation of $I(A : B)$ as measure for correlations.

Furthermore, we note that for a pure state $I(A : B)$ is given by

$$I(A : B) = S(A) + S(B) = 2S(A) \,, \tag{3.17}$$

as can be easily seen by applying the properties of entanglement entropy presented in Section 3.1.2. For pure states the correlations between A and B come from entanglement. Therefore, the fact that $I(A : B)$ essentially reduces to entanglement

entropy for pure states provides further support for the interpretation of $I(A:B)$ as measure for correlations between A and B.

Conditional Mutual Information

The mutual information quantifies the information shared by two subsystems A and B. It can be straightforwardly generalized to the conditional mutual information,

$$I(A:B|C) = S(AC) + S(BC) - S(ABC) - S(C) \,, \tag{3.18}$$

where C is a further subsystem. In particular, we find

$$I(A:B|C = \emptyset) = I(A:B) \,. \tag{3.19}$$

Moreover, the strong subadditivity of entanglement entropy (3.12) implies $I(A:B|C)$ to be non-negative,

$$I(A:B|C) \geq 0 \,. \tag{3.20}$$

Conditional mutual information is a measure for the information shared by A and B but not C (see e.g. [28]).[4] We visualize this in Figure 3.1. The motivation for this interpretation of (3.18) works in an analogous way as the motivation of the interpretation of mutual information presented below (3.15). In particular, the conditional mutual information quantifies the correlations between A and B that are not related to correlations with C. In order to justify this statement, we compute the conditional mutual information for the following example. We consider A and B to split into two parts A_1, A_2 and B_1, B_2, respectively, i.e. the Hilbert space for ABC is of the form

$$\begin{aligned} \mathcal{H}_{ABC} &= \mathcal{H}_A \otimes \mathcal{H}_B \otimes \mathcal{H}_C \,, \\ \text{where} \quad \mathcal{H}_A &= \mathcal{H}_{A_1} \otimes \mathcal{H}_{A_2} \,, \quad \mathcal{H}_B = \mathcal{H}_{B_1} \otimes \mathcal{H}_{B_2} \,. \end{aligned} \tag{3.21}$$

The state on ABC we work with in this example is given by

$$\rho^{ABC} = \rho^{A_1 B_1} \otimes \rho^{A_2 B_2 C} \,, \quad \text{with} \quad \rho^{A_2 B_2 C} = \sum_i p_i \left| i_{A_2} i_{B_2} i_C \right\rangle \left\langle i_{A_2} i_{B_2} i_C \right| \,. \tag{3.22}$$

Here we choose the states $\left| i_{A_2, B_2, C} \right\rangle$ to be orthonormal in $\mathcal{H}_{A_2, B_2, C}$, respectively and set $p_i > 0$ with $\sum_i p_i = 1$. The state ρ^{ABC} is constructed in such a way that the correlations between A and B are separated into two parts: correlations between A_1 and B_1, which are independent of C, and correlations between A_2 and B_2. The latter are inseparable from correlations with C. This is easy to be seen by

$$S(A_2 B_2 C) = S(A_2 B_2) = S(A_2 C) = S(B_2 C) = S(A_2) = S(B_2) = S(C) \,, \tag{3.23}$$

i.e. the entanglement entropy of all subsystems of $A_2 B_2 C$ is the same. By interpreting entanglement entropy as the amount of information contained in a subsystem

---

[4]We note that this interpretation of conditional mutual information is based on classical considerations. An operational interpretation for quantum systems is given in [160].
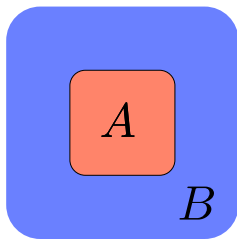
Figure 3.2: A constant time slice for a quantum field theory. We split the constant time slice into two entangling regions A and B. The entanglement entropy $S(A)$ is the von Neumann entropy of the reduced density matrix ρ^A, which encodes the expectation values of observables located in A.

(see Section 3.1.1), we see that all subsystems contain the same amount of information. Consequently, there are no correlations between A_2 and B_2 that are independent from correlations with C.

So we see that the only correlations between A and B that are not related to correlations with C come from A_1 and B_1. If the interpretation of conditional mutual information as measure for these correlations is correct, we should find

$$I(A : B|C) = I(A_1 : B_1) , \tag{3.24}$$

since the mutual information $I(A_1 : B_1)$ (3.15) measures the correlations between A_1 and B_1. By applying (3.23) to (3.18) we can indeed verify (3.24) and thus justify the interpretation of conditional mutual information presented above.

3.1.4 Entanglement Entropy for Quantum Field Theories

For systems Σ consisting of a discrete set of subsystems $A_1, \ldots, A_n$, i.e. for Hilbert spaces of the form

$$\mathcal{H}_\Sigma = \mathcal{H}_{A_1} \otimes \cdots \otimes \mathcal{H}_{A_n} , \tag{3.25}$$

the definition of the entanglement entropy (3.6) is easily applied to any subsystem $A = A_{i_1} \cdots A_{i_k}$. The state of interest is traced over the complement $A^c = B$ to obtain the reduced density matrix ρ^A which allows to compute $S(A)$ via (3.6). However, for continuous systems, such as quantum field theories, the computation of entanglement entropies is in general very involved and was performed only in a few cases (see e.g. [161]).[5] In quantum field theories the subsystems A and B are identified with complementary regions on a constant time slice of the space-time the field theory is defined on (see Figure 3.2). These regions are referred to as *entangling regions*. This approach may be interpreted as a continuum limit of the discrete setup.

The most straightforward approach for calculating entanglement entropies for field theories is to discretize the system by putting it on a lattice and send the lattice spacing to zero after directly computing the entanglement entropy via (3.6).

---

[5]Reviews for entanglement entropy in quantum field theories are [162–164].

For instance, this strategy has been pursued in [165] to determine the entanglement entropy of the ground state of a massless scalar field for a region outside a sphere.

A further method for determining entanglement entropies which is particularly successful for CFTs is the so-called *replica trick* [161, 162, 166]. Here an n-sheeted Riemann surface is used to compute

$$\text{tr}_A\left(\left(\rho^A\right)^n\right) \tag{3.26}$$

for the quantum theory on the lattice. The result is then analytically continued to complex n, which allows to determine $S(A)$ via

$$S(A) = -\lim_{n \to 1} \frac{\partial}{\partial n} \text{tr}_A\left(\left(\rho^A\right)^n\right). \tag{3.27}$$

For reviews regarding the replica trick we refer to [33, 163, 164]. In field theories the entanglement is in general UV divergent but expected to contain universal terms, i.e. terms that are independent of the chosen UV cut-off scheme. To clarify this statement, we consider the entanglement entropy regarding the vacuum state of a quantum field theory with d spatial dimensions. $S(A)$ is assumed to be of the form [164]

$$S(A) = \frac{g_{d-1}(\partial A)}{\epsilon^{d-1}} + \cdots + \frac{g_1(\partial A)}{\epsilon} + g_0(\partial A)\log(\epsilon) + S_0(A), \tag{3.28}$$

where ϵ is the UV cut-off. The term $S_0(A)$ is finite in the UV and the $g_i(\partial A)$ are extensive functions on the boundary ∂A. The coefficient g_0 in front of the logarithmical divergent term is considered to be universal. A simple motivation for this is the fact that g_0 does not change under rescalings of the UV cut-off $\epsilon \longrightarrow a\epsilon$, i.e.

$$\begin{aligned} S(A) \longrightarrow &\frac{g_{d-1}(\partial A)/a^{d-1}}{\epsilon^{d-1}} + \cdots + \frac{g_1(\partial A)/a}{\epsilon} + g_0(\partial A)\log(\epsilon) \\ &+ g_0(\partial A)\log(a) + S_0(A). \end{aligned} \tag{3.29}$$

Moreover, (3.29) shows that the g_i for $i > 0$ are not universal.

3.1.5   Entanglement Entropy for Gauge Theories

In gauge theories the definition of entanglement entropy is somewhat ambiguous due to the fact that a factorization of the form (3.1) of the Hilbert space of physical states $\mathcal{H}_\Sigma$ is not possible. We justify this subtlety following the arguments made in [167]. Gauge theories come with constraints the physical states have to satisfy. For instance, in quantum electrodynamics physical states have to obey Gauss' law

$$\nabla \cdot E = 0. \tag{3.30}$$

By splitting $\mathcal{H}_\Sigma$ into two parts for A and B we generate two subsystems separated by a boundary. However, the boundary electrical field on the A side may not be chosen independently from the boundary electrical field on the B side. They have
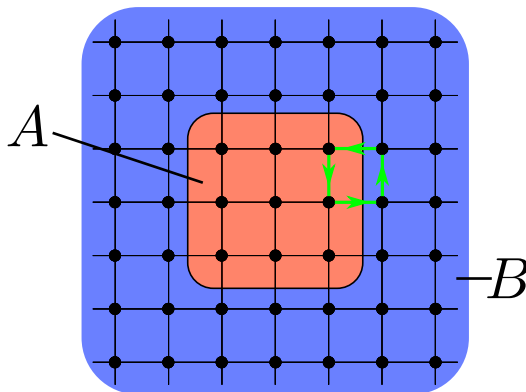
Figure 3.3: Issues with the definition of entanglement entropy in lattice gauge theories. In order to compute the entanglement entropy in a gauge theory, the system is discretized to a gauge theory on a lattice. The gauge field is not associated with the lattice sites but with the edges. Physical excitations of the gauge field correspond to loops on the lattice (green). When introducing the subregions A and B, the loops crossing the boundary between A and B are separated into a part lying in A and a part lying in B. Neither of them is gauge invariant. Only their combination has this property. This argument shows that it is not possible to find a factorization of the form $\mathcal{H}_A \otimes \mathcal{H}_B$ of the Hilbert space of physical states.

to be chosen in such a way that Gauss' law holds on the boundary. Thus, the degrees of freedom in A and B are not completely independent from each other, as required for a factorization of the form (3.1) for $\mathcal{H}_\Sigma$.

The issues caused by the introduction of two composite regions A and B may also be seen when considering the lattice gauge approach. As we depict in Figure 3.3, the gauge field is defined on the edges of the lattice, not on the lattice sites as it is the case for other fields (see Section 3.1.4). Physical excitations of the gauge field are not associated with its value on single edges but with closed loops of the edges. The boundary between A and B cuts the edges linking these two regions. Thus, loops crossing the boundary are split into two parts, one lying in A and one lying in B. Taken separately these two parts are not invariant under gauge transformations. Only together they are gauge invariant.

Without a factorization (3.1) of $\mathcal{H}_\Sigma$, it is not clear how to expand the concept of entanglement entropy to gauge theories. This is a topic of current research for which no unique solution was found so far. In the following we present the approach pursued in [167–169].[6] For an alternative approach, see e.g. [170].

In the lattice gauge approach, the Hilbert space $\mathcal{H}_\Sigma$ of physical states is given by the states satisfying the constraints imposed by the gauge group. It is considered to be a subspace of the space $\mathcal{H}_A \otimes \mathcal{H}_B$ including gauge dependent, unphysical states,

$$\mathcal{H}_\Sigma \subset \mathcal{H}_A \otimes \mathcal{H}_B \, . \tag{3.31}$$

---

[6]For the setup considered in [167], this procedure leads to the same result as the replica trick.
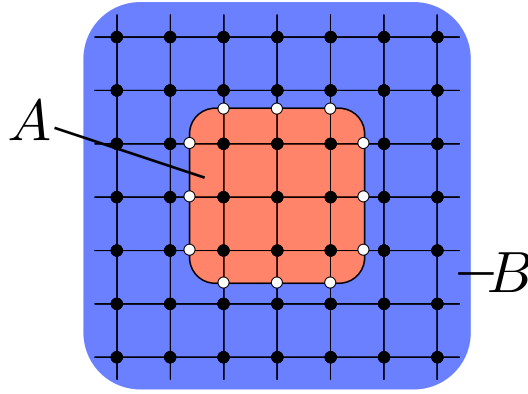
Figure 3.4: Introducing additional degrees of freedom. The Hilbert space of physical states is embedded into a space of the form $\mathcal{H}_A \otimes \mathcal{H}_B$ that also contains states that are not invariant under gauge transformations. The edges crossing the boundary between the regions A and B are cut into two pieces, one belonging to A and one belonging to B. On the boundary, where they meet, new degrees of freedom are introduced (white). These correspond to surface charges located at the boundary between A and B.

For $\mathcal{H}_A \otimes \mathcal{H}_B$ it is known how to define entanglement entropy (see Section 3.1.1, 3.1.4). The edges crossing the boundary between A and B are split into two parts, one belonging to A and one belonging to B. At the boundary, where these two parts meet, new degrees of freedom are introduced. These may be interpreted as surface charges attached to the boundary. This setup is depicted in Figure 3.4.

The entanglement entropy of physical states is defined to be the entanglement entropy of the states when interpreted as elements of the expanded Hilbert space described above.

3.1.6   The Ryu-Takayanagi Formula

Even though it is possible to formally define entanglement entropy for gauge theories, its calculation for explicit examples is mathematically very challenging. However, in $\mathrm{AdS}_{d+1}/\mathrm{CFT}_d$ the entanglement entropy of a CFT state with a classical gravitational dual has a very elegant and easy to calculate representation in the bulk. We restrict ourselves to static bulk geometries in this thesis. For a generalization of the bulk representation of entanglement entropy to a broader variety of geometries, we refer to [84]. A review of entanglement entropy in AdS/CFT can be found in [33].

The Gravity Dual of Entanglement Entropy

For an entangling region A on a constant time slice of the CFT side, Ryu and Takayanagi proposed that in the large N limit the entanglement entropy of a state
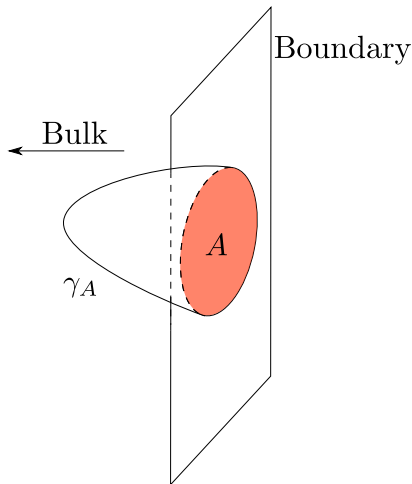
Figure 3.5: A Ryu-Takayanagi (RT) surface. For a given entangling region A of the CFT defined on the conformal boundary the RT formula (3.32) states that the entanglement entropy $S(A)$ is given by the area of the minimal $(d-1)$-dimensional bulk surface γ_A that is attached to the boundary of A and is homologous to A. This surface is referred to as RT surface. Due to the hyperbolic structure of the bulk geometry, γ_A stretches into the bulk.

with classical and static gravitational dual is given by [82, 171]

$$S(A) = \frac{\text{area}(\gamma_A)}{4G_{d+1}} \,, \tag{3.32}$$

which is known as the *Ryu-Takayanagi (RT) formula*. Here G_{d+1} is Newton's constant for the bulk (i.e. Newton's constant in $d+1$ dimensions for AdS_{d+1}) and γ_A is the static minimal $(d-1)$-dimensional bulk surface attached to the boundary ∂A and homologous to A. Note that we see A as part of the conformal boundary in this construction. The surface γ_A is referred to as *Ryu-Takayanagi (RT) surface*. We depict a typical example for a RT surface in Figure 3.5.

We emphasize that the RT formula is proposed to hold in the large N limit. For finite N bulk quantum effects will lead to $1/N$ corrections to (3.32) (see e.g. [172]). In this thesis we restrict our discussions to the large N limit, where these corrections are suppressed.

The RT formula states that the computation of entanglement entropies, which is very challenging on the field theory side, reduces to determining the area of a minimal surface on the gravity side. Being a proposal which has been confirmed for several examples [82] at first, the RT formula was later verified in [86, 173] by extending the replica trick for the boundary to the bulk. We note that the RT formula implies additional properties for entanglement entropy which do not hold for generic quantum systems. As an example, we mention the monogamy of mutual information [85]. Moreover, we refer to [157] for various implications of the RT formula.

Since the RT surface is a bulk surface that stretches out to the conformal boundary of the considered asymptotic AdS space, its area is divergent. This di-
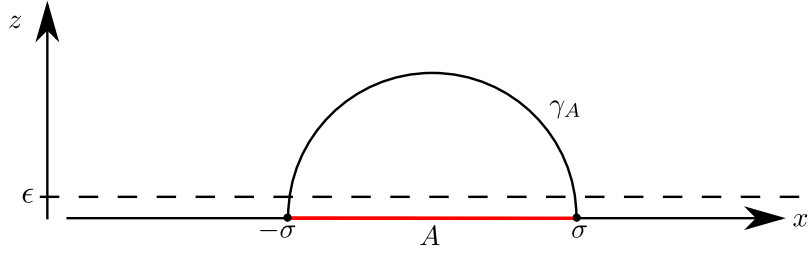
Figure 3.6: A constant time slice of the $(2+1)$-dimensional Poincaré patch (3.33). We consider the vacuum state of a CFT_2 defined on the real axis with the Poincaré patch as gravity dual. For an entangling interval $A = [-\sigma, \sigma]$ on the conformal boundary of the geometry, the RT surface γ_A is the geodesic connecting the two endpoints of A. This geodesic lies in the same constant time slice as A. The entanglement entropy of A is given by area(γ_A) (3.32), i.e. the length of γ_A. Since this length is divergent we introduce a radial cut-off at $z = \epsilon$. The resulting entanglement entropy is given by (3.39).

vergence requires the introduction of a radial cut-off which is identified with the UV cut-off of the entanglement entropy on the field theory side.

We note that in most of the examples studied in this thesis we consider $d = 2$, i.e. $\mathrm{AdS}_3/\mathrm{CFT}_2$. Here the RT surface has dimension one and is therefore not an actual surface but a curve. Nevertheless, we refer to this curve as RT "surface" and to its length as "area" in order to maintain a consistent notation throughout this thesis.

A Simple Example: Entangling Intervals for the Poincaré Patch

As a simple example to show how the RT formula (3.32) is applied, we consider the vacuum state of a CFT defined on the real axis in $\mathrm{AdS}_3/\mathrm{CFT}_2$. The dual geometry is the Poincaré patch (2.61),

$$ds_{\mathrm{PP}}^2 = \frac{L^2}{z^2}\left(-dt^2 + dx^2 + dz^2\right) \tag{3.33}$$

in $2 + 1$ dimensions. The conformal boundary, on which the CFT is defined, is located at $z = 0$. As entangling region A we consider the interval $[-\sigma, \sigma]$ – where $\sigma > 0$ – on a constant time slice $t = const.$ on the conformal boundary. Since the bulk is $(2+1)$-dimensional, the RT surface γ_A is simply the geodesic connecting the two endpoints of the boundary interval A. We depict this setup in Figure 3.6.

The following computation of $S(A)$ via (3.32) is taken from [82]. For symmetry reasons we assume γ_A to lie in the same constant time slice as A. We choose a parametrization of the form

$$\gamma_A(s) = \left(t = const., x = -\sigma\cos(s), z(s)\right), \quad \text{where} \quad s \in [0, \pi], \tag{3.34}$$

for the RT surface. The area of γ_A, i.e. the length of the geodesic (3.34), is given by

$$\text{area}(\gamma_A) = L \int_0^\pi ds \frac{\sqrt{(z')^2 + \sigma^2 \sin^2(s)}}{z}, \tag{3.35}$$

where the $'$ refers to a derivative w.r.t. s. This integral is minimized by the solution of the Euler-Lagrange equation

$$\frac{d}{ds}\left(\frac{z'}{z\sqrt{(z')^2 + \sigma^2 \sin^2(s)}}\right) + \frac{\sqrt{(z')^2 + \sigma^2 \sin^2(s)}}{z^2} = 0. \tag{3.36}$$

It is easy to verify that

$$z(s) = \sigma \sin(s) \tag{3.37}$$

is the solution of (3.36) that starts and ends on the conformal boundary, i.e. satisfies $z(0) = z(\pi) = 0$. Since the length of γ_A is divergent we need to introduce a radial cut-off $z = \epsilon$ (see Figure 3.6). We obtain

$$\text{area}(\gamma_A) = L \int_\varepsilon^{\pi-\varepsilon} ds \frac{1}{\sin(s)} = 2\log\big(\cot(\varepsilon/2)\big) = 2\log\left(\frac{2\sigma}{\epsilon}\right) + \mathcal{O}(\epsilon^2), \tag{3.38}$$

where $\varepsilon = \arcsin(\epsilon/\sigma)$ is the value of s where $\gamma_A(s)$ approaches the radial cut-off at $z = \epsilon$. By inserting (3.38) into the RT formula (3.32) and applying $c = 3L/2G_3$ (2.117), we find

$$S(A) = \frac{c}{3}\log\left(\frac{2\sigma}{\epsilon}\right), \tag{3.39}$$

which is the well known formula for the entanglement entropy of an entangling interval in CFT$_2$ [174].

3.1.7 Phase Transitions of the Ryu-Takayanagi Surface

In many cases there are several competing candidates for RT surfaces with different topologies. Which one is realized depends on the scales of the entangling region A. By changing these it is possible for the minimality condition to cause a phase transition of the RT surface γ_A from one candidate to another (see e.g. [83, 114, 115, 175, 176]). This transition was studied from the field theory side in e.g. [177, 178].

Two Entangling Intervals for the Poincaré Patch

To see this for a concrete example, we consider the entangling region A to be the union of two entangling intervals (see e.g. [176]),

$$A = A^1 A^2, \tag{3.40}$$

where $A^1 = [-a, -\sigma]$ and $A^2 = [\sigma, a]$ for $0 < \sigma < a$, for a CFT defined on the real axis. The dual geometry is the Poincaré patch (3.33). The interval between A^1 and A^2 is denoted by B, i.e. $B = [-\sigma, \sigma]$. There are two candidates for γ_A which we depict in Figure 3.7, $\gamma_{AB} \cup \gamma_B$ and $\gamma_{A^1} \cup \gamma_{A^2}$. Both these candidates are homologous to A. The RT surface γ_A is the surface with the minimal area.
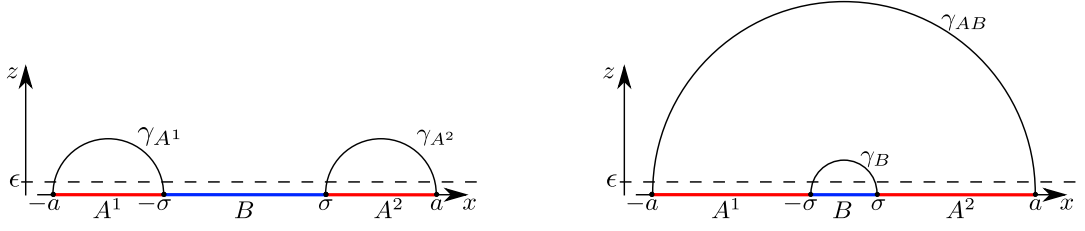
Figure 3.7: The two competing candidates for RT surfaces of two intervals $A^1 A^2$. We consider the vacuum state of a two-dimensional CFT on the real axis with the Poincaré patch (3.33) as gravity dual. For an entangling interval $A = A^1 A^2$ consisting of two intervals $A^1 = [-a, -\sigma]$ and $A^2 = [a, \sigma]$ there are two competing candidates for the RT surface γ_A: $\gamma_{A^1} \cup \gamma_{A^2}$ and $\gamma_{AB} \cup \gamma_B$, where $B = [-\sigma, \sigma]$ is the interval between A^1 and A^2. Both these candidates are homologous to A; the surface with the minimal area is γ_A. For σ sufficiently large we find $\gamma_A = \gamma_{A^1} \cup \gamma_{A^2}$ whereas for σ sufficiently small $\gamma_A = \gamma_{AB} \cup \gamma_B$ holds. So we see that γ_A undergoes a phase transition when σ decreases.

Therefore, the entanglement entropy is given by

$$S(A) = \frac{1}{4G_3} \min\{\text{area}(\gamma_{AB} \cup \gamma_B), \text{area}(\gamma_{A^1} \cup \gamma_{A^2})\}, \qquad (3.41)$$

via the RT formula (3.32). Which one of the surfaces $\gamma_{A^1} \cup \gamma_{A^2}$ and $\gamma_{AB} \cup \gamma_B$ has the minimal area changes with the value of σ as we now show. By using the formula (3.39) for the entanglement entropy of one interval, we find

$$\text{area}(\gamma_{AB} \cup \gamma_B) = \frac{c}{3} \log\left(\frac{2a}{\epsilon}\right) + \frac{c}{3} \log\left(\frac{2\sigma}{\epsilon}\right) \qquad (3.42)$$

and

$$\text{area}(\gamma_{A^1} \cup \gamma_{A^2}) = 2\frac{c}{3} \log\left(\frac{a - \sigma}{\epsilon}\right). \qquad (3.43)$$

By examining the behavior of

$$\text{area}(\gamma_{AB} \cup \gamma_B) - \text{area}(\gamma_{A^1} \cup \gamma_{A^2}) = \frac{c}{3} \log\left(\frac{4s}{(1 - s)^2}\right) \qquad (3.44)$$

in w.r.t. $s = \sigma/a$, it is easy to verify that

$$\text{area}(\gamma_{AB} \cup \gamma_B) < \text{area}(\gamma_{A^1} \cup \gamma_{A^2}) \quad \text{for} \quad \sigma < (3 - 2\sqrt{2})a \qquad (3.45)$$

and

$$\text{area}(\gamma_{AB} \cup \gamma_B) > \text{area}(\gamma_{A^1} \cup \gamma_{A^2}) \quad \text{for} \quad \sigma > (3 - 2\sqrt{2})a \qquad (3.46)$$

hold. Consequently, γ_A undergoes a phase transition when σ becomes smaller than $(3 - 2\sqrt{2})a$, i.e. it changes from $\gamma_{A^1} \cup \gamma_{A^2}$ to $\gamma_{AB} \cup \gamma_B$. The corresponding entanglement entropy is thus given by

$$S(A) = \begin{cases} \frac{c}{3} \log\left(\frac{2a}{\epsilon}\right) + \frac{c}{3} \log\left(\frac{2\sigma}{\epsilon}\right) & \text{for} \quad \sigma < (3 - 2\sqrt{2})a, \\ 2\frac{c}{3} \log\left(\frac{a - \sigma}{\epsilon}\right) & \text{else} \end{cases}, \qquad (3.47)$$

BTZ Black Hole   Conical Defect
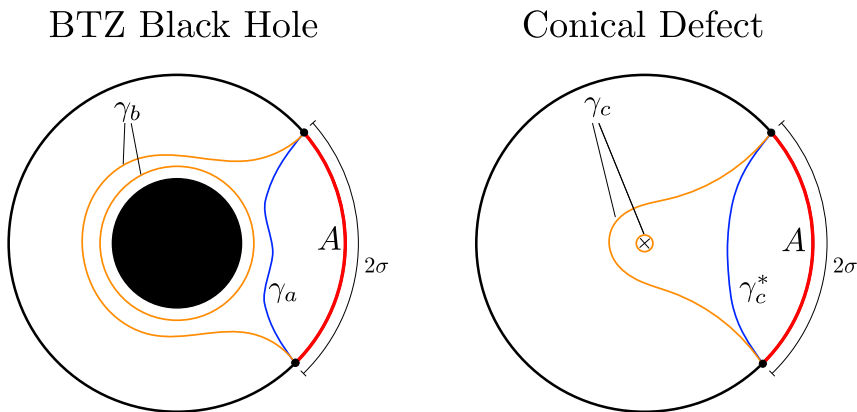
Figure 3.8: Two candidates for the RT surface of an interval in BTZ black hole (2.148) and conical defect (2.152) geometry. Given an entangling interval A (red) on the boundary of a constant time slice of a BTZ black hole (l.h.s.), there are two competing candidates for the RT surface γ_A. One is the geodesic γ_a (blue) lying on the same side of the black hole as A connecting the two endpoints of A. The other is the union γ_b (orange) of the black hole horizon and the geodesic lying on the other side of the black hole and connecting the endpoints of A. Which one of γ_a and γ_b is the RT surface of A depends on the angular size 2σ of A. We make an analogous observation for the conical defect (r.h.s.). Here one of the two competing candidates for γ_A is given by the geodesic γ_c^* (blue) lying on the same side of the conical defect as A and connecting the endpoints of A. The other γ_c (orange) is the union of the geodesic lying on the opposite side of the defect connecting the endpoints of A and an infinitesimal circle surrounding the defect. If $2\sigma \leq \pi$, we have $\gamma_A = \gamma_c^*$ and $\gamma_A = \gamma_c$ otherwise.

where we have used (3.42) and (3.43). We note that $S(A)$, written as in (3.47) and interpreted as a function of σ, has an non-analytic point at $\sigma = (3 - 2\sqrt{2})a$. This non-analyticity is a large N effect: The RT formula (3.32) only applies in the limit of large N. For finite N, $S(A)$ will become smooth at $\sigma = (3 - 2\sqrt{2})a$.

One Entangling Interval for the BTZ Black Hole

As a further example for a phase transition in the RT surface, we consider one entangling interval for a thermal CFT_2 state of inverse temperature β dual to the BTZ black hole (2.148). [7] This example is of particular importance for the Chapters 4, 5 and 6. Given an entangling interval A of angular size 2σ, there are two candidates for the RT surface γ_A (see Figure 3.8): the geodesic γ_a connecting the two endpoints of A which lies on the same side of the BTZ black hole as A and the union of the respective geodesic lying on the opposite side of the black hole and the black hole horizon, γ_b [175]. Note that it is necessary to include the black hole horizon in γ_b to ensure that it is homologous to A.

For sufficiently small angular size 2σ of A, the RT surface is given by γ_a, which

---

[7]The phase transition of the RT surface in this setup was discussed e.g. in [83, 114, 115, 175].
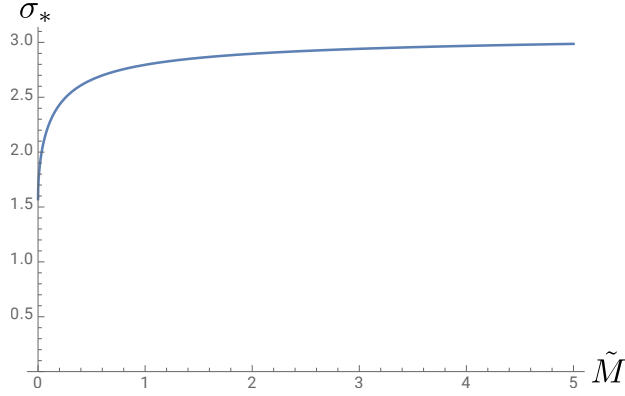
Figure 3.9: The transition angle σ_* (3.50) in terms of $\tilde{M} = 8G_3 M$. Here M is the mass of the black hole. It is easy to verify that σ_* grows monotonically with $\tilde{M}$ and $\pi/2 \leq \sigma_* \leq \pi$ holds. For a given entangling interval A with angular size 2σ, the corresponding RT surface is given by γ_a if $\sigma < \sigma_*$ and γ_b if $\sigma > \sigma_*$ (see Figure 3.8).

leads to the entanglement entropy [82]

$$S(A) = \frac{c}{3} \log\left(\frac{\beta}{\pi\epsilon} \sinh\left(\frac{2\pi\ell_{CFT}\sigma}{\beta}\right)\right), \tag{3.48}$$

via the RT formula (3.32). Here, ℓ_{CFT} is the radius of the circle the CFT is defined on and ϵ is a UV cut-off. However, if A is very large, the length of γ_b turns out to be smaller than the length of γ_a, i.e. γ_A undergoes a phase transition from γ_a to γ_b. After that transition, the entanglement entropy is given by [175]

$$S(A) = \frac{c}{3}\frac{2\pi^2\ell_{CFT}}{\beta} + \frac{c}{3} \log\left(\frac{\beta}{\pi\epsilon} \sinh\left(\frac{2\pi\ell_{CFT}(\pi - \sigma)}{\beta}\right)\right). \tag{3.49}$$

The first term in (3.49) corresponds to the circumference of the horizon, whereas the second is associated with the length of γ_a for the complement of A (see Figure 3.8).

The transition of the RT surface takes place for the $\sigma = \sigma_*$ where γ_a and γ_b have equal length. Applying the RT formula (3.32), we find that for $\sigma = \sigma_*$ (3.48) and (3.49) are equal. This leads to [114]

$$\sigma_* = \frac{\beta}{4\pi\ell_{\text{CFT}}} \log\left(\frac{\exp\left(4\pi^2\ell_{\text{CFT}}/\beta\right) + 1}{2}\right). \tag{3.50}$$

It is easy to verify that $\sigma_* \geq \pi/2$ holds. Therefore, the transition from γ_a to γ_b may only occur for A with angular size $2\sigma > \pi$. In preparation for our discussion of topological complexity in Chapter 4 we plot σ_* in terms of $\tilde{M} = 8G_3 M$ in Figure 3.9, where M is the mass of the black hole (2.149), (2.151).

One Entangling Interval for the Conical Defect

We conclude our discussion of phase transitions of the RT surface by presenting a further example for such a transition occurring for an entangling interval A of

a state dual to a conical defect geometry (2.152). Similar to the case of the BTZ black hole discussed above, the RT surface of A undergoes a phase transition if the angular size 2σ of A is sufficiently large (see e.g. [146]). Again we have two competing candidates for RT surfaces. One is the geodesic γ_c^* connecting the two endpoints of A which lies on the same side of the conical singularity as A. The other γ_c is the union of an infinitesimally small circle surrounding the conical singularity and the geodesic lying on the opposite side of the singularity, connecting the two endpoints of A. We depict γ_c^* and γ_c in Figure 3.8.

Note that the infinitesimal circle in γ_c does not contribute to the length of γ_c and may therefore be ignored when computing the entanglement entropy of A. However, it is necessary to make γ_c homologous to A and in particular plays a crucial role for topological complexity, as we discuss in Section 4.2.2.

Due to the symmetry of the setup, it is evident that γ_c^* is the minimal geodesic if A has angular size $2\sigma \leq \pi$ and γ_c is minimal otherwise. Therefore, the entanglement entropy of A is given by the length of γ_c^* via the RT formula (3.32) (see e.g. [146]),

$$S(A) = \frac{c}{3} \log \left(\frac{2\hat{N}\ell_{\mathrm{CFT}}}{\epsilon} \sin(\sigma/\hat{N}) \right), \tag{3.51}$$

if $2\sigma \leq \pi$. For $2\sigma \geq \pi$, the entanglement entropy is given by the length of γ_c,

$$S(A) = \frac{c}{3} \log \left(\frac{2\hat{N}\ell_{\mathrm{CFT}}}{\epsilon} \sin \left((\pi - \sigma)/\hat{N} \right) \right). \tag{3.52}$$

3.2 Complexity

Complexity (see e.g. [37]) is a quantity that was originally introduced in computer science to determine the minimal number of operations required to perform a given task. For instance, such a task could be to transform a set of n bits from an initial state, such as $(0, 0, \ldots, 0)$, to another configuration, e.g. $(1, 1, 1, 0, 0, 0, 1, 0, \ldots)$. For performing this task we are only allowed to apply certain fundamental operations to the initial state. These allowed operations are referred to as *gates*. Complexity is the minimal number of gates that are necessary to transform $(0, 0, \ldots, 0)$ into $(1, 1, 1, 0, 0, 0, 1, 0, \ldots)$.

This concept of mapping an initial configuration to a target configuration can be formulated for quantum systems as well.[8] Here the task is to map a reference state $|\psi_r\rangle$ to a target state $|\psi_t\rangle$ by applying unitary operators to $|\psi_r\rangle$. The unitary operators that are allowed to be applied are the (unitary) gates.

3.2.1 Complexity for Q-Bits

We now review the concept of complexity for a system consisting of a chain of n q-bits.[9] In this setup complexity is best understood – which is why we use it here to introduce the basic idea of the concept. As we show in the following,

---

[8]For a review of complexity for quantum systems we refer to [38].

[9]The following introduction to the concept of complexity for q-bits is motivated by [27], [38] and [179].

complexity essentially requires three ingredients: a set of gates, a reference state and a tolerance. The complexity of a given target state is the minimal number of gates required to transform the reference state into the target state, up to the tolerance.

Complexity for Pure States

First we focus on the complexity for a pure target state $|\psi_t\rangle$. For a set of n q-bits the reference state is usually taken to be

$$|\psi_r\rangle = |00 \cdots 0\rangle \ . \tag{3.53}$$

This reference state is very simple in the sense that it does not have any correlations between the q-bits. To be more precise, no subset of q-bits is entangled with the rest of the system as $|\psi_r\rangle$ is a product state.

In preparation of our analysis of holographic subregion complexity in Section 5.5 we now discuss the implications of this choice for $|\psi_r\rangle$. If we choose a target state with a lot of correlations between the q-bits, the gates transforming $|\psi_r\rangle$ into $|\psi_t\rangle$ necessarily have to build up all these correlations. Consequently, the choice of a product state as $|\psi_r\rangle$ implies that the correlations between subsystems of $|\psi_t\rangle$ play an important role for complexity. However, we need to stress that the correlations between subsystems is not the only thing complexity captures, as there are also product states to be expected that require many gates to generate, i.e. have a high complexity.

One possible choice for the set of unitary gates consists of the following four fundamental operations which act on one and two q-bits of the chain of n q-bits, respectively.

Hadamard Gate. This gate acts on a single q-bit of the n q-bit chain and is given by the matrix

$$\mathrm{H} = \frac{1}{\sqrt{2}} \begin{pmatrix} 1 & 1 \\ 1 & -1 \end{pmatrix} \ , \tag{3.54}$$

where we use the standard column vector representation of $|0\rangle$ and $|1\rangle$, i.e.

$$|0\rangle = \begin{pmatrix} 1 \\ 0 \end{pmatrix} \ , \quad |1\rangle = \begin{pmatrix} 0 \\ 1 \end{pmatrix} \ . \tag{3.55}$$

In particular, we find that H maps $|0\rangle$ to $|+\rangle = (|0\rangle + |1\rangle)/\sqrt{2}$ and $|1\rangle$ to $|-\rangle = (|0\rangle - |1\rangle)/\sqrt{2}$.

Phase Gate. As the Hadamard gate, the Phase gate S acts on a single q-bit. It introduces a relative complex phase between the $|0\rangle$ and $|1\rangle$ part of the q-bit,

$$\mathrm{S} = \begin{pmatrix} 1 & 0 \\ 0 & i \end{pmatrix} \ , \tag{3.56}$$

where we again use (3.55).

$\pi/8$ **Gate.** Also the $\pi/8$ gate T acts on a single q-bit. As the phase gate, it introduces a relative complex phase between $|0\rangle$ and $|1\rangle$,

$$T = \begin{pmatrix} 1 & 0 \\ 0 & e^{i\pi/4} \end{pmatrix} . \tag{3.57}$$

Controlled-NOT **Gate.** Unlike the Hadamard, Phase and $\pi/8$ gate, the controlled-NOT gate CNOT acts on two q-bits of the chain of n q-bits,

$$\text{CNOT} = \begin{pmatrix} 1 & 0 & 0 & 0 \\ 0 & 1 & 0 & 0 \\ 0 & 0 & 0 & 1 \\ 0 & 0 & 1 & 0 \end{pmatrix} , \tag{3.58}$$

where we use

$$\sum_{i,j=0}^{1} a_{ij} |ij\rangle = \begin{pmatrix} a_{00} \\ a_{01} \\ a_{10} \\ a_{11} \end{pmatrix} . \tag{3.59}$$

The gates H, S, T, CNOT may be applied to any q-bits of the considered chain of n q-bits. As an example we consider the target state

$$|\psi_t\rangle = \frac{1}{\sqrt{2}} \big(|000\ldots0\rangle + |110\ldots0\rangle \big) . \tag{3.60}$$

In order to transform $|\psi_r\rangle$ into $|\psi_t\rangle$ we need to apply the Hadamard gate to the first q-bit and the CNOT gate to the first two q-bits:

$$\begin{aligned} |00\ldots0\rangle \longmapsto & \big(\text{CNOT} \otimes \mathbb{1}_{n-2} \big) \big(\text{H} \otimes \mathbb{1}_{n-1} \big) |00\ldots0\rangle \\ = & \frac{1}{\sqrt{2}} \big(|000\ldots0\rangle + |110\ldots0\rangle \big) . \end{aligned} \tag{3.61}$$

This application of gates is visualized in Figure 3.10.

The set of gates $\{\text{H}, \text{S}, \text{T}, \text{CNOT}\}$ is universal, which means that it is possible to approximate any target state arbitrarily well by applying these gates to the reference state.[10] This universality is a necessary condition a set of gates is required to have. Otherwise, there would be states that cannot be reached from the target state by applying the gates and thus complexity could not be defined for these states.

It is not possible to map $|\psi_r\rangle$ to any target state by applying only a finite number of gates. This is evident since the number of states that can be generated by acting with a finite number of gates on $|\psi_r\rangle$ is countable but the number of

---

[10]A proof for this can be found [27].
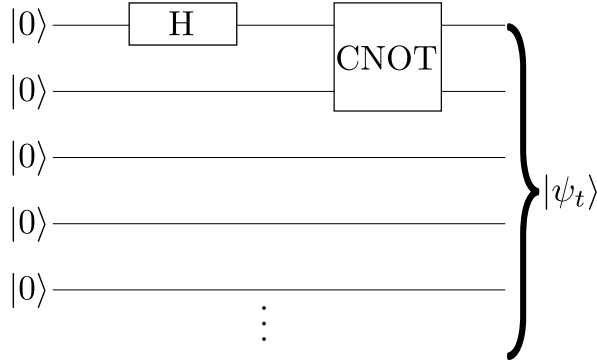
Figure 3.10: Hadamard and CNOT gate applied to the reference state $|\psi_r\rangle = |00\cdots 0\rangle$. When applying the Hadamard (3.54) and CNOT (3.58) gate to the first two q-bits as depicted above, we obtain the target state $|\psi_t\rangle$ given in (3.60).

all states is of course uncountable. It is only possible to approximate any state arbitrarily well with a finite set of gates. So in order to define the complexity of a state $|\psi_t\rangle$ as the minimal number of gates that need to be applied to $|\psi_r\rangle$, a tolerance $\tilde{\epsilon}$ is required. To be more precise, we define the complexity $\mathcal{C}_{\tilde{\epsilon}}(|\psi_t\rangle)$ as the minimal number of gates that need to be applied to $|\psi_r\rangle$ in order to generate a state $|\psi_t^{\tilde{\epsilon}}\rangle$ sufficiently close to $|\psi_t\rangle$ in trace norm, i.e.

$$|| \, |\psi_t\rangle \langle\psi_t| - \left|\psi_t^{\tilde{\epsilon}}\right\rangle \left\langle\psi_t^{\tilde{\epsilon}}\right| \, ||_{\mathrm{tr}} \le \tilde{\epsilon} \,. \tag{3.62}$$

This number of gates is finite.[11] So we see that the definition of complexity for q-bits requires three ingredients: the reference state $|\psi_r\rangle$, a set of universal unitary gates, e.g. $\{\mathrm{H}, \mathrm{S}, \mathrm{T}, \mathrm{CNOT}\}$, and a tolerance $\tilde{\epsilon}$. In (3.62) we have defined the tolerance to refer to the trace-norm-induced distance between the target state $|\psi_t\rangle$ and the state generated by the gates. In principle other concepts of tolerance, such as the difference between expectation values of certain operators, are possible, as pointed out in [179].

Complexity for Mixed States

So far we have only considered the complexity for pure states. It is a non-trivial problem to generalize this concept to mixed states. This is due to the fact that it is not possible to generate any mixed state from the reference state $|\psi_r\rangle$ (3.53) by applying unitary gates to it.[12] In [179] several generalizations of complexity to mixed states were discussed, which we now review.

---

[11] We note that in the definition of complexity via (3.62) additional ancilla q-bits may be considered (see e.g. [38]). In our discussion of complexity for mixed states (see below) we discuss this concept in more detail.

[12] We note that there exist formulations of complexity that involve non-unitary gates that resolve this issue [180]. However, in this thesis we only consider unitary gates.

Purification Complexity. This generalization of complexity to mixed states adds additional q-bits to the chain of n q-bits. These additional q-bits are referred to as ancilla q-bits. The reference state of the resulting extended Hilbert space is

$$|\Psi_r\rangle = |\psi_r\rangle \otimes |00\cdots 0\rangle_{ancilla} \,, \tag{3.63}$$

i.e. the ancilla q-bits are all set to $|0\rangle$, just as the q-bits in $|\psi_r\rangle$. The number of ancilla q-bits is kept arbitrary. The purification complexity $\mathcal{C}_P$ of a mixed state ρ_t on the n q-bits of interest is defined as the minimal number of gates required to transform $|\Psi_r\rangle$ – up to a tolerance – into a purification $|\Psi_t\rangle$ of ρ_t for some number of ancilla q-bits. To ensure that this concept of complexity reduces to the complexity for pure states discussed above if ρ_t is pure, the gates are only allowed to act on ancilla q-bits if these are entangled with the n q-bits in $|\Psi_t\rangle$. Note that the purification $|\Psi_t\rangle$ of a target state $|\psi_t\rangle$ that is already pure is always of the form

$$|\Psi_t\rangle = |\psi_t\rangle \otimes |\phi\rangle_{ancilla} \,, \tag{3.64}$$

where $|\phi\rangle_{ancilla}$ is some state on the ancilla q-bits. States like this obviously describe no entanglement between the n q-bits and the ancilla q-bits. Therefore the restriction stated above ensures that only the original n q-bits are allowed to be used when applying the gates to the reference state. Consequently, we recover the concept of pure state complexity discussed above if ρ_t is pure.[13]

Spectrum and Basis Complexity. The concepts of spectrum and basis complexity are results of the so-called *spectrum approach* [179]. This approach pursues the idea to separate the effort it takes to generate a state with the same spectrum $\tilde{\rho}_t$ as the target state ρ_t from the effort to transform the basis of eigenstates of $\tilde{\rho}_t$ into the one of ρ_t. We consider the same setup as for purification complexity: We add an arbitrary amount of ancilla q-bits to the system of n q-bits. The spectrum complexity $\mathcal{C}_S$ is defined to be the minimal number of gates that are required to transform the reference state $|\Psi_r\rangle$ – up to tolerance – into a purification of a state $\tilde{\rho}_t$ with the same spectrum as ρ_t. Analogous to the definition of purification complexity, the gates may only act on the ancilla q-bits if they are entangled with the n q-bits in the purification of $\tilde{\rho}_t$. It is easy to see that the spectrum complexity is in general smaller than the purification complexity, i.e.

$$\mathcal{C}_S \leq \mathcal{C}_P \,, \tag{3.65}$$

as the purifications of ρ_t considered for $\mathcal{C}_P$ are included in the set of purifications of all states with the same spectrum as ρ_t, which is required for $\mathcal{C}_S$. The spectrum complexity may be interpreted as the effort it takes to generate the spectrum of ρ_t.

Having generated a state $\tilde{\rho}_t$ with the correct spectrum, we now need to transform the eigenvectors of $\tilde{\rho}_t$ into the corresponding ones of ρ_t in order to map $\tilde{\rho}_t$ to

---

[13]We note that the original formulation of purification complexity in [179] slightly differs from the one we present here. In this paper the gates are also allowed to act on the ancilla if these are entangled with the n q-bits in the approximation of $|\Psi_t\rangle$ they generate. This may cause the purification complexity of pure states to differ from the pure state complexity discussed above. I brought this subtlety to the attention of the authors of [179].

ρ_t. The effort it takes to perform this task is referred to as basis complexity. The easiest way to define this quantity is via

$$\mathcal{C}_B = \mathcal{C}_P - \mathcal{C}_S \,. \tag{3.66}$$

The inequality (3.65) guaranties that $\mathcal{C}_B$ is always non-negative. We note that this definition of basis complexity suggests that the purification complexity splits into two independent pieces: the effort it takes to generate the spectrum of ρ_t ($\mathcal{C}_S$) and the effort to generate the correct basis ($\mathcal{C}_B$),

$$\mathcal{C}_P = \mathcal{C}_S + \mathcal{C}_B \,. \tag{3.67}$$

Whether these two tasks may really be considered to be independent from each other in $\mathcal{C}_P$ is not clear, as already pointed out in [179].

An alternative definition $\tilde{\mathcal{C}}_B$ of basis complexity is the number of unitary gates that need to be applied to $\tilde{\rho}_t$ in order to transform it into ρ_t – up to tolerance. Since $\tilde{\rho}_t$ has per definicionem the same spectrum as ρ_t, there exists a unitary transformation that maps $\tilde{\rho}_t$ to ρ_t. Thus this procedure is well defined.

It is easy to see that both $\mathcal{C}_B$ and $\tilde{\mathcal{C}}_B$ are equal to $\mathcal{C}_P$ if ρ_t is pure. Moreover, $\mathcal{C}_S$ is zero for pure ρ_t, since the reference state $|\psi_r\rangle \langle\psi_r|$ has the same spectrum as a pure target state $|\psi_t\rangle \langle\psi_t|$. So we see that the spectrum approach to complexity reduces to the pure state complexity discussed above for pure target states. In the spectrum approach we see that new ingredient for the complexity of mixed states is the effort it takes to generate the spectrum.

The concepts of complexity for mixed states are particularly interesting in view of the complexity of reduced states, the so-called *subregion complexity*. If we consider a pure entangled state of a system Σ consisting of two subsystems A, B, the results of Section 3.1 imply that the reduced state on A is mixed. So, a concept of complexity that measures the effort it takes to generate the reduced state on A necessarily needs to be applicable to mixed states. Here it is important to mention that the purification, spectrum and basis complexity do not take into account if a state is reduced, i.e. part of a bigger system. It is not clear whether a concept of complexity for reduced states should ignore this property.[14] In particular, in my discussion about holographic subregion complexity in Section 5.5, I argue that there is evidence for the bulk quantity, which is suggested to be related to the complexity of reduced CFT states, to take the fact that the state is part of a larger system into account.

3.2.2   Complexity for Quantum Field Theories

For a quantum system that is described by a finite dimensional Hilbert space – such as q-bits – the concept of complexity is easily defined (see Section 3.2.1). However, for a system on an infinite dimensional Hilbert space, such as quantum field theories, it is a highly non-trivial task to introduce a notion of complexity. According to [48] there are four main challenges that need to be addressed for a

---

[14]This has already been pointed out in [179].

definition of complexity in field theories:

Choice of the Reference State. In order to follow the motivation for complexity as a measure for the correlations of a state (see Section 3.2.1), we require the reference state to be the field theory analogue of a product state in position space, i.e. there should be no spatial correlations present in the reference state, as it was the case for q-bits (3.53). For generic quantum field theories there is no clear or natural choice for such a state. We emphasize that the vacuum state is in general highly entangled as can be seen from the entanglement entropy (3.39) for a CFT_2 vacuum state, for instance. Thus the vacuum state is not a good choice for the reference state.

Set of Gates. It is not clear at all how to choose a suitable set of unitary gates for field theories. A discrete set of gates – as in the case of q-bits – is not expected to be able to generate all possible states. Approaches for field theory complexities usually consider a continuum of gates (see e.g. [48, 49]).

Measure for Gates. In the q-bit system discussed in Section 3.2.1 complexity simply counted the number of gates required to map the reference state $|\psi_r\rangle$ to the target state $|\psi_t\rangle$. For field theories we expect the number of gates required to approximate a generic $|\psi_t\rangle$ to be divergent. So we need to introduce a measure function to the set of gates and a concept of minimality for the gates. A very popular approach for this problem was given in [181, 182], where a Finsler metric was on the set of all unitary operators was considered.

UV Divergencies. In Section 3.1.4 we saw that the entanglement entropy is UV divergent in field theories. We expect a similar effect for complexity. So we require a concept of regulating these UV divergencies.

Even though the concept of complexity has been studied intensively for field theories in recent years and some progress has been made (see e.g. [48–51, 183]), a rigorous and formal definition for complexity in field theories is still subject of current research.

3.2.3 Complexity in AdS/CFT

The AdS/CFT correspondence allows us to approach complexity for field theories from a new perspective. Since a formal definition of complexity is not known in field theories, we may ask if it is possible to find a proper definition in the bulk. To be more precise, the aim of this approach is to introduce bulk quantities that appear to be good candidates for encoding a concept of complexity of the boundary state. This allows us to work with the complexity of the boundary state on the gravity side. We need to stress that – since a field theory formulation for complexity is not available – this method does not introduce a gravity dual of a known boundary quantity, as it is the case for the RT formula (see Section 3.1.6). It may rather be seen as a strategy for defining complexity via the bulk. The main
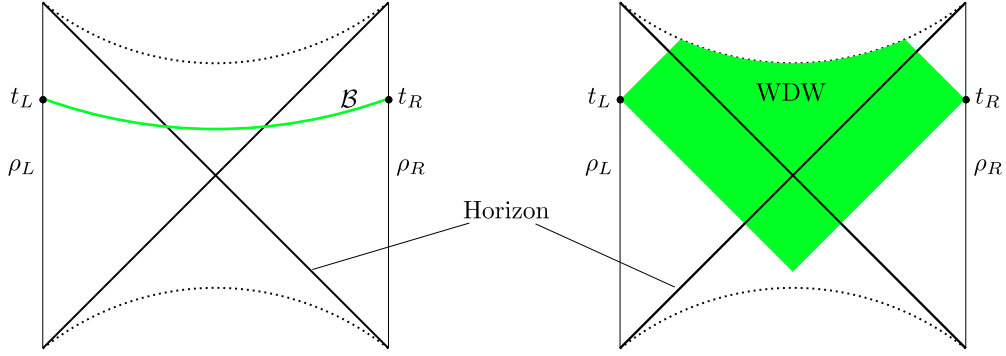
Figure 3.11: The Penrose diagram of the two sided eternal AdS black hole. (This graphic is inspired by a similar visualization in [49].) This geometry is dual to the thermofield double state (3.68) which describes two copies of the same CFT state on the asymptotic boundaries of the two sides of the black hole. We denote these two states by ρ_L and ρ_R. The two sides of the black hole are connected via an Einstein-Rosen bridge. There are two proposals for the bulk dual of the complexity of the boundary state. The CV conjecture (3.69) considers the maximal codimension one bulk surface $\mathcal{B}$ stretching from the left boundary at time t_L to the right at time t_R (l.h.s.). The complexity at times t_L, t_R is proposed to be given by the volume of $\mathcal{B}$. The CA conjecture (3.70) evaluates the gravitational action over the Wheeler-DeWitt (WDW) patch to compute complexity at times t_L, t_R. The WDW patch is defined as the union of all spatial slices connecting the conformal boundaries on the two sides of the black hole at times t_L, t_R (r.h.s.).

challenge in this approach is to test whether a given bulk quantity actually is a suitable bulk dual for complexity.

Complexity Equals Volume and Complexity Equals Action

Susskind was the first who pursued an holographic approach to complexity [56–59, 184, 185].[15] Together with his collaborators, he introduced two new bulk quantities – proposed to correspond to complexity – for the thermofield double state,

$$|TFD(t_L, t_R)\rangle = \frac{1}{\sqrt{Z_\beta}} \sum_i e^{-\beta E_i/2} e^{-iE_i(t_L + t_R)} |i\rangle_L |i\rangle_R \ . \qquad (3.68)$$

This state describes an entangled state between two copies of the same CFT at times t_L and t_R on the two copies. The holographic dual of $|TFD(t_L, t_R)\rangle$ is the two sided eternal AdS black hole [60, 61]. The two copies of the CFT defined on the asymptotic boundaries of the two sides of the black hole are connected by an Einstein-Rosen bridge. We depict this geometry in Figure 3.11. Susskind and his collaborators made the following two proposals for a bulk dual of complexity on the field theory side:

---

[15]We also mention [186] here for related work.

Complexity Equals Volume (CV). [57, 58] We consider the maximal codimension one bulk surface $\mathcal{B}$ connecting the constant time slices at t_L and t_R of the two CFT copies on the asymptotic boundaries of the two-sided black hole (see l.h.s. of Figure 3.11). The complexity = volume (CV) conjecture proposes the complexity of the boundary state to be proportional to the volume of $\mathcal{B}$,

$$\mathcal{C}_V = \frac{\text{vol}(\mathcal{B})}{G_{d+1}s} \,, \tag{3.69}$$

where s is a characteristic length scale in the bulk geometry, e.g. it may chosen to be the AdS radius or the radius of the black hole.

Complexity Equals Action (CA). [59, 187] Alternatively to CV, the complexity = action (CA) conjecture proposes complexity to be given by the gravitational action evaluated over the Wheeler-DeWitt patch,

$$\mathcal{C}_A = \frac{\mathcal{S}_{WDW}}{\pi \hbar} \,. \tag{3.70}$$

The Wheeler-DeWitt patch is given by the union of all spatial slices connecting the constant time slices at t_L and t_R on the conformal boundaries of the black hole (see r.h.s. of Figure 3.11).

The motivation for these two proposals for complexity goes as follows.[16] The boundary reaches thermal equilibrium very fast in time, i.e. in $t_L + t_R$, but both $\mathcal{C}_V$ and $\mathcal{C}_A$ keep growing in $t_L + t_R$ even after this thermalization [57, 59, 187]. So $\mathcal{C}_V$ and $\mathcal{C}_A$ capture aspects of the field theory state that continue to evolve after thermal equilibrium has been reached. These aspects were associated with complexity in [57] and [59]. Moreover, $\mathcal{C}_V$ and $\mathcal{C}_A$ turn out to grow linearly in $t_L + t_R$ for large $t_L + t_R$ [57, 59, 187]. This property is to be expected from complexity, as argued in [57, 58].

Holographic Subregion Complexity (HSRC)

Inspired by the CV proposal, Alishahiha introduced a bulk quantity known as *holographic subregion complexity (HSRC)* for reduced states on entangling regions A on the CFT side [63]. We only consider static bulk geometries, where the RT surface γ_A lies in the same constant time slice as A. A generalization of HSRC to non-static space-times can be found in [52]. For a given entangling region A on the CFT side, the HSRC for static bulk geometries is given by the volume of the codimension one bulk region $\mathcal{B}_A$ bounded by γ_A and A on the constant time slice [63],

$$\mathcal{C}_{\text{HSRC}}(A) = \frac{\text{vol}(\mathcal{B}_A)}{8\pi L G_{d+1}} \,, \tag{3.71}$$

where L is the *AdS* radius. We depict this construction in Figure 3.12. HSRC was studied in various papers, e.g. [53, 54, 188–191].

---

[16]This motivation is based on [49, 57].
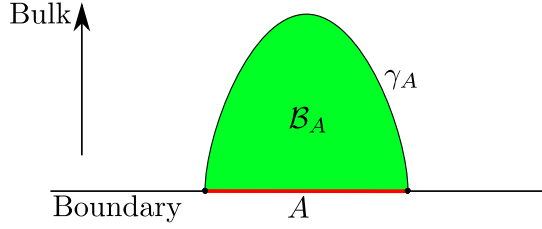
Figure 3.12: Alishahiha's proposal for holographic subregion complexity (HSRC) [63]. Given an entangling region A on a constant time slice, HSRC is given by the volume of the codimension one bulk region $\mathcal{B}_A$ on that time slice, bounded by A and the corresponding RT surface γ_A (3.71). Here A is interpreted as a region on the conformal boundary of the bulk.

One possible motivation for this proposal goes as follows [52]. The AdS/CFT correspondence implies that it is possible to reconstruct the whole bulk space-time from the dual CFT state on the conformal boundary of the considered geometry. This fact raises the question what bulk region is encoded in the reduced density matrix ρ^A corresponding to an entangling region A on the CFT side, i.e. which bulk region can be reconstructed from ρ^A? In [192, 193] it was argued that the bulk region associated with ρ^A is the so-called entanglement wedge $\mathcal{W}_A$.

Given an entangling region A and the corresponding RT surface γ_A, $\mathcal{W}_A$ is defined to be the domain of dependence of $\mathcal{B}_A$. So $\mathcal{W}_A$ is the set of all bulk points p for which any inextensible causal curve that passes through p necessarily intersects $\mathcal{B}_A$. We depict the typical form of $\mathcal{W}_A$ in Figure 3.13.

Following the above discussion, it is reasonable for the bulk dual of the subregion complexity of ρ^A to be related to $\mathcal{W}_A$. Combining this observation with the CV conjecture, which essentially states that complexity is related to volumes of codimension one bulk surfaces, motivates the proposal (3.71) for HSRC.

As a simple example we compute $\mathcal{C}_{\text{HSRC}}(A)$ for $A = [-\sigma, \sigma]$, where we consider a CFT$_2$ on the real axis with the Poincaré patch (3.33) as holographic dual.[17] As pointed out in Section 3.1.6, the RT surface for A is given by

$$\gamma_A = (t = const., x = -\sigma \cos(s), z = \sigma \sin(s)), \quad \text{where} \quad s \in [0, \pi]. \qquad (3.72)$$

Thus we find the volume of the bulk region $\mathcal{B}_A$ enclosed by A and γ_A to be given by

$$\text{vol}(\mathcal{B}_A) = \int_{-\sigma}^{\sigma} dx \int_{\epsilon}^{\sqrt{\sigma^2 - x^2}} dz \frac{L^2}{z^2} = \frac{2\sigma L^2}{\epsilon} - L^2 \pi, \qquad (3.73)$$

where we have introduced a cut-off at $z = \epsilon$, analogous to the computation of the entanglement entropy (3.38). We find

$$\mathcal{C}_{\text{HSRC}}(A) = \frac{c\sigma}{6\pi\epsilon} - \frac{c}{12}, \qquad (3.74)$$

---

[17]The HSRC for this setup was computed in [63].
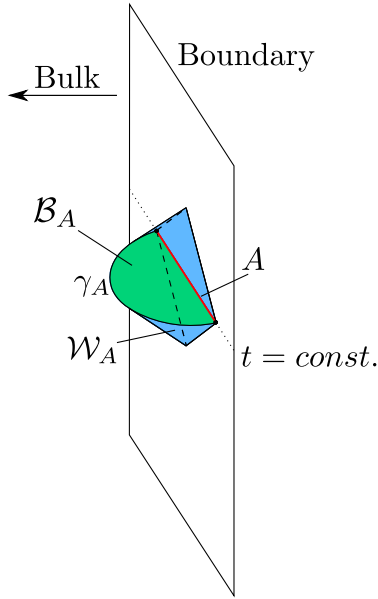
Figure 3.13: The entanglement wedge $\mathcal{W}_A$. For an entangling region A on a constant time slice of the conformal boundary of the bulk space-time, $\mathcal{W}_A$ (blue) is given by the domain of dependence of $\mathcal{B}_A$ (green). Here $\mathcal{B}_A$ is the codimension one bulk region lying in the same constant time slice as A and bounded by A and the corresponding RT surface γ_A. The domain of dependence of $\mathcal{B}_A$ is the set of all bulk points p for which any inextensible causal curve intersecting p passes through $\mathcal{B}_A$.

where we have applied $G_3 = 3L/2c$ in (3.71). In (3.74) we see that the second term, i.e. -c/12, does not change under rescalings of the cut-off. In [63] it was suggested that this term is universal, i.e. independent of the cut-off scheme.

3.3 Modular Hamiltonian

A further object in quantum information that we study in this thesis (see Chapter 6) is the *modular Hamiltonian* [73]. Given a subregion A on a constant time slice of a quantum field theory, the modular Hamiltonian $K(A)$ of a reduced state ρ^A on A is defined via

$$\rho^A = \frac{e^{-K(A)}}{\mathrm{tr}_A(e^{-K(A)})} \, . \tag{3.75}$$

The hermiticity and positive-definiteness of ρ^A imply that K is hermitian as well. The modular Hamiltonian is an important ingredient for quantum information measures such as the relative entropy,[18] which we introduce in Section 3.3.3). It has been studied intensively in recent years [41,64–72]. However, the explicit form of K is only known for a few cases, some of which we present in Section 3.3.2.

---

[18]see e.g. [31] for a review and [194–196] for work involving the relative entropy.

3.3.1   Aspects of Modular Hamiltonians

We begin our review of the modular Hamiltonian K (3.75) by presenting some properies of this object. The modular Hamiltonian has been studied in great detail and many non-trivial results have been obtained for it. For instance, in [197,198] a quantum version of the Bekenstein bound involving K has been derived. Moreover, in [66] the authors presented a method for determining the matrix elements of K for excited CFT states in terms of correlation functions. In [65, 194] bulk duals of the modular Hamiltonian were studied in the context of AdS/CFT.

Here we present two aspects of modular Hamiltonians we consider particularly interesting: a symmetry which is naturally induced by the modular Hamiltonian and a general statement about the form of modular Hamiltonians for two-dimensional CFTs.

A Symmetry Induced by the Modular Hamiltonian

The modular Hamiltonian provides a particular symmetry which leaves the expectation values of operators $\mathcal{O}$ located in the region A invariant.[19]   The transformation associated with this symmetry is induced by the one-parameter family of unitary operators

$$U_K(s) = \left(\rho^A\right)^{is} = e^{-isK}\,, \tag{3.76}$$

where $s \in \mathbb{R}$. Considering the definition of K (3.75), it is evident that the expectation value of an operator located in A does not change under U_K,

$$\mathrm{tr}\left(\rho^A \mathcal{O}(s)\right) = \mathrm{tr}\left(\rho^A \mathcal{O}\right), \tag{3.77}$$

where $\mathcal{O}(s) = U_K(s)\mathcal{O}U_K(-s)$. Moreover, we note that $U_K(s)$ maps the operator algebra of the domain of dependence $\mathfrak{D}_A$ of A into itself.[20] Therefore, the $U_K(s)$ form a one-parameter group of transformations for the operator algebra of $\mathfrak{D}_A$, the so-called *modular group* [73]. We need to emphasize that the modular flow, i.e. the flow generated by $U_K(s)$ on $\mathfrak{D}_A$, is usually not local. This is due to the fact that K is usually not a local operator. Only in a few cases K turns out to be local and therefore provides a local modular flow. We present some of these cases in Section 3.3.2.

Modular Hamiltonians for Two-Dimensional CFTs

In [200] a topological criterion for a local modular Hamiltonian in two-dimensional CFTs was introduced. In particular, when fulfilled, this criterion provides a modular Hamiltonian which is a local integral over the energy momentum tensor. The basic statement of [200] goes as follows. Consider a state in a two-dimensional CFT in Euclidean signature and an entangling region A on a constant time slice. Remove a small circle around every boundary point of A from the space-time region. If the resulting space-time $\mathfrak{M}$ is conformally equivalent to an annulus, then K is a local integral over the energy momentum tensor. In topological terms this means

---

[19]The following discussion of the symmetry is based on [199].
[20]The domain of dependence $\mathfrak{D}_A$ is defined analogously to $\mathcal{W}_A$ in Section 3.2.3.

that the prerequisites of the above statement are fulfilled if $\mathfrak{M}$ may be mapped to a sphere with two holes in such a way that A becomes a simple curve connecting these two holes.

In a couple of simple cases, the integral over the energy momentum tensor providing the modular Hamiltonian is given by

$$K(A) = \int_A dx \frac{2\pi}{f'(x)} T_{00}(x)\,. \tag{3.78}$$

Here $z \longmapsto w = f(z)$ is the conformal transformation that maps $\mathfrak{M}$ to an annulus in form of a rectangle with 2π periodic $Im(w)$. The term $f'(x)$ in (3.78) is the first derivative of the (real) restriction of $f(z)$ to the constant time slice. For instance, the expression (3.78) holds for a CFT defined on flat space, where the considered state is either thermal or the vacuum and A is a single interval. Moreover, (3.78) is also true for the vacuum and an interval A when the spatial direction is taken to be a circle. For more complicated configurations, such as quantum quenches, where K has a different form than (3.78), we refer to [200].

We emphasize that even though the result of [200] applies for the ground state of a CFT defined on a circle, it is not applicable to a thermal state on the circle. As already pointed out in [200], the space-time of such a state has the shape of a torus in Euclidean signature, since both the spatial and the time direction are periodic. Therefore, the resulting $\mathfrak{M}$ for an interval A is not conformally equivalent to an annulus and thus the prerequisites of the statement are not fulfilled. In the context of AdS/CFT, the BTZ black hole (see Section 2.5.2) is the gravity dual of such a thermal state on the circle. We discuss the modular Hamiltonian for this setup in more detail in Section 6.4.3.

3.3.2 Explicit Examples for Modular Hamiltonians

An explicit expression for the modular Hamiltonian was only derived in a few cases. Here we present two prominent examples. Further examples are given in Chapter 6 and [74–78].

Half Space in d Dimensions. Consider the ground state of a generic quantum field theory in d-dimensional Minkowski space $\mathbb{R}^{d-1,1}$. The modular Hamiltonian of the half-space

$$\mathscr{H} = \{x^i \in \mathbb{R}^{d-1} | x^1 > 0\} \tag{3.79}$$

of a constant time slice is given by the boost generator in x^1 direction [201, 202] (see also [115]),

$$K(\mathscr{H}) = 2\pi \int_{\mathscr{H}} d^{d-1}x\, x^1 T_{00}(x)\,. \tag{3.80}$$

We note that in [67] the behavior of the modular Hamiltonian under variations of the half space was studied.

Sphere in d Dimensions. For the vacuum of a CFT on d-dimensional Minkowski space the modular Hamiltonian for a ball shaped region B_R of radius

R on a constant time slice takes the form [199, 203]

$$K(B_R) = \int_{B_R} d^{d-1}x \frac{R^2 - r^2}{2R} T_{00}(x) \,, \tag{3.81}$$

where $r = \sum_{i=1}^{d-1} \left(x^i\right)^2$. The center of the ball is set to the origin. The expression (3.81) for $K(B_R)$ may be derived from the modular Hamiltonian (3.80) of half space (3.79) via a conformal transformation (see e.g. [199]).

3.3.3 Relative Entropy

Studying the modular Hamiltonian directly is in general a very challenging task. A very popular approach for obtaining results for the modular Hamiltonian is to work with quantities that are better understood and for which the modular Hamiltonian plays a non-trivial role. One such quantity is the *relative entropy*,[21] which has been studied extensively in the context of modular Hamiltonians [41, 67, 68, 115, 197, 198, 204].

Given two reduced states ρ_0^A, ρ_1^A on an entangling region A, the relative entropy of them is defined via

$$S_{rel}(A) = \text{tr}_A(\rho_1^A \log \rho_1^A) - \text{tr}_A(\rho_1^A \log \rho_0^A) = \Delta \langle K_0 \rangle (A) - \Delta S(A) \,, \tag{3.82}$$

where $K_0(A)$ is the modular Hamiltonian of ρ_0^A and

$$\Delta \langle K_0 \rangle (A) = \text{tr}_A(\rho_1^A K_0(A)) - \text{tr}_A(\rho_0^A K_0(A)) \,. \tag{3.83}$$

Moreover, $\Delta S(A)$ denotes the difference of the entanglement entropies of ρ_1^A and ρ_0^A. The second equality in (3.82) is an immediate consequence of the definition of the modular Hamiltonian (3.75). The presence of the modular Hamiltonian in (3.82) allows us to use S_{rel} as a tool to obtain non-trivial results for K_0. For instance, S_{rel} has been used to derive the first law of entanglement [115] (see Section 6.2) and a quantum version of the Beckenstein bound [197, 198] for K_0.

Relative Entropy in Terms of Surprise

The relative entropy allows us to compare the two states ρ_0^A and ρ_1^A with each other. To provide some intuition for the physical meaning of relative entropy, we review the interpretation of S_{rel} in terms of *surprise* as presented in [31]. For simplicity we restrict our discussion to the classical case, where the relative entropy of two discrete probability distributions $\{p_i\}_i$, $\{q_i\}_i$ is given by

$$S_{rel} = \sum_i p_i(\log(p_i) - \log(q_i)) \,. \tag{3.84}$$

Evidently, this corresponds to the quantum case, where both density matrices ρ_0^A and ρ_1^A are diagonal.

---

[21]For an introduction to the concept of relative entropy we refer to [31]. The mathematical rigorous definition of relative entropy for quantum field theories is reviewed e.g. in [34, 35].

The concept of surprise, mentioned above, pursues the idea of quantifying how unexpected a given event is. Consider an event that may happen with probability p. As pointed out in [31], the quantity $-\log(p)$ is a good measure for the amount of surprise the event would cause. We may use this concept of surprise for motivating relative entropy as follows. We consider a system which we mistakenly assume to come with a probability distribution $\{q_i\}_i$ whereas the actual probability distribution is $\{p_i\}_i$. The average amount of surprise we would obtain from a measurement is therefore given by

$$-\sum_i p_i \log(q_i)\,. \tag{3.85}$$

The relative entropy (3.84) thus is the difference between the average of surprise we experience due to our false assumption and the actual average of surprise,

$$-\sum_i p_i \log(p_i)\,, \tag{3.86}$$

provided by the correct probability distribution. So in a sense, S_{rel} measures how much our assumed probability distribution $\{q_i\}_i$ deviates from the actual probability distribution $\{p_i\}_i$ of the system. We note that this motivation of S_{rel} via the average of surprise can be made mathematically more concrete. For this we refer to e.g. [31, 98]. For quantum systems the above interpretation may be straightforwardly adopted: given an quantum system in a state ρ_1^A which is mistakenly assumed to be ρ_0^A, the relative entropy measures the deviation of ρ_0^A from ρ_1^A.

Properties of Relative Entropy

We conclude our introduction to relative entropy (3.82) by presenting two properties of S_{rel} which are of particular importance for our results presented in Chapter 6.

Non-Negativity. The relative entropy of two states ρ_0^A, ρ_1^A is non-negative [34],

$$S_{rel}(A) \geq 0\,. \tag{3.87}$$

In particular, $S_{rel}(A)$ is zero if and only if $\rho_0^A = \rho_1^A$.

Monotonicity. The relative entropy is monotonous, i.e.

$$S_{rel}(A) \leq S_{rel}(A')\,, \tag{3.88}$$

for two entangling regions A, A' with $A \subset A'$ [34, 205].

Chapter 4

Topological Complexity

In this chapter we present the results of [1], where my collaborators and I introduced the concept of *topological complexity* for AdS_3/CFT_2. This is a further proposal for a gravity dual of the subregion complexity corresponding to an entangling region A, next to Alishahiha's proposal [63] presented in Section 3.2.3. Alishahiha considers the subregion complexity of A for a CFT state with static gravitational dual to be proportional to the volume of the codimension one bulk region $\mathcal{B}_A$ enclosed by the boundary interval A and the corresponding RT surface γ_A (see Figure 3.12). This proposal – as Susskind's volume proposal (3.69) – requires to introduce the length scale L in (3.71) by hand in order for the complexity to be dimensionless. Our concept of topological complexity avoids this subtlety: for a CFT state with static gravitational dual we define the topological complexity of an entangling region A to be

$$\mathcal{C}_T(A) = -\frac{1}{2} \int_{\mathcal{B}_A} \mathcal{R}_{ct} d\mathfrak{a} \,, \tag{4.1}$$

where $\mathcal{R}_{ct}$ is the Ricci scalar of the induced metric on the constant time slice in the bulk and $d\mathfrak{a}$ is the corresponding area element. By construction, $\mathcal{C}_T$ is dimensionless and therefore no additional scale needs to be introduced. The prefactor $-1/2$ ensures the non-negativity of $\mathcal{C}_T$ as $\mathcal{R}_{ct}$ is negative for the examples considered here. As we show in the following section, the topology of $\mathcal{B}_A$ and A is of significant importance for $\mathcal{C}_T(A)$, which justifies the term "topological complexity". In particular, if the topology of $\mathcal{B}_A$ changes due to a phase transition in γ_A (see Section 3.1.7), we find that $\mathcal{C}_T$ changes by a discrete, finite jump.[1] Moreover, we see that our concept of complexity (4.1) allows us to interpret $\mathcal{R}_{ct}$ in a natural way as a *complexity density* in the bulk.

Note that we only consider geometries with constant $\mathcal{R}_{ct}$. In these cases, $\mathcal{C}_T(A)$ is obviously proportional to $\mathrm{vol}(\mathcal{B}_A)$ and thus agrees with Alishahiha's proposal (3.71) up to a multiplicative prefactor.[2] However, interpreting $\mathrm{vol}(\mathcal{B}_A)$ in the context of topological complexity reveals a clear relation between the terms in

---

[1]We refer to [188] for related work.

[2]We note that in [188] some of the examples we discuss in this chapter have been studied in the context of holographic subregion complexity. Since topological complexity and holographic subregion complexity differ only by a constant prefactor in these examples, the results we present in (4.11), (4.13), (4.21), (4.23) effectively have already been computed in [188]. However, the

Alishahiha's holographic subregion complexity and the topology of $\mathcal{B}_A$ and A, as we discuss below. Therefore, our topological approach to complexity provides new insight to the interpretation of the terms appearing in Alishahiha's formula (3.71). Moreover, our topological approach allows us to formulate a general expression for the complexity[3] of an arbitrary entangling region A for CFT_2 states with static gravity dual.

We present our results regarding topological complexity in the following way. In Section 4.1 we show how to express topological complexity in terms of the geodesic curvature and the Euler characteristic using the Gauss-Bonnet theorem. In particular, we show how this result may be used to determine the form of topological complexity for static asymptotic AdS_3 spaces. We apply the expression for topological complexity obtained in Section 4.1 to CFT_2 states dual to global AdS_3, BTZ black holes and conical defects in Section 4.2. In particular, we present an explicit expression for the topological complexity of an arbitrary entangling region for the CFT_2 vacuum state – which is dual to global AdS_3. Moreover, we show how the topological complexity changes with the mass of BTZ black holes and continue this analysis to conical defects by allowing the mass of the BTZ black hole to become negative (see Section 2.5.2). We conclude this chapter by discussing the obtained results in Section 4.3.

Note that [1] not only considers the study of topological complexity via the Gauss-Bonnet theorem. Also subregion complexity for tensor networks and a field theory expression for subregion complexity are discussed. The latter is presented in Chapter 5. Since I did not participate in the study of subregion complexity for tensor networks, I do not include it in this thesis.

4.1 Topological Complexity from the Gauss-Bonnet Theorem

The topological complexity (4.1) may be reformulated in terms of the geodesic curvature of $\partial\mathcal{B}_A$ and the Euler characteristic of $\mathcal{B}_A$ via the Gauss-Bonnet theorem. This observation allows us to conclude that for static asymptotic AdS_3 space-times many aspects of topological complexity are determined by the topology of the considered entangling region A and the topology of $\mathcal{B}_A$.

---

approach we present in the following sections provides a topological interpretation of the results. Moreover, we find that they all may be obtained from the same, general expression (4.10).

[3]The term complexity may refer to both our topological and Alishahiha's holographic subregion complexity as they only differ by a multiplicative prefactor in the examples we consider here.

4.1.1 Application of the Gauss-Bonnet Theorem to Topological Complexity

Using the Gauss-Bonnet theorem (see e.g. [103]), we find that the topological complexity (4.1) of an entangling region A can be rewritten as[4]

$$\mathcal{C}_T(A) = \int_{\partial \mathcal{B}_A} k_g ds - 2\pi \chi(\mathcal{B}_A) \,, \tag{4.2}$$

where $\chi(\mathcal{B}_A)$ is the Euler characteristic of $\mathcal{B}_A$, k_g the geodesic curvature (see e.g. [103]) of $\partial \mathcal{B}_A$ on the constant time slice and ds the corresponding line element.[5]

For a given curve γ, the geodesic curvature may be interpreted as a measure for the deviation of γ from a geodesic. In particular, k_g vanishes if γ is a geodesic. Moreover, if γ is only piecewise differentiable, the integral over k_g along γ includes angular contributions from the points where γ is not differentiable.

4.1.2 Topological Complexity for Asymptotic AdS$_3$

We now discuss topological complexity (4.2) for static asymptotic AdS$_3$ geometries. In particular, we focus on asymptotic AdS$_3$ geometries of the form

$$ds^2_{\text{AAdS}_3} = -f(\tilde{r})d\tilde{t}^2 + \frac{1}{f(\tilde{r})}d\tilde{r}^2 + \tilde{r}^2 d\phi^2 \,, \tag{4.3}$$

where $0 < \tilde{r}$, $\tilde{t} \in \mathbb{R}$, $\phi \sim \phi + 2\pi$ and f is a positive function with $f(\tilde{r}) \longrightarrow \tilde{r}^2/L^2$ for $\tilde{r} \longrightarrow \infty$. Considering (2.116), it is easy to see that such geometries in fact asymptote to AdS$_3$ for large $\tilde{r}$. For geometries of the form (4.3) we may use (4.2) to construct a general expression for the topological complexity of a generic entangling region, as we now show. We introduce a radial cut-off at

$$\tilde{r} = \tilde{r}_\epsilon = \frac{L\ell_{\text{CFT}}}{\epsilon} \,, \tag{4.4}$$

where ℓ_{CFT} is the radius of the circle the CFT is defined on. In order to determine the topological complexity for a given boundary region A, we replace the region $\mathcal{B}_A$ in (4.2) by the subset $\mathcal{B}_A^\epsilon$ lying above the cut-off (see Figure 4.1),

$$\mathcal{C}_T(A) = \int_{\partial \mathcal{B}_A^\epsilon} k_g ds - 2\pi \chi(\mathcal{B}_A) \,. \tag{4.5}$$

Here we assume ϵ to be sufficiently small for the topologies of $\mathcal{B}_A^\epsilon$ and $\mathcal{B}_A$ to agree. Note that RT surfaces for $(2+1)$-dimensional bulk geometries are mostly

---

[4]We note that the Gauss-Bonnet theorem was also used in [155] in the context of holographic subregion complexity. The authors applied it to hyperbolic polygons corresponding to the difference of the holographic subregion complexities of certain boundary intervals. Our formula (4.2) may be used to reproduce their findings as a special case.

[5]Note that the Gauss-Bonnet theorem is usually formulated in terms of the Gaussian curvature, not the Ricci scalar. However, in two dimensions the Ricci scalar is given by the Gaussian curvature times two (see e.g. [103]). This allows us to apply the Gauss-Bonnet theorem to (4.1) to obtain (4.2).
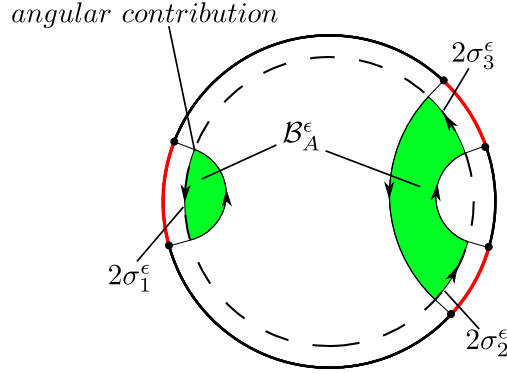
Figure 4.1: Visualization of the terms appearing in the expression (4.6) for topological complexity. We may compute topological complexity for an entangling region A (red) via the Gauss-Bonnet theorem. The resulting formula is (4.2). In order to obtain a finite result we need to introduce a cut-off $\tilde{r}_\epsilon$ (4.4) (dashed circle). The integral in (4.2) then goes in direction of the arrows along the boundary of the green region $\mathcal{B}_A^\epsilon$ enclosed by the cut-off and the RT surface γ_A. This region is by construction the part of $\mathcal{B}_A$ lying above the cut-off. Note that the angles between the RT surface and the cut-off contribute additively to the integral in (4.2). Evidently, there are as many angular contributions as endpoints of A. Since the RT surfaces are geodesics, they do not contribute to the integral over the geodesic curvature in (4.2). These considerations result in the formula (4.6) for topological complexity, where the total angular size $2\sigma_A^\epsilon$ is the sum of the angular sizes of all segments of $\partial\mathcal{B}_A^\epsilon$ on the cut-off (in the depicted example we have $2\sigma_A^\epsilon = 2(\sigma_1^\epsilon + \sigma_2^\epsilon + \sigma_3^\epsilon)$).

geodesics.[6] Consequently, they do not contribute to the integral over the geodesic curvature in (4.5). This allows us to conclude that in the integral over the geodesic curvature in (4.5) only the part of $\partial\mathcal{B}_A^\epsilon$ lying on the cut-off circle $\tilde{r} = \tilde{r}_\epsilon$ and the intersection angles between γ_A and this circle contribute. Consequently, we find the topological complexity of A to be given by

$$\mathcal{C}_T(A) = 2\sqrt{f(\tilde{r}_\epsilon)}\sigma_A^\epsilon - 2\pi\chi(\mathcal{B}_A) + angular\ contributions\,. \qquad (4.6)$$

Here $2\sigma_A^\epsilon$ is the total angular size of the part of $\partial\mathcal{B}_A^\epsilon$ on the cut-off and the *angular contributions* are given by the angles between the RT surface γ_A and the cut-off (see Figure 4.1). Moreover, we have used the fact that along the cut-off, i.e. the circle of radius $\tilde{r}_\epsilon$, the geodesic curvature is given by

$$k_g = \frac{\sqrt{f(\tilde{r}_\epsilon)}}{\tilde{r}_\epsilon}\,, \qquad (4.7)$$

which is easy to verify.

---

[6]We use the term "mostly" here since this statement is not correct for conical defects (2.152). These geometries have a naked singularity, which leads to RT surfaces that not only consist of geodesics. We discuss this situation in Section 4.2.2.

4.2 Examples for Topological Complexity

In this section we compute topological complexity for explicit examples. We consider the geometries of global AdS$_3$ (2.116), the BTZ black hole (2.148) and the conical defect (2.152). All these geometries can be written in the form (4.3), however only for global AdS$_3$ and the BTZ geometry may (4.6) be applied for the computation of topological complexity. The reason for that is the naked singularity of the conical defect geometry. As we discuss in Section 3.1.7, this causes the RT surface for sufficiently large entangling intervals to include an infinitesimally small circle around the singularity. This circle happens to be no geodesic. Since the derivation of (4.6) included the assumption that the RT surface is a geodesic, we conclude that it is not applicable for conical defects. We discuss topological complexity for conical defects in Section 4.2.2.

Before we present the explicit calculations, we simplify (4.6) for global AdS$_3$ and the BTZ black hole by sending ϵ to zero and only considering the constant and divergent part of $\mathcal{C}_T$. Since the remaining parts of $\mathcal{C}_T$ are of order ϵ, they may be neglected. We pursue as follows. It is easy to verify that $\sqrt{f(\tilde{r}_\epsilon)}$ behaves as

$$\sqrt{f(\tilde{r}_\epsilon)} = \frac{\ell_{\text{CFT}}}{\epsilon} + \mathcal{O}(\epsilon)\,, \tag{4.8}$$

for the considered geometries (see (2.116) and (2.148)). Moreover, the angles under which the RT surface intersects the cut-off at $\tilde{r} = \tilde{r}_\epsilon$ asymptote to $\pi/2$, as this is the angle under which geodesics asymptote to the conformal boundary in global AdS$_3$ (see e.g. [33]). Since the RT surface is attached to the endpoints of the entangling region A, there are as many angular contributions to $\mathcal{C}_T$ as endpoints of A (see Figure 4.1). By denoting the number of endpoints as n, we find

$$\mathcal{C}_T(A) = \frac{2\ell_{\text{CFT}}\sigma_A}{\epsilon} + \frac{\pi}{2}n - 2\pi\chi(\mathcal{B}_A) + \mathcal{O}(\epsilon)\,, \tag{4.9}$$

where σ_A is the total angular size of A. [7] We also note that an entangling region A for a $(1+1)$-dimensional CFT is always the disjoint union of a given number $q \in \mathbb{N}$ of intervals A_i, $i = 1, \ldots, q$. By setting the angular size of A_i to $2\sigma_i$, we conclude[8]

$$\mathcal{C}_T(A) = \frac{2\ell_{\text{CFT}}}{\epsilon}\sum_{i=1}^{q}\sigma_i + \frac{\pi}{2}n - 2\pi\chi(\mathcal{B}_A) + \mathcal{O}(\epsilon)\,. \tag{4.10}$$

Here we see that the constant – i.e. ϵ^0 – term of topological complexity is completely determined by topological quantities. This term is assumed to be universal (see Section 3.2.3). For any configuration of entangling intervals it is fixed by the total number of endpoints of the intervals and the Euler characteristic of $\mathcal{B}_A$.

---

[7]We note that in (4.9) we used $\sigma_A^\epsilon = \sigma_A + \mathcal{O}(\epsilon^2)$. Given the previously mentioned fact that γ_A approaches the conformal boundary under the angle $\pi/2$, this is easy to verify.

[8]We note that in [1] we have set $n = 2q$, since every interval A_i has two boundary points. However, this is not applicable to the case when A is the complete circle providing the constant time slice, since this may be seen as one interval with no boundary points.

4.2.1　Topological Complexity for Global AdS$_3$

We now apply our formula for topological complexity (4.10) to entangling regions for the CFT$_2$ vacuum state, which is dual to global AdS$_3$ (2.116). We particularly focus on the behavior of topological complexity under phase transitions of the RT surface (see Section 3.1.7). As we show below, these phase transitions lead to a finite jump in complexity which is caused only by the change of the topology of $\mathcal{B}_A$.

Topological Complexity for One Interval

As a first simple application of (4.10) we consider A to be a single interval of angular size $2\sigma_A$ in global AdS$_3$. The bulk region $\mathcal{B}_A$ is of the form depicted in Figure 3.12, which implies $\chi(\mathcal{B}_A) = 1$. Moreover, the number n of endpoints for one interval is two. Consequently, we find

$$\mathcal{C}_T = \frac{2\ell_{\text{CFT}}\sigma_A}{\epsilon} - \pi + \mathcal{O}(\epsilon)\,. \tag{4.11}$$

Furthermore, we may also consider the special case when the considered entangling region is the whole constant time slice, i.e. the circle of radius ℓ_{CFT}. In this situation, $\mathcal{C}_T$ may be computed analogously to the situation with one interval discussed above. However, since the considered entangling region does not have any endpoints, we need to set $n = 0$ in (4.10) which leads to

$$\mathcal{C}_T = \frac{2\pi\ell_{\text{CFT}}}{\epsilon} - 2\pi + \mathcal{O}(\epsilon)\,. \tag{4.12}$$

Topological Complexity for Two Intervals

For an entangling region A consisting of two intervals A_1 and A_2, we need to consider two different phases of the RT surface. As for the analogous setup in the Poincaré patch, discussed in Section 3.1.7 and depicted in Figure 3.7, the RT surface γ_A is given by $\gamma_{A_1} \cup \gamma_{A_2}$ if the distance between A_1 and A_2 is sufficiently large. We denote this phase of the RT surface as *Phase I*. Moreover, if A_1 and A_2 are close to each other, γ_A is given by $\gamma_{AB} \cup \gamma_B$, where B is the interval between A_1 and A_2. We refer to this phase as *Phase II*.

By denoting the angular size of A_i as $2\sigma_i$, $i = 1, 2$, we find via (4.10) that the topological complexity of two intervals is given by

$$\mathcal{C}_T(A_1 A_2) = \begin{cases} \frac{2\ell_{\text{CFT}}(\sigma_1 + \sigma_2)}{\epsilon} - 2\pi + \mathcal{O}(\epsilon) & \text{Phase I} \\ \frac{2\ell_{\text{CFT}}(\sigma_1 + \sigma_2)}{\epsilon} + \mathcal{O}(\epsilon) & \text{Phase II} \end{cases}\,. \tag{4.13}$$

Here we have used the fact that two intervals have $n = 4$ endpoints and the additivity of the Euler characteristic, which implies $\chi(\mathcal{B}_A) = 2$ in Phase I. Since the contributions of order ϵ may be ignored, we find that the complexity (4.13) changes by a discrete value of 2π at the transition from Phase I to Phase II. In particular, this jump only concerns the finite, i.e. ϵ^0 part of complexity, which is proposed to be universal (see Section 3.2.3).[9]

---

[9]We note that this jump has already been determined in [188] in the context of holographic subregion complexity.
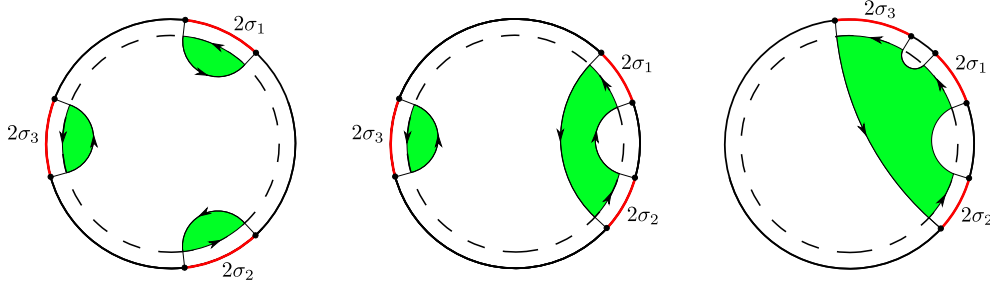
Figure 4.2: Different phases of the RT surface of several intervals. Given an entangling region A (red) being the union of q disjoint entangling intervals (here we visualize $q = 3$) of angular size $2\sigma_1, \ldots, 2\sigma_q$, we see that the RT surface γ_A has different phases, depending on the position of the entangling intervals relative to each other. When the RT surface changes its phase, the topology of the bulk region $\mathcal{B}_A$ enclosed by γ_A and A changes as well. This causes a discrete jump in the topological complexity $\mathcal{C}_T(A)$ (4.17) as the number $\mathcal{E}$ of disjoint pieces of $\mathcal{B}_A$ changes. We depict the part of $\mathcal{B}_A$ above the cut-off (dashed circle) in green.

Topological Complexity for an Arbitrary Number of Intervals

Our result for the topological complexity of two intervals (4.13) may be straight-forwardly generalized to an entangling region A consisting of an arbitrary number of intervals $A_1, \ldots A_q$, $q \in \mathbb{N}$. We denote the angular size of A_i by $2\sigma_i$. When we neglect the special case where the considered entangling region is the whole constant time slice (4.12), we find that the number of endpoints is the given by

$$n = 2q\,. \tag{4.14}$$

The RT surface of q intervals has several different phases depending on the position of the intervals relative to each other (see Figure 4.2). Depending on the phase, we find different values for the Euler characteristic $\chi(\mathcal{B}_A)$. The quantity determining $\chi(\mathcal{B}_A)$ is the number of disjoint regions $\mathcal{B}_A$ consists of: consider $\mathcal{B}_A$ to consist of $\mathcal{E}$ disjoint regions, each of which is assumed to be connected (see Figure 4.2). Then $\chi(\mathcal{B}_A)$ is given by the sum of all Euler characteristics of these regions. As we visualize in Figure 4.2, none of these regions has any holes for any configuration of entangling intervals. Consequently, their Euler characteristic is always one. Therefore, we find

$$\chi(\mathcal{B}_A) = \mathcal{E}\,. \tag{4.15}$$

In particular, we note

$$\chi(\mathcal{B}_A) \leq q\,, \tag{4.16}$$

which is an immediate consequence of the above discussion.

Inserting (4.14) and (4.15) into (4.10) we find

$$\mathcal{C}_T(A) = \frac{2\ell_{\mathrm{CFT}}}{\epsilon} \sum_{i=1}^{q} \sigma_i + \pi(q - 2\mathcal{E}) + \mathcal{O}(\epsilon)\,. \tag{4.17}$$

So we see that the different phases of γ_A correspond to different integer values of $\mathcal{E}$. Consequently, we find that at the transition point between two phases, the topological complexity jumps by a multiple of 2π.

4.2.2   Topological Complexity for BTZ Black Holes and Conical Defects

The behavior of the topological complexity of an arbitrary number of entangling intervals discussed above also applies for CFT states dual to BTZ black holes and conical defects. The results presented in Section 4.2.1 regarding the discrete jump of topological complexity when the RT surface undergoes a phase transition in global AdS$_3$ evidently may also be found for the geometries discussed here. In addition to these aspects of topological complexity, there is a further kind of phase transition for the RT surface that may occur here and is not present for global AdS$_3$: as discussed in Section 3.1.7 the RT surface for a single interval wraps around the black hole horizon (or conical defect) if the interval is sufficiently large. In this section we focus on this type of phase transition.

Topological Complexity for BTZ Black Holes

We now discuss the behavior of topological complexity under the phase transition of the RT surface mentioned above for thermal CFT states dual BTZ black holes. For this purpose we write the BTZ metric (2.148) in terms of the black hole mass (2.149)

$$M = \frac{\tilde{r}_h^2}{8G_3 L^2}\,,\tag{4.18}$$

which may be identified with the square of the temperature T on the field theory side via (2.151)

$$LM = \frac{\pi^2 \ell_{CFT}^2 c}{3}T^2\,,\tag{4.19}$$

where $c = 3L/2G_3$ (2.117) is the central charge of the CFT. Using the mass M, the BTZ metric (2.148) may be written as

$$ds_{\mathrm{BTZ}}^2 = -\Big(\frac{\tilde{r}^2}{L^2} - \tilde{M}\Big)d\tilde{t}^2 + \frac{1}{\frac{\tilde{r}^2}{L^2} - \tilde{M}}d\tilde{r}^2 + \tilde{r}^2 d\phi^2\,,\tag{4.20}$$

where $\tilde{M} = 8G_3 M$.

In order to discuss the behavior of topological complexity under the phase transition, we consider the following setup. We set the angular size of the boundary entangling interval A to a fixed value $2\sigma_A > \pi$ and vary $\tilde{M}$. Following the discussion in Section 3.1.7, we find that for sufficiently large $\tilde{M}$ the corresponding RT surface γ_A is given by the geodesic lying in the same constant time slice and on the same side of the black hole as A (see Figure 4.3). We refer to this type of RT surface as *Phase a*. The corresponding topological complexity is given by (4.10)

$$\mathcal{C}_T(A, \text{Phase a}) = \frac{2\ell_{\mathrm{CFT}}\sigma_A}{\epsilon} - \pi + \mathcal{O}(\epsilon)\,.\tag{4.21}$$
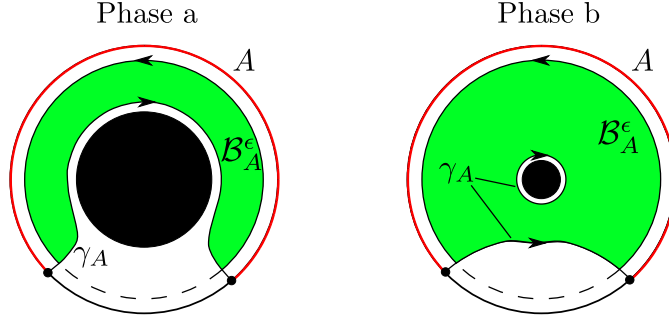
Figure 4.3: Change of topology in $\mathcal{B}_A$ for BTZ black holes. Consider an entangling interval A (red) with angular size larger than π for a state dual to a BTZ black hole. If the mass of the black hole is sufficiently large, the RT surface γ_A lies on the same side of the BTZ black hole as A (Phase a). The topology of $\mathcal{B}_A$ is then trivial (we depict the part $\mathcal{B}_A^\epsilon$ of $\mathcal{B}_A$ lying above the cut-off in green). If the mass of the black hole becomes too small, the RT surface undergoes a phase transition and then consists of the geodesic lying on the other side of the black hole and the black hole horizon (Phase b). In this situation, $\mathcal{B}_A$ has the topology of an annulus. Consequently, its Euler characteristic is zero. This change of the Euler characteristic leads to a discrete jump in topological complexity by 2π (4.21), (4.23).

By decreasing $\tilde{M}$, $\mathcal{C}_T$ does not change until the RT surface undergoes the phase transition turning it into the union of the black hole horizon and the geodesic connecting the two endpoints of A and lying on the other side of the black hole (see Figure 4.3). We refer to this kind of RT surface as *Phase b*. Evidently, the bulk region $\mathcal{B}_A$ enclosed by the RT surface and A now has a different topology than in Phase a: it surrounds the horizon and consequently has a hole, as depicted in Figure 4.3. Thus its Euler characteristic is given by

$$\chi(\mathcal{B}_A) = 0\,. \tag{4.22}$$

Therefore, the topological complexity in Phase b is given by (4.10) [10]

$$\mathcal{C}_T(A, \text{Phase b}) = \frac{2\ell_{\text{CFT}}\sigma_A}{\epsilon} + \pi + \mathcal{O}(\epsilon)\,. \tag{4.23}$$

So we see once more that the change of topological complexity at the point of the transition from Phase a to Phase b may be explained purely in topological terms: at the transition point the topology and therefore the Euler characteristic of $\mathcal{B}_A$ changes. This leads to a discrete jump by 2π in $\mathcal{C}_T$. [11]

We note that from the above analysis we find that topological complexity is mostly independent of the temperature of the thermal state dual to the BTZ black hole. [12] This is evident since the temperature is essentially given by $\tilde{M}$ (4.19) and

---

[10]For the sake of completeness we note that the black hole horizon – which is part of the boundary of $\mathcal{B}_A$, is a geodesic. Therefore its contribution to the integral over the geodesic curvature k_g in (4.2) vanishes. Consequently (4.10) may be applied in order to compute $\mathcal{C}_T$.

[11]This jump has already been observed in [188] by computing the holographic subregion complexity via a direct integration in the bulk.

[12]This was also pointed out in [188] in the context of holographic subregion complexity.

(4.21) and (4.23) are independent of $\tilde{M}$. Only at the transition point of the RT surface, i.e. at $\tilde{M} = \tilde{M}_*$, with[13]

$$\sigma_A = \frac{1}{2\sqrt{\tilde{M}_*}} \log\left(\frac{\exp(2\pi\sqrt{\tilde{M}_*}) + 1}{2}\right), \qquad (4.24)$$

the temperature dependence is present due to the discrete jump in $\mathcal{C}_T$.

Topological Complexity for the Conical Defect

As a final example, we now consider topological complexity for conical defects (2.152). Just as for the BTZ black hole, the RT surface of a single entangling interval A undergoes a phase transition for sufficiently large A (see Section 3.1.7). If the angular size of A is larger than π, i.e. $2\sigma_A > \pi$, the RT surface consists of two parts: a geodesic connecting the two endpoints of A and lying on the other side of the defect and an infinitesimally small circle circumventing the conical defect (see Section 3.1.7). We refer to this configuration of the RT surface as *Phase c*. Note that the circle around the defect is usually ignored since its circumference is zero and therefore does not contribute to the entanglement entropy when computed via the RT formula (3.32). However, formally the circle is necessary for ensuring that the RT surface is homologous to A (see Section 3.1.7 for more details). The circle also plays a crucial role for topological complexity, as we demonstrate in this section.

The BTZ metric in the form (4.20) may be used for conical defects (2.152) as well by considering $\tilde{M} \in [-1, 0)$. Here, $\tilde{M}$ is associated with $\hat{N}$ via (2.154). In order to compute the topological complexity (4.2) for Phase c, we need to determine the geodesic curvature of the infinitesimal circle surrounding the conical defect. We do that by considering a circle of finite radius $\tilde{r} = \tilde{r}_*$ and taking the limit $\tilde{r}_* \longrightarrow 0$,

$$\oint_{\tilde{r}=\tilde{r}_*} k_g ds = 2\pi\sqrt{\frac{\tilde{r}_*^2}{L^2} - \tilde{M}} \longrightarrow 2\pi\sqrt{-\tilde{M}} \quad \text{for} \quad \tilde{r}_* \longrightarrow 0. \qquad (4.25)$$

Moreover – in analogy to the computation of $\mathcal{C}_T$ in Phase b for the BTZ black hole – we find the Euler characteristic of the bulk region $\mathcal{B}_A$ to be zero,

$$\chi(\mathcal{B}_A) = 0. \qquad (4.26)$$

By inserting (4.25) and (4.26) together with the value of the geodesic curvature at the cut-off (4.7) and the angular contribution π into (4.2), we find

$$\mathcal{C}_T(A, \text{Phase c}) = \frac{2\ell_{\text{CFT}}\sigma_A}{\epsilon} + \pi - 2\pi\sqrt{-\tilde{M}} + \mathcal{O}(\epsilon). \qquad (4.27)$$

Note that the contribution (4.25) of the infinitesimal circle around the defect appears with a minus sign in (4.27) since the circle needs to be integrated over in mathematically negative direction in order to obtain the correct term for $\mathcal{C}_T$ (see Figure 4.4).

---

[13]This is a consequence of (3.50).

For $\tilde{M} = -1$, which corresponds to global AdS_3 (2.116), we find that (4.27) agrees with the value of $\mathcal{C}_T$ we obtained in Section 4.2.1 for a single interval in global AdS_3 (4.11).

Behavior of the Universal Part of Topological Complexity

We conclude our analysis of topological complexity for BTZ black holes and conical defects by discussing the behavior of the term c_T^0 in $\mathcal{C}_T$ constant in ϵ as a function of $\tilde{M}$. This term is proposed to be universal (see Section 3.2.3 and [63]). For the BTZ black hole, we find that c_T^0 is completely determined by topological quantities, i.e. the number of endpoints of the considered entangling region A and the topology of the codimension one bulk region $\mathcal{B}_A$. [14] As long as these topological aspects do not change, c_T^0 is constant in $\tilde{M}$. For one entangling interval of angular size $2\sigma_A > 2\pi$ we see that the value of c_T^0 jumps by 2π when the corresponding RT surface changes its phase from Phase a to Phase b (see (4.21) and (4.23)). By taking $\tilde{M}$ to negative values and therefore considering conical defects, we find that c_T^0 (4.27) is now no longer strictly topological, as its value depends on $\tilde{M}$, i.e. the geometry we consider. We depict the behavior of c_T^0 as a function of $\tilde{M}$ in Figure 4.4.

4.3   Discussion

The focus of this chapter was the topological complexity $\mathcal{C}_T$ (4.1) for CFT_2 states with static asymptotic AdS_3 spaces as gravity duals. Topological complexity is a quantity my collaborators and I introduced in [1] as a candidate for a holographic dual of subregion complexity. We studied topological complexity for entangling regions of CFT_2 states dual to global AdS_3, BTZ black holes and conical defects. For these static bulk geometries $\mathcal{C}_T$ agrees with Alishahiha's holographic subregion complexity (3.71) – up to a proportionality factor. The reason for this is the scalar curvature on the constant time slice, which is constant for the considered geometries. The advantage of our topological approach is the fact that it allows us to apply the Gauss-Bonnet theorem straightforwardly to compute the topological complexity. In particular, this provided us with an universal expression (4.10) for $\mathcal{C}_T$ for global AdS_3 and BTZ black holes. This expression is valid for any entangling region on the CFT side. Remarkably, our expression (4.10) for $\mathcal{C}_T$ reveals that the term c_T^0 which is of order zero in the cut-off expansion of $\mathcal{C}_T$ is solely determined by topological quantities. These quantities are the number of endpoints of the considered entangling region A and the Euler characteristic of the bulk region $\mathcal{B}_A$ bounded by the RT surface γ_A and A on the conformal boundary of the bulk. This result allowed us to systematically study the behavior of topological complexity during phase transitions of the RT surface (see Sections 4.2.1 and 4.2.2). If the RT surface undergoes a phase transition, the topology and therefore the Euler characteristic of $\mathcal{B}_A$ changes. This led us to the conclusion that c_T^0 performs a discrete jump by multiples of 2π at the transition point of the RT surface. Such

---

[14]We have recovered this behavior for one entangling interval above (see (4.21) and (4.23)). It is easy to see that it is also valid for an arbitrary set of entangling intervals.
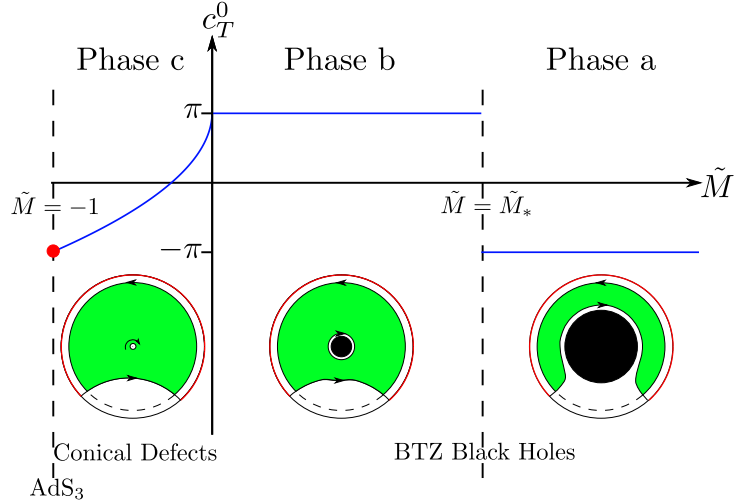
Figure 4.4: Plot of the cut-off independent part of topological complexity for BTZ black holes, conical defects and global AdS$_3$. We depict the term c_T^0 of topological complexity independent of the cut-off for $\tilde{M} \geq -1$. The cut-off corresponds to the dashed circle in the depicted constant time slices. Since the Ricci scalar is constant for all $\tilde{M}$, topological complexity is proportional to the volume of the region $\mathcal{B}_A$ (green) enclosed by the considered boundary entangling interval A (red) and the corresponding RT surface. We assume the angular size of A to be larger than π. For sufficiently large $\tilde{M}$, $\mathcal{B}_A$ lies on the same side of the BTZ black hole as A (Phase a) and has trivial topology, which leads to $c_T^0 = -\pi$ (4.21). If $\tilde{M}$ becomes smaller than $\tilde{M}_*$ (4.24), $\mathcal{B}_A$ wraps around the BTZ black hole and assumes the topology of an annulus. This causes c_T^0 to jump to π (4.23). When $\tilde{M}$ becomes negative, the considered geometry corresponds to a conical defect (Phase c). Here $\mathcal{B}_A$ still has the topology of an annulus. Moreover, c_T^0 is now no longer constant but depends on $\tilde{M}$ via $c_T^0 = \pi - 2\pi\sqrt{-\tilde{M}}$ (4.27). For $\tilde{M} = -1$ the geometry becomes global AdS$_3$ (red dot).

phase transitions occur when A consists of multiple entangling intervals as the phase of the RT surface depends on the position of these intervals relative to each other. Moreover, for thermal states dual to BTZ black holes γ_A also undergoes a phase transition if A consists of only one interval. When the angular size of A becomes sufficiently large, γ_A changes from a geodesic lying on the same side of the black hole as A to the union of the respective geodesic on the other side and the horizon (see Figure 4.3). In Section 4.2.2 we concluded that the only temperature dependence of c_T^0 is given by the discrete jump occurring at this transition of the RT surface.

Furthermore, we studied the topological complexity of CFT states dual to conical defects for large entangling intervals A (see Section 4.2.2). In this case the RT surface consists of a geodesic connecting the endpoints of A and an infinitesimally small circle circumventing the conical singularity. We found that the circle wrapping around the singularity is of great importance for the calculation of $\mathcal{C}_T$. In particular, it provides a contribution to c_T^0 which is not purely topological but

depends on the specific conical defect under consideration. This fact distinguishes the topological complexity of the conical defect from the one of global AdS$_3$ and BTZ black holes.

The results presented in this chapter are easily understood from the bulk perspective. However, they raise several non-trivial questions for the interpretation of topological complexity[15] on the field theory side. In the following we assume that the proposal that topological complexity corresponds to subregion complexity on the field theory side is true. In this context, we consider the following aspects of our results of particular interest for future projects. We find that the subregion complexity jumps by multiples of 2π when the RT surface undergoes a phase transition. It is a non-trivial question whether this discrete jump actually occurs on the field theory side. It might well be that it is a large N effect that is replaced by a rapid change in subregion complexity for finite N. [16] Moreover, even if the discrete jump turns out to be a large N effect, why this rapid change in subregion complexity happens is not clear at all and requires further investigation. Also the fact that the subregion complexity always seems to jump by multiples of 2π is an intriguing property that should be studied in detail. Furthermore, we only computed topological complexity for static situations so far. In order to develop a better understanding for $\mathcal{C}_T$ and in particular to decide whether it is actually suitable to describe subregion complexity, time-dependent systems need to be considered. In particular, this is important in order to investigate the differences between topological complexity and holographic subregion complexity (3.71). In the cases we studied so far, these two concepts differed only by a proportionality factor.

---

[15]Note that these questions also play a role for Alishahiha's holographic subregion complexity (3.71). This is due to the fact that for the examples we considered here topological complexity only deviates from holographic subregion complexity by a multiplicative factor.

[16]An analogous behavior for holographic subregion complexity has been suggested in [188].

Chapter 5

Holographic Subregion Complexity from Kinematic Space

This chapter is devoted to the results about holographic subregion complexity (HSRC) (3.71) I found together with my collaborators. These results were published in [1] and [2]. We developed a method for expressing the volume of codimension one bulk regions lying in constant time slices of AdS_3 in terms of CFT_2 quantities, namely entanglement entropies.

The concept of *kinematic space* [96], which is the space of all boundary anchored geodesics in a constant time slice of AdS_3, allowed us to express the volumes of codimension one bulk regions in terms of lengths of geodesics starting and ending on the conformal boundary. We refer to this expression as the *volume formula*. Since the lengths of boundary anchored geodesics on a constant time slice may be interpreted as entanglement entropies via the RT formula (3.32) in AdS_3/CFT_2, the volume formula can be rewritten in terms of entanglement entropies, leading to an expression for bulk volumes in terms of entanglement entropies. We may interpret this result as a new entry to the dictionary as it offers a way to calculate volumes in the bulk on the CFT side.

This is a particularly exciting result in the context of holographic subregion complexity (HSRC), i.e. the bulk volume enclosed by an entangling interval on the boundary and the respective RT surface: we are able to convert the defining formula (3.71) of HSRC into a field theory expression. To be more explicit, we managed to find a field theory dual for the HSRC of vacuum states (i.e. states dual to global AdS_3 or the $(2+1)$-dimensional Poincaré patch). This is of significant importance for testing the proposal that HSRC is related to the complexity of reduced CFT states. Since we now have a field theory expression for HSRC we may examine whether it has properties which are to be expected from complexity. We study HSRC in this context in Section 5.5, where we compare it with the proposals for mixed state complexity of [179] (see Section 3.2.1). Moreover, if HSRC actually turns out to be a good measure for the complexity of reduced states, our results provide an explicit field theory expression for this quantity, which does not require the bulk for constructing it. In particular, it may therefore be generalized

to field theories with no gravity dual.

This chapter is structured as follows. In Section 5.1 we review the aspects of kinematic space required for the construction of the volume formula, which we discuss and prove in Section 5.2 for global AdS$_3$ and the $(2+1)$-dimensional Poincaré patch. Section 5.3 focuses on the expression of bulk volumes in terms of entanglement entropy resulting from the volume formula. We apply this expression to several examples for bulk regions associated with HSRC. We generalize the volume formula to quotient spaces of AdS$_3$ such as conical defects and BTZ black holes in Section 5.4 and discuss the resulting relation between entanglement entropies and HSRC for these geometries. In Section 5.5 we study our expression for HSRC obtained from the volume formula under the assumption that HSRC is in fact a measure for the complexity of reduced CFT states and provide an outlook and concluding remarks in Section 5.6.

5.1   Kinematic Space

In this section we introduce the concept of kinematic space $\mathcal{K}$ as presented in [96]. We note that there are alternative formulations of kinematic space [206–208] which we do not discuss here. Moreover, we refer to [94, 95] for early developments regarding kinematic space and [97] for a discussion of the subject in the context of tensor networks.

Consider a CFT$_2$ state whose dual geometry is a static asymptotic AdS$_3$ space, i.e. a static space-time that behaves as global AdS$_3$ (2.116),

$$ds^2_{\text{AAdS}_3} \sim -\frac{\tilde{r}^2}{L^2}d\tilde{t}^2 + \frac{L^2}{\tilde{r}^2}d\tilde{r}^2 + \tilde{r}^2 d\phi^2 \,, \tag{5.1}$$

for $\tilde{r} \longrightarrow \infty$. Here $\phi \in [0, 2\pi]$ is 2π-periodic. Moreover, we assume that for two boundary points u, v on a constant time slice there is a unique bulk geodesic running from u to v. In this setup there are two different ways to introduce $\mathcal{K}$. It can be seen as the space of all oriented boundary anchored geodesics on a constant time slice but also as the space of all entangling intervals on the boundary of the constant time slice [96,97]. These two interpretations are referred to as the *bulk* and the *boundary perspective*, respectively. The existence of these two ways to see $\mathcal{K}$ is due to our above assumption that the geodesic running from one boundary point u to another boundary point v is unique. This implies a one-to-one correspondence between the geodesic in the bulk and the entangling interval $[u, v]$ lying between the two endpoints of the geodesic, as we depict in Figure 5.1.

So we see that $\mathcal{K}$ has an interpretation that is easy to grasp both on the gravity and the field theory side, making it a valuable tool for expressing bulk objects in terms of field theory quantities (see e.g. [95, 206]). In particular, it was shown in [95] that $\mathcal{K}$ comes with a volume form $\omega_{\mathcal{K}}$ that is naturally constructed in the bulk perspective. It consists only of derivatives of lengths of boundary anchored geodesics. Since these lengths may be interpreted as entanglement entropies via the RT formula (3.32), $\omega_{\mathcal{K}}$ can also be understood from the boundary perspective.
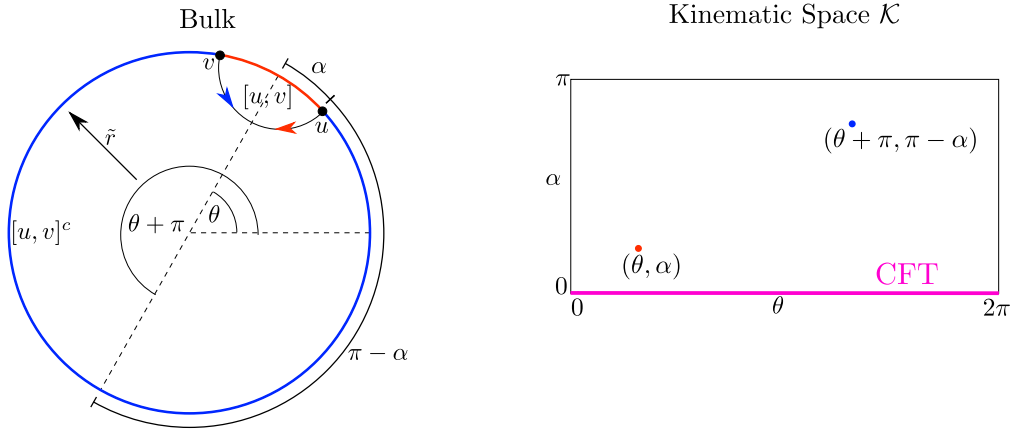
Figure 5.1: Coordinates for kinematic space $\mathcal{K}$. Kinematic space is the space of all boundary anchored geodesics on a constant time slice of the bulk. We can use the boundary points u, v as coordinates for a geodesic. Alternatively, the position θ of the center of the corresponding boundary interval $[u, v]$ and the opening angle α of $[u, v]$ may be used as coordinates (5.2). Each bulk geodesic appears twice in $\mathcal{K}$, namely with two different orientations, as visualized by the arrows on the l.h.s. By interpreting $\mathcal{K}$ as the space of all entangling intervals on the boundary CFT, we see that the two orientations of a geodesic correspond to an entangling interval and its complement (red and blue). Taking the opening angle α to zero shows that the lower boundary of $\mathcal{K}$ corresponds to the points on the conformal boundary of the bulk.

In [95–97] the authors demonstrated how properties of the bulk geometry may be computed in $\mathcal{K}$. In particular, the length of an arbitrary bulk curve can be expressed as an integral over $\omega_\mathcal{K}$, where each bulk geodesic, i.e. each point in $\mathcal{K}$, is weighted with the number of its intersections with the curve. The interpretation of $\omega_\mathcal{K}$ in the boundary perspective then allows us to interpret the integral over $\omega_\mathcal{K}$ determining the length of the curve as an integral over entanglement entropies. Thus $\mathcal{K}$ offers a way to compute the lengths of arbitrary bulk curves from the field theory side. This approach is closely related to the concept of differential entropy (see e.g. [94, 95, 209, 210]).

5.1.1 Kinematic Space from the Bulk Perspective

We now review the bulk perspective of kinematic space $\mathcal{K}$. [1] Here $\mathcal{K}$ is defined as the space of all oriented boundary anchored geodesics. We may use the endpoints $\phi = u, v$ of the geodesic as natural coordinates on $\mathcal{K}$, i.e. the point $(u, v) \in \mathcal{K}$ is associated with the geodesic starting at the boundary point u and ending at the boundary point v (see Figure 5.1). As $\mathcal{K}$ is the space of "oriented" geodesics we may distinguish between the geodesic starting at u and ending at v and the geodesic starting at v and ending at u, i.e. $(u, v) \neq (v, u)$. A further very useful set of coordinates – which we frequently use in this chapter – is given by $(\theta, \alpha) \in$

---

[1]This review is based on [96].
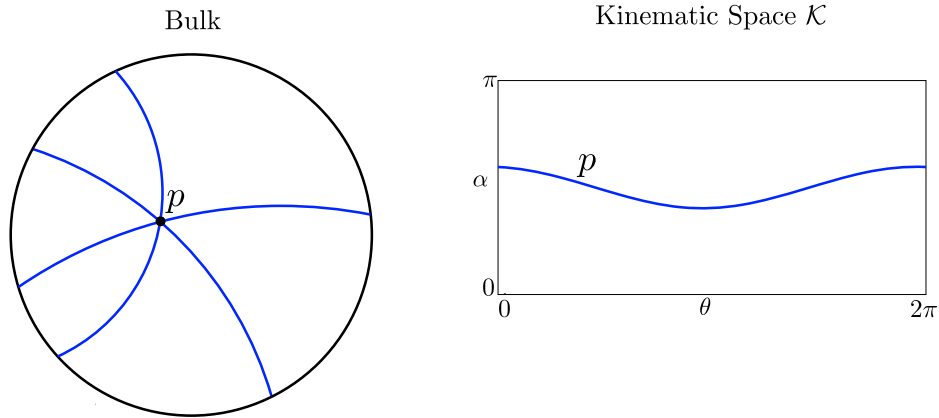
Figure 5.2: Bulk points in kinematic space. A point p in the bulk constant time slice is identified with the set of all geodesics intersecting p (l.h.s.). This set is a curve in kinematic space which is referred to as point curve (r.h.s.).

$[0, 2\pi] \times [0, \pi]$, where

$$u = \theta - \alpha \quad \text{and} \quad v = \theta + \alpha \,. \tag{5.2}$$

As depicted in Figure 5.1, θ may be interpreted as the midpoint of the boundary interval $[u, v]$ and α as its opening angle. Evidently, the angle θ is 2π-periodic. The geodesic with the opposite orientation as (θ, α) is given by $(\theta + \pi, \pi - \alpha)$. Moreover, using the coordinates θ, α it is easy to see that the line $\alpha = 0$ in $\mathcal{K}$ may be interpreted as the conformal boundary of the bulk [96, 97]: when we consider a geodesic (θ, α) in the bulk and send α to zero, this geodesic moves closer and closer to the conformal boundary at $\tilde{r} = \infty$ (see Figure 5.1). When α reaches zero, the geodesic is reduced to a point at $\tilde{r} = \infty$, i.e. a point on the conformal boundary. Thus we see that the points $(\theta, 0) \in \mathcal{K}$ correspond to the points on the conformal boundary of the bulk.

Furthermore, there is a very natural way to describe a bulk point p in $\mathcal{K}$. We identify p with the set of all geodesics that intersect it (see Figure 5.2). This set turns out to be a curve in $\mathcal{K}$ – which is referred to as *point curve* [95, 96].

Since we aim at using kinematic space as an auxiliary space to associate geometric aspects of the bulk with quantities on the boundary, we require to encode the bulk geometry in $\mathcal{K}$. This is achieved by defining a volume form $\omega_{\mathcal{K}}$ for $\mathcal{K}$ that allows us to compute the length ℓ of an arbitrary bulk curve γ – lying on the constant time slice – as an integral over $\mathcal{K}$. More specifically, we demand the following equation to hold,

$$\frac{\ell(\gamma)}{4G_3} = \frac{1}{4} \int_{\mathcal{K}} \omega_{\mathcal{K}} n_{\gamma} \,, \tag{5.3}$$

where we have introduced Newton's constant G_3 ($(2+1)$-dimensional) as it will simplify the expressions discussed in the rest of this chapter. Here $n_{\gamma}(u, v)$ is the number of intersections the geodesic (u, v) has with γ. So (5.3) essentially states that the length of a bulk curve γ is given by the integral over all geodesics

Bulk   Kinematic Space $\mathcal{K}$
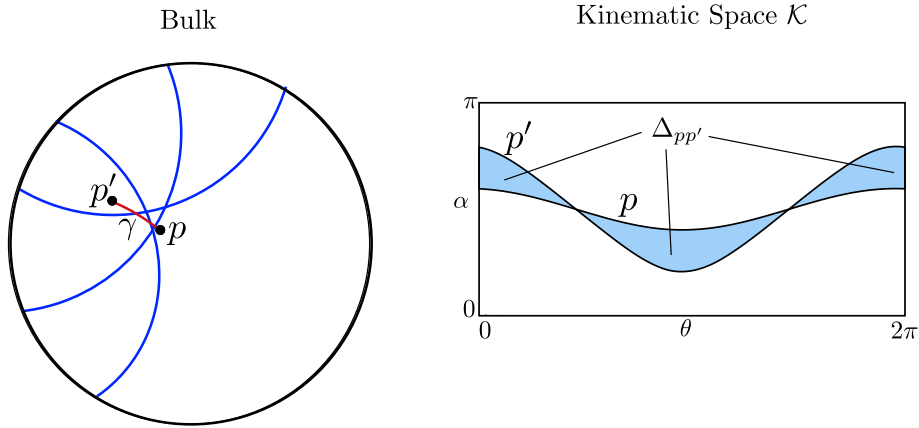
Figure 5.3: Lenghts of bulk curves in the constant time slice from kinematic space. In order to compute the length of a generic bulk curve γ in $\mathcal{K}$, we consider the set of all geodesics intersecting γ (l.h.s.). The length of γ is given by an integral over this set in kinematic space, where each geodesic is weighted with the number of its intersections with γ (5.3). If γ is a geodesic between two bulk points p, p', the number of intersections of each boundary anchored geodesic with γ is either zero or one. Therefore (5.3) reduces to an integral over the set $\Delta_{pp'}$ of all geodesics intersecting γ (5.5) (r.h.s.). This set is bounded by the point curves of p and p'.

intersecting γ weighted with the number of intersections. We visualize this concept in Figure 5.3. It was shown in [96] that the condition (5.3) leads to

$$\omega_{\mathcal{K}} = \frac{1}{4G_3}\partial_u\partial_v\ell(u,v)du \wedge dv = \frac{1}{8G_3}(\partial_\theta^2 - \partial_\alpha^2)\ell(\theta,\alpha)d\theta \wedge d\alpha\,, \qquad (5.4)$$

where $\ell(u,v)$ is the length of the geodesic (u,v). The volume form $\omega_{\mathcal{K}}$ given in (5.4) is referred to as *Crofton form*.

A special case of (5.3) that plays an important role in the following sections is the integral expression in $\mathcal{K}$ for the geodesic distance $d(p,p')$ between two bulk points p, p' [96],

$$\frac{d(p,p')}{4G_3} = \frac{1}{4}\int_{\Delta_{pp'}} \omega_{\mathcal{K}}\,, \qquad (5.5)$$

where $\Delta_{pp'} \subset \mathcal{K}$ is the set of all boundary anchored geodesics intersecting the geodesic $\gamma_{pp'}$ starting at p and ending at p'. Equation (5.5) is a simple consequence of the fact that any boundary anchored geodesic intersects $\gamma_{pp'}$ at most once, since $\gamma_{pp'}$ is a geodesic itself. We depict $\Delta_{pp'}$ in Figure 5.3. It turns out to be the set bounded by the point curves of p and p'.

5.1.2 Kinematic Space from the Boundary Perspective

In the boundary perspective, $\mathcal{K}$ is interpreted as the space of all entangling intervals on a constant time slice of the CFT.[2] A point $(u,v) \in \mathcal{K}$ which corresponds to a

---

[2]This review is based on [96].

geodesic stretching from u to v in the bulk perspective is now interpreted as the entangling interval $[u, v]$. Using the coordinates θ, α (5.2) it is easy to see that the point $(\theta + \pi, \pi - \alpha)$ in $\mathcal{K}$ – which refers to the same geodesic as (θ, α) but with opposite orientation in the bulk perspective – corresponds to the complement of the entangling interval (θ, α) in the boundary perspective.

The RT formula (3.32) allows us to interpret the Crofton form $\omega_\mathcal{K}$ (5.4) in terms of quantum information [95, 96]. It relates the length $\ell(u, v)$ of the geodesic starting at u and ending at v to the entanglement entropy $S(u, v)$ of the interval $[u, v]$. This allows us to express $\omega_\mathcal{K}$ in terms of entanglement entropy,

$$\omega_\mathcal{K} = \partial_u \partial_v S du \wedge dv = \frac{1}{2}(\partial_\theta^2 - \partial_\alpha^2) S d\theta \wedge d\alpha \,. \tag{5.6}$$

In this form, $\omega_\mathcal{K}$ may be interpreted as an infinitesimal version of conditional mutual information (3.18) [96]. By considering the intervals $A = [u - du, u]$, $B = [v, v + dv]$, $C = [u, v]$ and expanding $I(A : B|C)$ to leading order in du and dv, we find

$$I(A : B|C) \sim \partial_u \partial_v S du dv \,, \tag{5.7}$$

which coincides with $\omega_\mathcal{K}$. So in the boundary perspective $\omega_\mathcal{K}$ measures quantum information aspects of the CFT. Since $\omega_\mathcal{K}$ was originally constructed to encode aspects of the bulk geometry in $\mathcal{K}$ (see Section 5.1.1) this indicates a close relationship between quantum information on the CFT side and geometry on the AdS side.

Furthermore, we can define a metric $ds_\mathcal{K}^2$ for $\mathcal{K}$ in a very natural way [95, 96]. This is done by demanding the causal structure induced by the metric to encode the partially ordered structure of the set of all entangling intervals. To be more precise, (u_1, v_1) is supposed to lie in the past of (u_2, v_2) if $[u_1, v_1] \subset [u_2, v_2]$ and in the future of (u_3, v_3) if $[u_3, v_3] \subset [u_1, v_1]$. A point $(u_4, v_4) \in \mathcal{K}$ is considered spatially separated from (u_1, v_1) if $[u_1, v_1] \not\subset [u_4, v_4]$ and $[u_4, v_4] \not\subset [u_1, v_1]$. These considerations in particular imply that intervals of the form $[u_1, v_5]$ and $[u_5, v_1]$ correspond to points in $\mathcal{K}$ that are light-like separated from (u_1, v_1), as they lie in the future/past of (u_1, v_1) according to the above definition but a slight shift is sufficient to spatially separate them from (u_1, v_1). A metric that is supposed to carry the above causal structure necessarily has to be of the form

$$ds_\mathcal{K}^2 \propto du dv \,. \tag{5.8}$$

By demanding the volume form induced by $ds_\mathcal{K}^2$ to be the Crofton form (5.6), we may fix the prefactor in (5.8) to $2\partial_u \partial_v S$,

$$ds_\mathcal{K}^2 = 2\partial_u \partial_v S du dv = \frac{1}{2}(\partial_\theta^2 - \partial_\alpha^2) S\big({-}d\alpha^2 + d\theta^2\big) \,. \tag{5.9}$$

We see that it is possible to introduce the geometry of kinematic space from the boundary perspective without any reference to the interpretation of $\mathcal{K}$ as space of geodesics in the bulk or the bulk in general. The Crofton form (5.6) has an immediate interpretation as infinitesimal conditional mutual information (5.7) and the metric (5.9) is motivated by the partially ordered structure of the set of all

intervals and the Crofton form. The fact that the geometry of $\mathcal{K}$ can be defined directly from the field theory side without referencing the bulk plays an important role for the construction of a field theory dual of holographic subregion complexity which we perform in the sections below.

In this chapter we focus on bulk geometries that are invariant under rotations, i.e. constant shifts of ϕ (5.1). In these situations the entanglement entropy $S(u, v)$ only depends on the length $v - u = 2\alpha$ of the corresponding interval $[u, v]$, not its position, as is easy to see via the *RT* formula (3.32). Thus $ds^2_{\mathcal{K}}$ and $\omega_{\mathcal{K}}$ simplify in the following way,

$$ds^2_{\mathcal{K}} = -\frac{1}{2}\partial^2_\alpha S\left(-d\alpha^2 + d\theta^2\right),\tag{5.10}$$

$$\omega_{\mathcal{K}} = -\frac{1}{2}\partial^2_\alpha S d\theta \wedge d\alpha\,.\tag{5.11}$$

We note that the prefactor $-\partial^2_\alpha S/2$ is always non-negative [96]. This is an immediate consequence of the non-negativity of the conditional mutual information (3.20) and the interpretation of $\omega_{\mathcal{K}}$ as infinitesimal version of the conditional mutual information (5.7).

Point curves have a very natural interpretation in the context of the metric (5.10) when the bulk is chosen to be global AdS$_3$ (2.116). In [95] it was shown that in this case point curves are space-like geodesics w.r.t. the metric (5.10). [3] When we consider a bulk point p_* in the limit where it approaches the conformal boundary, the respective point curve asymptotes to light rays emitted from a point on the $\alpha = 0$ slice of $\mathcal{K}$. This point in $\mathcal{K}$ corresponds to p_* when the $\alpha = 0$ slice is associated with the conformal boundary of the bulk (see Figure 5.1). Considering the causal structure of $\mathcal{K}$ introduced above, these conclusions are easy to see.

5.2 Bulk Volumes from Kinematic Space: the Volume Formula

In [1] my collaborators and I introduced an integral in $\mathcal{K}$ computing the volume of an arbitrary codimension one bulk region $\mathcal{Q}$ on a constant time slice,

$$\frac{\text{vol}(\mathcal{Q})}{4G_3} = \frac{1}{2\pi}\int_{\mathcal{K}}\omega_{\mathcal{K}}\lambda_{\mathcal{Q}}\,,\tag{5.12}$$

which we refer to as volume formula. [4] Here $\lambda_{\mathcal{Q}}(\theta, \alpha)$ is the length of the segment of the geodesic (θ, α) that lies inside of $\mathcal{Q}$ (see Figure 5.4). We refer to $\lambda_{\mathcal{Q}}$ as the *chord length*. The volume formula may be interpreted as an adaptation of the integral expression of the length of a bulk curve in $\mathcal{K}$ (5.3): to obtain the length of a bulk curve, we need to integrate over kinematic space, where we weight each

---

[3]Analogous results were found for conical defects and BTZ black holes [95].

[4]We note that formulae of the form (5.12) are well established in integral geometry (see e.g. [211]).
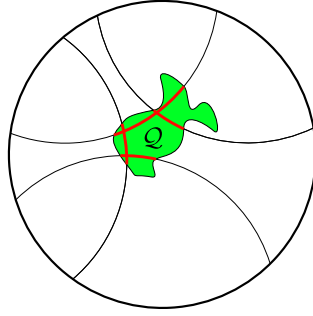
Figure 5.4: Volumes of codimension one bulk regions from kinematic space. In order to obtain the volume of an arbitrary bulk region $\mathcal{Q}$ (green) in the constant time slice by a kinematic space computation, we consider the set of all geodesics intersecting $\mathcal{Q}$. The volume of $\mathcal{Q}$ may then be computed by an integral over $\mathcal{K}$ (5.12) where each bulk geodesic (θ, α) is weighted with the length $\lambda_{\mathcal{Q}}(\alpha, \theta)$ of the segment it shares with $\mathcal{Q}$ (red).

geodesic, i.e. each point in $\mathcal{K}$, with the number of its intersections with the curve. Analogously, the volume of a bulk region is given by an integral over $\mathcal{K}$ where each geodesic is weighted with the length of the segment that intersects the region (5.12).

The remainder of this chapter is based on [2], where my collaborators and I studied the volume formula in great detail.

5.2.1 Proof of the Volume Formula for Global AdS$_3$

Expressions like the volume formula (5.12) are known in integral geometry [211] but not very well established in the AdS/CFT community. Here we present a simple proof of the volume formula that I constructed for the special case of global AdS$_3$. This geometry is dual to the CFT vacuum state. We use the coordinates (2.116) for AdS$_3$,

$$ds^2_{\text{AdS}} = -\Big(1 + \frac{\tilde{r}^2}{L^2}\Big)d\tilde{t}^2 + \frac{1}{1 + \frac{\tilde{r}^2}{L^2}}d\tilde{r}^2 + \tilde{r}^2 d\phi^2 \,. \tag{5.13}$$

The entanglement entropy of an interval with opening angle α is given by [82, 161]

$$S(\alpha) = \frac{c}{3} \log\Big(\frac{2\ell_{\text{CFT}}}{\epsilon} \sin(\alpha)\Big) \,, \tag{5.14}$$

where ℓ_{CFT} is the radius of the circle the CFT is defined on and ϵ is a UV cutoff. Moreover, $c = 3L/2G_3$ is the central charge (2.117). The metric (5.10) and Crofton form (5.11) on $\mathcal{K}$ corresponding to (5.14) are [96]

$$ds^2_{\mathcal{K}} = \frac{c}{6} \frac{1}{\sin^2(\alpha)}\big(-d\alpha^2 + d\theta^2\big) \quad \text{and} \quad \omega_{\mathcal{K}} = \frac{c}{6} \frac{1}{\sin^2(\alpha)} d\theta \wedge d\alpha \,, \tag{5.15}$$

where we have used the coordinates θ, α (5.2) for $\mathcal{K}$.

By defining

$$V(\mathcal{Q}) = \frac{2G_3}{\pi} \int_{\mathcal{K}} \omega_{\mathcal{K}} \lambda_{\mathcal{Q}} = \frac{L}{2\pi} \int_{\mathcal{K}} d\theta d\alpha \frac{\lambda_{\mathcal{Q}}}{\sin^2(\alpha)}, \tag{5.16}$$

the volume formula (5.12) may be written as

$$\mathrm{vol}(\mathcal{Q}) = V(\mathcal{Q}). \tag{5.17}$$

We prove (5.17) as follows. First we show the validity of (5.17) for a disc $\mathcal{D}_R$ with radius R lying in the constant time slice of AdS$_3$ and centered around $\tilde{r} = 0$. We do this via a direct computation. Second we verify certain properties of $V(\mathcal{Q})$, such as additivity and non-negativity, which are characteristic for volumes. These properties together with the validity of (5.17) for discs allow us in the third step to verify (5.17) for annular arcs. These annular arcs can be used to construct Riemann sums that approximate the volume of a generic bulk region arbitrarily well. This completes the proof of the volume formula.

Discs in AdS$_3$

We now show that (5.17) holds for $\mathcal{Q} = \mathcal{D}_R$, where $\mathcal{D}_R$ is a disc with radius R in the constant time slice of AdS$_3$ centered around $\tilde{r} = 0$. By pulling the metric ds^2_{AdS} (5.13) back to the constant time slice, it is easy to verify that

$$\mathrm{vol}(\mathcal{D}_R) = 2\pi L \int_0^R d\tilde{r} \frac{\tilde{r}}{\sqrt{L^2 + \tilde{r}^2}} = 2\pi L(\sqrt{L^2 + R^2} - L) \tag{5.18}$$

holds. We now compute $V(\mathcal{D}_R)$ to see that it gives the same result. The chord length $\lambda_{\mathcal{D}_R}(\alpha, \theta)$ associated with the geodesic (θ, α) is given by [82]

$$\lambda_{\mathcal{D}_R}(\theta, \alpha) = \begin{cases} L \operatorname{arcosh}(1 + 2\frac{R^2}{L^2} \sin^2(\alpha_R)), & \text{if } \alpha_* \leq \alpha \leq \pi - \alpha_* \\ 0, & \text{otherwise.} \end{cases} \tag{5.19}$$

The angle α_R is the opening angle of the geodesic (θ, α) on the boundary of $\mathcal{D}_R$ (see Figure 5.5). It is given by (see e.g. [96])

$$\frac{R}{\sqrt{L^2 + R^2}} \cos(\alpha_R) = \cos(\alpha). \tag{5.20}$$

Moreover, the angle $\alpha = \alpha_*$ corresponds to $\alpha_R = 0$ and refers to a geodesic that is tangent to $\mathcal{D}_R$ (see Figure 5.5)

$$\cos(\alpha_*) = \frac{R}{\sqrt{L^2 + R^2}}. \tag{5.21}$$

By inserting (5.19) into (5.16) we find

$$V(\mathcal{D}_R) = L \int_0^{2\pi} d\theta \int_{\alpha_*}^{\pi - \alpha_*} d\alpha \frac{\lambda_{\mathcal{D}_R}}{\sin^2(\alpha)} = L \int_0^{2\pi} d\theta \int_{\alpha_*}^{\pi - \alpha_*} d\alpha \, \partial_\alpha \lambda_{\mathcal{D}_R} \cot(\alpha), \tag{5.22}$$
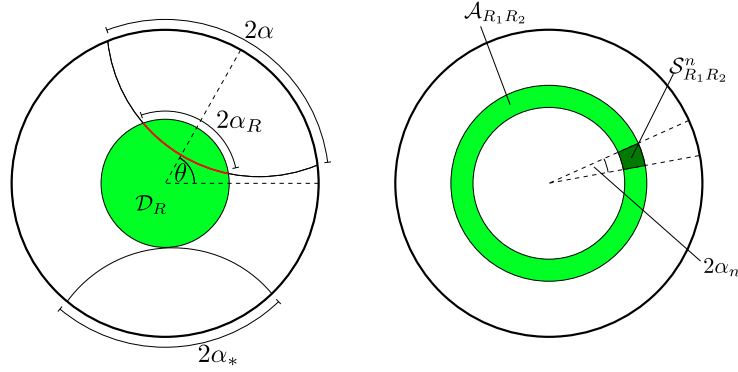
Figure 5.5: The volume formula for discs and annular arcs. The first step in the proof of the volume formula (5.12) is to verify it for a disc $\mathcal{D}_R$ centered at $\tilde{r} = 0$ (l.h.s.). The opening angle of a geodesic (θ, α) at the boundary of the disc is denoted by α_R. With (θ, α_*) we refer to geodesics tangent to the boundary of $\mathcal{D}_R$. From the validity of the volume formula for discs we can conclude that it is also valid for a segment $\mathcal{S}^n_{R_1 R_2}$ of an annulus $\mathcal{A}_{R_1 R_2}$ with inner radius R_1 and outer radius R_2 (r.h.s.). The opening angle of $\mathcal{S}^n_{R_1 R_2}$ is given by (5.33).

where we have used $1/\sin^2(\alpha) = -\partial_\alpha \cot(\alpha)$ to perform a partial integration in order to obtain the second equality. Performing the coordinate transformation $\alpha = \alpha(\alpha_R)$ and using the fact that $\lambda_{\mathcal{D}_R}$ (5.19) does not depend on θ, we find

$$V(\mathcal{D}_R) = \int_0^\pi d\alpha_R \frac{2L^2 R^2 \cos^2(\alpha_R)}{L^2 + R^2 \sin^2(\alpha_R)} = 2\pi L\left(\sqrt{L^2 + R^2} - L\right), \qquad (5.23)$$

which is equal to $\text{vol}(\mathcal{D}_R)$ (5.18). [5] Thus (5.17) holds for discs.

Properties of $V(\mathcal{Q})$ Associated with Volumes

The next step leading to the proof of (5.17) is to verify certain properties of $V(\mathcal{Q})$ (5.16) which are known to hold for volumes.

Non-Negativity. The integral $V(\mathcal{Q})$ (5.16) obeys

$$V(\mathcal{Q}) \geq 0 \qquad (5.24)$$

for any region $\mathcal{Q}$, where equality only holds for $\mathcal{Q} = \emptyset$. This property is an immediate implication of the fact that the integrand in (5.16) is non-negative and only vanishes if $\mathcal{Q} = \emptyset$. Note that we define $\mathcal{Q}$ to be a codimension one bulk region. Therefore, we do not consider the cases where $\mathcal{Q}$ is a curve, etc. for which $V(\mathcal{Q})$ would vanish as well.

Additivity. Given two regions $\mathcal{Q}, \mathcal{Q}'$ on the constant time slice of AdS$_3$, V satisfies the additivity relation

$$V(\mathcal{Q} \cup \mathcal{Q}') = V(\mathcal{Q}) + V(\mathcal{Q}') - V(\mathcal{Q} \cap \mathcal{Q}'), \qquad (5.25)$$

---

[5]The integration in (5.23) was performed via *Mathematica*.

which follows from the evident additivity of the chord length $\lambda_{\mathcal{Q}}$,

$$\lambda_{\mathcal{Q} \cup \mathcal{Q}'} = \lambda_{\mathcal{Q}} + \lambda_{\mathcal{Q}'} - \lambda_{\mathcal{Q} \cap \mathcal{Q}'}. \tag{5.26}$$

Monotonicity. Given two regions $\mathcal{Q}, \mathcal{Q}'$ with $\mathcal{Q} \subset \mathcal{Q}'$, we find

$$V(\mathcal{Q}) \leq V(\mathcal{Q}'). \tag{5.27}$$

The verification of this monotonicity is a simple application of the non-negativity and additivity of V.

Rotational Invariance. The value of $V(\mathcal{Q})$ for any region $\mathcal{Q}$ in the constant time slice of AdS_3 does not change under rotations of $\mathcal{Q}$ around $\tilde{r} = 0$. This is an immediate consequence of the invariance of ds^2_{AdS} (5.13) under such rotations.

Construction of Riemann Sums

The properties of V listed above can now be used to verify the validity of (5.17) first for annuli and then for annular arcs. An arbitrary bulk region $\mathcal{Q}$ may then be approximated arbitrarily well by annular arcs which completes the proof of the volume formula (5.12).

Consider an annulus $\mathcal{A}_{R_1 R_2}$ of inner radius R_1 and outer radius R_2 lying in the constant time slice of AdS_3 and centered around $\tilde{r} = 0$. Evidently, $\mathcal{A}_{R_1 R_2}$ is given by the difference of the two discs $\mathcal{D}_{R_1}$ and $\mathcal{D}_{R_2}$,

$$\mathcal{A}_{R_1 R_2} = \mathcal{D}_{R_2} \backslash \mathcal{D}_{R_1}. \tag{5.28}$$

Consequently, the volume of $\mathcal{A}_{R_1 R_2}$ is given by

$$\text{vol}(\mathcal{A}_{R_1 R_2}) = \text{vol}(\mathcal{D}_{R_2}) - \text{vol}(\mathcal{D}_{R_1}). \tag{5.29}$$

We now show that $V(\mathcal{A}_{R_1 R_2})$ gives the same result, verifying (5.17) of annuli. The additivity of V (5.25) implies

$$V(\mathcal{D}_{R_2}) = V(\mathcal{D}_{R_1}) + V(\mathcal{A}_{R_1 R_2}), \tag{5.30}$$

via (5.28). Since (5.17) is known to be true for discs (5.23), (5.18), we therefore conclude

$$V(\mathcal{A}_{R_1 R_2}) = \text{vol}(\mathcal{D}_{R_2}) - \text{vol}(\mathcal{D}_{R_1}). \tag{5.31}$$

Using (5.29) we find

$$V(\mathcal{A}_{R_1 R_2}) = \text{vol}(\mathcal{A}_{R_1 R_2}), \tag{5.32}$$

i.e. the validity of (5.17) for annuli.

We can conclude the validity of (5.17) for annular arcs from (5.32). Consider a segment $\mathcal{S}^n_{R_1 R_2}$ of the annulus $\mathcal{A}_{R_1 R_2}$ with opening angle

$$2\alpha_n = \frac{2\pi}{n}, \quad n \in \mathbb{N}, \tag{5.33}$$
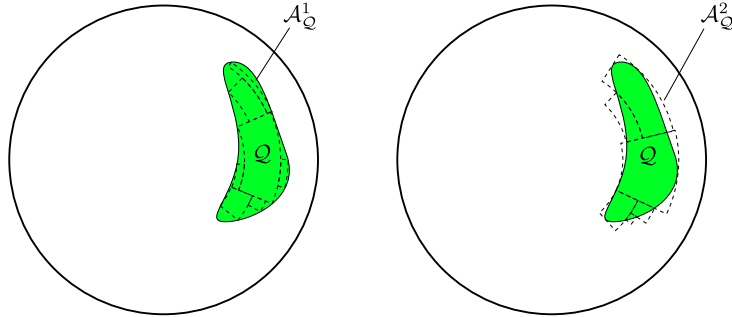
Figure 5.6: Approximation of an arbitrary codimension one bulk region $\mathcal{Q}$ in the constant time slice. We use disjoint unions of annular arcs $\mathcal{A}_{\mathcal{Q}}^1, \mathcal{A}_{\mathcal{Q}}^2$ to approximate $\mathcal{Q}$. Here we assume $\mathcal{A}_{\mathcal{Q}}^1 \subset \mathcal{Q} \subset \mathcal{A}_{\mathcal{Q}}^2$. By taking the limit where $\mathcal{A}_{\mathcal{Q}}^1$ and $\mathcal{A}_{\mathcal{Q}}^2$ converge to $\mathcal{Q}$, we can prove the volume formula (5.12) for an arbitrary $\mathcal{Q}$.

as depicted in Figure 5.5. The rotational invariance and additivity of V, together with (5.32) imply

$$V(\mathcal{S}_{R_1 R_2}^n) = \frac{1}{n} V(\mathcal{A}_{R_1 R_2}) = \frac{1}{n} \text{vol}(\mathcal{A}_{R_1 R_2}) = \text{vol}(\mathcal{S}_{R_1 R_2}^n). \tag{5.34}$$

To conclude the proof of (5.17) we now consider an arbitrary codimension one bulk region $\mathcal{Q}$ lying in the constant time slice of AdS$_3$. We can approximate $\mathcal{Q}$ by disjoint unions of annular arcs, as depicted in Figure 5.6. We choose two such approximations $\mathcal{A}_{\mathcal{Q}}^1, \mathcal{A}_{\mathcal{Q}}^2$ satisfying

$$\mathcal{A}_{\mathcal{Q}}^1 \subset \mathcal{Q} \subset \mathcal{A}_{\mathcal{Q}}^2. \tag{5.35}$$

The monotonicity of V (5.27) implies

$$V(\mathcal{A}_{\mathcal{Q}}^1) \leq V(\mathcal{Q}) \leq V(\mathcal{A}_{\mathcal{Q}}^2), \tag{5.36}$$

which leads to

$$\text{vol}(\mathcal{A}_{\mathcal{Q}}^1) \leq V(\mathcal{Q}) \leq \text{vol}(\mathcal{A}_{\mathcal{Q}}^2), \tag{5.37}$$

via the additivity of V (5.25) and the validity of (5.17) for annular arcs. By taking the limit where $\mathcal{A}_{\mathcal{Q}}^1$ and $\mathcal{A}_{\mathcal{Q}}^2$ converge to $\mathcal{Q}$, (5.37) leads to

$$\text{vol}(\mathcal{Q}) \leq V(\mathcal{Q}) \leq \text{vol}(\mathcal{Q}) \quad \Leftrightarrow \quad \text{vol}(\mathcal{Q}) = V(\mathcal{Q}), \tag{5.38}$$

which completes the proof of (5.17) and thus shows the validity of the volume formula (5.12) for arbitrary $\mathcal{Q}$.

5.2.2 The Volume Formula for the Poincaré Patch

In addition to the proof of the volume formula for global AdS$_3$ discussed in Section 5.2.1 my collaborators and I also presented a proof for the Poincaré patch in [2], which we now review.

Kinematic Space for the Poincaré Patch

The kinematic space $\mathcal{K}$ for the Poincaré patch [212] is constructed in an analogous way as for asymptotic global AdS$_3$ spaces (see Section 5.1). The geodesics may again be parametrized by their endpoints $x = u, v$ on the boundary, where we use the coordinates x and z (3.33) for the constant time slice of the Poincaré patch. In analogy to (5.2) we introduce the coordinates $\chi \in \mathbb{R}$ and $\sigma \in \mathbb{R}$ corresponding to the center and radius of the boundary interval $[u, v]$ via

$$u = \chi - \sigma \,, \quad v = \chi + \sigma \,. \tag{5.39}$$

The geodesic with opposite orientation as (χ, σ) is then given by $(\chi, -\sigma)$. Using (5.11) – where σ takes the role of α – and (3.39), we find

$$\omega_\mathcal{K} = \frac{c}{6} \frac{1}{\sigma^2} d\chi \wedge d\sigma \tag{5.40}$$

for the Crofton form.

Proof of the Volume Formula for the Poincaré Patch

In analogy to the case of global AdS$_3$ (see Section 5.2.1), we introduce

$$V(\mathcal{Q}) = \frac{L}{2\pi} \int_\mathcal{K} d\chi d\sigma \frac{\lambda_\mathcal{Q}}{\sigma^2} \,, \tag{5.41}$$

in order to prove the volume formula (5.12) by showing

$$\mathrm{vol}(\mathcal{Q}) = V(\mathcal{Q}) \tag{5.42}$$

for a codimension one bulk region $\mathcal{Q}$ lying in the constant time slice of the Poincaré patch.

As in the case of global AdS$_3$, discussed in Section 5.2.1, V is additive (5.25), monotonous (5.27) and non-negative (5.24). Moreover, it is invariant under translations in x direction, i.e. the value of V for a region $\mathcal{Q}$ does not change when $\mathcal{Q}$ is shifted in x-direction. This is an easily verified consequence of the invariance of ds^2_{PP} (3.33) under shifts in x-direction.

For proving (5.42) we pursue the following strategy. First we show that (5.42) holds for an generic infinitesimal rectangular strip $\mathcal{S}^{x_0}_{z_1 z_2}$ at $x = x_0$ with width δx and stretching from $z = z_1$ to $z = z_2$. We then prove (5.42) for an arbitrary bulk region $\mathcal{Q}$ by approximating it by a disjoint union of such strips, as depicted in Figure 5.7. The properties of V mentioned above then imply that (5.42) holds for $\mathcal{Q}$. This follows analogously to the case of global AdS$_3$ in Section 5.2.1, where $\mathcal{Q}$ was approximated with annular arcs instead of rectangular strips.

Since $\mathcal{S}^{x_0}_{z_1 z_2}$ has infinitesimal width, we may only distinguish between geodesics that enter $\mathcal{S}^{x_0}_{z_1 z_2}$ on the l.h.s. and exit it on the r.h.s. and geodesics that do not intersect $\mathcal{S}^{x_0}_{z_1 z_2}$ (see Figure 5.7). The latter do not contribute to V, as their chord
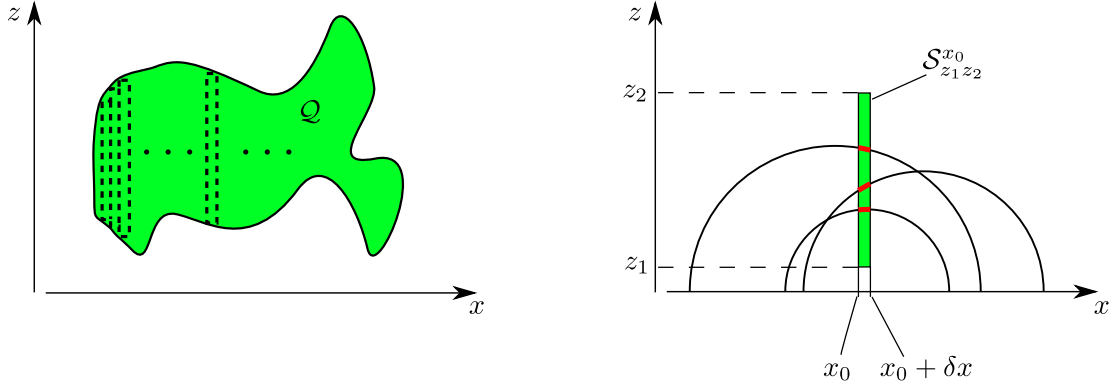
Figure 5.7: The strategy for proving the volume formula (5.12) for the Poincaré patch. We approximate a generic codimension one bulk region $\mathcal{Q}$ in the constant time slice of the Poincaré patch by a disjoint union of rectangular strips with infinitesimal width δx (l.h.s.). We verify the volume formula for a generic strip $\mathcal{S}^{x_0}_{z_1 z_2}$ of this kind, located a $x = x_0$ and stretching from $z = z_1$ to $z = z_2$ (r.h.s.). For the integral (5.41) appearing in the volume formula we only distinguish between geodesics entering at one side and exiting at the other side of $\mathcal{S}^{x_0}_{z_1 z_2}$ and geodesics that do not intersect $\mathcal{S}^{x_0}_{z_1 z_2}$, since the strip has infinitesimal width. The validity of the volume formula for a generic $\mathcal{S}^{x_0}_{z_1 z_2}$ then implies that the volume formula holds for any $\mathcal{Q}$.

length is zero. As may be easily deduced from (3.72), the geodesic (χ, σ) obeys the equation

$$z^2 = \sigma^2 - (x - \chi)^2 \,. \tag{5.43}$$

So only geodesics which satisfy

$$z_1 \leq \sigma^2 - (x_0 - \chi)^2 \leq z_2 \tag{5.44}$$

contribute to $V(\mathcal{S}^{x_0}_{z_1 z_2})$. By setting $\sigma_{1,2} = \sqrt{z_{1,2}^2 + (x_0 - \chi)^2}$ we obtain[6]

$$V(\mathcal{S}^{x_0}_{z_1 z_2}) = 2 \cdot \frac{L}{2\pi} \int_{-\infty}^{\infty} d\chi \int_{\sigma_1}^{\sigma_2} \frac{d\sigma}{\sigma^2} \lambda_{\mathcal{S}^{x_0}_{z_1 z_2}} \tag{5.45}$$

from (5.41). Using (3.33) and (5.43) we find for the contributing geodesics in the infinitesimal limit

$$\begin{aligned}
\lambda_{\mathcal{S}^{x_0}_{z_1 z_2}}(\chi, \sigma) = ds_{PP} &= \frac{L}{z} \sqrt{\delta x^2 + \delta z^2} = \frac{L \delta x}{z^2} \sqrt{z^2 + (x_0 - \chi)^2} \\
&= \frac{L \sigma}{\sigma^2 - (x_0 - \chi)^2} \delta x \,,
\end{aligned} \tag{5.46}$$

and thus conclude

$$V(\mathcal{S}^{x_0}_{z_1 z_2}) = \frac{L^2 \delta x}{\pi} \int_{-\infty}^{\infty} d\chi \int_{\sigma_1}^{\sigma_2} d\sigma \frac{1}{\sigma\left(\sigma^2 - (x_0 - \chi)^2\right)} = L^2\left(\frac{1}{z_1} - \frac{1}{z_2}\right) \delta x \,. \tag{5.47}$$

---

[6]Note that since we assume $\sigma_{1,2} > 0$, we only consider one orientation of the geodesic. We compensate this by the multiplicative factor 2 in (5.45).

It is easy to verify that the volume of $\mathcal{S}_{z_1 z_2}^{x_0}$ is also given by

$$\text{vol}(\mathcal{S}_{z_1 z_2}^{x_0}) = L^2 \Big(\frac{1}{z_1} - \frac{1}{z_2} \Big) \delta x \,. \tag{5.48}$$

Therefore we find that (5.42) is true for $\mathcal{Q} = \mathcal{S}_{z_1 z_2}^{x_0}$.

We can use this result to show that (5.42) holds for any $\mathcal{Q}$. By approximating $\mathcal{Q}$ with a disjoint union of infinitesimal strips we come to this conclusion analogously to the case of global AdS$_3$, where we used annular arcs instead of infinitesimal strips (see Section 5.2.1). This completes the proof of the volume formula (5.12) for the Poincaré patch.

5.3 Holographic Subregion Complexity for Vacuum States

The holographic subregion complexity (HSRC) (see Section 3.2.3) of an entangling interval A is given – up to a proportionality factor – by the volume of the codimension one bulk region $\mathcal{B}_A$ enclosed by A and the corresponding RT surface γ_A (3.71). As we discussed in [1] and [2], the volume formula (5.12) can be used to construct a field theory expression for HSRC for the CFT states dual to the global AdS$_3$ geometry (5.13) and the $(2+1)$-dimensional Poincaré patch (3.33). These states are the vacuum states for a CFT defined on a circle and the real axis, respectively. In the following we use the kinematic space notation for entangling intervals introduced in Section 5.1.2. In particular, we refer to A as (θ_A, α_A). Moreover, we choose the proportionality factor that relates vol($\mathcal{B}_A$) to HSRC to be $1/L^2$ and not $(8\pi L G_3)^{-1}$ as in (3.71). We make this choice in order stay consistent with our definition of topological complexity (4.1). For the geometries we consider here, the Ricci scalar $\mathcal{R}_{ct}$ appearing in the formula for topological complexity takes the constant value $-2/L^2$. Therefore, the topological complexity is given by vol($\mathcal{B}_A$) multiplied with the same proportionality factor we choose here. So the concept of complexity we are using in the following is given by

$$\mathcal{C}(\theta_A, \alpha_A) = \frac{\text{vol}(\mathcal{B}_A)}{L^2} \,. \tag{5.49}$$

Note that we still refer to $\mathcal{C}$ as HSRC and not topological complexity. This is due to the fact that the results we present in this chapter are based on the proportionality of $\mathcal{C}$ to vol($\mathcal{B}_A$) and are therefore closer related to HSRC (3.71) than to topological complexity (4.1).

5.3.1 Holographic Subregion Complexity in Terms of Entanglement Entropies

We now construct an integral expression for HSRC (5.49) that only contains entanglement entropies by applying the volume formula (5.12) to $\mathcal{B}_A$. Since entanglement entropy is a CFT quantity, this integral expression provides a CFT formula

for HSRC. The volume formula leads to

$$\frac{\text{vol}(\mathcal{B}_A)}{4G_3} = \frac{1}{2\pi} \int_{\mathcal{K}} \omega_{\mathcal{K}} \lambda_{\mathcal{B}_A} \,. \tag{5.50}$$

Note that $\omega_{\mathcal{K}}$ (5.11) only depends on entanglement entropies. Thus, in order to derive a field theory expression for HSRC from (5.50), we only need to find a field theory expression for $\lambda_{\mathcal{B}_A}$. The chord length $\lambda_{\mathcal{B}_A}(\theta, \alpha)$ of a geodesic (θ, α) is the length of the segment of (θ, α) lying inside of $\mathcal{B}_A$. By construction, $\mathcal{B}_A$ is a convex set, i.e. any geodesic (θ, α) has either no or two intersection points p, p' with the boundary of $\mathcal{B}_A$. If there are no intersection points, the geodesic does not intersect $\mathcal{B}_A$ and the corresponding chord length is zero. If there are two intersection points, the chord length $\lambda_{\mathcal{B}_A}(\theta, \alpha)$ is simply the geodesic distance between p and p' (see Figure 5.8). In (5.5) we presented an expression for the geodesic distance between two bulk points as an integral in $\mathcal{K}$. Applying this expression to the present situation yields

$$\frac{\lambda_{\mathcal{B}_A}(\theta, \alpha)}{4G_3} = \frac{1}{4} \int_{\Delta_A(\theta, \alpha)} \omega_{\mathcal{K}} \,, \tag{5.51}$$

where $\Delta_A(\theta, \alpha) \subset \mathcal{K}$ is the region in kinematic space bounded by the point curves corresponding to p and p' (see Figure 5.9). If p and p' do not exist, i.e. if (θ, α) does not intersect $\mathcal{B}_A$, we find $\Delta_A(\theta, \alpha)$ to be empty, which implies $\lambda_{\mathcal{B}_A}(\theta, \alpha) = 0$ via (5.51). Since $\omega_{\mathcal{K}}$ only contains entanglement entropies, (5.51) is a field theory expression for $\lambda_{\mathcal{B}_A}$.

We can now insert (5.51) into (5.50),

$$\begin{aligned}
\frac{\text{vol}(\mathcal{B}_A)}{4G_3^2} &= \frac{1}{2\pi} \int_{\mathcal{K}} \omega_{\mathcal{K}} \left(\int_{\Delta_A(\theta, \alpha)} \omega_{\mathcal{K}} \right) \\
&= \frac{1}{8\pi} \int_{\mathcal{K}} d\theta d\alpha \int_{\Delta_A(\theta, \alpha)} d\theta' d\alpha' \partial_\alpha^2 S(\alpha) \partial_{\alpha'}^2 S(\alpha') \,,
\end{aligned} \tag{5.52}$$

where we have used (5.11) for $\omega_{\mathcal{K}}$. This provides us with the desired expression of HSRC in terms of entanglement entropy,

$$\mathcal{C}(\theta_A, \alpha_A) = \frac{9}{8\pi c^2} \int_{\mathcal{K}} d\theta \, d\alpha \int_{\Delta_A(\theta, \alpha)} d\theta' d\alpha' \partial_\alpha^2 S(\alpha) \partial_{\alpha'}^2 S(\alpha') \,. \tag{5.53}$$

By considering the boundary perspective for kinematic space (see Section 5.1.2) we see that HSRC is given by a double integral over entangling intervals containing only entanglement entropies. The formula (5.53) is one of the main results of this chapter. In the following sections we will review the detailed discussion of (5.53) which my collaborators and I provided in [2].

We emphasize that it is possible to generalize (5.52) to an integral expression in terms of entanglement entropies for an arbitrary codimension one bulk region $\mathcal{Q}$ on the constant time slice. This expression can be derived analogously to (5.52). Therefore the volume formula provides a field theory interpretation for any $\text{vol}(\mathcal{Q})$ in terms of entanglement entropies. This observation may be seen as an extension of the expression of the lengths of bulk curves in terms of entanglement entropies via (5.3) [96] and the closely related concept of differential entropy (see e.g. [94, 95, 209, 210]).
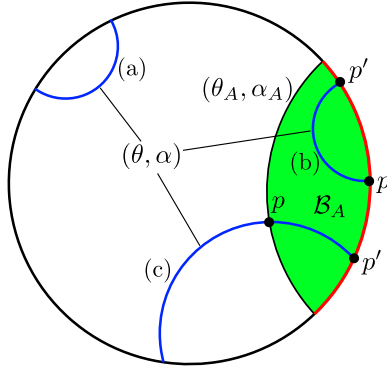
Figure 5.8: Three different types of geodesics in a constant time slice. When computing the volume of $\mathcal{B}_A$ (green) by an integral over kinematic space (5.50), we may distinguish three types of geodesics. Type (a) geodesics do not intersect with $\mathcal{B}_A$ and therefore do not contribute. Geodesics of type (b) lie completely inside of $\mathcal{B}_A$ and type (c) geodesics lie only partially inside of $\mathcal{B}_A$. For type (b) and (c) geodesics (θ, α), the chord length $\lambda_{\mathcal{B}_A}$ is given by the geodesic distance between the two intersection points p, p' of (θ, α) with $\partial \mathcal{B}_A$.

5.3.2 Regions of Integration in the CFT Formula for Holographic Subregion Complexity

Even though the expression for subregion complexity (5.53) only contains entanglement entropies, it still relies implicitly on the bulk since we require the interpretation of (θ, α) as geodesic in order to construct the region of integration $\Delta_A(\theta, \alpha)$. We now present a procedure that allows us to construct $\Delta_A(\theta, \alpha)$ directly from the field theory side. This construction requires extensive use of the geometry (5.10) imposed on $\mathcal{K}$. Since this geometry can be motivated from the CFT side (see Section 5.1.2), we effectively only require knowledge about the field theory side in order to perform this construction. This fact justifies the statement that the following procedure is a field theory construction of $\Delta_A(\theta, \alpha)$.

We begin by noting that the region of integration $\Delta_A(\theta, \alpha)$ is always bounded by the point curves corresponding to the intersection points of (θ, α) with the boundary of $\mathcal{B}_A$, as pointed out below (5.51). So if we can find a procedure for constructing these point curves from the boundary perspective, we accomplish the same for $\Delta_A(\theta, \alpha)$. As pointed out in Section 5.1.2, point curves are geodesics in $\mathcal{K}$. So there is a straightforward way for constructing them from the geometry of kinematic space and thus from the CFT side. Therefore, the only thing left to do is to find a way for identifying the specific point curves required for $\Delta_A(\theta, \alpha)$. In order to develop such a procedure, we first study these point curves from the bulk perspective and then interpret our results from the boundary perspective. This procedure was developed by me and published in [2]. We present it for the kinematic space of global AdS$_3$. It can be formulated in an analogous way for the Poincaré patch.

We note that in [95] it has only been shown for the kinematic space of global AdS$_3$ that point curves are geodesics in $\mathcal{K}$. [7] This can also be verified for the kinematic space of the Poincaré patch via a direct calculation. The computation is easily done by noting that the point curve of a bulk point (x, z) is given by (5.43). Since we are only considering the kinematic spaces of global AdS$_3$ and the Poincaré patch in this section, the assumption that point curves are geodesics in $\mathcal{K}$ is legitimate. We are unaware of the existence of an argument that proves this statement for arbitrary asymptotic AdS$_3$ spaces. However, we note that in the appendix of [96] a procedure for constructing point curves from the boundary perspective for generic bulk geometries was discussed.

Δ_A from the Bulk Perspective

For studying the shape of $\Delta_A(\theta, \alpha)$, we introduce the following three types of bulk geodesics (θ, α) (see Figure 5.8).

Type (a) Bulk Geodesics. We refer to a geodesic (θ, α) as type (a) if it does not intersect $\mathcal{B}_A$ at all. Consequently, the chord length vanishes for type (a) geodesics, i.e. $\lambda_{\mathcal{B}_A}(\theta, \alpha) = 0$, which leads to $\Delta_A(\theta, \alpha) = \emptyset$.

Type (b) Bulk Geodesics. If a geodesic (θ, α) lies completely inside of $\mathcal{B}_A$, we denote it to be of type (b). As depicted in Figure 5.8, the intersection points of type (b) geodesics with the boundary of $\mathcal{B}_A$ lie on the conformal boundary of the constant time slice of the bulk. They are the endpoints of the entangling interval corresponding to (θ, α) on the CFT side. As pointed out in Section 5.1.1, the constant time slice of the CFT may be identified with the lower boundary of kinematic space, i.e. the points in $\mathcal{K}$ with $\alpha = 0$. The point curves in $\mathcal{K}$ associated with the intersection points of (θ, α) and $\partial \mathcal{B}_A$ are therefore light rays in $\mathcal{K}$ emitted from the points on the boundary of $\mathcal{K}$ corresponding to the endpoints of the entangling interval belonging to (θ, α) (see Section 5.1.2). As we depict in Figure 5.9, these point curves bound a $\Delta_A(\theta, \alpha)$ that is the union of causal diamonds in $\mathcal{K}$.

Type (c) Bulk Geodesics. A bulk geodesic (θ, α) that has one intersection point with $\mathcal{B}_A$ located on the conformal boundary of the constant time slice and one on the RT surface γ_A is referred to as type (c). As we depict in Figure 5.8, these geodesics lie only partially in $\mathcal{B}_A$. In analogy to the discussion of type (b) geodesics presented above, the intersection point of (θ, α) on the conformal boundary may be identified with one endpoint of the corresponding entangling interval on the CFT side. The point curve in $\mathcal{K}$ associated with this endpoint again consists of light rays in $\mathcal{K}$ emitted form the corresponding boundary point of $\mathcal{K}$. The intersection point of (θ, α) with γ_A evidently is the bulk point where the geodesics (θ, α) and (θ_A, α_A) intersect. The point curve in $\mathcal{K}$ associated with this intersection point is therefore the space-like geodesic in $\mathcal{K}$ running through the kinematic space

---

[7]In [95] analogous properties have also been shown for the conical defect and the BTZ black hole. However, as we discuss in Section 5.4, the geodesic connecting two boundary points is not unique in these geometries. Here however, we assume uniqueness of this geodesic. Therefore the following discussion does not apply to the conical defect and the BTZ black hole.
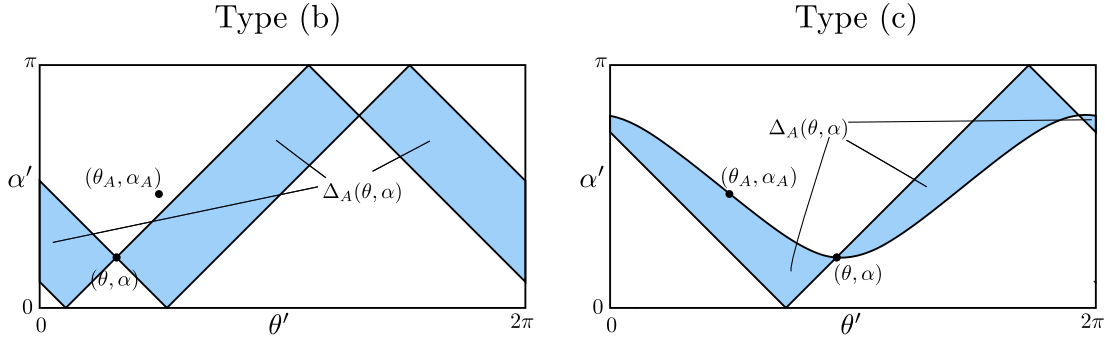
Figure 5.9: The region of integration $\Delta_A(\theta, \alpha)$ for bulk geodesics of type (b) and (c). L.h.s.: We depict the region of integration $\Delta_A(\theta, \alpha)$ (blue) appearing in (5.53) for (θ, α) of type (b). It is given by the causal diamonds in $\mathcal{K}$ bounded by the light rays emitted from the points on the lower boundary of $\mathcal{K}$ which correspond to the endpoints of the geodesic (entangling interval) associated with (θ, α). R.h.s.: We depict $\Delta_A(\theta, \alpha)$ for (θ, α) of type (c). One boundary of $\Delta_A(\theta, \alpha)$ consists of light rays in $\mathcal{K}$. These light rays are emitted from the kinematic space point corresponding to the endpoint of the geodesic (entangling interval) (θ, α) lying inside of the interval associated with (θ_A, α_A). The other boundary of $\Delta_A(\theta, \alpha)$ is the geodesic in $\mathcal{K}$ connecting (θ_A, α_A) and (θ, α) (see discussion in the introduction of Section 5.3.2).

points (θ, α) and (θ_A, α_A). So we see that $\Delta_A(\theta, \alpha)$ is bounded by a light-like and a space-like geodesic in $\mathcal{K}$. In Figure 5.9 we depict the typical form of $\Delta_A(\theta, \alpha)$ for a bulk geodesic of type (c).

The three types of bulk geodesics presented above only consider geodesics that intersect the RT surface part of $\partial\mathcal{B}_A$ once (type (c)) or not at all (types (a) and (b)). For completeness we note that there are no geodesics intersecting the RT surface γ_A twice. This is due to the fact that γ_A is a geodesic itself. Therefore, a geodesic intersecting γ_A twice would correspond to a situation where two geodesics intersect twice, which is not possible in the geometries we consider. Thus, the types (a) – (c) are sufficient to classify all possible ways a geodesic (θ, α) may intersect $\mathcal{B}_A$.

Δ_A from the Boundary Perspective

We now interpret the three types of bulk geodesics from the boundary perspective of kinematic space, i.e. we see the points (θ, α) in $\mathcal{K}$ as the entangling intervals on the constant time slice of the CFT (see Section 5.1.2). So the three types of bulk geodesics give rise to three types of boundary intervals. We note that in the discussion of the different types of geodesics, we constructed the corresponding regions of integration Δ_A solely by using the geometry of $\mathcal{K}$. This allows us to translate the construction of Δ_A to the boundary perspective. The resulting method for defining Δ_A goes as follows.

Type (a) Boundary Intervals. The boundary intervals (θ, α) associated
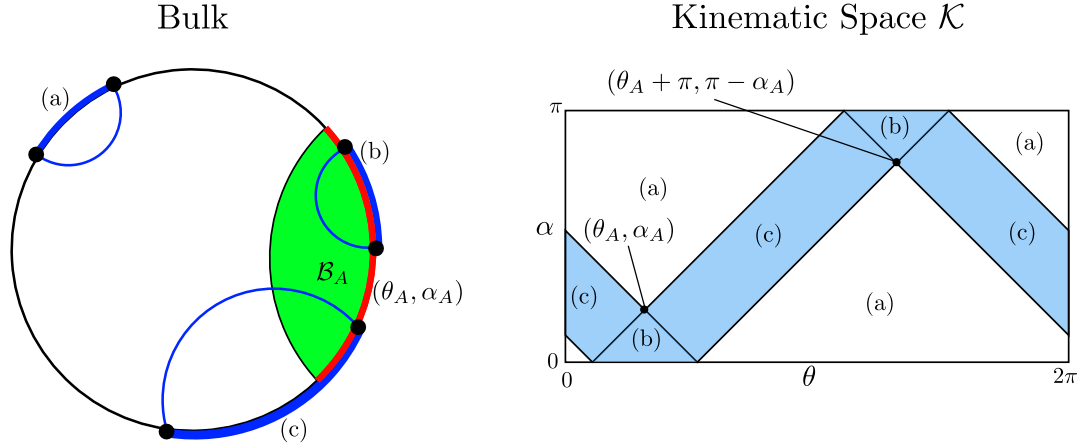
Figure 5.10: Three different types of boundary intervals on a constant time slice. L.h.s.: The bulk geodesics of type (a), (b) and (c) depicted in Figure 5.8 may be associated with boundary intervals of type (a), (b) and (c) in the boundary perspective of kinematic space. By doing so we conclude that type (a) intervals have none of their endpoints lying in the interval (θ_A, α_A), whereas for type (b) intervals both endpoints lie inside of (θ_A, α_A). Moreover, an interval is of type (c) if only one of its endpoints lies in (θ_A, α_A). R.h.s: In kinematic space, type (a) intervals either lie in the future light cone of the interval (θ_A, α_A) or in the past light cone of the complementary interval, $(\theta_A + \pi, \pi - \alpha_A)$. Intervals of type (b) lie in the past of (θ_A, α_A) or the future of $(\theta_A + \pi, \pi - \alpha_A)$. Type (c) intervals are causally disconnected from (θ_A, α_A) and $(\theta_A + \pi, \pi - \alpha_A)$. The set of type (c) intervals is referred to as causal wings.

with type (a) bulk geodesics are referred to as type (a) as well. It is easy to see that the defining property of type (a) intervals is the fact that both of its boundary points do not lie inside of the interval (θ_A, α_A) (see Figure 5.10). The region of integration $\Delta_A(\theta, \alpha)$ is the empty set in this situation.

Type (b) Boundary Intervals. A bulk geodesic of type (b) corresponds to a boundary interval (θ, α) with both endpoints located in the interval (θ_A, α_A) (see Figure 5.10). These boundary intervals are called type (b). The two endpoints of (θ, α) may be interpreted as points on the lower boundary of $\mathcal{K}$, as pointed out in Section 5.1.1. The region of integration $\Delta_A(\theta, \alpha)$ is given by the subset of $\mathcal{K}$ that is bounded by the light rays starting at these points (see Figure 5.9).

Type (c) Boundary Intervals. As depicted in Figure 5.10, bulk geodesics of type (c) correspond to boundary intervals (θ, α) that only partially lie inside of (θ_A, α_A). We refer to them as type (c) as well. We find that one endpoint of type (c) intervals lies inside of (θ_A, α_A) and the other lies outside of (θ_A, α_A). The corresponding region of integration $\Delta_A(\theta, \alpha)$ is bounded by the light rays in $\mathcal{K}$ starting at the boundary point of $\mathcal{K}$ associated with the endpoint of (θ, α) inside of (θ_A, α_A) and the space-like geodesic in $\mathcal{K}$ that intersects (θ, α) and (θ_A, α_A) (see Figure 5.9).

The construction rule of $\Delta_A(\theta, \alpha)$ for the three types of entangling intervals only requires knowledge of the position of the endpoints of (θ, α) relative to (θ_A, α_A) and the geometry (5.10) of kinematic space. Both these aspects are well understood from the boundary perspective (see Section 5.1.2) and do not require any reference to the bulk. Thus we see that $\Delta_A(\theta, \alpha)$ can be constructed from the CFT side, which justifies the statement that (5.53) is a field theory expression for HSRC.

As a side remark we note that only entangling intervals with at least one endpoint inside of (θ_A, α_A) contribute to the double integral (5.53) over $\mathcal{K}$ giving subregion complexity. For the outer integral over θ and α this is evident since $\Delta_A(\theta, \alpha)$ is empty for all intervals with both endpoints outside of (θ_A, α_A), i.e. type (a) intervals.

In order to see this for the inner integral over θ' and α' we interpret the points in $\mathcal{K}$ as bulk geodesics. In this picture, the inner integral over $\Delta_A(\theta, \alpha)$ computes the length of the chord of (θ, α) lying inside of $\mathcal{B}_A$. Therefore, $\Delta_A(\theta, \alpha)$ only contains geodesics that intersect this chord (see Section 5.1.1). If there would be such a geodesic with both endpoints lying outside of $\mathcal{B}_A$, it would evidently intersect the geodesic (θ_A, α_A) twice, which is not possible for the bulk geometries we consider. Consequently, any geodesic contained in $\Delta_A(\theta, \alpha)$ is of type (b) or (c) and therefore corresponds to a boundary interval of the same type. Per definicionem, boundary intervals of type (b) and (c) have at least one endpoint lying inside of the boundary interval (θ_A, α_A).

Position of the Three Types of Boundary Intervals in Kinematic Space

We conclude our discussion of the regions of integration Δ_A appearing in our CFT expression for HSRC (5.53) by discussing the location of the three types of entangling intervals in kinematic space. As we depict in Figure 5.10, the causal structure of $\mathcal{K}$ (5.10) allows us to identify the intervals of types (a), (b) and (c) in a very straightforward way in $\mathcal{K}$.

Location of Type (a) Intervals. An interval of type (a) has both its endpoints lying outside of (θ_A, α_A). Consequently, it either completely contains (θ_A, α_A) or is completely contained in the complement of (θ_A, α_A). Using the interpretation of the causal structure of $\mathcal{K}$ in terms of the partial ordered structure of entangling intervals presented in Section 5.1.2, we therefore find that type (a) intervals either lie in the future of (θ_A, α_A) or the past of its complement, $(\theta_A + \pi, \pi - \alpha_A)$ (see Figure 5.10).

Location of Type (b) Intervals. Intervals of type (b) have both endpoints contained in (θ_A, α_A) (see Figure 5.10). Consequently, they are either intervals completely contained in (θ_A, α_A) or the complement of such intervals. Just as for type (a) intervals, the interpretation of the causal structure of $\mathcal{K}$ in terms of entangling intervals allows us to associate a certain region in $\mathcal{K}$ with type (b) intervals: they either lie in the past of (θ_A, α_A) or the future of its complement, $(\theta_A + \pi, \pi - \alpha_A)$.

Location of Type (c) Intervals. The remaining intervals are of type (c). They are characterized by the fact that they have one endpoint lying in (θ_A, α_A) and one in its complement $(\theta_A + \pi, \pi - \alpha_A)$ (see Figure 5.10). Therefore, they are causally disconnected from (θ_A, α_A) and $(\theta_A + \pi, \pi - \alpha_A)$, as we may conclude by interpreting once more the causal structure of $\mathcal{K}$ in terms of entangling intervals. The region in $\mathcal{K}$ containing points with this property is bounded by the light rays emitted from the points on the lower boundary of $\mathcal{K}$ that correspond to the endpoints of (θ_A, α_A). It takes the form of two causal diamonds attached to the past light cone of (θ_A, α_A) (see Figure 5.10). These squares are referred to as *causal wings* [97].

5.3.3   Holographic Subregion Complexity for Global AdS$_3$

We now demonstrate how to apply our CFT formula for HSRC (5.53) to explicit examples. The CFT state we consider is the vacuum state dual to global AdS$_3$. First we calculate the HSRC for the whole circle forming the constant time slice of the CFT and then for half of that circle.

Cut-Off in Kinematic Space

Since our formula (5.53) for the HSRC of an entangling interval (θ_A, α_A) is constructed to give the volume of a bulk region $\mathcal{B}_A$ expanding to the conformal boundary, it is easy to see that (5.53) is divergent and a cut-off procedure is required. When computing HSRC by determining $\mathrm{vol}(\mathcal{B}_A)$ directly in the bulk, usually a radial cut-off at $\tilde{r} = L\ell_{\mathrm{CFT}}/\epsilon$ is introduced, where we use the coordinates (5.13) for global AdS$_3$ and ℓ_{CFT} is the radius of the circle the CFT is defined on (see Sections 3.2.3, 4.1.2). Here however, we aim at computing HSRC from the field theory side. Therefore, the use of a radial cut-off would be counter intuitive. Instead we introduce a cut-off procedure that is natural for calculations in kinematic space. By using the coordinates θ and α (5.2) for $\mathcal{K}$, we may introduce a horizontal cut-off at $\alpha = \xi$ and $\alpha = \pi - \xi$, where $\xi \ll 1$ (see Figure 5.11). Since bulk geodesics with small opening angle α asymptote to the conformal boundary of the bulk (see Section 5.1.1), it is easy to see that the integrand in (5.53) diverges for $\alpha \longrightarrow 0$. This justifies the cut-off at $\alpha = \xi$. Moreover, the geodesics with opening angle $\alpha \longrightarrow \pi$ also asymptote to the conformal boundary, which is evident by considering Figure 5.1. Therefore, a further cut-off is required at $\alpha = \pi - \xi$. In the boundary perspective of kinematic space this cut-off procedure implies that we only consider entangling intervals with an opening angle larger than ξ and whose complement also have an opening angle larger than ξ.

We note that this cut-off scheme may not be associated with a radial cut-off in the bulk. To be more precise, we cannot find a radial cut-off $\tilde{r} = L\ell_{\mathrm{CFT}}/\epsilon$ such that the kinematic space formula (5.53) with cut-off at $\alpha = \xi$ and $\alpha = \pi - \xi$ computes the volume of the part $\mathcal{B}_A^\epsilon$ of the bulk region $\mathcal{B}_A$ above the radial cut-off for any entangling interval (θ_A, α_A). We can see this by making the following consideration. Our formula (5.53) is an application of the volume formula (5.12) to $\mathcal{B}_A$. In order for the kinematic space cut-off ξ to correspond to a radial cut-off ϵ we would require the cut-off version of the kinematic space integral (5.53)
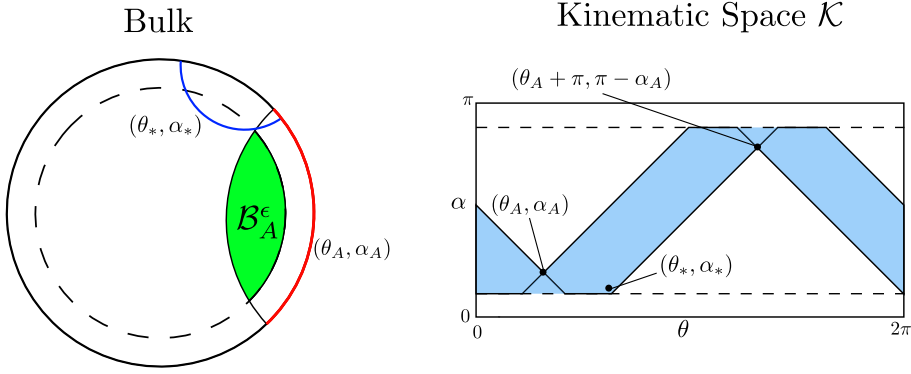
Figure 5.11: Comparing the kinematic space cut-off (r.h.s.) with the radial cut-off in the bulk (l.h.s.). R.h.s.: when working with our field theory expression for HSRC (5.53), which is based on integrals over kinematic space, it is natural to introduce a cut-off at $\alpha = \xi$ and $\alpha = \pi - \xi$ in kinematic space. The resulting region in $\mathcal{K}$ contributing to the integrals in (5.53), i.e. type (b) and (c) geodesics (intervals) are depicted in blue. L.h.s.: Considering a kinematic space cut-off ξ is not the same as working with a radial cut-off in the bulk (dashed circle). For instance, the geodesic (θ_*, α_*) does not contribute to the volume of $\mathcal{B}_A^\epsilon$ (green), which is the volume providing HSRC in the radial cut-off scheme (5.50). The reason for that is the fact that (θ_*, α_*) does not intersect $\mathcal{B}_A^\epsilon$ and therefore does not contribute to the kinematic space integral (5.12) providing $\mathrm{vol}(\mathcal{B}_A^\epsilon)$. However, (θ_*, α_*) does contribute in the kinematic space cut-off scheme, since it is contained in the blue region in $\mathcal{K}$ (r.h.s.).

to correspond to the volume formula applied to $\mathcal{B}_A^\epsilon$. However, as follows from our discussion of the volume formula in Section 5.2, this would imply that only geodesics (θ, α) intersecting $\mathcal{B}_A^\epsilon$ contribute to the cut-off version of the kinematic space integral (5.53), which is not the case, as we show in Figure 5.11.

Subregion Complexity for the Whole Constant Time Slice

In order to apply our CFT formula (5.53) to the circle which is the whole constant time slice of the field theory, we introduce the cut-off at $\alpha, \alpha' = \xi$ and $\alpha, \alpha' = \pi - \xi$, as explained above,

$$
\begin{aligned}
\mathcal{C}(circle) =& \frac{9}{8\pi c^2} \int_{\mathcal{K}} d\theta d\alpha \int_{\Delta_A(\theta,\alpha)} d\theta' d\alpha' \partial_\alpha^2 S(\alpha) \partial_{\alpha'}^2 S(\alpha') \\
\longrightarrow & \frac{9}{8\pi c^2} \int_0^{2\pi} d\theta \int_\xi^{\pi-\xi} d\alpha \, \partial_\alpha^2 S(\alpha) \int_{\Delta_A^\xi(\theta,\alpha)} d\theta' d\alpha' \partial_{\alpha'}^2 S(\alpha') \, ,
\end{aligned}
\tag{5.54}
$$

where $\Delta_A^\xi(\theta, \alpha)$ is the part of $\Delta_A(\theta, \alpha)$ containing only points (θ', α') in $\mathcal{K}$ for which $\xi \leq \alpha' \leq \pi - \xi$ holds (see Figure 5.12). Since (θ_A, α_A) is the whole CFT constant time slice, all entangling intervals (θ, α) are of type (b) (see Section 5.3.2). We first determine the integral over θ' and α' in (5.54). By using the expression (5.14)
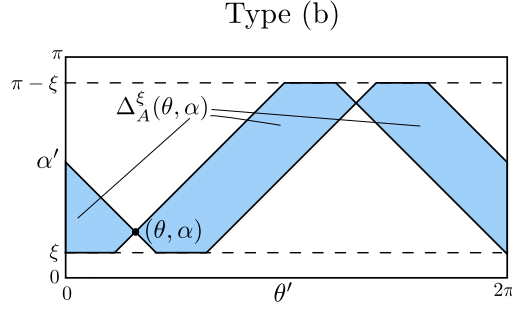
Type (b)

Figure 5.12: The region of integration $\Delta_A^\xi(\theta, \alpha)$ for a type (b) geodesics (intervals). By introducing the kinematic space cut-off at $\alpha' = \xi$ and $\alpha' = \pi - \xi$, the region of integration $\Delta_A(\theta, \alpha)$ (see Figure 5.9) in (5.53) is replaced by $\Delta_A^\xi(\theta, \alpha)$ (blue).

for the entanglement entropy, it is easy to verify that

$$\int_{\Delta_A^\xi(\theta,\alpha)} d\theta' d\alpha' \partial_{\alpha'}^2 S(\alpha') = -\frac{8c}{3} \left(\log\left(\frac{\sin(\alpha)}{\sin(\xi)}\right) + \xi \cot(\xi) \right) \qquad (5.55)$$

holds. Now we insert this result into (5.54), which leads to

$$\mathcal{C}(circle) = 4\left(\xi \cot^2(\xi) + \cot(\xi) + \xi - \frac{\pi}{2} \right) = \frac{8}{\xi} - 2\pi + \mathcal{O}(\xi^2). \qquad (5.56)$$

In the limit $\xi \longrightarrow 0$ this result for HSRC can be matched to the expression (4.12) obtained in Section 4.2.1 from the Gauss-Bonnet theorem by setting $\xi = 4\epsilon/\pi\ell_{\text{CFT}}$. Note that even though the cut-off scheme for kinematic space does not correspond to a radial cut-off scheme in the bulk, it is still possible to recover the same divergent behavior and the same ξ^0 term, i.e. -2π, from both schemes. In particular, this supports the idea that the constant term in HSRC is universal (see Section 3.2.3).

Subregion Complexity for Half of the Constant Time Slice

We now apply our CFT formula for HSRC (5.53) to the semicircle corresponding to half of the constant time slice of the CFT, i.e. we set $(\theta_A, \alpha_A) = (0, \pi/2)$. As for the computation of the HSRC for the whole circle (5.54), we introduce cut-offs at $\alpha, \alpha' = \xi$ and $\alpha, \alpha' = \pi - \xi$ in $\mathcal{K}$. This leads to the following expression for HSRC,

$$\mathcal{C}(0, \pi/2) = \frac{9}{8\pi c^2} \int_0^{2\pi} d\theta \int_\xi^{\pi-\xi} d\alpha \, \Lambda_\xi(\theta, \alpha) \partial_\alpha^2 S(\alpha), \qquad (5.57)$$

where

$$\Lambda_\xi(\theta, \alpha) = \int_{\Delta_A^\xi(\theta,\alpha)} d\theta' d\alpha' \partial_{\alpha'}^2 S(\alpha'). \qquad (5.58)$$

When computing the HSRC for the whole constant time slice, all contributing entangling intervals (θ, α) were of type (b). Here however, also intervals of type (c) are present. The location of type (b) and (c) boundary intervals in kinematic
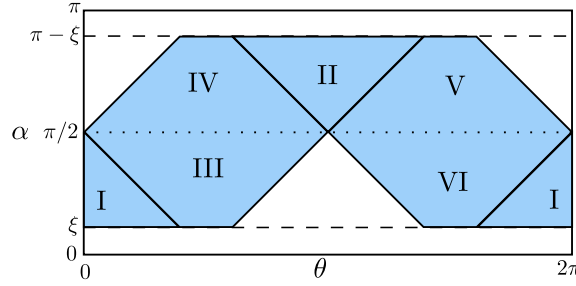
Figure 5.13: Location of type (b) and (c) intervals for $(\theta_A, \alpha_A) = (0, \pi/2)$. If we consider the complexity for half of the full constant time slice, i.e. a semicircle, we find the corresponding type (b) and (c) intervals located in the blue region in kinematic space. Regions I and II contain type (b) intervals, whereas type (c) intervals are located in III - VI. The symmetry of the Crofton form (5.15) implies that the region I contributes in the same way to the integrals in HSRC (5.57) as II. Moreover, the contributions of regions III - VI are also the same. This allows us to write (5.57) as an integral over I and III (5.59).

space is depicted in Figure 5.13. Intervals of type (b) are contained in the regions I and II, while type (c) intervals can be found in regions III – VI. By using the symmetry of the Crofton form (5.15), it is easy to verify that the regions I and II give the same contribution to $\mathcal{C}(0, \pi/2)$. The same statement holds for the regions III – VI. Therefore, we can rewrite (5.57) in terms of integrals over the regions I and III,

$$
\mathcal{C}(0, \pi/2) = \frac{9}{4\pi c^2} \left(\int_{\xi}^{\pi/2} d\alpha \int_{\alpha-\pi/2}^{\pi/2-\alpha} d\theta \, \Lambda_\xi(\theta, \alpha) \partial_\alpha^2 S(\alpha) \right.
$$
$$
\left. + 2 \int_{\xi}^{\pi/2} d\alpha \int_{\pi/2-\alpha}^{\pi/2+\alpha} d\theta \, \Lambda_\xi(\theta, \alpha) \partial_\alpha^2 S(\alpha) \right).
$$

(5.59)

Here, the first term corresponds to region I and computes the contributions of type (b) intervals, while the second corresponds to region III and is therefore associated with the type (c) intervals. We already determined $\Lambda_\xi(\theta, \alpha)$ for type (b) intervals (θ, α) in (5.55). Inserting the corresponding result into (5.59) yields

$$
\mathcal{C}(0, \pi/2) = \frac{9}{4\pi c^2} \left[-\frac{8c}{3} \int_{\xi}^{\pi/2} d\alpha \int_{\alpha-\pi/2}^{\pi/2-\alpha} d\theta \left(\log\left(\frac{\sin(\alpha)}{\sin(\xi)}\right) + \xi \cot(\xi) \right) \partial_\alpha^2 S(\alpha) \right.
$$
$$
\left. + 2 \int_{\xi}^{\pi/2} d\alpha \int_{\pi/2-\alpha}^{\pi/2+\alpha} d\theta \, \Lambda_\xi(\theta, \alpha) \partial_\alpha^2 S(\alpha) \right].
$$

(5.60)

Computing $\Lambda_\xi(\theta, \alpha)$ for (θ, α) of type (c) turns out to be a challenging task. In this case $\Delta_A(\theta, \alpha)$ is not just bounded by light rays – as it is the case for type (b) intervals – but also by generic point curves. In particular, these point curves cross the cut-off at $\alpha = \xi$ and $\alpha = \pi - \xi$ in some cases (see Figure 5.14). This would require to distinguish several special cases for the shape of the region of integration $\Delta_A^\xi(\theta, \alpha)$ when determining $\Lambda_\xi(\theta, \alpha)$ via the integral given in (5.58).
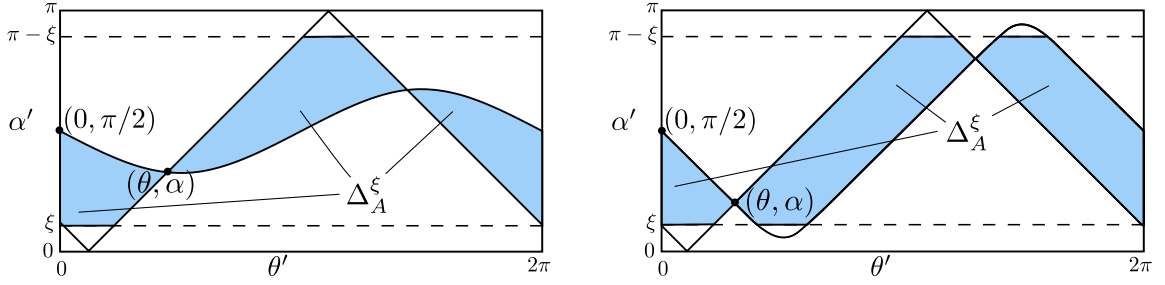
Figure 5.14: The region of integration Δ_A^ξ for type (c) intervals. When computing the HSRC of the semicircle, i.e. half of the constant time slice, via (5.53) we need to distinguish two different cases for the region of integration Δ_A^ξ for type (c) intervals: The space like geodesic bounding Δ_A^ξ may lie completely above the kinematic space cut-off i.e. the dashed line, (l.h.s.) or partially below it (r.h.s.). The fact that we need to take both these cases into account makes the computation of HSRC via (5.53) particularly involved.

However, we can avoid this rather technical computation in the special case of the semicircle by making use of the symmetry of this setup, as we now explain. In the following we effectively only use symmetries of the Crofton form (5.15) and the region of integration in $\mathcal{K}$, i.e. $\Delta_A^\xi(\theta, \alpha)$, but since discussing these symmetries is most easily done in the bulk perspective of kinematic space, we now treat points (θ, α) in $\mathcal{K}$ as bulk geodesics.

Following the derivation of our CFT formula for HSRC (5.53), we see that $\Lambda_\xi(\theta, \alpha)$ computes, up to a multiplicative factor and differences in the cut-off scheme, the length of the chord of (θ, α) lying inside of the bulk region $\mathcal{B}_A$ (5.51). Having a type (c) bulk geodesic (θ, α) in region III (see Figure 5.13), it is easy to see that region III also contains a geodesic $(\tilde{\theta}, \alpha)$ whose chord length is given by the length of the segment of (θ, α) lying outside of $\mathcal{B}_A$. We depict this setup in Figure 5.15. So we find that the sum of these two chord lengths give the total length of (θ, α). Moreover, since the cut-off in kinematic space is independent of θ, it is easy to see that this statement also holds in the kinematic space cut-off scheme, i.e.

$$\Lambda_\xi(\theta, \alpha) + \Lambda_\xi(\tilde{\theta}, \alpha) = -\frac{8c}{3}\left(\log\left(\frac{\sin(\alpha)}{\sin(\xi)}\right) + \xi \cot(\xi) \right), \tag{5.61}$$

where the r.h.s. of this equality gives, up to a multiplicative factor, the full length of (θ, α) when computed by using the kinematic space cut-off scheme, i.e. (5.55). Thus we can replace the remaining $\Lambda_\xi(\theta, \alpha)$ for type (c) in (5.60) by (5.61) when we multiply the corresponding term by $1/2$. This leads to

$$\mathcal{C}(0, \pi/2) = -\frac{6}{\pi c} \int_\xi^{\pi/2} d\alpha \int_{\alpha - \pi/2}^{\alpha + \pi/2} d\theta \left(\log\left(\frac{\sin(\alpha)}{\sin(\xi)}\right) + \xi \cot(\xi) \right) \partial_\alpha^2 S(\alpha)$$
$$= 2\xi \cot^2(\xi) + 2 \cot(\xi) + 2\xi - \pi = \frac{4}{\xi} - \pi + \mathcal{O}(\xi^2). \tag{5.62}$$

Just as for the HSRC of the whole constant time slice (5.56), we see that in the
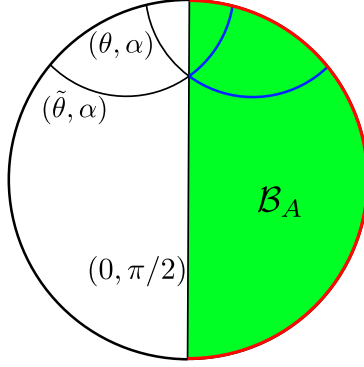
Figure 5.15: Visualization of the symmetry argument used to compute HSRC for the semicircle. Consider a geodesic (θ, α) in the constant time slice of the bulk which we w.l.o.g. assume to correspond to a point in region III in kinematic space (see Figure 5.13). Using the symmetry of the bulk region $\mathcal{B}_A$ (green) we may find a bulk geodesic $(\tilde{\theta}, \alpha)$ corresponding to a point in region III such that the sum of the chord lengths of (θ, α) and $(\tilde{\theta}, \alpha)$ (blue) gives the total length of (θ, α). This observation allows us to simplify the integral expression (5.60) for the HSRC of the semicircle to (5.62).

limit $\xi \longrightarrow 0$, we can match this result for HSRC obtained by a computation in kinematic space with the one presented in (4.11) derived by a computation in the bulk. This matching is obtained by setting $\xi = 4\epsilon/\pi\ell_{\text{CFT}}$. Once more we see that both the kinematic space cut-off scheme as well as the radial cut-off scheme in the bulk (4.4) provide the same constant term, i.e. $-\pi$, for complexity. This gives further support to the statement that this term is universal (see Section 3.2.3).

5.3.4 Holographic Subregion Complexity for the Poincaré Patch

Our CFT formula for HSRC (5.53) provides us with a way to compute the HSRC for a generic entangling interval (χ_A, σ_A) for the Poincaré patch (3.33) in field theory. We work with the kinematic space coordinates (χ, σ) defined in (5.39). Here we only consider the $\sigma \geq 0$, i.e. we do not distinguish between different orientations of bulk geodesics. Evidently, the two orientations of a bulk geodesic contribute in the same way to the volume formula. Therefore, restricting to one orientation just requires us to adapt the integrals over $\mathcal{K}$ in the volume formula (5.50) and the chord length (5.51) by a multiplicative factor of two. We therefore find, by adapting our formula for HSRC (5.53) accordingly,

$$\mathcal{C}(\chi_A, \sigma_A) = \frac{9}{2\pi c^2} \int_{-\infty}^{\infty} d\chi \int_{\xi}^{\infty} d\sigma \Lambda_\xi(\chi, \sigma) \partial_\sigma^2 S(\sigma) \,, \qquad (5.63)$$

where

$$\Lambda_\xi(\chi, \sigma) = \int_{\Delta_A^\xi(\chi, \sigma)} d\chi' d\sigma' \partial_{\sigma'}^2 S(\sigma') \,. \qquad (5.64)$$

Here, the entanglement entropy $S(\sigma)$ is given by (3.39). Moreover, analogously to our discussion of HSRC for global AdS$_3$, we have introduced the cut-off ξ for the σ and σ' coordinate. The region of integration Δ_A^ξ is again the part of Δ_A lying above the cut-off. As discussed in Section 5.3.2, we need to distinguish between entangling intervals (χ, σ) of type (a), (b) and (c) for the construction of $\Delta_A(\chi, \sigma)$. The region of integration $\Delta_A(\chi, \sigma)$ is only non-vanishing if (χ, σ) is of type (b) or (c).

If (χ, σ) is of type (b), $\Delta_A(\chi, \sigma)$ is bounded by the light rays

$$(\tilde{\chi}, \tilde{\sigma}_\pm(\tilde{\chi})), \quad \text{where} \quad \tilde{\sigma}_\pm(\tilde{\chi}) = |\chi \pm \sigma - \tilde{\chi}|. \tag{5.65}$$

In this case, $\Lambda_\xi(\chi, \sigma)$ is given by

$$\Lambda_\xi^{(b)}(\sigma) = -\frac{4c}{3}\left(\log\left(\sigma/\xi\right) + 1\right). \tag{5.66}$$

For type (c) intervals (χ, σ), $\Delta_A(\chi, \sigma)$ is bounded by the point curve in $\mathcal{K}$ intersecting (χ, σ) and (χ_A, σ_A) and the light rays in $\mathcal{K}$ corresponding to the boundary point of the interval (χ, σ) lying inside of (χ_A, σ_A). The latter is of the form (5.65), where the $-$ $(+)$ corresponds to the case where the left (right) endpoint of (χ, σ) lies inside of (χ_A, σ_A).

The point curve intersecting (χ, σ) and (χ_A, σ_A) may be constructed as follows. We consider the bulk perspective of $\mathcal{K}$, i.e. we interpret the elements of $\mathcal{K}$ as geodesics in the bulk. By considering the equation (5.43) for a generic bulk geodesic on the constant time slice of the Poincaré patch, it is easy to see that the point curve $(\tilde{\chi}, \tilde{\sigma}(\tilde{\chi}))$, associated with an arbitrary bulk point (x, z) in the constant time slice, is given by

$$\tilde{\sigma}(\tilde{\chi}) = \sqrt{(x - \tilde{\chi})^2 + z^2}. \tag{5.67}$$

By imposing that this point curve crosses (χ, σ) and (χ_A, σ_A), i.e. $\tilde{\sigma}(\chi) = \sigma$ and $\tilde{\sigma}(\chi_A) = \sigma_A$, we find

$$x = \frac{\sigma^2 - \sigma_A^2 - \chi^2 + \chi_A^2}{2(\chi - \chi_A)} \quad \text{and} \quad z = \sqrt{\sigma^2 - (x - \chi)^2}. \tag{5.68}$$

Therefore, the point curve $(\tilde{\chi}, \tilde{\sigma}(\tilde{\chi}))$ bounding $\Delta_A(\chi, \sigma)$ is given by

$$\tilde{\sigma}(\tilde{\chi}) = \sqrt{(x - \tilde{\chi})^2 + \sigma^2 - (x - \chi)^2}, \tag{5.69}$$

where x is given by (5.68).

For an interval (χ, σ) of type (c) we find $\Lambda_\xi(\chi, \sigma)$ (5.64) to be

$$\Lambda_\xi^{(c),\pm}(\chi, \sigma) = \frac{1}{2}\Lambda_\xi^{(b)}(\sigma) + \Xi^\pm(\chi, \sigma), \tag{5.70}$$

where x and $\Lambda_\xi^{(b)}(\sigma)$ are given by (5.68) and (5.66) respectively and

$$\Xi^\pm(\chi, \sigma) = -\frac{c}{3}\log\left(\frac{\sigma \pm (\chi - x)}{\sigma \mp (\chi - x)}\right) \tag{5.71}$$
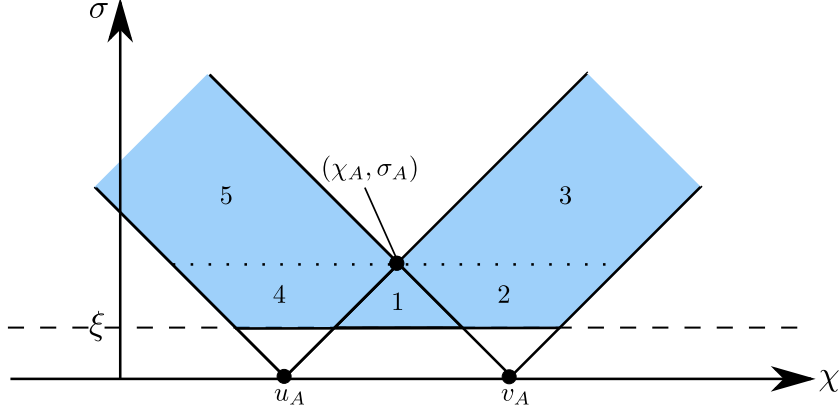
Figure 5.16: The five regions of integration in $\mathcal{K}$ appearing in (5.72). The region i $(i = 1, \ldots, 5)$ is integrated over in the ith term in (5.72). By identifying the χ axis of $\mathcal{K}$ with the constant time slice of the CFT (see Section 5.1.1) we may identify the lower edges of the regions of integration with the endpoints u_A, v_A of the considered entangling interval A.

holds. Here, Ξ^+ (Ξ^-) refers to the situation where the right (left) endpoint of the interval (χ, σ) lies inside of (χ_A, σ_A). Note that in the computation of $\Lambda_\xi^{(c),\pm}$ we assumed that the point curve (5.69) stays above the cut-off. The error for $\mathcal{C}$ that is caused by this assumption is of order ξ and therefore irrelevant in the $\xi \longrightarrow 0$ limit.

Separating the type (b) and (c) intervals in (5.63) from each other and inserting (3.39), we obtain

$$\mathcal{C}(\chi_A, \sigma_A) = \frac{-3}{2\pi c} \Big[\int_\xi^{\sigma_A} d\sigma \int_{u_A+\sigma}^{v_A-\sigma} \frac{d\chi}{\sigma^2} \Lambda_\xi^{(b)} + \int_\xi^{\sigma_A} d\sigma \int_{v_A-\sigma}^{v_A+\sigma} \frac{d\chi}{\sigma^2} \Lambda_\xi^{(c),-}$$
$$+ \int_{\sigma_A}^\infty d\sigma \int_{u_A+\sigma}^{v_A+\sigma} \frac{d\chi}{\sigma^2} \Lambda_\xi^{(c),-} + \int_\xi^{\sigma_A} d\sigma \int_{u_A-\sigma}^{u_A+\sigma} \frac{d\chi}{\sigma^2} \Lambda_\xi^{(c),+} \qquad (5.72)$$
$$+ \int_{\sigma_A}^\infty d\sigma \int_{u_A-\sigma}^{v_A-\sigma} \frac{d\chi}{\sigma^2} \Lambda_\xi^{(c),+} \Big] \,,$$

where $u_A = \chi_A - \sigma_A$ and $v_A = \chi_A + \sigma_A$ are the endpoints of the interval (χ_A, σ_A). The five integrals in (5.72) correspond to the five regions in $\mathcal{K}$ depicted in Figure 5.16. By using the expression (5.70) for $\Lambda_\xi^{(c),\pm}$, we can bring (5.72) into the form

$$\mathcal{C}(\chi_A, \sigma_A) = \frac{-3}{2\pi c} \Big[\int_\xi^\infty d\sigma \frac{2\sigma_A}{\sigma^2} \Lambda_\xi^{(b)} + \int_\xi^{\sigma_A} d\sigma \int_{v_A-\sigma}^{v_A+\sigma} \frac{d\chi}{\sigma^2} \Xi^- + \int_{\sigma_A}^\infty d\sigma \int_{u_A+\sigma}^{v_A+\sigma} \frac{d\chi}{\sigma^2} \Xi^-$$
$$+ \int_\xi^{\sigma_A} d\sigma \int_{u_A-\sigma}^{u_A+\sigma} \frac{d\chi}{\sigma^2} \Xi^+ + \int_{\sigma_A}^\infty d\sigma \int_{u_A-\sigma}^{v_A-\sigma} \frac{d\chi}{\sigma^2} \Xi^+ \Big] \,.$$
$$(5.73)$$

The first integral in (5.73) provides the divergent part of $\mathcal{C}(\chi_A, \sigma_A)$,

$$\frac{-3}{2\pi c} \int_\xi^\infty d\sigma \frac{2\sigma_A}{\sigma^2} \Lambda_\xi^{(b)} = \frac{8\sigma_A}{\pi \xi} \,. \qquad (5.74)$$

The remaining integrals stay finite in the limit $\xi \longrightarrow 0$ and can be brought into the form

$$\int_0^\infty d\sigma \, \frac{2}{\pi \sigma^2} \left[\sigma_A \log \left| \frac{\sigma_A^2}{\sigma_A^2 - \sigma^2} \right| + \sigma \log \left| \frac{\sigma_A - \sigma}{\sigma_A + \sigma} \right| \right] + \mathcal{O}(\xi) = -\pi + \mathcal{O}(\xi). \quad (5.75)$$

Combining (5.74) and (5.75), we obtain

$$\mathcal{C}(\chi_A, \sigma_A) = \frac{8\sigma_A}{\pi \xi} - \pi + \mathcal{O}(\xi). \quad (5.76)$$

We can match the divergent part of $\mathcal{C}$ to the one obtained in (3.74), where the radial bulk cut-off $z = \epsilon$ was used, by setting $\xi = 4\epsilon/\pi$ and adapting the convention for the prefactor of HSRC (see beginning of Section 5.3). As for the HSRC for global AdS$_3$ (see Section 5.3.3), we find that the constant term, i.e. $-\pi$, in $\mathcal{C}$ obtained by the kinematic space cut-off scheme agrees with the constant term in (3.74) obtained from the radial cut-off scheme in the bulk. This supports the proposal stating that this term is universal (see Section 3.2.3).

5.3.5 Holographic Subregion Complexity in Terms of Mutual Information for the Poincaré Patch

As a side remark we present an alternative formulation of our expression (5.50) for the volume $\mathrm{vol}(\mathcal{B}_A)$ associated with HSRC (5.49) for the Poincaré patch. This reformulation may be more accessible for physical interpretation than our CFT expression for HSRC (5.53). It is based on the bulk perspective of kinematic space, i.e. points (χ, σ) in $\mathcal{K}$ will be interpreted as geodesics in the bulk. Just as in Section 5.3.4 we are only working with one orientation of the geodesics, i.e. we only consider $\sigma \geq 0$. Therefore, we again adapt the volume formula (5.50) by a multiplicative factor of two,

$$\frac{\mathrm{vol}(\mathcal{B}_A)}{4G_3} = \frac{1}{\pi} \int_{\sigma \geq 0} \omega_{\mathcal{K}} \lambda_{\mathcal{B}_A}, \quad (5.77)$$

where $\omega_{\mathcal{K}}$ is given by (5.40). Following the discussion of Section 5.3.2, we may distinguish geodesics lying completely inside of $\mathcal{B}_A$ (type (b)) and geodesics lying only partially inside of $\mathcal{B}_A$ (type (c)). For geodesics of type (b) the chord length $\lambda_{\mathcal{B}_A}$ is the total length of the geodesic. The RT formula (3.32) implies that this chord length may be interpreted as the entanglement entropy of the corresponding entangling interval. These considerations allow us to rewrite (5.77) as follows,

$$\frac{\mathrm{vol}(\mathcal{B}_A)}{4G_3} = -\frac{2G_3}{\pi} \int_{\text{type (b)}} d\chi d\sigma S \partial_\sigma^2 S - \frac{1}{2\pi} \int_{\text{type (c)}} d\chi d\sigma \lambda_{\mathcal{B}_A} \partial_\sigma^2 S, \quad (5.78)$$

where the regions of integration of the two integrals are the geodesics of type (b) and (c) respectively. Before we continue with our discussion, we need to stress that the entanglement entropy S, chord length $\lambda_{\mathcal{B}_A}$ and the integrals over them are divergent in (5.78). Thus, a proper cut-off scheme is necessary for applying (5.78) to explicit examples.
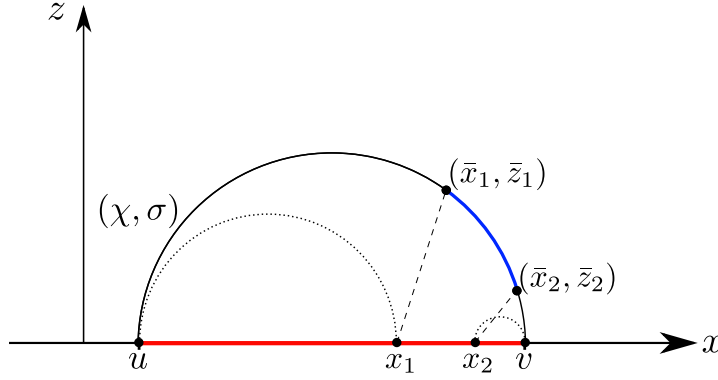
Figure 5.17: Associating points on a geodesic in the constant time slice of the Poincaré patch with boundary points. The mapping (5.79) may be used to identify points $(\bar{x}_i, \bar{z}_i)$, $i = 1, 2$ on the bulk geodesic (χ, σ) with points x_i on the conformal boundary at $z = 0$. The points x_i lie in the interval $[u, v]$ (red) associated with (χ, σ). Assuming $(x_1 - u)(v - x_2)$ to be sufficiently small, the RT surface of $[x_1, x_2] \cup [u, v]^c$ is given by the dotted curves. This allows us to express the geodesic distance between $(\bar{x}_1, \bar{z}_1)$ and $(\bar{x}_2, \bar{z}_2)$ (length of the blue curve) i.t.o. the mutual information $I([x_1, x_2] : [u, v]^c)$ (see (5.80), (5.82) and (5.84)).

In (5.78) we see that we can interpret the contribution of type (b) geodesics in terms of entanglement entropy. In the rest of this section we present an expression for the remaining integral over type (c) geodesics in terms of mutual information (3.15). This expression is based on the interpretation of geodesic distances in the bulk in terms of mutual information introduced in [213]. We first review this interpretation and then apply it to the chord lengths of type (c) geodesics.

Consider two bulk points $p_1 = (\bar{x}_1, \bar{z}_1)$ and $p_2 = (\bar{x}_2, \bar{z}_2)$ on the constant time slice lying on the same geodesic (χ, σ). [8] In [213] the bulk modular flow was used to assign boundary points x_1, x_2 to p_1 and p_2 respectively which lie inside the entangling interval associated with (χ, σ),

$$x_i = \frac{\sigma^2 - \sqrt{\sigma^4 - (\bar{x}_i - \chi)^2 \sigma^2}}{\bar{x}_i - \chi} + \chi, \quad i = 1, 2. \tag{5.79}$$

We depict this procedure in Figure 5.17. Assuming w.l.o.g. $x_1 \leq x_2$, the length of the geodesic segment between p_1 and p_2 is given by [213]

$$d(p_1, p_2) = L \log \left(\frac{2\sigma(x_2 - x_1)}{(x_1 - u)(v - x_2)} + 1 \right) = L \log \eta, \tag{5.80}$$

where u, v are the boundary points of the entangling interval associated with (χ, σ) (5.39) and η is the conformal cross-ratio

$$\eta = \frac{(v - x_1)(x_2 - u)}{(v - x_2)(x_1 - u)}. \tag{5.81}$$

---

[8]We use the coordinates (3.33) for the Poincaré patch.

By using the formula (3.39) for entanglement entropy, we may express η in terms of entanglement entropies,

$$\eta = e^{\frac{3}{c}\kappa} + 1\,,\tag{5.82}$$

where

$$\kappa = S([x_1, x_2]) + S([u, v]) - S([x_2, v]) - S([u, x_1])\,.\tag{5.83}$$

For sufficiently small $(x_1 - u)(v - x_2)$ the RT surface of $[x_1, x_2] \cup [u, v]^c$ is given by $\gamma_{[u,x_1]} \cup \gamma_{[x_2,v]}$, as visualized in Figure 5.17. [9] In this case, the RT formula (3.32) implies that κ is equal to the mutual information (3.15) of $[x_1, x_2]$ and $[u, v]^c$,

$$\kappa = I([x_1, x_2] : [u, v]^c)\,.\tag{5.84}$$

Therefore, we see that we may express the geodesic distance (5.80) of the two bulk points p_1 and p_2 in terms of mutual information.

We may now apply this result to the chord length $\lambda_{\mathcal{B}_A}(\chi, \sigma)$ of type (c) geodesics in order to formulate the corresponding integral in (5.78) in terms of mutual information. By doing so, we obtain the alternative expression for subregion complexity mentioned at the beginning of this section. Evidently, $\lambda_{\mathcal{B}_A}(\chi, \sigma)$ is the geodesic distance between the endpoint of (χ, σ) lying inside of $\mathcal{B}_A$ and the point where (χ, σ) and (χ_A, σ_A) meet.[10] Therefore, combining (5.80) and (5.82), we find

$$\lambda_{\mathcal{B}_A}(\chi, \sigma) = L \log\left(e^{\frac{3}{c}\kappa} + 1\right)\,.\tag{5.85}$$

By sending p_1 or p_2 to one endpoint of the geodesic (χ, σ) – as required for $\lambda_{\mathcal{B}_A}$ – x_1 or x_2 asymptotes to u or v respectively. This is easy to see from (5.79). Consequently, we find $(x_1 - u)(v - x_2) \longrightarrow 0$. Therefore, the interpretation of κ as mutual information (5.84) is valid for (5.85). We find

$$\kappa = I([u, \hat{x}] : [u, v]^c)\,,\tag{5.86}$$

if the endpoint u of (χ, σ) lies inside of $\mathcal{B}_A$ and

$$\kappa = I([\hat{x}, v] : [u, v]^c)\,,\tag{5.87}$$

if v lies inside of $\mathcal{B}_A$. Here $\hat{x}$ denotes the boundary point associated with the bulk point where (χ, σ) and (χ_A, σ_A) meet (see Figure 5.18 and (5.79)).

By inserting (5.85) into (5.78) we obtain the following expression for subregion complexity,

$$\mathcal{C}(\chi_A, \sigma_A) = -\frac{9}{\pi c^2} \int_{\text{type (b)}} d\chi d\sigma S \partial_\sigma^2 S$$
$$-\frac{3}{2\pi c} \int_{\text{type (c)}} d\chi d\sigma \log\left(e^{\frac{3}{c}\kappa} + 1\right) \partial_\sigma^2 S\,,\tag{5.88}$$

where we used (5.49) and (2.117).

---

[9]This may be easily verified by considering our discussion of phase transitions of the RT surface in Section 3.1.7.

[10]We note again that this distance is divergent. Thus a proper cut-off procedure is required.
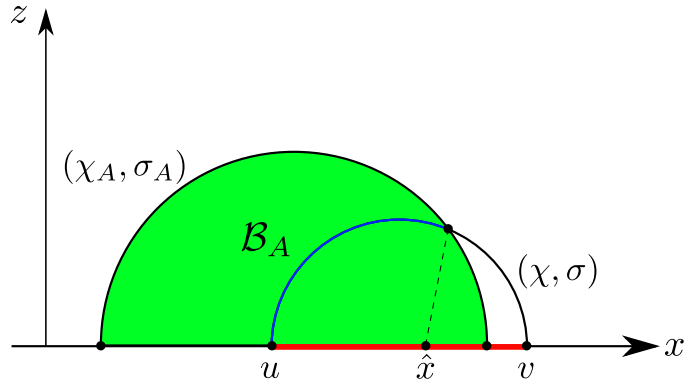
Figure 5.18: Identification of the intersection point of the bulk geodesics (χ_A, σ_A) and (χ, σ). By associating the intersection point of (χ_A, σ_A) and (χ, σ) with a boundary point $\hat{x}$ on the entangling interval corresponding to (χ, σ) (red), we may express the chord length of (χ, σ) (length of the blue curve) in terms of mutual information (see (5.85) and (5.86))

We see that the expression (5.88) for HSRC is a single integral over kinematic space not a double integral as (5.53). However, the derivation of (5.88) heavily relies on the bulk since the bulk modular flow is required to identify $\hat{x}$ in (5.86) and (5.87). Thus (5.88) is strictly speaking no CFT expression for HSRC. We nevertheless consider it a valuable result for HSRC which may provide some inspiration for field theory expressions for HSRC in the future.

5.4 Holographic Subregion Complexity for Excited States

Until now we have discussed HSRC only for vacuum states. Applying the volume formula (5.12) we were able to derive a field theory expression for HSRC only containing entanglement entropies. We now generalize this approach to two types of geometries that are quotients of pure AdS_3: conical defects and BTZ black holes. These geometries are dual to primary excitations and thermal states of the CFT, respectively (see Section 2.5.2).

The main difference between the gravity duals of these excited states and the vacuum states is the fact that the geodesics anchored at the boundary of a constant time slice are no longer uniquely determined by their endpoints. To be more precise, given two points on the constant time slice of the conformal boundary, there are several geodesics running between them. Consequently, the one-to-one correspondence between entangling intervals on the CFT side and boundary anchored geodesics on the gravity side no longer exists. This one-to-one correspondence allowed us to interpret the kinematic space for the vacuum from both the bulk and the boundary perspective and thus offered a very natural way to associate bulk volumes with CFT integrals (see Section 5.3). For excited states this strategy for constructing CFT expressions for bulk volumes is no longer possible.

The kinematic space for the geometries we consider here is again defined as the space of all boundary anchored geodesics on a constant time slice. Both the conical defect and the BTZ black hole may be defined as a quotient of AdS$_3$. As discussed below, we may apply the quotienting procedure providing these geometries to construct their kinematic space as a quotient of the kinematic space of the vacuum state. This construction makes it evident that the volume formula (5.12) may also be applied to the quotient geometries, when inheriting the volume form $\omega_\mathcal{K}$ from the vacuum kinematic space.

Since there are several geodesics attached to the same pair of boundary points, only the geodesic with minimal length corresponds to a RT surface providing entanglement entropy. The CFT interpretation of the lengths of the other – so-called – *long geodesics* is a subject of current research. There is evidence that they are related to the entanglement of inner degrees of freedom which are not spatially organized [146]. This interpretation is referred to as *entwinement* [146]. Entwinement has been discussed in e.g. [95, 97, 214] and made more concrete in [215, 216]. We note that in quotient geometries there are regions that cannot be reached by minimal geodesics but only by non-minimal ones (see Figure 5.19 for the conical defect geometry). Since these regions are – by construction – not intersected by RT surfaces, they are called *entanglement shadows* [146, 217]. The existence of entanglement shadows makes it clear that a kinematic space which is supposed to provide a volume formula of the form (5.12) necessarily needs to include non-minimal geodesics. If it would only contain minimal geodesics, a bulk region $\mathcal{Q}$ lying completely inside of the entanglement shadow could not be reached by the geodesics associated with such a kinematic space and thus vol($\mathcal{Q}$) could not be computed via the volume formula.

Due to the presence of non-minimal geodesics in kinematic space, we may no longer interpret the volume form $\omega_\mathcal{K}$ in terms of entanglement entropies. This interpretation only applies to the geodesics of minimal length. Consequently, our expression for HSRC as an integral over kinematic space no longer consists only of entanglement entropies, as for the vacuum state (5.53), but also includes entwinement. We present a formulation of HSRC as an integral over the space of entangling intervals below. This expression includes length contributions from non-minimal geodesics and may be seen as a first approach towards finding a CFT formula for HSRC.

Furthermore, we find that for thermal states (BTZ black holes) – besides the minimal and non-minimal geodesics connecting boundary points – there is a third type of geodesic: these geodesics run between the boundary and the horizon of the black hole. Consequently, they only have one endpoint at the conformal boundary and may thus not be associated with any boundary interval. We consider the contribution of these geodesics to HSRC as related to the fact that the dual CFT state is thermal.

5.4.1   Conical Defects

In this section we discuss kinematic space and HSRC for conical defects (see Section 2.5.2). We start by reviewing the construction of the conical defect geometry by

quotienting AdS_3. The same procedure may be used to derive the corresponding kinematic space. The conical defect geometry $CD_{\hat{N}}$ is obtained from global AdS_3 (5.13) by considering the identification

$$\phi \sim \phi + 2\pi/\hat{N} \,, \quad \hat{N} \in \mathbb{N} \tag{5.89}$$

for the angular coordinate of global AdS_3 (5.13) (see e.g. [146, 147]).[11] Therefore, $CD_{\hat{N}}$ is given by the quotient

$$CD_{\hat{N}} = \frac{AdS_3}{\mathbb{Z}_{\hat{N}}} \,. \tag{5.90}$$

By introducing the coordinates $\hat{t} = \hat{N}\tilde{t}$, $\hat{r} = \tilde{r}/\hat{N}$ and $\hat{\phi} = \hat{N}\phi$, we obtain the metric of the conical defect (2.152) (see e.g. [146]).[12]

$$ds_{CD}^2 = -\Big(\frac{\hat{r}^2}{L^2} + \hat{N}^{-2}\Big)d\hat{t}^2 + \frac{1}{\frac{\hat{r}^2}{L^2} + \hat{N}^{-2}}d\hat{r}^2 + \hat{r}^2 d\hat{\phi}^2 \,, \tag{5.91}$$

where the dual field theory is defined on the circle $\hat{\phi} \sim \hat{\phi} + 2\pi$ at $\hat{r} = \infty$. As we depict in Figure 5.19, the quotienting procedure (5.89) results in a geometry where the geodesic on a constant time slice connecting two points on the conformal boundary at $\hat{r} = \infty$ is not unique. The RT formula (3.32) states that the entanglement entropy of a boundary interval is then given by the length of the minimal geodesic connecting the two endpoints of the interval.

Kinematic Space for Conical Defects

In the following we work with the kinematic space $\mathcal{K}_{CD}$ for $CD_{\hat{N}}$ introduced in [147], which is the space of all boundary anchored geodesics on a constant time slice of $CD_{\hat{N}}$, including the non-minimal ones.[13]

As pointed out in [147], the kinematic space of the conical defect is most easily obtained from the kinematic space of global AdS_3 (5.15). Due to the identification (5.89) in the ϕ coordinate of global AdS_3 required for the construction of $CD_{\hat{N}}$, we need to introduce the same identification in the θ coordinate (5.2) for the kinematic space of global AdS_3 to obtain $\mathcal{K}_{CD}$,

$$\theta \sim \theta + \frac{2\pi}{\hat{N}} \,. \tag{5.92}$$

A point (θ, α) in AdS_3 kinematic space refers to a geodesic corresponding to a boundary interval centered around $\phi = \theta$ with opening angle α (5.2). Therefore, (5.92) is an immediate consequence of the identification (5.89) in the ϕ coordinate

---

[11]For simplicity we assume $\hat{N} \in \mathbb{N}$ here. In principle it is possible to consider conical defects for non-integer $\hat{N}$ as well.

[12]Note that in (2.152) we use $\tilde{t}$, $\tilde{r}$ and ϕ to refer to $\hat{t}$, $\hat{r}$ and $\hat{\phi}$.

[13]We mention [95] for related work. For an alternative formulation of kinematic space for conical defects we refer to [212].

Bulk

Kinematic Space $\mathcal{K}_{\mathrm{CD}}$
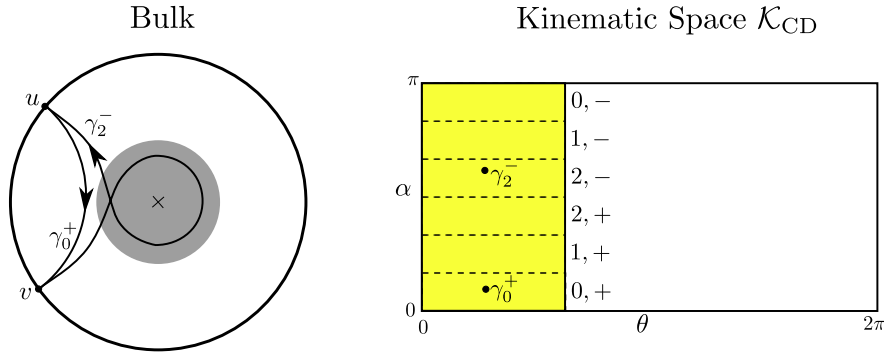
Figure 5.19: Constant time slice (l.h.s.) and kinematic space (r.h.s.) for the conical defect. We consider a constant time slice for the conical defect with $\hat{N} = 3$ (5.89). As depicted on the l.h.s. the geodesic connecting two points u, v on the conformal boundary at $\hat{r} \longrightarrow \infty$ is not unique. Besides the geodesic of minimal length there are further geodesics winding around the conical defect at $\hat{r} = 0$. Moreover, there is a region (grey) surrounding the conical defect that may not be accessed by the geodesics providing the minimal distance between two boundary points but only by non-minimal geodesics. This region is called entanglement shadow. The kinematic space for the conical defect (r.h.s.) – i.e. the space of all boundary anchored geodesics – is given by a quotient of the kinematic space of global AdS$_3$ (5.92). We depict the corresponding fundamental domain in yellow. The geodesics in $\mathcal{K}_{\mathrm{CD}}$ come with an orientation $(\pm)$ and a winding number $n = 0, 1, 2$ indicating how often a geodesic winds around the defect. A geodesic with winding number n and orientation $\pm$ has $\alpha \in \mathcal{W}_n^{\pm}$ (5.93).

of global AdS$_3$. The opening angle α still runs from 0 to π in $\mathcal{K}_{\mathrm{CD}}$. The elements in $\mathcal{K}_{\mathrm{CD}}$ with $\alpha \in \mathcal{W}_n^{\pm}$, where

$$\mathcal{W}_n^+ = \left(\frac{n\pi}{2\hat{N}}, \frac{(n+1)\pi}{2\hat{N}} \right], \quad \mathcal{W}_n^- = \left[\frac{(2\hat{N} - n - 1)\pi}{2\hat{N}}, \frac{(2\hat{N} - n)\pi}{2\hat{N}} \right), \qquad (5.93)$$

refer to bulk geodesics winding $n = 0, \ldots, \hat{N} - 1$ times around the conical defect at $\hat{r} = 0$ [147] (see Figure 5.19). Here the $\pm$ correspond to the two different orientations of each geodesic. In particular, $\mathcal{W}_0^{\pm}$ contain the minimal geodesics, i.e. the RT surfaces.[14]

The metric and volume form of $\mathcal{K}_{\mathrm{CD}}$ are given by

$$ds^2_{\mathcal{K}_{\mathrm{CD}}} = -\frac{1}{8G_3} \partial_\alpha^2 \ell \left(-d\alpha^2 + d\theta^2 \right), \quad \omega_{\mathcal{K}_{\mathrm{CD}}} = -\frac{1}{8G_3} \partial_\alpha^2 \ell d\theta \wedge d\alpha, \qquad (5.94)$$

where

$$\ell(\alpha) = 2L \log \left(\frac{2\ell_{\mathrm{CFT}}}{\epsilon} \sin(\alpha) \right) \qquad (5.95)$$

---

[14]Note that, strictly speaking, some RT surfaces also include an infinitesimal circle around the conical defect (see Section 3.1.7). Since we are only interested in the length of the RT surface here, we neglect this circle.

is the length of the geodesic associated with (θ, α) [147]. [15] Note that ℓ does not depend on θ due to the symmetry of the geometry. We note that $\ell(\alpha)$ may only be associated with entanglement entropy for $\alpha \in \mathcal{W}_0^{\pm}$, since only these points in $\mathcal{K}_{\mathrm{CD}}$ correspond to geodesics with minimal length.

Volume Formula for Conical Defects

Since CD_N is a quotient of global AdS_3 (5.90), it is easy to see that the volume formula (5.12) also holds here,

$$\frac{\mathrm{vol}(\mathcal{Q})}{4G_3} = \frac{1}{2\pi} \int_{\mathcal{K}_{\mathrm{CD}}} \omega_{\mathcal{K}_{\mathrm{CD}}} \lambda_{\mathcal{Q}} = -\frac{1}{16\pi G_3} \int_0^{2\pi/\hat{N}} d\theta \int_0^{\pi} d\alpha \lambda_{\mathcal{Q}}(\theta, \alpha) \partial_\alpha^2 \ell(\alpha), \quad (5.96)$$

where $\mathcal{Q}$ is an arbitrary codimension one bulk region in the constant time slice of $\mathrm{CD}_{\hat{N}}$. The chord length $\lambda_{\mathcal{Q}}(\theta, \alpha)$ is the length of the segment of the geodesic associated with (θ, α) lying in $\mathcal{Q}$.

Holographic Subregion Complexity for Conical Defects

In analogy to (5.53) we may use the kinematic space integral (5.5) determining the distance between two bulk points to derive a double integral expression over $\mathcal{K}_{\mathrm{CD}}$ from (5.96) for the volume of the region $\mathcal{B}_A$ associated with HSRC (5.49). We obtain the following expression for HSRC,

$$\mathcal{C}(\hat{\theta}_A, \hat{\alpha}_A) = \frac{1}{32\pi L^2} \int_0^{2\pi/\hat{N}} d\theta \int_0^{\pi} d\alpha \int_{\Delta_A(\theta, \alpha)} d\theta' d\alpha' n_{(\theta, \alpha)}^A(\theta', \alpha') \partial_\alpha^2 \ell \partial_{\alpha'}^2 \ell, \quad (5.97)$$

where $\Delta_A(\theta, \alpha) \subset \mathcal{K}_{\mathrm{CD}}$ corresponds to the geodesics intersecting the chord of the geodesic (θ, α) lying inside of $\mathcal{B}_A$. We use the coordinates $(\hat{\theta}_A, \hat{\alpha}_A)$ to refer to an entangling interval on the CFT side with endpoints $\hat{\phi} = \hat{\theta}_A - \hat{\alpha}_A$ and $\hat{\phi} = \hat{\theta}_A + \hat{\alpha}_A$. By construction, (5.97) not only includes minimal geodesics connecting two boundary points but also non-minimal ones. Since non-minimal geodesics may intersect the chord of (θ, α) more than once we need to weight each (θ', α') with the number $n_{(\theta, \alpha)}^A(\theta', \alpha')$ of its intersections (5.3).

Due to the contribution of non-minimal geodesics to (5.97), a field theory interpretation of HSRC not only includes entanglement entropy – as it was the case for global AdS_3 (5.53) – but also entwinement.

As a first step towards a field theory interpretation of (5.97) we conclude our discussion of HSRC for conical defects by reformulating (5.97) as an integral over the space of entangling intervals. This reformulation was constructed by me and published in [2] with less details than presented here. Since $\mathcal{K}_{\mathrm{CD}}$ is the space of all boundary anchored geodesics, the one-to-one correspondence between points in $\mathcal{K}_{\mathrm{CD}}$ and entangling intervals on the boundary which we had for global AdS_3 is not

---

[15]Here ϵ is a radial cut-off and ℓ_{CFT} the radius of the circle the CFT is defined on. We have chosen the factor in front of $\sin(\alpha)$ to be $2\ell_{\mathrm{CFT}}/\epsilon$ in order to get in touch with the entanglement entropy (5.14) of global AdS_3.

present here. Nevertheless, we may interpret (5.97) as an integral over entangling intervals.

We begin by making the following observation. Consider an integral over kinematic space of the form

$$\int_{\mathcal{K}_{\mathrm{CD}}} d\theta d\alpha f(\theta, \alpha) \partial_\alpha^2 \ell \,, \tag{5.98}$$

where f is an arbitrary function on $\mathcal{K}_{\mathrm{CD}}$. When using $\hat{\theta} \in [0, 2\pi]$ and $\hat{\alpha} \in [0, \pi]$ to parametrize the entangling intervals on the circle corresponding to the CFT constant time slice,[16] it is easy to see that (5.98) can be reformulated as

$$\int_{\mathcal{K}_{\mathrm{CD}}} d\theta d\alpha f(\theta, \alpha) \partial_\alpha^2 \ell = \int_0^{2\pi} d\hat{\theta} \int_0^\pi d\hat{\alpha} \sum_{n=0}^{\hat{N}-1} f_n(\hat{\theta}, \hat{\alpha}) \partial_{\hat{\alpha}}^2 \ell_n(\hat{\alpha}) \,, \tag{5.99}$$

where $f_n(\hat{\theta}, \hat{\alpha})$ is the value of f at the point in $\mathcal{K}_{\mathrm{CD}}$ corresponding to the geodesic winding n times around the defect and ending at the endpoints of the interval $(\hat{\theta}, \hat{\alpha})$. Analogously, $\ell_n(\hat{\alpha})$ is the length of the geodesic with winding number n attached to $(\hat{\theta}, \hat{\alpha})$ (see Figure 5.19). Applying the reformulation (5.99) to (5.97), we find that HSRC can be written as an integral over the space of entangling intervals,

$$\mathcal{C}(\hat{\theta}_A, \hat{\alpha}_A) = \int d\hat{\theta} d\hat{\alpha} \Big(F_A^{\mathrm{CD}}(\hat{\theta}, \hat{\alpha}) + G_A^{\mathrm{CD}}(\hat{\theta}, \hat{\alpha}) \Big) \,. \tag{5.100}$$

Here $F_A^{\mathrm{CD}}(\hat{\theta}, \hat{\alpha})$ refers to all contributions of geodesics with winding number $n = 0$ to the double integral (5.97) and $G_A^{\mathrm{CD}}(\hat{\theta}, \hat{\alpha})$ corresponds to the contribution of geodesics of higher winding, i.e. $n > 0$. The RT formula (3.32) implies that the integral over F_A^{CD} in (5.100) can be expressed solely in terms of entanglement entropies, since geodesics with $n = 0$ are RT surfaces. In particular, if we set $\hat{N} = 1$, we find that G_A^{CD} vanishes and (5.100) becomes the integral over entanglement entropies giving HSRC for global AdS$_3$ (5.53). This is easy to be seen, since $\mathrm{CD}_{\hat{N}=1} = \mathrm{AdS}_3$. For $\hat{N} > 1$ HSRC not only consists of entanglement entropies but additional contributions containing the length of non-minimal geodesics are present, i.e. $G_A^{\mathrm{CD}} \neq 0$. As pointed out in the introduction to this section, the length of non-minimal geodesics are considered to correspond to inner correlations of the corresponding CFT state which are referred to as entwinement.

Since F_A^{CD} and G_A^{CD} essentially consist of volume integrals over regions in $\mathcal{K}_{\mathrm{CD}}$ (see (5.97)), it is easy to see that they are non-negative. So we find that the integral over F_A^{CD} provides a lower bound for HSRC,

$$\int d\hat{\theta} d\hat{\alpha} \, F_A^{\mathrm{CD}}(\hat{\theta}, \hat{\alpha}) \leq \mathcal{C}(\hat{\theta}_A, \hat{\alpha}_A) \,. \tag{5.101}$$

Consequently, HSRC for conical defects is bounded from below by a term only depending on entanglement entropies.

---

[16] $(\hat{\theta}, \hat{\alpha})$ corresponds to an entangling interval with endpoints $\hat{\phi} = \hat{\theta} - \hat{\alpha}$ and $\hat{\phi} = \hat{\theta} + \hat{\alpha}$.

5.4.2 BTZ Black Holes

We now discuss the kinematic space $\mathcal{K}_{\text{BTZ}}$ for the non-rotating BTZ black hole geometry (2.148)

$$ds^2_{\text{BTZ}} = -\frac{\tilde{r}^2 - \tilde{r}_h^2}{L^2} d\tilde{t}^2 + \frac{L^2}{\tilde{r}^2 - \tilde{r}_h^2} d\tilde{r}^2 + \tilde{r}^2 d\phi^2 \tag{5.102}$$

and the resulting expression for subregion complexity.

BTZ Geometry

Similar as for the conical defect (see Section 5.4.1), the quotienting procedure for AdS$_3$ providing the BTZ geometry (5.102) leads to a method for obtaining $\mathcal{K}_{\text{BTZ}}$ from the vacuum kinematic space. We therefore briefly review the quotienting procedure that allows us to construct the BTZ black hole (5.102) from the Poincaré patch [141, 142]. Considering the coordinates t, z and x (3.33) for the Poincaré patch, we may perform the coordinate transformation $x_\pm = x \pm t$, leading to

$$ds^2_{\text{PP}} = \frac{L^2}{z^2} \big(-dt^2 + dx^2 + dz^2 \big) = \frac{L^2}{z^2} \big(dx_+ dx_- + dz^2 \big) . \tag{5.103}$$

By defining $\tilde{r}$, $\tilde{t}$, ϕ via

$$x_\pm = L \Big(1 - \frac{\tilde{r}_h^2}{\tilde{r}^2} \Big)^{1/2} e^{\tilde{r}_h(\phi \pm \tilde{t}/L)/L} , \quad z = L \frac{\tilde{r}_h}{\tilde{r}} e^{\tilde{r}_h \phi/L} , \tag{5.104}$$

and imposing the periodicity $\phi \sim \phi + 2\pi$, we obtain the identification

$$(t, x, z) \sim e^{2\pi \tilde{r}_h/L}(t, x, z) , \tag{5.105}$$

which turns the Poincaré patch into the BTZ black hole (5.102). In particular, the constant time slice $t = 0$ of the Poincaré patch is transformed into the BTZ constant time slice $\tilde{t} = 0$. The identification imposed on the constant time slice resulting from this transformation is

$$(x, z) \sim e^{2\pi \tilde{r}_h/L}(x, z) . \tag{5.106}$$

More precisely, the quotient space resulting from the identification (5.106) is globally equivalent to the constant time slice of the two-sided BTZ black hole, as we depict in Figure 5.20. [17] In the following we work with this constant time slice of the BTZ black hole. The identification (5.106) offers the region

$$L^2 \leq x^2 + z^2 < L^2 e^{4\pi \tilde{r}_h/L} \tag{5.107}$$

as fundamental domain of the BTZ constant time slice (see Figure 5.20). The vertical line $x = 0$ corresponds to the horizon of the black hole, whose circumference is given by

$$L \int_L^{L \exp(2\pi \tilde{r}_h/L)} \frac{dz}{z} = 2\pi \tilde{r}_h , \tag{5.108}$$

as may be easily deduced from (5.103) and (5.107).

---

[17]The emergence of the two-sided BTZ black hole is related to the fact that the identification (5.105) generates an extended version of the BTZ geometry presented in (5.102). To be more precise, the coordinates $\tilde{r}$, $\tilde{t}$, ϕ only cover a part of the space generated by (5.105). This is evident, since (5.104) is only defined for $x_\pm > 0$.
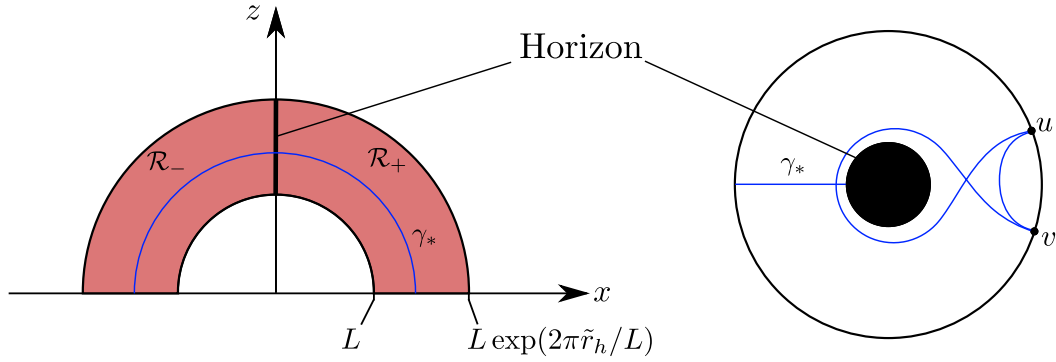
Figure 5.20: Fundamental domain of the constant time slice of the two-sided BTZ black hole. We depict the constant time slice $t = 0$ of the Poincaré patch (l.h.s.) which may be transformed into the constant time slice $\tilde{t} = 0$ of the two sided BTZ black hole via (5.106). The z axis separates the corresponding fundamental domain (red) into two regions $\mathcal{R}_\pm$ each providing one side of the BTZ black hole. Considering one side of the black hole (r.h.s.), there are infinitely many geodesics (blue) connecting any pair of boundary points u, v. Moreover, there are also geodesics γ_* passing through the horizon to the other side of the black hole.

Kinematic Space of the BTZ Black Hole

We consider $\mathcal{K}_{\mathrm{BTZ}}$ to be the space of all boundary anchored geodesics on the constant time slice $\tilde{t} = 0$ of the BTZ geometry (5.102). This definition of $\mathcal{K}_{\mathrm{BTZ}}$ is considered in [97, 218]. [18] As for the conical defect (see Section 5.4.1), the geodesic connecting two boundary points is not unique. In fact, for any pair of boundary points $\phi = u, v$ there are infinitely many geodesics running from u to v (see Figure 5.20). Moreover, as we show in Figure 5.20, there are also geodesics starting at a boundary point ϕ and passing through the horizon to the other side of the black hole. These geodesics are included in $\mathcal{K}_{\mathrm{BTZ}}$ as well.

We may define $\mathcal{K}_{\mathrm{BTZ}}$ as a quotient of the Poincaré patch kinematic space in the following way.[19] Using the kinematic space coordinates (χ, σ) (5.39) to parametrize a geodesic in the constant time slice of the Poincaré patch with endpoints $u_{\mathrm{PP}} = \chi - \sigma$ and $v_{\mathrm{PP}} = \chi + \sigma$ on the boundary, we find that the identification (5.106) leads to

$$(\chi, \sigma) \sim e^{2\pi\tilde{r}_h/L}(\chi, \sigma)\,, \tag{5.109}$$

which turns the Poincaré kinematic space into $\mathcal{K}_{\mathrm{BTZ}}$. The metric and volume form of $\mathcal{K}_{\mathrm{BTZ}}$ are inherited from the Poincaré kinematic space,

$$ds^2_{\mathcal{K}_{\mathrm{BTZ}}} = -\frac{1}{8G_3}\partial^2_\sigma\ell\big(-d\sigma^2 + d\chi^2\big)\,, \quad \omega_{\mathcal{K}_{\mathrm{BTZ}}} = -\frac{1}{8G_3}\partial^2_\sigma\ell\,d\chi \wedge d\sigma\,, \tag{5.110}$$

---

[18]We mention [95] for related work. Note that there are also alternative definitions of $\mathcal{K}_{\mathrm{BTZ}}$ as the space of geodesics with minimal length [212].

[19]Quotient constructions (for the BTZ kinematic space) of the type presented here were also considered in [97, 218].
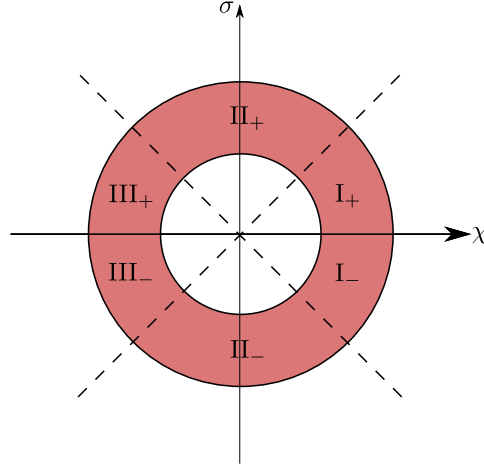
Figure 5.21: Kinematic space $\mathcal{K}_{\mathrm{BTZ}}$ constructed as a quotient of the kinematic space of the Poincaré patch via (5.109). The fundamental domain (red) may be separated into six regions by the χ axis and the light rays emitted from the origin (dashed lines). As may be seen by associating the χ axis with the constant time slice of the field theory, the regions $\mathrm{I}_\pm$, $\mathrm{III}_\pm$ correspond to the geodesics lying completely on one side of the BTZ black hole, where the sign $\pm$ refers to their orientation. Moreover, the geodesics represented by $\mathrm{II}_\pm$ have one endpoint on each side of the BTZ black hole.

where

$$\ell(\sigma) = 2L \log\left(\frac{2\sigma}{\epsilon}\right) \tag{5.111}$$

is the length of the geodesic associated with (χ, σ) (3.38). Here, ϵ corresponds to a cut-off. Due to the symmetry of the system, ℓ is independent of χ. Using the coordinates $u_{\mathrm{PP}} = \chi - \sigma$ and $v_{\mathrm{PP}} = \chi + \sigma$ in the covering space of $\mathcal{K}_{\mathrm{BTZ}}$, i.e. the Poincaré patch kinematic space, we may distinguish the following six sectors of $\mathcal{K}_{\mathrm{BTZ}}$.

Sector I_+. Geodesics with $0 < u_{\mathrm{PP}} < v_{\mathrm{PP}}$ all have the same orientation and are restricted to the r.h.s. of the two sided BTZ black hole (see Figure 5.21). Both their endpoints are attached to the conformal boundary of the BTZ geometry at $\tilde{r} = \infty$.

Sector II_+. The sector with $u_{\mathrm{PP}} < 0 < v_{\mathrm{PP}}$ corresponds to geodesics which pass from one side of the black hole to the other, as depicted in Figure 5.21. Moreover, they all have the same orientation.

Sector III_+. Complementary to sector I_+, sector III_+, contains geodesics with $u_{\mathrm{PP}} < v_{\mathrm{PP}} < 0$. They all share the same orientation and all lie on the l.h.s. of the black hole (see Figure 5.21).

Sectors I_-, II_-, III_-. By exchanging u_{PP} and v_{PP} in the above definitions of

sectors I_+, II_+, III_+, we obtain the sectors I_-, II_-, III_-, respectively. They share the same properties as their counterparts but have opposite orientation (see Figure 5.21).

We may parametrize the geodesics corresponding to the points in sector I_+ by their endpoints $\phi = \theta - \alpha$ and $\phi = \theta + \alpha$ on the conformal boundary of the BTZ geometry (5.21) by setting

$$ u_{\text{PP}} = Le^{\tilde{r}_h(\theta - \alpha)/L}\,, \quad v_{\text{PP}} = Le^{\tilde{r}_h(\theta + \alpha)/L}\,, \quad \text{where} \quad \theta \sim \theta + 2\pi\,, \quad \alpha \in \mathbb{R}\,. \quad (5.112) $$

This allows us to identify the geodesics in sector I_+ winding n times around the horizon. They are given by $\alpha \in \mathcal{V}_n$, where

$$ \mathcal{V}_n = [\pi n, \pi(n+1))\,, \quad n \in \mathbb{N}_0\,. \quad (5.113) $$

Analogous parametrizations can be found for the geodesics in sectors I_- and III_+. Moreover, (5.112) – together with (2.117) – provides us with the expression

$$ \omega_{\mathcal{K}_{\text{BTZ}}} = \frac{c}{6} \frac{\tilde{r}_h^2}{L^2 \sinh^2(\tilde{r}_h \alpha/L)} d\theta \wedge d\alpha \quad (5.114) $$

for the volume form (5.110) in sector I_+. By considering the formula (3.48) for the entanglement entropy for BTZ black holes, we see that (5.114) is of the form

$$ \omega_{\mathcal{K}_{\text{BTZ}}} = -\frac{1}{2}\partial_\alpha^2 S(\alpha) d\theta \wedge d\alpha \quad (5.115) $$

for

$$ 0 < \alpha < \frac{L}{2\tilde{r}_h} \log\left(\frac{e^{2\pi\tilde{r}_h/L} + 1}{2}\right)\,, \quad (5.116) $$

since the corresponding geodesics are the RT surfaces of the associated entangling intervals.[20]

Volume Formula for BTZ Black Holes

The BTZ black hole is a quotient of the Poincaré patch (5.105). Consequently, the volume formula (5.12) also holds here, i.e. we may compute the volume of an arbitrary codimension one bulk region $\mathcal{Q}$ lying in the constant time slice of the BTZ black hole via

$$ \frac{\text{vol}(\mathcal{Q})}{4G_3} = \frac{1}{2\pi} \int_{\mathcal{K}_{\text{BTZ}}} \omega_{\mathcal{K}_{\text{BTZ}}} \lambda_{\mathcal{Q}} = -\frac{1}{16\pi G_3} \int_{\mathcal{K}_{\text{BTZ}}} d\chi d\sigma \lambda_{\mathcal{Q}}(\chi, \sigma) \partial_\sigma^2 \ell(\sigma)\,. \quad (5.117) $$

Here $\lambda_{\mathcal{Q}}(\chi, \sigma)$ is the length of the chord lying inside of $\mathcal{Q}$ of the geodesic associated with (χ, σ).

---

[20]For larger α the RT surface undergoes a phase transition (see Section 3.1.7).

Holographic Subregion Complexity for BTZ Black Holes

Just as for the conical defect (see Section 5.4.1), we may apply the expression for the geodesic distance between two bulk points (5.5) to derive a double integral expression over $\mathcal{K}_{\mathrm{BTZ}}$ for the HSRC,

$$\mathcal{C}(\hat{\theta}_A, \hat{\alpha}_A) = \frac{1}{32\pi L^2} \int_{\mathcal{K}_{\mathrm{BTZ}}} d\chi d\sigma \int_{\Delta_A(\chi,\sigma)} d\chi' d\sigma' n^A_{(\chi,\sigma)}(\chi',\sigma') \partial^2_\sigma \ell(\sigma) \partial^2_{\sigma'} \ell(\sigma').$$
(5.118)

Here, we denote the considered entangling interval with endpoints $\phi = \hat{\theta}_A - \hat{\alpha}_A$ and $\phi = \hat{\theta}_A + \hat{\alpha}_A$ as $(\hat{\theta}_A, \hat{\alpha}_A)$. Moreover, $\Delta_A(\chi,\sigma)$ is the region in $\mathcal{K}_{\mathrm{BTZ}}$ corresponding to the bulk geodesics which intersect the chord of the geodesic associated with (χ,σ) lying in $\mathcal{B}_A$. The bulk region $\mathcal{B}_A$ is – as usual – the codimension one region enclosed by the boundary interval $(\hat{\theta}_A, \hat{\alpha}_A)$ and the corresponding RT surface. Since geodesics (χ',σ') of higher winding may intersect the chord of (χ,σ) more than once, we need to weight them with their number of intersections $n^A_{(\chi,\sigma)}(\chi',\sigma')$.

The integrals in (5.118) obviously not only consider the bulk geodesics which are RT surfaces but all geodesics in the constant time slice of the BTZ geometry. Consequently, an interpretation of (5.118) solely in terms of entanglement entropies is not possible.

We now introduce a reformulation of (5.118) similar to (5.100) for the conical defect in order to provide a first step towards a field theory interpretation of (5.118). I contributed this reformulation to [2], where I discussed it with less details than here. For this reformulation we need to analyze the contribution of the different sectors ($\mathrm{I}_\pm$, $\mathrm{II}_\pm$, $\mathrm{III}_\pm$) of kinematic space to (5.118). Without loss of generality, we consider the boundary interval $(\hat{\theta}_A, \hat{\alpha}_A)$ to be located on the r.h.s. of the two sided BTZ black hole (see Figure 5.20). Since the bulk region $\mathcal{B}_A$ therefore lies on the r.h.s. as well, it is easy to see that the geodesics lying completely on the l.h.s. (sectors $\mathrm{III}_\pm$) do not contribute to HSRC. So only the sectors $\mathrm{I}_\pm$ and $\mathrm{II}_\pm$ need to be considered. The geodesics in sector $\mathrm{I}_\pm$ have both their endpoints attached to the conformal boundary on the r.h.s. of the BTZ black hole. Therefore, in analogy to (5.99), we can reformulate the integral of a function f over $\mathrm{I}_\pm$ as an integral over the space of all entangling intervals,

$$\int_{\mathrm{I}_+ \cup \mathrm{I}_-} d\chi d\sigma f(\chi,\sigma) \partial^2_\sigma \ell = \int_0^{2\pi} d\hat{\theta} \int_0^\pi d\hat{\alpha} \sum_n f_n(\hat{\theta}, \hat{\alpha}) \partial^2_{\hat{\alpha}} \ell_n(\hat{\alpha}).$$
(5.119)

Here $f_n(\hat{\theta}, \hat{\alpha})$ and $\ell_n(\hat{\alpha})$ are the functions f and ℓ evaluated at the point in $\mathrm{I}_\pm$ corresponding to the geodesic with endpoints $\phi = \hat{\theta} \pm \hat{\alpha}$ and winding number n (see paragraph of (5.113)). We note that these geodesics are considered with two different orientations – as usual. This guarantees that we may interpret (5.119) as an integral over all entangling intervals. We may now apply the reformulation (5.119) to subregion complexity (5.118), which leads to

$$\mathcal{C}(\hat{\theta}_A, \hat{\alpha}_A) = \int d\hat{\theta} d\hat{\alpha} \left(F^{\mathrm{BTZ}}_A(\hat{\theta}, \hat{\alpha}) + G^{\mathrm{BTZ}}_A(\hat{\theta}, \hat{\alpha}) \right) + thermal\ contributions.$$
(5.120)

As for the conical defect (5.100), the function F_A^{BTZ} refers to all contributions to the double integral (5.118) only containing entanglement entropies. The function G_A^{BTZ} contains all contributions from geodesics in $\mathrm{I}_\pm$ that are no RT surfaces. The remaining *thermal contributions* in (5.120) refer to contributions involving the sectors $\mathrm{II}_\pm$. The geodesics corresponding to these sectors cannot be associated with entangling intervals on the conformal boundary of one side of the black hole, since they have one endpoint on each side of the black hole. So by only considering one side of the black hole, they run between the conformal boundary and the horizon. Since contributions like this may only occur in geometries with an horizon, we refer to them as thermal. We see that subregion complexity for BTZ black holes not only consists of entanglement entropies (F_A^{BTZ}) but also has thermal contributions as well as contributions from non-minimal geodesics connecting two boundary points (G_A^{BTZ}). The latter are proposed to correspond to inner correlations of the dual CFT state called entwinement, as mentioned at the beginning of this section.

Regarding the contribution of entanglement entropies to subregion complexity, i.e. F_A^{BTZ}, we note that only the RT surfaces for entangling intervals with opening angle

$$\hat{\alpha} < \frac{L}{2\tilde{r}_h} \log\left(\frac{e^{2\pi\tilde{r}_h/L}+1}{2}\right) \tag{5.121}$$

are contained in $\mathcal{K}_{\mathrm{BTZ}}$. The reason for that is the fact that the RT surface undergoes a phase transition for larger $\hat{\alpha}$ and is no longer just a geodesic attached to the considered boundary interval but also includes the horizon of the black hole (see Section 3.1.7). However, there are still terms included in F_A^{BTZ} which may be associated with the entanglement entropy of large entangling intervals, as we now show. The length of a geodesic corresponding to a RT surface for large $\hat{\alpha}$ is given by (3.49),

$$\ell(\hat{\alpha}) = 2\pi\tilde{r}_h + 2L \log\left(\frac{2L\ell_{\mathrm{CFT}}}{\tilde{r}_h\epsilon}\sinh\left(\tilde{r}_h(\pi-\hat{\alpha})/L\right)\right), \tag{5.122}$$

where ℓ_{CFT} is the radius of the circle the CFT is defined on and ϵ is a UV cut-off.[21] The first term in (5.122) is the circumference of the horizon, while the second gives the length ℓ_{min} of the minimal geodesic connecting the two endpoints of the interval $(\hat{\theta},\hat{\alpha})$. The length of this minimal geodesic is present in the integral over sector I_- contributing to subregion complexity (5.118). To be more precise, ℓ_{min} appears in the integral in form of its second derivative with respect to the opening angle. The circumference of the horizon appearing in (5.122) is independent of the opening angle and thus the second derivatives of $\ell(\hat{\alpha})$ and ℓ_{min} are identical. This allows us to interpret the contributions of ℓ_{min} to subregion complexity as contributions of the RT surfaces of large entangling intervals. Consequently, we find that the entanglement entropy of boundary intervals of any size is present in F_A^{BTZ}.

Since F_A^{BTZ}, G_A^{BTZ} as well as the thermal contributions in (5.120) essentially encode integrals of positive functions over certain regions in $\mathcal{K}_{\mathrm{BTZ}}$ (see (5.118)), we find that they are all non-negative. Consequently, we find subregion complexity

---

[21]We have defined the cut-off ϵ in such a way that ℓ_{CFT} is present in (5.122) in order to get in touch with the entanglement entropy (3.49) of the CFT state dual to the BTZ geometry.

to be always greater than the integral over F_A^{BTZ},

$$\int d\hat{\theta} d\hat{\alpha} \; F_A^{\text{BTZ}}(\hat{\theta}, \hat{\alpha}) \leq \mathcal{C}(\hat{\theta}_A, \hat{\alpha}_A) \,. \tag{5.123}$$

Since F_A^{BTZ} is an expression only depending on entanglement entropies, we may therefore interpret (5.123) as a lower bound for subregion complexity only containing entanglement entropies.

5.5 Interpretation of Holographic Subregion Complexity as Complexity for Reduced States

Given our results for HSRC for vacuum states, conical defects and BTZ black holes (5.53), (5.100), (5.120), we may now study the implications of these results for the complexity of CFT states. In the following we assume that the volume enclosed by an entangling region and the corresponding RT surface is indeed a measure for the complexity of the corresponding reduced CFT state. We examine our formulae for HSRC obtained from kinematic space in that context. By doing so I made the following observations.

HSRC Takes Correlations Between Subsystems Into Account. We find that in our formulae (5.53), (5.100), (5.120) for HSRC the correlations between subsystems play an important role. To see this we first consider the pure states dual to AdS$_3$ or the conical defect on the whole constant time slice. In (5.53), (5.101) we see that our formulae for HSRC are bounded from below by an integral over entanglement entropies. The entanglement entropy of every possible entangling interval contributes to this integral. Entanglement entropy for pure states captures the correlations between an entangling interval and its complement (see Section 3.1). Therefore, the integral over entanglement entropies, appearing in our expressions for complexity (5.53), (5.100) and bounding them from below, seems to summarize the correlations between all entangling intervals and their complements for the considered state. The appearance of such an integral term measuring correlations as a lower bound for complexity in field theory is consistent with our discussion of complexity for q-bits in Section 3.2.1. In this discussion we state that the gates required to map the reference state to the target state $|\psi_t\rangle$ necessarily need to build up the correlations between the subsystems present in $|\psi_t\rangle$. Therefore, these correlations should contribute to complexity.

When we combine the fact that the HSRC of global AdS$_3$ (5.53) only contains contributions involving entanglement entropies and the interpretation of these contributions as lower bound for complexity we conclude: the CFT vacuum satisfies a minimality condition regarding complexity. This is easy to see since the HSRC of global AdS$_3$ saturates the corresponding lower bound.

For reduced states – including states dual to BTZ black holes – on an entangling interval A we make analogous observations. We note that for these states entanglement entropy not only captures correlations between subsystems but also takes into account that the states are mixed (see Section 3.1.1). However, correlations still contribute to entanglement entropy and consequently play a role for

HRSC as well. We note that for reduced states the integral over entanglement entropies in (5.53), (5.100) and (5.120) not only contain entanglement entropies corresponding to subintervals of A but also entanglement entropies corresponding to intervals that only partially lie in A, as depicted in Figure 5.10. Despite these additional contributions, there are contributions of all subintervals of A present in the integral under consideration. It is easy to see these contributions, which again may be interpreted in terms of correlations between subintervals of A and their complements, provide a positive lower bound for complexity.

Further evidence for the importance of correlations for HSRC may be obtained from the interpretation of the volume form of kinematic space in terms of conditional mutual information (see Section 5.1.2). In Section 3.1.3 we argued that conditional mutual information captures certain correlations between subsystems. However, the argument leading to this conclusion was based on classical considerations. Therefore a more careful analysis is required in order to make the relation between correlations and HSRC more concrete.

HSRC Takes Correlations with the Complement of the Considered Entangling Interval Into Account. In the previous paragraph we noted that in our formulae (5.53), (5.100) and (5.120) for the complexity of a reduced state on an entangling interval A, there are contributions of entanglement entropies corresponding to intervals that partially lie in A and partially in its complement. This fact gives strong evidence that a concept of complexity for reduced CFT states based on HSRC takes into account that the considered state is part of a larger system. To be more precise, a reduced state is not just interpreted as a generic mixed state which needs to be generated from a reference state. The fact that this mixed state is obtained by reducing a state from a larger system to A plays a role for complexity.

In particular, this result shows that the concept of complexity for mixed states introduced in [179] and discussed in Section 3.2.1 cannot be straightforwardly applied to reduced states in order to construct a CFT dual of HSRC. This is due to the fact that this concept does not consider the subtlety that a given mixed state might be a reduced state.

The Reference State has the Properties of a Product State. In Section 3.2.1 we used the product state $|\psi_r\rangle = |00\cdots0\rangle$ (3.53) as reference state for q-bits. This state does not carry any correlations between its subsystems. Our results for HSRC are in agreement with a CFT reference state that has the same property, i.e. no interval $[u, v]$ is entangled with its complement $[u, v]^c$ in the reference state. This may be seen as follows. In the previous paragraphs we argued that our formulae for complexity (5.53), (5.100), (5.120) for the states we considered always contain an integral term over entanglement entropies that functions as a lower bound for complexity. Moreover, it is easy to see that any state with a classical, static space-time as gravitational dual has such an integral term as lower bound for HSRC.[22] This is an immediate consequence of the construction

---

[22]For the sake of this paragraph we assume that the volume formula (5.12) holds for these geometries, even though we have only proven it for global AdS$_3$ and the Poincaré patch (see

of kinematic space and the RT formula (3.32). We take this observation as a motivation for the hypothesis that the complexity of any state is bounded from below by such an integral over entanglement entropies. Given this assumption we expect that in the reference state no interval is entangled with its complement: when we consider a state on the whole constant time slice, we find the integral discussed above to include the entanglement entropies of all possible intervals on the constant time slice. The complexity of the reference state is per definicionem zero. Therefore, the integral including entanglement entropies has to be zero, since it is a lower bound for complexity. This condition is satisfied if the entanglement entropy of any entangling interval is zero. A state for which the entanglement entropy vanishes for each entangling interval by construction has no correlations between any interval and its complement. States with this property may be seen as the CFT analogue of the factorizing reference state $|\psi_r\rangle = |00\cdots0\rangle$ (3.53) introduced for q-bits in Section 3.2.1.

Given our discussion of entanglement in QFTs in Section 1.1 this is an intriguing result, as we stated that states in QFTs are usually entangled. So the reference state is expected to be a very exotic state of the CFT. We consider the vanishing of all entanglement entropies for the reference state to be a large N effect. For finite N corrections to HSRC may allow the reference state have non-vanishing entanglement entropies. Nevertheless, our observations allow us to conclude that the entanglement entropies of the reference state are suppressed in the large N limit. So we see that the reference state is weakly entangled compared to more common states in the CFT, such as the vacuum.

HSRC Encodes More than Just Spatial Correlations. In our formulae (5.100) and (5.120) for the complexity of conical defect and BTZ black hole geometries we see that not only entanglement entropy for entangling intervals is considered. There are also additional contributions associated with entwinement, which correspond to contributions of non-minimal geodesics to the volume enclosed by an entangling region and the corresponding RT surface. As stated in the introduction of Section 5.4, entwinement is proposed to be related to the entanglement of inner degrees of freedom which are not spatially organized. The presence of these additional contributions is in agreement with the statement that correlation play an important role for complexity (see Section 3.2.1). In the previous paragraphs we argued that correlations between spatial regions contribute to HSRC. In an analogous way we may argue that the contribution of entwinement to HSRC indicates that correlations between inner degrees of freedom are also present in complexity.

Moreover, we note that for the BTZ black hole also thermal contributions are present in HSRC (5.120). We see them as a consequence of the fact that the dual CFT state is mixed. However, a clear interpretation of these contributions is yet to be found. A careful analysis of them might provide a strategy for constructing a formulation of complexity for mixed states which may be compared with the formulations presented in Section 3.2.

Section 5.2).

5.6 Discussion

The subject of this chapter was the results regarding a field theory expression for HSRC my collaborators and I presented in [1] and [2]. We constructed an expression for the HSRC of states dual to global AdS_3 and the Poincaré patch only containing entanglement entropies (see Section 5.3). Since entanglement entropies are CFT quantities, this expression may be seen as a field theory formulation for HSRC.

We obtained this result by making use of the concept of kinematic space, which we reviewed in Section 5.1. The kinematic space $\mathcal{K}$ for asymptotic AdS_3 is the space of all boundary anchored geodesics on a constant time slice. For the considered vacuum states the one-to-one correspondence between such geodesics in the bulk and entangling intervals on the boundary allows to interpret $\mathcal{K}$ in the field theory perspective as the space of all entangling intervals (see Section 5.1.2). The fact that $\mathcal{K}$ has a very intuitive interpretation both from the bulk and the boundary point of view makes it a very powerful tool for systematically constructing CFT duals for given bulk quantities (see e.g. [95, 206]).

In Section 5.2 we presented and proved the volume formula, which provides a way for computing volumes on the constant time slice in the bulk as an integral over lengths of geodesics. The RT formula (3.32) allowed us to interpret these lengths appearing in the volume formula as entanglement entropies. We used this procedure to express the bulk volume $\mathrm{vol}(\mathcal{B}_A)$ associated with HSRC in terms of entanglement entropies in Section 5.3.1. Consequently, we obtained a formula for HSRC (5.53) which only depends on entanglement entropies. We see this formula as the field theory dual of HSRC for vacuum states. In particular, we developed a strategy for constructing this formula directly from the field theory side in Section 5.3.2. This procedure only requires the geometry (5.10) imposed on kinematic space, which can be motivated directly from the CFT side without any reference to the bulk.

Furthermore, we generalized our field theory expression for HSRC of vacuum states to excited states dual to conical defects and BTZ black holes in Section 5.4. For these geometries the geodesic attached to two points on the conformal boundary is not unique. Consequently, the CFT interpretation of kinematic space as the space of all entangling intervals is no longer possible. Therefore, the field theory interpretation of our formulae (5.97) and (5.118) for the HSRC of excited states is more involved than for the vacuum states corresponding to global AdS_3 and the Poincaré patch. Similar to the HSRC of vacuum states (5.53), the corresponding expressions for excited states (5.97), (5.118) contain terms that can be associated with entanglement entropy. However, they also include contributions for which this association is not possible. These contributions originate from the presence of additional (non-minimal) geodesics connecting two boundary points. Moreover, our expression (5.118) for the HSRC of states dual to BTZ black holes also contains terms originating from bulk geodesics running from the conformal boundary to the black hole horizon. These geodesics have only one endpoint attached to the boundary and therefore cannot be associated with entangling intervals. The additional contributions from non-minimal geodesics appearing in our HSRC formulae for ex-

cited states may be associated with a quantity called entwinement [146] which is seen as the field theory dual of the lengths of non-minimal geodesics (see beginning of Section 5.4).

As a first step towards a field theory interpretation of our formulae (5.97), (5.118) for HSRC of excited states, we rearranged the terms appearing in them in such a way that (5.97) and (5.118) may be written as integrals in the space of entangling intervals (5.100), (5.120). This procedure allowed us to separate the contributions of entanglement entropies from the additional contributions that cannot be associated with entanglement entropies. For the conical defect the resulting expression for HSRC consists of an integral only containing entanglement entropies and an integral containing contributions from entwinement.

For BTZ black holes we came to a similar conclusion but in addition found contributions that cannot be written as an integral over the space of entangling intervals. These contributions originate from the presence of geodesics in the bulk running from the boundary to the horizon. Due to their relation to the horizon we refer to them as *thermal contributions*.

HSRC is conjectured to be a measure for the complexity of subregions on the CFT side (see Section 3.2.3). Whether this conjecture is true is subject of current research. Since a satisfactory definition for subregion complexity has not yet been formulated, this conjecture is difficult to test. The results we presented in this chapter provide some valuable insights that may help to establish a field theory interpretation for HSRC. We saw that in all the considered cases (global AdS$_3$, Poincaré patch, conical defects and BTZ black holes) HSRC contains terms determined solely by entanglement entropies (5.53), (5.100) and (5.120). For excited states further terms are present (5.100), (5.120). The terms completely determined by entanglement entropy work as a lower bound for HSRC which is saturated for vacuum states, i.e. global AdS$_3$ and the Poincaré patch. In Section 5.5 we studied the above observations under the assumption that HSRC is indeed a reasonable measure for subregion complexity on the CFT side. We concluded that in this case, the reference state may be understood as a field theory analogue of a product state. Moreover, we found that HSRC seems to take correlations between the considered subsystem and its complement into account. This led us to the conclusion that HSRC may not be interpreted as the type of complexity for mixed states discussed in [179] (see Section 3.2.1), since the corresponding correlations are not considered there.

Even though the role of HSRC on the field theory side is still under debate, our observations show that the correlations present in the state under consideration play a crucial role for HSRC (see Section 5.5). Following our introduction to complexity in Section 3.2, this is a property that is also associated with complexity. However, to come to a rigorous field theory interpretation of HSRC further investigations are required. For instance, a generalization of our expressions for HSRC towards states with non-static gravity dual is required in order to see whether our interpretation of HSRC in terms of entanglement entropies and entwinement also holds for these situations. Moreover, the presence of entwinement in our expression suggest that this quantity and its role on the field theory side should also

be further examined. Furthermore, we restricted our study of HSRC to $(2+1)$-dimensional bulk geometries. It is an open question whether our results also apply for higher dimensional cases.

Chapter 6

Modular Hamiltonians on Entanglement Plateaux

In [3] I examined the inner structure of modular Hamiltonians (3.75) by using the relative entropy (3.82). Here we review the corresponding results. We consider a one-parameter family of states ρ_λ^Σ on a region Σ. The parameter λ may correspond to the energy density or the temperature of the system, for instance. For this one-parameter family we study the λ-dependence of

$$\Delta \langle K_0 \rangle (A, \lambda) = \mathrm{tr}_A(\rho_\lambda^A K_0(A)) - \mathrm{tr}_A(\rho_{\lambda_0}^A K_0(A)), \qquad (6.1)$$

where A is a subregion of Σ and $K_0(A)$ is the modular Hamiltonian of a reduced reference state $\rho_{\lambda_0}^A$. In particular, we focus on the situation where A and $B = \Sigma \backslash A$ form an entanglement plateau[1] that is stable under variations of the size of A. My result for this setup provides a relation between the λ-dependence of $\Delta \langle K_0 \rangle (A, \lambda)$ and the second derivative w.r.t. λ of the entanglement entropies $S(A, \lambda)$ and $S(B, \lambda)$ corresponding to ρ_λ^A and ρ_λ^B, respectively. In simple terms, my result states that if both $\Delta \langle K_0 \rangle (A, \lambda)$ and $\Delta \langle K_0 \rangle (B, \lambda)$ are linear in $\lambda - \lambda_0$ for a given A and variations of it, then $\partial_\lambda^2 S(A, \lambda)$ and $\partial_\lambda^2 S(B, \lambda)$ are constant under variations of the size of A. We present the exact statement of this result in Section 6.3.1.

This observation for the behavior of $\Delta \langle K_0 \rangle (A, \lambda)$ and $\Delta \langle K_0 \rangle (B, \lambda)$ may be derived from the monotonicity (3.88) of the relative entropy. The relative entropy is known to be a valuable quantity for the study of modular Hamiltonians and has been used to obtain many non-trivial results for these (see Section 3.3.3). My result offers a further application of the relative entropy to modular Hamiltonians providing deeper insight into their dependence on the parameter λ. It employs a non-trivial relation between the λ-dependence of modular Hamiltonians and entanglement entropies for one-parameter families of states. We note that the first law of entanglement [115], which we discuss in Section 6.2, provides such a relation as well. However, the first law of entanglement focuses on the linear term in the series expansion of $\Delta \langle K_0 \rangle (A, \lambda)$ in terms of $\lambda - \lambda_0$, whereas my result is subject to higher order contributions in $\lambda - \lambda_0$.

---

[1]The term entanglement plateau is explained and discussed in Section 6.1 in detail. For the sake of this introduction we state that A and B form an entanglement plateau if they saturate the Araki-Lieb inequality (3.10).

In AdS/CFT entangling regions forming an entanglement plateau are very common. This allows to apply my result to several setups in AdS/CFT. However, we need to stress that it is not only valid for holographic setups but holds in any quantum system.

Moreover, my result is of particular interest in the context of [200], where a topological condition was presented under which the modular Hamiltonian may be written as a local integral over the energy momentum tensor in two-dimensional CFTs (see Section 3.3.1). By choosing the parameter λ to be the energy density, my result offers a strategy for deciding when such an integral expression is not possible.

This chapter has the following structure. In Section 6.1 we review the concept of entanglement plateaux. This allows us to present the overall setup for my result in Section 6.2. We proof the result in Section 6.3 and apply it to several examples in Section 6.4, including states dual to black strings, black branes and BTZ black holes. We conclude with a discussion and final remarks in Section 6.5.

6.1 Entanglement Plateaux

As already mentioned at the beginning of this chapter my result is about the modular Hamiltonians for entangling regions forming entanglement plateaux. In this section we introduce the concept of entanglement plateaux and discuss some of their properties we require for my result.

6.1.1 Definition of Entanglement Plateaux

The term "entanglement plateau" was introduced in [114] and refers to a pair of entangling regions A, B for which

$$S(\Sigma) = |S(A) - S(B)| \tag{6.2}$$

holds. Here Σ is the union of A and B, i.e.

$$\Sigma = AB \,, \tag{6.3}$$

and $S(A)$ is the entanglement entropy corresponding to the reduced state ρ^A of the region A. $S(B)$ and $S(\Sigma)$ are defined in an analogous way. The defining equation (6.2) may be seen as the extremal case where the Araki-Lieb inequality (3.10) is saturated.[2]

There are many examples for entanglement plateaux. The most prominent is the situation of a pure state ρ^Σ on Σ. In this case we find

$$S(A) = S(B) \quad \text{and} \quad S(\Sigma) = 0 \,, \tag{6.4}$$

---

[2]We note that holographic situations where the Araki-Lieb inequality is saturated were also discussed in [157].
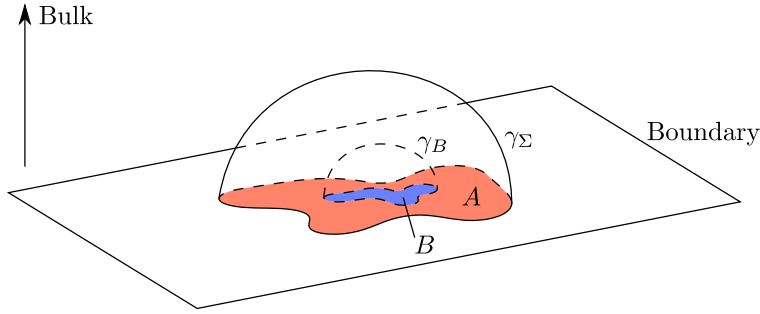
Figure 6.1: A typical example for an entanglement plateau in AdS/CFT. We consider two entangling regions A (red) and B (blue) on a constant time slice of the CFT on the conformal boundary of the bulk geometry. Here B is taken to be completely surrounded by A. Moreover, we assume the RT surfaces γ_Σ and γ_B of $\Sigma = AB$ and B not to intersect. In this situation we find that the union of γ_Σ and γ_B is homologous to A. If B is sufficiently small, we expect $\gamma_\Sigma \cup \gamma_B$ to be the RT surface of A.

so (6.2) trivially holds. Another entanglement plateau that is easily constructed is a state ρ^Σ of the form

$$\rho^\Sigma = \rho^A \otimes \rho^B \,, \tag{6.5}$$

where ρ^B is assumed to be pure, i.e. $S(B) = 0$. Due to the additivity of the entanglement entropy for product states (3.14), we find

$$S(\Sigma) = S(A) + S(B) = S(A) = |S(A) - S(B)| \tag{6.6}$$

for this setup, i.e. (6.2).

6.1.2 Holographic Examples for Entanglement Plateaux

In AdS/CFT entanglement plateaux are very common due to the Ryu-Takayanagi (RT) formula (3.32) as we now explain. The RT formula – which we discuss in Section 3.1.6 – states that in the AdS/CFT correspondence the entanglement entropy of a region Σ is given by the area of the minimal surface γ_Σ in the bulk homologous to Σ – the RT surface. We restrict our discussion to static space-times, where the RT surface lies in the same constant time slice as the entangling region A at the conformal boundary. If we choose $B \subset \Sigma$ in such a way that it has no boundary points in common with Σ and $\gamma_\Sigma \cap \gamma_B = \emptyset$ holds, we find that the surface $\gamma_\Sigma \cup \gamma_B$ is homologous to $A = \Sigma \backslash B$, as depicted in Figure 6.1. This may be seen as follows: by construction $\gamma_B \cup B$ and $\gamma_\Sigma \cup \Sigma$ enclose bulk regions R_B and R_Σ, respectively. Since γ_Σ and γ_B do not intersect we conclude that $R_\Sigma \backslash R_B$ is a region that is enclosed by $\gamma_\Sigma \cup \gamma_B$ and $\Sigma \backslash B = A$, i.e. $\gamma_\Sigma \cup \gamma_B$ is homologous to A.

So we see that $\gamma_\Sigma \cup \gamma_B$ is a very natural candidate for the RT surface γ_A. If $\gamma_\Sigma \cup \gamma_B$ turns out to be the RT surface of A it is easy to see that

$$S(A) = S(\Sigma) + S(B) \quad \Leftrightarrow \quad S(\Sigma) = S(A) - S(B) \tag{6.7}$$
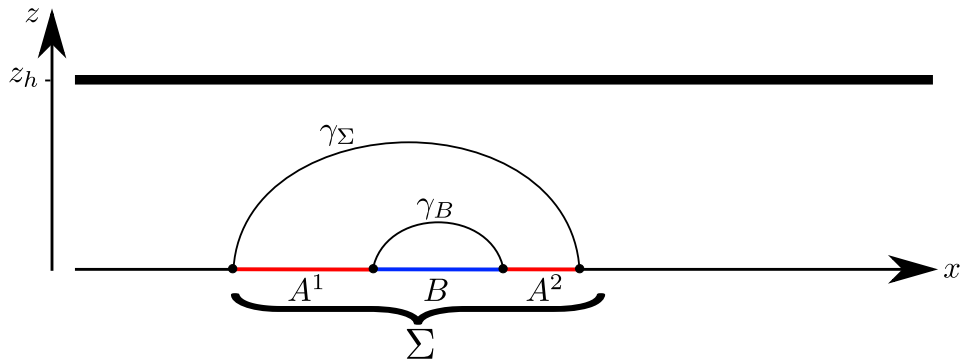
Figure 6.2: An entanglement plateau in black string geometry. The graphic shows a constant time slice of the black string geometry (6.8). The CFT_2 state dual to this geometry is thermal and defined on the real axis. An entangling region A that is the union of two sufficiently close intervals A^1 and A^2 forms an entanglement plateau with the interval B between A^1 and A^2, since $\gamma_A = \gamma_\Sigma \cup \gamma_B$, where $\Sigma = AB$.

holds, i.e. A and B form an entanglement plateau. We need to emphasize that there is no guarantee for $\gamma_\Sigma \cup \gamma_B = \gamma_A$ to hold since there are explicit counterexamples, such as two intervals on the Poincaré patch that are sufficiently far apart from each other (see Section 3.1.7). However, for a sufficiently small B we expect it to be true, since in the limit of vanishing B γ_A should asymptote to γ_Σ [157] (see Figure 6.1).

We now present explicit holographic examples for entanglement plateaux.

Two Intervals in Black String Geometry

We consider a thermal state on the real axis in AdS_3/CFT_2 dual to the geometry of a black string

$$ds^2_{BS} = \frac{L^2}{z^2}\Big(-\frac{z_h^2 - z^2}{z_h^2}dt^2 + \frac{z_h^2}{z_h^2 - z^2}dz^2 + dx^2 \Big), \tag{6.8}$$

where $0 < z < z_h$ and $x, t \in \mathbb{R}$. [3] The conformal boundary of this geometry is located at $z = 0$ and the horizon of the black string corresponds to $z = z_h$. The entangling region A is defined to be the union of two intervals A^1 and A^2. Moreover, B is given by the interval between A^1 and A^2, i.e. we choose B in such a way that $\Sigma = AB$ is an interval. We present this setup in Figure 6.2.

If A^1 and A^2 are sufficiently close, i.e. if B is sufficiently small, the RT surface γ_A is given by $\gamma_\Sigma \cup \gamma_B$ as depicted in Figure 6.2. This may be seen in an analogous way as for the corresponding setup for the Poincaré patch geometry presented in Section 3.1.7. Following the discussion above (6.7), we conclude that A and B form an entanglement plateau

---

[3]This geometry is a planar AdS_3 black hole. It may be seen as the 3-dimensional analogue of the metric (2.139) obtained from black $D3$-branes (see e.g. [219]).
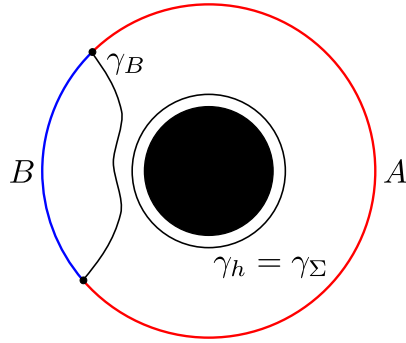
Figure 6.3: An entanglement plateau for a thermal state dual to a *BTZ* black hole. We depict a constant time slice of the BTZ black hole (6.9). This geometry is dual to a thermal CFT_2 state on a circle. If we choose the entangling region A to be sufficiently large the corresponding RT surface is given by $\gamma_A = \gamma_h \cup \gamma_B$, where γ_h is the horizon of the black hole and $B = A^c$. This choice of B implies that $\Sigma = AB$ is the whole circle. Therefore, $\gamma_h = \gamma_\Sigma$ holds and consequently A and B form an entanglement plateau.

One Interval in the BTZ Black Hole Geometry

The BTZ black hole is an asymptotic AdS_3 geometry that resembles the gravity dual of a thermal CFT_2 state on a circle (see Section 2.5.2). The corresponding metric is given by (2.148)

$$ds^2_{BTZ} = -\frac{\tilde{r}^2 - \tilde{r}_h^2}{L^2}d\tilde{t}^2 + \frac{L^2}{\tilde{r}^2 - \tilde{r}_h^2}d\tilde{r}^2 + \tilde{r}^2 d\phi^2 \,, \tag{6.9}$$

where $t \in \mathbb{R}$, $0 < \tilde{r}_h < \tilde{r}$ and $\phi \sim \phi + 2\pi$. The black hole horizon is located at $\tilde{r} = \tilde{r}_h$ and the conformal boundary corresponds to $\tilde{r} \longrightarrow \infty$. If we choose A to be an interval in ϕ that is sufficiently large, the RT surface γ_A is the union of γ_{A^c} and the horizon γ_h (see Section 3.1.7), as we depict in Figure 6.3. The length of the curve γ_h circumventing the horizon corresponds to the thermal entropy of the state. Thus, if we choose $B = A^c$, i.e. if we set Σ to be the whole circle the CFT is defined on, we find $\gamma_h = \gamma_\Sigma$ and in particular (6.7). Therefore we see that A and B form an entanglement plateau.[4]

6.1.3 One-Parameter Families of Entanglement Plateaux

We now introduce a continuous parameter σ to the entangling regions A and B forming an entanglement plateau, i.e.

$$A \longrightarrow A_\sigma \,, \quad B \longrightarrow B_\sigma \,. \tag{6.10}$$

This parameter is essential for the formulation of my result for modular Hamiltonians presented in Section 6.3. It allows us to continuously vary the size of A_σ

---

[4]The BTZ black hole is the original example for an entanglement plateau that was discussed in [114].
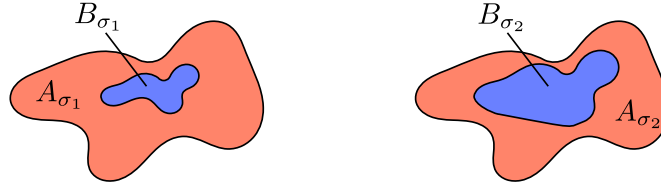
Figure 6.4: One-parameter families of entangling regions. We consider two one-parameter families of entangling regions A_σ and B_σ. The dependence of these regions on the parameter σ is chosen in such a way that $\Sigma = A_\sigma B_\sigma$ is constant in σ and $A_{\sigma_2} \subset A_{\sigma_1}$ for $\sigma_1 < \sigma_2$. These two properties imply $B_{\sigma_1} \subset B_{\sigma_2}$.

and B_σ in a systematic way. The parameter dependency of A_σ and B_σ is chosen in such a way that the following properties hold,

$$A_{\sigma_2} \subset A_{\sigma_1} \quad \text{for} \quad \sigma_1 < \sigma_2 \tag{6.11}$$

$$\Sigma = const. \quad \text{for all } \sigma \,, \tag{6.12}$$

i.e. σ varies the size of A_σ while keeping $\Sigma = A_\sigma B_\sigma$ fixed. In particular, this implies

$$B_{\sigma_1} \subset B_{\sigma_2} \quad \text{for} \quad \sigma_1 < \sigma_2 \,. \tag{6.13}$$

We depict this setup in Figure 6.4. Moreover, we assume A_σ and B_σ to form an entanglement plateau for all σ. This is a restriction to the amount A_σ is allowed to vary. To see this, we consider $A = [-a, -\sigma] \cup [\sigma, a]$ to be the union of two intervals for a CFT state with the Poincaré patch as holographic dual (see Section 3.1.7). If σ is too small, the RT surface γ_{A_σ} undergoes a phase transition which causes the defining property (6.2) for entanglement plateaux to no longer hold in this setup (3.47). So we see that in general the variation of A_σ has to be sufficiently small.

The defining equation (6.2) for entanglement plateaux implies

$$S(\Sigma) = \pm\big(S(A_\sigma) - S(B_\sigma)\big) \,, \tag{6.14}$$

where the $+$ is chosen if $S(A_\sigma) - S(B_\sigma) \geq 0$ and the $-$ if $S(A_\sigma) - S(B_\sigma) < 0$. We now show that the sign of $S(A_\sigma) - S(B_\sigma)$ does not change in σ, i.e. the sign on the r.h.s. of (6.14) is the same for all σ. This plays an important role for proving my result for modular Hamiltonians (see Section 6.3.2). First we consider the case $S(\Sigma) = 0$. Here the σ-independence of the sign is obvious. Second we discuss the situation $S(\Sigma) > 0$. If there were values σ_+ and σ_- for σ such that

$$S(A_{\sigma_+}) - S(B_{\sigma_+}) > 0 \quad \text{and} \quad S(A_{\sigma_-}) - S(B_{\sigma_-}) < 0 \tag{6.15}$$

hold, we would find a value σ_0 between σ_+ and σ_- with

$$S(A_{\sigma_0}) - S(B_{\sigma_0}) = 0 \,, \tag{6.16}$$

due to the continuity of σ. However, this contradicts (6.14) since $S(\Sigma)$ is assumed to be strictly positive. Therefore, either σ_+ or σ_- cannot exist. This completes the proof that the sign of $S(A_\sigma) - S(B_\sigma)$ is constant in σ.

6.2 Setup and Motivation

In order to discuss my result for modular Hamiltonians in Section 6.3 we now introduce the setup necessary for formulating it as well as a motivation. In [3] I was considering the object

$$\Delta \langle K_0 \rangle (A, \lambda) = \text{tr}_A(\rho_\lambda^A K_0(A)) - \text{tr}_A(\rho_{\lambda_0}^A K_0(A)) \tag{6.17}$$

for a family of states ρ_λ that depend on a parameter λ. Here $K_0(A)$ is the modular Hamiltonian of the reference state ρ_{λ_0} reduced to an entangling region A, i.e.

$$\rho_{\lambda_0}^A = \frac{e^{-K_0(A)}}{\text{tr}_A \left(e^{-K_0(A)} \right)}, \quad \text{where} \quad \rho_{\lambda_0}^A = \text{tr}_{A^c}(\rho_{\lambda_0}). \tag{6.18}$$

As can be seen in (3.82) $\Delta \langle K_0 \rangle (A, \lambda)$ plays a crucial role for the relative entropy of the reduced states ρ_λ^A and $\rho_{\lambda_0}^A$,

$$S_{rel}(A, \lambda) = \Delta \langle K_0 \rangle (A, \lambda) - \Delta S(A, \lambda), \tag{6.19}$$

where $\Delta S(A, \lambda)$ is given by

$$S(A, \lambda) - S(A, \lambda_0) \tag{6.20}$$

and $S(A, \lambda)$ denotes the entanglement entropy of ρ_λ^A. In AdS/CFT a systematic approach is known for determining ΔS since the entanglement entropies it consist of are given by the RT formula (3.32). However, for $\Delta \langle K_0 \rangle$ there is no such procedure. Thus, when computing the relative entropy of two states, calculating $\Delta \langle K_0 \rangle$ is the most challenging part. There are only a view cases where $\Delta \langle K_0 \rangle$ known explicitly.[5] The importance of $\Delta \langle K_0 \rangle$ for S_{rel} as well as the fact that very little is known about it motivated me to study $\Delta \langle K_0 \rangle$ in [3].

Even though there are many things about $\Delta \langle K_0 \rangle$ that are yet to be understood, the first order contribution in $\tilde\lambda = \lambda - \lambda_0$ [6] is known to be $\partial_\lambda \Delta S(A, \lambda)|_{\lambda=\lambda_0} \tilde\lambda$ [115], i.e.

$$\Delta \langle K_0 \rangle (A, \lambda) = \partial_\lambda \Delta S(A, \lambda)|_{\lambda=\lambda_0} \tilde\lambda + \mathcal{O}(\tilde\lambda^2), \tag{6.21}$$

or equivalently

$$\partial_\lambda \Delta \langle K_0 \rangle (A, \lambda)|_{\lambda=\lambda_0} = \partial_\lambda \Delta S(A, \lambda)|_{\lambda=\lambda_0}. \tag{6.22}$$

The relation (6.22) is referred to as the *first law of entanglement*. It is a simple consequence of the non-negativity of the relative entropy (3.87), as we now show.[7]

From (6.19) it is easy to see that $S_{rel}(A, \lambda_0) = 0$ holds. Since S_{rel} is always non-negative we conclude that S_{rel} has a minimum at $\lambda = \lambda_0$. Consequently, we find

$$\partial_\lambda S_{rel}(A, \lambda)|_{\lambda=\lambda_0} = \partial_\lambda \left(\Delta \langle K_0 \rangle (A, \lambda) - \Delta S(A, \lambda) \right)|_{\lambda=\lambda_0} = 0 \tag{6.23}$$

---

[5]For instance, in the cases where K_0 is known (see e.g. (3.80), (3.81)), $\Delta \langle K_0 \rangle$ may be determined as well.

[6]Since $\Delta \langle K_0 \rangle (A, \lambda_0) = 0$, it is reasonable to treat $\Delta \langle K_0 \rangle$ as a function of $\tilde\lambda$ rather than λ.

[7]The following argument is taken from [115].

and therefore (6.22).

So we see that if $\Delta \langle K_0 \rangle$ is linear in $\tilde{\lambda}$, its explicit form is completely determined by entanglement entropy. We present an explicit example for such a situation in (6.35). However, in general $\Delta \langle K_0 \rangle$ cannot be expected to be linear in $\tilde{\lambda}$.

In [3] I was examining how $\Delta \langle K_0 \rangle (A, \lambda)$ depends on $\tilde{\lambda}$ for entangling regions that form an entanglement plateau. To be more precise, I investigated when we can be sure that $\Delta \langle K_0 \rangle (A, \lambda)$ or $\Delta \langle K_0 \rangle (B, \lambda)$ is not linear in $\tilde{\lambda}$ if A and B form an entanglement plateau that is stable under variations of the size of A and B for all states ρ_λ.

6.3   Non-Linearities of One-Parameter Families of Modular Hamiltonians

We now formulate the exact statement of the result for one-parameter families of states on entanglement plateaux I published in [3]. Moreover, we present a proof for it in this section.

6.3.1   A Result for Modular Hamiltonians on Entanglement Plateaux

My result considers two entangling regions A and B that form an entanglement plateau for a family of states ρ_λ. The plateau is considered to be stable under variations of the size of A and B that keep AB fixed, i.e. if the sizes of A and B are varied in this way, the resulting regions are assumed to still form an entanglement plateau for all ρ_λ. For this setup I was able to show that the only way how both $\Delta \langle K_0 \rangle (A, \lambda)$ and $\Delta \langle K_0 \rangle (B, \lambda)$ may be linear in $\tilde{\lambda}$ is if $\partial_\lambda^2 S(A, \lambda)$ and $\partial_\lambda^2 S(B, \lambda)$ are constant under the considered variations of A and B [3].

This result can be used to check whether an entangling region A is expected to lead to higher order contributions of $\tilde{\lambda}$ in $\Delta \langle K_0 \rangle (A, \lambda)$: If we can find an entangling region B in such a way that A and B form an entanglement plateau stable under small variations of the size of A and B that keep AB invariant, it suffices to examine $\partial_\lambda^2 S(A, \lambda)$ and $\partial_\lambda^2 S(B, \lambda)$. If one of them is not constant under variations of the respective entangling region, we can conclude that $\Delta \langle K_0 \rangle (A, \lambda)$, $\Delta \langle K_0 \rangle (B, \lambda)$ or both are non-linear in $\tilde{\lambda}$. We demonstrate this method on several examples in Section 6.4. Furthermore, we emphasize that this result is true for any quantum system, i.e. it is not restricted to holographic situations.

We conclude this section with presenting the explicit statement of my result in the form we prove it in Section 6.3.2.

Let ρ_λ be a one-parameter family of states and A_σ and B_σ two families of entangling regions depending on a continuous parameter σ. We assume $A_{\sigma_2} \subset A_{\sigma_1}$ for $\sigma_1 < \sigma_2$ and $\Sigma = A_\sigma B_\sigma$ to be constant in σ. Moreover, A_σ and B_σ are considered to form entanglement plateaux for all σ and all states ρ_λ, i.e.

$$S(\Sigma, \lambda) = |S(A_\sigma, \lambda) - S(B_\sigma, \lambda)| \quad \forall \sigma, \lambda \,. \tag{6.24}$$

Also, $S(A_\sigma, \lambda)$, $S(B_\sigma, \lambda)$ and $S(\Sigma, \lambda)$ are taken to be differentiable in λ for all σ and the reference parameter λ_0 is assumed to be no boundary point of the domain of λ.

If there is an interval $[\xi, \eta]$ such that $\Delta \langle K_0 \rangle (A_\sigma, \lambda)$ and $\Delta \langle K_0 \rangle (B_\sigma, \lambda)$ are linear in $\tilde{\lambda} = \lambda - \lambda_0$ for all $\sigma \in [\xi, \eta]$, then both $\partial_\lambda^2 S(A_\sigma, \lambda)$ and $\partial_\lambda^2 S(B_\sigma, \lambda)$ are constant in σ on $[\xi, \eta]$ for all λ.

6.3.2   Proof of the Result for Modular Hamiltonians

The proof of the result presented in Section 6.3.1 is based on properties of the relative entropy S_{rel} (3.82). This quantity is known to be a very powerful tool for studying modular Hamiltonians (see Section 3.3.3). For instance, the derivation of the first law of entanglement (6.22) presented in Section 6.2 is an application of the non-negativity of S_{rel}. For my result we require the monotonicity of S_{rel} (3.88),

$$S_{rel}(A) \leq S_{rel}(A') \,, \tag{6.25}$$

where A and A' are two entangling regions with $A \subseteq A'$.

Proof for Black Strings

Before we present the proof for generic entanglement plateaux in Section 6.3.2, we first consider a special case to demonstrate the basic idea and to make the statement of the result (see Section 6.3.1) more accessible.

For the one-parameter family of states ρ_λ we take thermal CFT_2 states on the real axis that are dual to the geometry of black strings (6.8). The parameter λ is chosen to be the energy density (see e.g. [115, 219]),

$$\lambda = \frac{L}{16\pi G_3 z_h^2} = \frac{\pi c}{6\beta^2} \,. \tag{6.26}$$

Here $c = 3L/2G_3$ (2.117) is the central charge of the CFT and β is the inverse temperature of the state ρ_λ. In Section 6.1.2 we pointed out that an entangling region $A = A^1 A^2$ that is the union of two sufficiently close disjoint intervals forms an entanglement plateau with the interval B lying between A^1 and A^2. We use this setup to construct one-parameter families A_σ and B_σ of entanglement plateaux: consider two real numbers $a_1 < 0 < a_2$ as well as a parameter σ satisfying $a_1 < -\sigma$ and $\sigma < a_2$. We now define

$$A_\sigma^1 = [a_1, -\sigma] \,, \quad A_\sigma^2 = [\sigma, a_2] \,, \quad A_\sigma = A_\sigma^1 A_\sigma^2 \quad \text{and} \quad B_\sigma = [-\sigma, \sigma] \,, \tag{6.27}$$
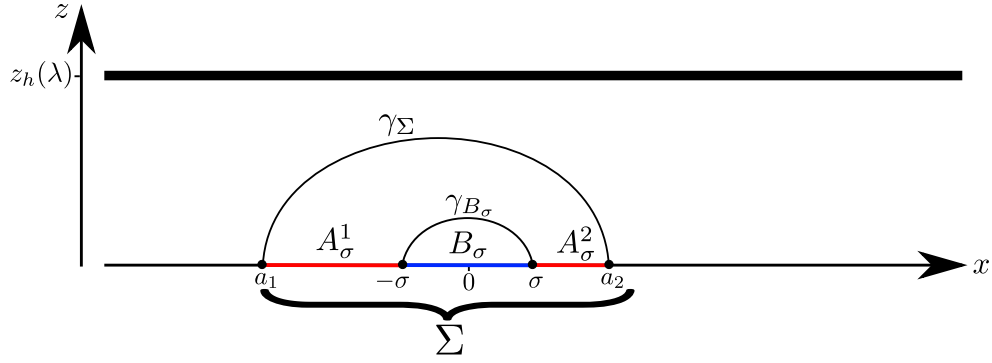
Figure 6.5: A family entangling regions forming entanglement plateaux. We consider an entangling interval $B_\sigma = [-\sigma, \sigma]$ and the union A_σ of two entangling intervals $A_\sigma^1 = [a_1, -\sigma]$ and $A_\sigma^2 = [\sigma, a_2]$ for states dual to black strings (6.8). The union of $\Sigma = A_\sigma B_\sigma$ is constant in σ. If σ is sufficiently small, A_σ and B_σ form an entanglement plateau, i.e. the RT surface of γ_{A_σ} is the union of γ_{B_σ} and γ_σ, which implies (6.2).

where the range of σ is restricted in such a way that A_σ and B_σ form an entanglement plateau for all λ that we consider. We depict this setup in Figure 6.5. Note that the maximal distance, i.e. the maximal value of σ, A_σ^1 and A_σ^2 are allowed to have so that A_σ and B_σ form an entanglement plateau depends on λ. To be more precise, if we choose σ too large for a given λ, the RT surface γ_{A_σ} undergoes a phase transition and A_σ and B_σ no longer form an entanglement plateau.[8] The critical value of σ where the phase transition occurs depends on λ. So the deviation of λ from a given reference value λ_0 and the range of allowed σ has to be chosen in such a way that γ_{A_σ} does not undergo the phase transition for all λ and σ, i.e. A_σ and B_σ have to form an entanglement plateau for all λ and σ.

In this setup we now demonstrate how the monotonicity of the relative entropy (6.25) may be used to show that $\Delta \langle K_0 \rangle (A_\sigma, \lambda)$ is not linear in $\tilde\lambda$ for all σ except possibly one. We argue that under the assumption that $\Delta \langle K_0 \rangle (A_\sigma, \lambda)$ is linear for more than one particular value of σ the monotonicity of S_{rel} would be violated.

So we now assume $\Delta \langle K_0 \rangle (A_\sigma, \lambda)$ to be linear in $\tilde\lambda$ and compute $S_{rel}(A_\sigma, \lambda)$. For $S_{rel}(A_\sigma, \lambda)$ we need to determine $\Delta \langle K_0 \rangle (A_\sigma, \lambda)$ and $\Delta S(A_\sigma, \lambda)$ (3.82). Since A_σ and B_σ form an entanglement plateau, the latter is given by

$$\Delta S(A_\sigma, \lambda) = \Delta S(\Sigma, \lambda) + \Delta S(B_\sigma, \lambda) = \Delta S(\Sigma, \lambda) + \frac{c}{3} \log \left(\frac{\beta \sinh(2\pi\sigma/\beta)}{\beta_0 \sinh(2\pi\sigma/\beta_0)} \right),$$
(6.28)

where $\Sigma = A_\sigma B_\sigma = [a_1, a_2]$ and $\beta_0 = \beta(\lambda_0)$ is the inverse temperature (6.26) of the reference state. In the second equality we used [82, 161]

$$S(B_\sigma, \lambda) = \frac{c}{3} \log \left(\frac{\beta}{\pi\epsilon} \sinh\left(\frac{2\pi\sigma}{\beta} \right) \right),$$
(6.29)

---

[8]This phase transition is analogous to the situation for the Poincaré patch discussed in Section 3.1.7.
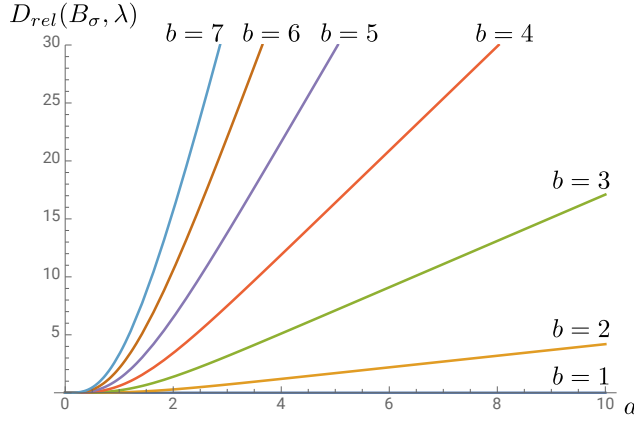
Figure 6.6: Plot of $D_{rel}(B_\sigma, \lambda)$ (6.32) for $a = 2\pi\sigma/\beta_0 \in [0, 10]$ and $b = \beta_0/\beta = 0, 1, \ldots, 7$. The global multiplicative factor $c/3$ is set to 1. We see that for fixed b D_{rel} grows monotonically with a. Consequently, D_{rel} grows monotonically with σ for fixed β and β_0. For $b = 1$ we find $D_{rel} = 0$. This is an immediate consequence of the fact that $b = 1$ corresponds to $\lambda = \lambda_0$ (6.26).

where ϵ is a UV cut-off.

Since we assume $\Delta \langle K_0 \rangle (A_\sigma, \lambda)$ to be linear in $\tilde{\lambda}$ we may determine it via the first law of entanglement (6.22), i.e.

$$\Delta \langle K_0 \rangle (A_\sigma, \lambda) = \Delta S'(A_\sigma, \lambda_0)\tilde{\lambda}, \tag{6.30}$$

where the $'$ refers to a derivative w.r.t. λ, i.e. $\partial_\lambda S(A_\sigma, \lambda)|_{\lambda=\lambda_0}$. Combining this result with (6.28) we obtain

$$S_{rel}(A_\sigma, \lambda) = \Delta S'(\Sigma, \lambda_0)\tilde{\lambda} - \Delta S(\Sigma, \lambda) + D_{rel}(B_\sigma, \lambda), \tag{6.31}$$

where

$$\begin{aligned} D_{rel}(B_\sigma, \lambda) &= \Delta S'(B_\sigma, \lambda_0)\tilde{\lambda} - \Delta S(B_\sigma, \lambda) \\ &= \frac{c}{3}\left(\frac{1}{2}(1 - b^2)(1 - a\coth(a)) + \log\left(b\frac{\sinh(a)}{\sinh(b\,a)}\right)\right), \end{aligned} \tag{6.32}$$

with $a = 2\pi\sigma/\beta_0$ and $b = \beta_0/\beta$.

From (6.31) we see that $S_{rel}(A_\sigma, \lambda)$ depends on σ only via $D_{rel}(B_\sigma, \lambda)$. In Figure 6.6 we show that $D_{rel}(B_\sigma, \lambda)$ grows monotonically with a for fixed b and consequently $D_{rel}(B_\sigma, \lambda)$ grows with σ for fixed λ and λ_0.

If we now assume that there are two values ξ, η of σ, where we w.l.o.g. assume $\xi < \eta$, for which $\Delta \langle K_0 \rangle (A_\sigma, \lambda)$ is linear in $\tilde{\lambda}$, we conclude

$$S_{rel}(A_\xi, \lambda) < S_{rel}(A_\eta, \lambda). \tag{6.33}$$

However, this is a contradiction to the monotonicity of S_{rel} (6.25) since $A_\eta \subset A_\xi$. Thus we conclude that there is at most one value for σ such that $\Delta \langle K_0 \rangle (A_\sigma, \lambda)$ is

linear in $\tilde{\lambda}$.

We see that in the example presented above the monotonicity of the relative entropy allows us to argue that $\Delta \langle K_0 \rangle (A_\sigma, \lambda)$ cannot be linear in $\tilde{\lambda}$ except for possibly one particular σ. This conclusion relies heavily on the fact that an explicit expression for $S(B_\sigma, \lambda)$ is known. This allowed us to compute $D_{rel}(B_\sigma, \lambda)$ (6.32) and conclude that the monotonicity of S_{rel} would be violated if $\Delta \langle K_0 \rangle (A_\sigma, \lambda)$ were linear in $\tilde{\lambda}$ for more than one value of σ. If we want to expand the discussion of this section to generic entanglement plateaux we do not have an explicit expression for $D_{rel}(B_\sigma, \lambda)$. We now demonstrate how to conclude that there is a conflict between the linearity of $\Delta \langle K_0 \rangle (A_\sigma, \lambda)$ and the monotonicity of S_{rel} without knowing the explicit form of $D_{rel}(B_\sigma, \lambda)$. The corresponding argument is based on the fact that $D_{rel}(B_\sigma, \lambda)$ is the relative entropy $S_{rel}(B_\sigma, \lambda)$ as we now show.

The modular Hamiltonian of the reduced reference state $\rho_{\lambda_0}^{B_\sigma}$ on B_σ is given by [220, 221]

$$K_0(B_\sigma) = \int_{-\sigma}^{\sigma} dx \, \beta_0 \frac{\cosh(\frac{2\pi\sigma}{\beta_0}) - \cosh(\frac{2\pi x}{\beta_0})}{\sinh(\frac{2\pi\sigma}{\beta_0})} T_{00}(x) \,, \tag{6.34}$$

where $T_{\mu\nu}$ is the energy momentum tensor of the CFT. The expectation value of T_{00} is the energy density, i.e. the parameter λ (6.26). Thus we find

$$\Delta \langle K_0 \rangle (B_\sigma, \lambda) = \beta_0 \left(2\sigma \coth \left(\frac{2\pi\sigma}{\beta_0} \right) - \frac{\beta_0}{\pi} \right) \tilde{\lambda} = \Delta S'(B_\sigma, \lambda_0) \tilde{\lambda} \,. \tag{6.35}$$

The second equality is an implication of the first law of entanglement (6.22) but can also be derived directly using (6.29). So by considering (6.32) we find

$$D_{rel}(B_\sigma, \lambda) = S_{rel}(B_\sigma, \lambda) \,. \tag{6.36}$$

This observation allows us to rewrite (6.31) as

$$S_{rel}(A_\sigma, \lambda) = \Delta S'(\Sigma, \lambda_0) \tilde{\lambda} - \Delta S(\Sigma, \lambda) + S_{rel}(B_\sigma, \lambda) \,. \tag{6.37}$$

Here we see now that the monotonicity of S_{rel} (6.25) is in conflict with the linearity of $\Delta \langle K_0 \rangle (A_\sigma, \lambda)$: If $S_{rel}(B_\sigma, \lambda)$ grows with σ as it should since $B_{\sigma_1} \subset B_{\sigma_2}$ for $\sigma_1 < \sigma_2$, $S_{rel}(A_\sigma, \lambda)$ does the same. But since $A_{\sigma_2} \subset A_{\sigma_1}$ this contradicts the monotonicity of S_{rel}.

Proof for Generic Entanglement Plateaux

We now present the proof of my result as formulated in Section 6.3.1. In the following we assume that both $\Delta \langle K_0 \rangle (A_\sigma, \lambda)$ and $\Delta \langle K_0 \rangle (B_\sigma, \lambda)$ are linear in $\tilde{\lambda}$ for $\sigma \in [\xi, \eta]$ and show that, given the prerequisites from Section 6.3.1, $\partial_\lambda^2 S(A_\sigma, \lambda)$ and $\partial_\lambda^2 S(B_\sigma, \lambda)$ are constant on $[\xi, \eta]$. This result is a consequence of the monotonicity of S_{rel}.

From (6.24) it is easy to see that

$$S(A_\sigma, \lambda) = S(B_\sigma, \lambda) \pm S(\Sigma, \lambda) \tag{6.38}$$

holds, where for $S(A_\sigma, \lambda) \geq S(B_\sigma, \lambda)$ we have $+$ and $-$ otherwise. In Section 6.1.3 we show that this sign is independent of σ, i.e. only λ determines whether $+$ or $-$ appears in (6.38). By assuming w.l.o.g. $S(A_\sigma, \lambda_0) \geq S(B_\sigma, \lambda_0)$ we find

$$\Delta S'(A_\sigma, \lambda_0) = \Delta S'(B_\sigma, \lambda_0) + \Delta S'(\Sigma, \lambda_0) , \tag{6.39}$$

where the $'$ corresponds to a derivative w.r.t. λ, as we now show. We need to distinguish the situations $S(\Sigma, \lambda_0) > 0$ and $S(\Sigma, \lambda_0) = 0$. First consider $S(\Sigma, \lambda_0) > 0$. This inequality also holds in a small neighborhood of λ_0. Thus (6.38) reduces to

$$S(A_\sigma, \lambda) = S(B_\sigma, \lambda) + S(\Sigma, \lambda) , \tag{6.40}$$

for λ sufficiently close to λ_0. This implies (6.39).

In the second case, $S(\Sigma, \lambda_0) = 0$, the non-negativity of the entanglement entropy implies that $S(\Sigma, \lambda)$ is minimal for $\lambda = \lambda_0$. By assumption $S(\Sigma, \lambda)$ is differentiable in λ and λ_0 is not a boundary point of the domain of λ. So we conclude $S'(\Sigma, \lambda_0) = 0$ which implies via (6.24)

$$0 = S'(\Sigma, \lambda_0) = \partial_\lambda |S(A_\sigma, \lambda) - S(B_\sigma, \lambda)| \Big|_{\lambda=\lambda_0} = \partial_\lambda \sqrt{\left(S(A_\sigma, \lambda) - S(B_\sigma, \lambda)\right)^2}\Big|_{\lambda=\lambda_0}$$

$$= \lim_{\lambda \to \lambda_0} \left(S'(A_\sigma, \lambda) - S'(B_\sigma, \lambda)\right) \frac{S(A_\sigma, \lambda) - S(B_\sigma, \lambda)}{|S(A_\sigma, \lambda) - S(B_\sigma, \lambda)|}$$

$$\tag{6.41}$$

and therefore (6.39),

$$\Delta S'(A_\sigma, \lambda_0) = \Delta S'(B_\sigma, \lambda_0) = \Delta S'(B_\sigma, \lambda_0) + \Delta S'(\Sigma, \lambda_0) , \tag{6.42}$$

where in the second equality we applied $\Delta S'(\Sigma, \lambda_0) = 0$.

The relation (6.39) allows us to express $S_{rel}(A_\sigma, \lambda)$ in terms of $S_{rel}(B_\sigma, \lambda)$: since both $\Delta \langle K_0 \rangle (A_\sigma, \lambda)$ and $\Delta \langle K_0 \rangle (B_\sigma, \lambda)$ are considered linear in $\tilde{\lambda}$, (6.39) together with the first law of entanglement (6.22) gives

$$\Delta \langle K_0 \rangle (A_\sigma, \lambda) = \left(\Delta S'(B_\sigma, \lambda_0) + \Delta S'(\Sigma, \lambda_0)\right)\tilde{\lambda} = \Delta \langle K_0 \rangle (B_\sigma, \lambda) + \Delta S'(\Sigma, \lambda_0)\tilde{\lambda} . \tag{6.43}$$

By applying (6.38) to $\Delta S(A_\sigma, \lambda)$ we conclude

$$S_{rel}(A_\sigma, \lambda) = \Delta S'(\Sigma, \lambda_0)\tilde{\lambda} \mp \Delta S(\Sigma, \lambda) + S_{rel}(B_\sigma, \lambda) . \tag{6.44}$$

The monotonicity of the relative entropy (6.25) implies

$$S_{rel}(B_\xi, \lambda) \leq S_{rel}(B_\eta, \lambda) \tag{6.45}$$

and

$$S_{rel}(A_\xi, \lambda) \geq S_{rel}(A_\eta, \lambda) , \tag{6.46}$$

since $A_\eta \subset A_\xi$ and $B_\xi \subset B_\eta$. However, (6.44) together with (6.45) also implies

$$S_{rel}(A_\xi, \lambda) \leq S_{rel}(A_\eta, \lambda) \tag{6.47}$$

and consequently we find

$$S_{rel}(A_\xi, \lambda) = S_{rel}(A_\eta, \lambda). \tag{6.48}$$

The monotonicity of S_{rel} then allows us to conclude that $S_{rel}(A_\sigma, \lambda)$ is constant in σ for all $\sigma \in [\xi, \eta]$. Since the only σ-dependent term in (6.44) is $S_{rel}(B_\sigma, \lambda)$, this implies that $S_{rel}(B_\sigma, \lambda)$ is constant in σ on $[\xi, \eta]$ as well.

So we see that the monotonicity of the relative entropy leads us to the conclusion that both

$$S_{rel}(A_\sigma, \lambda) = \Delta \langle K_0 \rangle (A_\sigma, \lambda) - \Delta S(A_\sigma, \lambda) \tag{6.49}$$

and

$$S_{rel}(B_\sigma, \lambda) = \Delta \langle K_0 \rangle (B_\sigma, \lambda) - \Delta S(B_\sigma, \lambda) \tag{6.50}$$

are constant in σ on $[\xi, \eta]$ if $\Delta \langle K_0 \rangle (A_\sigma, \lambda)$ and $\Delta \langle K_0 \rangle (B_\sigma, \lambda)$ are linear in $\tilde{\lambda}$. By taking two derivatives w.r.t. λ and considering once more the linearity of $\Delta \langle K_0 \rangle (A_\sigma, \lambda)$ and $\Delta \langle K_0 \rangle (B_\sigma, \lambda)$, we find that

$$- \partial_\lambda^2 S_{rel}(A_\sigma, \lambda) = \partial_\lambda^2 S(A_\sigma, \lambda) \quad \text{and} \quad - \partial_\lambda^2 S_{rel}(B_\sigma, \lambda) = \partial_\lambda^2 S(B_\sigma, \lambda) \tag{6.51}$$

are constant in σ on $[\xi, \eta]$. This completes the proof of my result as stated in Section 6.3.1.

6.3.3 Discussion of the Proof for Generic Entanglement Plateaux

We now comment on various aspects of the result of Section 6.3.1 including its prerequisites and possible generalizations.

Continuity of σ

The continuity of the parameter σ controlling the size of the entangling regions A_σ and B_σ is required in order to guarantee that the sign in (6.38) only depends on λ but not on σ. The argument leading to the σ-independence of the sign is presented in Section 6.1.3. We may formulate a version of my result that also applies to discrete σ when we assume the sign of (6.38) to be constant in σ from the start. The proof of this version can be formulated in an analogously to the one presented Section 6.3.2.

A Stronger Statement

We note that in the proof presented in Section 6.3.2 we show the validity of a statement that is stronger than the one presented in Section 6.3.1 as an intermediate step. In the paragraph above (6.49) we conclude that given the prerequisites for my result the relative entropies $S_{rel}(A_\sigma, \lambda)$ and $S_{rel}(B_\sigma, \lambda)$ are constant in σ on $[\xi, \eta]$ if $\Delta \langle K_0 \rangle (A_\sigma, \lambda)$ and $\Delta \langle K_0 \rangle (B_\sigma, \lambda)$ are linear in $\tilde{\lambda}$. Taking two derivatives of $S_{rel}(A_\sigma, \lambda)$ and $S_{rel}(B_\sigma, \lambda)$ w.r.t. λ then leads to the conclusion that $\partial_\lambda^2 S(A_\sigma, \lambda)$

and $\partial_\lambda^2 S(B_\sigma, \lambda)$ are constant in σ on $[\xi, \eta]$. So we see that the fact that $\partial_\lambda^2 S$ is constant in σ for A_σ and B_σ is a consequence of the stronger result that the respective relative entropies are constant in σ.

In Section 6.3.1 we present the weaker version with $\partial_\lambda^2 S$ for practical reasons. We aim at applying my result for deciding when $\Delta \langle K_0 \rangle$ contains higher order contributions in $\tilde{\lambda}$. Determining the relative entropy is in general more complicated than determining the entanglement entropy. In particular for holographic setups, where the relative entropy is given via the RT formula, this is evident. So, a result that only requires the examination of entanglement entropies is easier to apply than one where relative entropies need to be computed.

Reverse Direction

The statement of the result presented in Section 6.3.1 is that a necessary condition for both $\Delta \langle K_0 \rangle (A_\sigma, \lambda)$ and $\Delta \langle K_0 \rangle (B_\sigma, \lambda)$ to be linear in $\tilde{\lambda}$ for all $\sigma \in [\xi, \eta]$ is that $\partial_\lambda^2 S(A_\sigma, \lambda)$ and $\partial_\lambda^2 S(B_\sigma, \lambda)$ are constant in σ on $[\xi, \eta]$. We now demonstrate at an example that the reverse direction of this statement does not hold, i.e. $\partial_\lambda^2 S(A_\sigma, \lambda)$ and $\partial_\lambda^2 S(B_\sigma, \lambda)$ being constant in σ is necessary but not sufficient for the linearity of $\Delta \langle K_0 \rangle (A_\sigma, \lambda)$ and $\Delta \langle K_0 \rangle (B_\sigma, \lambda)$.

Consider the CFT_2 of a free massless bosonic field Φ on a circle with radius ℓ_{CFT}. We define the following one-parameter family $|\lambda\rangle$ of states with conformal dimension $(\lambda, 0)$,

$$|\lambda\rangle = e^{i\sqrt{2\lambda}\Phi} |0\rangle \ , \tag{6.52}$$

where $|0\rangle$ is the vacuum state.[9] This setup was discussed in [66]. The entangling regions A_σ and B_σ are chosen to be an interval of angular size $2(\pi - \sigma)$ and its compliment – which is of angular size 2σ – respectively. This choice of entangling regions implies that $\Sigma = A_\sigma B_\sigma$ is the whole circle the CFT is defined on and therefore invariant under changes of σ. Moreover, we note that A_σ and B_σ form an entanglement plateau for all σ and λ as the states $|\lambda\rangle$ are pure. The reference state may correspond to any value $\lambda_0 > 0$ of λ.

According to [66] the entanglement entropies $S(A_\sigma, \lambda)$ and $S(B_\sigma, \lambda)$ are independent of λ. Thus we find

$$\partial_\lambda^2 S(A_\sigma, \lambda) = \partial_\lambda^2 S(B_\sigma, \lambda) = 0 \tag{6.53}$$

to be constant in σ on any interval $[\xi, \eta]$. However, $\Delta \langle K_0 \rangle (A_\sigma, \lambda)$ and $\Delta \langle K_0 \rangle (B_\sigma, \lambda)$ are not linear in $\tilde{\lambda}$: as discussed in [66], the relative entropies of A_σ and B_σ are given by

$$S_{rel}(A_\sigma, \lambda) = (1 + (\pi - \sigma)\cot(\sigma))\left(\sqrt{2\lambda} - \sqrt{2\lambda_0}\right)^2 , \tag{6.54}$$

$$S_{rel}(B_\sigma, \lambda) = (1 - \sigma\cot(\sigma))\left(\sqrt{2\lambda} - \sqrt{2\lambda_0}\right)^2 . \tag{6.55}$$

---

[9]Note that we assume in this section that the parameter λ is continuous. This is necessary in order to discuss this example in view of the result presented in Section 6.3.1 since the differentiability of the entanglent entropies implicitly assumes λ to be a continuous parameter.

Since $S(A_\sigma, \lambda)$ and $S(B_\sigma, \lambda)$ are constant in λ we find

$$\Delta S(A_\sigma, \lambda) = \Delta S(B_\sigma, \lambda) = 0 \tag{6.56}$$

and therefore conclude, by considering (6.19),

$$\Delta \langle K_0 \rangle (A_\sigma, \lambda) = (1 + (\pi - \sigma) \cot(\sigma)) \left(\sqrt{2\lambda} - \sqrt{2\lambda_0} \right)^2, \tag{6.57}$$

$$\Delta \langle K_0 \rangle (B_\sigma, \lambda) = (1 - \sigma \cot(\sigma)) \left(\sqrt{2\lambda} - \sqrt{2\lambda_0} \right)^2. \tag{6.58}$$

Evidently, the $\Delta \langle K_0 \rangle$ of A_σ and B_σ are not linear in $\tilde{\lambda}$ for any σ. So we see that the example we just discussed provides $\partial_\lambda^2 S(A_\sigma, \lambda)$ and $\partial_\lambda^2 S(B_\sigma, \lambda)$ constant in σ but no $\Delta \langle K_0 \rangle$ linear in $\tilde{\lambda}$. Therefore we conclude that $\partial_\lambda^2 S(A_\sigma, \lambda)$ and $\partial_\lambda^2 S(B_\sigma, \lambda)$ being constant in σ is not sufficient for $\Delta \langle K_0 \rangle (A_\sigma, \lambda)$ and $\Delta \langle K_0 \rangle (B_\sigma, \lambda)$ to be linear in $\tilde{\lambda}$.

Choice of the Reference State

In Section 6.3.1 we state that the parameter value $\lambda = \lambda_0$ of the reference state is not allowed to be a boundary point of the domain of λ. In other words, λ_0 is assumed to be in the interior of the domain of λ. We use this property in the following two ways.

First when considering the special case $S(\Sigma, \lambda_0) = 0$ below (6.40). We conclude $S'(\Sigma, \lambda_0) = 0$ to hold since $S(\Sigma, \lambda)$ is minimal for $\lambda = \lambda_0$. However, the vanishing of the first derivative at the minimum requires it to lie in the interior of the domain.

Second when using the first law of entanglement (6.22) to express $\Delta \langle K_0 \rangle$ in terms of entanglement entropies (6.43). The first law of entanglement is a consequence of the minimality of S_{rel} at the reference parameter as we argue in Section 6.2. Since S_{rel} is minimal at λ_0 the derivative of S_{rel} w.r.t. λ vanishes at λ_0 which implies the first law of entanglement. Just as for $S(\Sigma, \lambda)$, the vanishing of the derivative may only be concluded if λ_0 is in the interior of the domain of λ.

If λ_0 is a boundary point, we have no guarantee for the first law of entanglement to hold, as we now show at an explicit example. We consider the setup of excited states $|\lambda\rangle$ for the CFT$_2$ of a free boson on the circle discussed above in the paragraph about the reverse direction of my result. From (6.52) it is easy to see that $\lambda \geq 0$ holds. If we choose $\lambda_0 = 0$ as reference parameter value we find via (6.54)

$$S_{rel}(A_\sigma, \lambda) = 2(1 + (\pi - \sigma) \cot(\sigma))\lambda. \tag{6.59}$$

We see that $\partial_\lambda S_{rel}(A_\sigma, \lambda)|_{\lambda=\lambda_0}$ is not zero. Therefore, the first law of entanglement does not apply here.

As a final remark regarding this example we note that even though the first law of entanglement does not hold here, the system behaves just as we would expect considering the result of Section 6.3.1: both $\Delta \langle K_0 \rangle (A_\sigma, \lambda)$ and $\Delta \langle K_0 \rangle (B_\sigma, \lambda)$ are linear in $\tilde{\lambda}$ (see (6.57) and (6.58) for $\lambda_0 = 0$) and $\partial_\lambda^2 S(A_\sigma, \lambda) = \partial_\lambda^2 S(B_\sigma, \lambda) = 0$ are constant in σ. However, the prerequisites for my result are not satisfied here since λ_0 is a boundary point and therefore we cannot apply it. In particular, from

(6.59) we see that $S_{rel}(A_\sigma, \lambda)$ is not constant in σ. Thus, the stronger version of my result we discuss above does not hold here.

Generalization to Multi-Parameter Families of States

The result of Section 6.3.1 is formulated for a family of states ρ_λ that only depends on one-parameter λ. It can be generalized to a n-parameter family of states ρ_Λ, where $\Lambda = (\lambda^1, \dots, \lambda^n)$, in a straightforward way. The result for an n-parameter family of states may be formulated as follows.

If both $\Delta \langle K_0 \rangle (A_\sigma, \Lambda)$ and $\Delta \langle K_0 \rangle (B_\sigma, \Lambda)$ are linear in $\Lambda - \Lambda_0$ for all $\sigma \in [\xi, \eta]$, then

$$\frac{\partial}{\partial \lambda^i} \frac{\partial}{\partial \lambda^j} S(A_\sigma, \Lambda) \quad \text{and} \quad \frac{\partial}{\partial \lambda^i} \frac{\partial}{\partial \lambda^j} S(B_\sigma, \Lambda) \tag{6.60}$$

are constant in σ on $[\xi, \eta]$. Here Λ_0 corresponds to the reference state.

The proof of this statement is analogous to the proof presented in Section 6.3.2 for the case of a one-parameter family of states. The n-parameter version of the first law of entanglement required for the proof is

$$\begin{aligned}
\frac{\partial}{\partial \lambda^i} \Delta \langle K_0 \rangle (A_\sigma, \Lambda)|_{\Lambda = \Lambda_0} &= \frac{\partial}{\partial \lambda^i} \Delta S(A_\sigma, \Lambda)|_{\Lambda = \Lambda_0}, \\
\frac{\partial}{\partial \lambda^i} \Delta \langle K_0 \rangle (B_\sigma, \Lambda)|_{\Lambda = \Lambda_0} &= \frac{\partial}{\partial \lambda^i} \Delta S(B_\sigma, \Lambda)|_{\Lambda = \Lambda_0}.
\end{aligned} \tag{6.61}$$

6.4 Applications

We now demonstrate on a series of examples how the result presented in Section 6.3.1 can be applied to show that $\Delta \langle K_0 \rangle (A_\sigma, \lambda)$ for given one-parameter families of states ρ_λ and entangling regions A_σ is not linear in $\tilde{\lambda} = \lambda - \lambda_0$. The strategy we pursue goes as follows: for a given A_σ we construct a family of entangling regions B_σ such that $\Sigma = A_\sigma B_\sigma$ does not change with σ and A_σ forms an entanglement plateau with B_σ for all σ and λ. If $\partial_\lambda^2 S(A_\sigma, \lambda)$ or $\partial_\lambda^2 S(B_\sigma, \lambda)$ are not constant in σ on any interval, my result (see Section 6.3.1) implies that there are only single values of σ where both $\Delta \langle K_0 \rangle (A_\sigma, \lambda)$ and $\Delta \langle K_0 \rangle (B_\sigma, \lambda)$ are linear in $\tilde{\lambda}$, i.e. there is no interval $[\xi, \eta]$ such that the $\Delta \langle K_0 \rangle$ are linear in $\tilde{\lambda}$ for all $\sigma \in [\xi, \eta]$.

As can be seen from the above discussion, my result does in general not allow us to decide whether $\Delta \langle K_0 \rangle (A_\sigma, \lambda)$, $\Delta \langle K_0 \rangle (B_\sigma, \lambda)$ or both are non-linear in $\tilde{\lambda}$. However, in many cases we are able to make the stronger observation that $\Delta \langle K_0 \rangle (A_\sigma, \lambda)$ is non-linear in $\tilde{\lambda}$ for all σ with possibly one exception. We come to this conclusion by studying

$$D_{rel}(B_\sigma, \lambda) = \Delta S'(B_\sigma, \lambda_0)\tilde{\lambda} - \Delta S(B_\sigma, \lambda), \tag{6.62}$$

as we did in Section 6.3.2 for the black string geometry. By assuming that $\Delta \langle K_0 \rangle (A_\sigma, \lambda)$ is linear in $\tilde{\lambda}$ we can use the same arguments as presented in the proof of my result in Section 6.3.2 to obtain

$$S_{rel}(A_\sigma, \lambda) = \Delta S'(\Sigma, \lambda_0)\tilde{\lambda} \mp \Delta S(\Sigma, \lambda) + D_{rel}(B_\sigma, \lambda), \tag{6.63}$$

instead of (6.44). [10] If $D_{rel}(B_\sigma, \lambda)$ grows strictly monotonically with σ we can use the same arguments as for the black string geometry (see paragraph of (6.33)) to conclude that there is at most one value of σ where $\Delta \langle K_0 \rangle (A_\sigma, \lambda)$ is linear in $\tilde{\lambda}$. Otherwise the monotonicity of S_{rel} (6.25) would be violated. Note that in (6.63) we implicitly assume $S(A_\sigma, \lambda_0) \geq S(B_\sigma, \lambda_0)$, as we do in Section 6.3.2. The examples we present below all have this property. For $S(A_\sigma, \lambda_0) \leq S(B_\sigma, \lambda_0)$ a relation similar to (6.63) can be derived in an analogous way.

6.4.1 Multiple Intervals in Black String Geometries

My result may be used to study $\Delta \langle K_0 \rangle (A_\sigma, \lambda)$ for thermal CFT$_2$ states with the black string geometry (6.8) as holographic dual. We first confirm the results presented in Section 6.3.2 for the case where A_σ is the union of two disjoint intervals and then generalize it to generic configurations of entangling intervals. Moreover, we study the corresponding results in the context of [200] (see Section 3.3.1 for a review.)

Non-Linearity of $\Delta \langle K_0 \rangle$

We apply the strategy presented at the beginning of this section to confirm the results for the black string geometry (6.8) obtained in Section 6.3.2. The corresponding setup is shown in Figure 6.5: we consider A_σ to be the union of the two intervals $[a_1, -\sigma]$ and $[\sigma, a_2]$, where σ is chosen sufficiently small so that the RT surface γ_{A_σ} has the form depicted in Figure 6.5 for all considered energy densities λ. To show that $\Delta \langle K_0 \rangle (A_\sigma, \lambda)$ is in general not linear in $\tilde{\lambda}$ we define $B_\sigma = [-\sigma, \sigma]$. By construction A_σ and B_σ form an entanglement plateau and $\Sigma = A_\sigma B_\sigma = [a_1, a_2]$ is constant in σ. Since $\partial_\lambda^2 S(B_\sigma, \lambda)$ is not constant in σ (see (6.29)) we find that there are only single values of σ where $\Delta \langle K_0 \rangle$ is linear in $\tilde{\lambda}$ for both A_σ and B_σ. Furthermore, $\Delta \langle K_0 \rangle (B_\sigma, \lambda)$ (6.35) is known to be linear in $\tilde{\lambda}$ for all σ which brings us to the conclusion that $\Delta \langle K_0 \rangle (A_\sigma, \lambda)$ is linear in $\tilde{\lambda}$ only for single values of σ. By studying $D_{rel}(B_\sigma, \lambda)$ (6.62) we can narrow the number of these points down to one: as pointed out in Section 6.3.2 $D_{rel}(B_\sigma, \lambda)$ is given by (6.32) and grows strictly monotonically with σ. Thus, considering the discussion at the beginning of this section we conclude that $\Delta \langle K_0 \rangle (A_\sigma, \lambda)$ is non-linear in $\tilde{\lambda}$ for all σ with possibly one exception. We can identify this exception with the asymptotic situation $\sigma = 0$, i.e. when B_σ vanishes and A_σ becomes a single interval, for which $\Delta \langle K_0 \rangle$ is known to be linear in $\tilde{\lambda}$ (6.35).

The above analysis for A_σ being the union of two intervals can be straightforwardly generalized to a setup where A_σ is the union of an arbitrary number of intervals. For this we require two neighboring intervals A_σ^1, A_σ^2 belonging to A_σ to be sufficiently close so that the RT surface γ_{A_σ} is of the form depicted in Figure 6.7. We then can choose B_σ to be the interval between A_σ^1 and A_σ^2 and define the σ dependence of A_σ in such a way that it varies the size of B_σ while keeping

---

[10]If $\Delta \langle K_0 \rangle (B_\sigma, \lambda)$ is considered to be linear in $\tilde{\lambda}$ we find $D_{rel}(B_\sigma, \lambda) = S_{rel}(B_\sigma, \lambda)$ due to the first law of entanglement. This assumption led to (6.44).
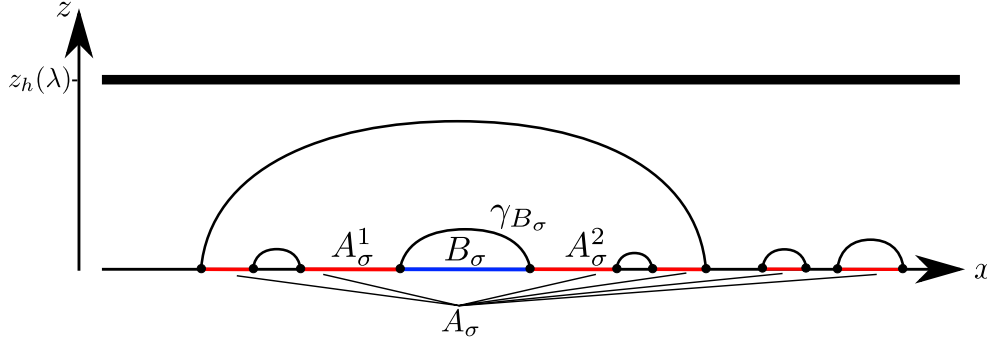
Figure 6.7: An entangling region consisting of multiple intervals. We consider a family of entangling regions A_σ consisting of intervals for states dual to black string geometries (6.8). If we choose two neighboring intervals A_σ^1, A_σ^2 belonging to A_σ to be sufficiently close, the RT surface γ_{A_σ} includes the *RT* surface γ_{B_σ} corresponding to the interval B_σ between A_σ^1 and A_σ^2. In this setup A_σ and B_σ form an entanglement plateau. When the parameter σ is defined to vary the size of B_σ we may apply my result presented in Section 6.3.1 to this configuration.

$\Sigma = A_\sigma B_\sigma$ fixed. As discussed above, $\partial_\lambda^2 S(B_\sigma, \lambda)$ is not constant in σ and furthermore $D_{rel}(B_\sigma, \lambda)$ grows strictly monotonically with σ. Consequently, we conclude that there is at most one value of σ where $\Delta \langle K_0 \rangle (A_\sigma, \lambda)$ is linear in $\tilde{\lambda}$.

Observation Regarding Integral Expressions for K_0

The above result, stating that $\Delta \langle K_0 \rangle (A_\sigma, \lambda)$ is not linear in $\tilde{\lambda}$ for the considered interval configurations A_σ, provides further insight related to the results of [200]. Here the authors introduced a criterion for two-dimensional CFTs under which the modular Hamiltonian can be written as a local integral over the energy momentum tensor. We review this criterion in Section 3.3.1. In particular, in [200] the corresponding result was used to derive the expression (6.34) for the modular Hamiltonian of one entangling interval. However, for an arbitrary number of intervals the result of [200] cannot be applied as its prerequisites are not satisfied. Considering our review in Section 3.3.1, this is easy to see. The fact that [200] cannot be used for an arbitrary set of intervals may be taken as a hint that it is not possible to write $K_0(A_\sigma)$ as a local integral over the energy momentum tensor in this case. However, it is certainly no formal proof for that. My result may be used to construct such a proof, as we now show.[11] To be more precise, we present an argument which implies that $K_0(A_\sigma)$ is not of the form

$$K_0(A_\sigma) = \int_{A_\sigma} dx h(x) T_{00}(x),\qquad (6.64)$$

---

[11]Note that in this proof we restrict ourselves to the situation where the thermal CFT_2 state on the real axis has the black string geometry (6.8) as holographic dual. The result of [200] however, is not just valid in AdS/CFT but applies to any CFT_2.

for the configurations A_σ of entangling intervals considered above – except for possibly one particular value of σ. [12] Here h is a local scaling function and $T_{\mu\nu}$ is the energy momentum tensor. For this purpose we assume that $K_0(A_\sigma)$ is of the form (6.64). Since we consider the parameter λ to be the energy density, we conclude that $\Delta \langle K_0 \rangle (A_\sigma, \lambda)$ is linear in $\tilde{\lambda}$ in this case,

$$\Delta \langle K_0 \rangle (A_\sigma, \lambda) = \tilde{\lambda} \int_{A_\sigma} dx h(x) . \tag{6.65}$$

However, as pointed out above, $\Delta \langle K_0 \rangle (A_\sigma, \lambda)$ is not linear in $\tilde{\lambda}$ except for possibly one particular value of σ. Thus, $K_0(A_\sigma)$ cannot be of the form (6.64) for any but possibly one particular value of σ.

6.4.2 Annuli in Black Brane Geometries

The discussion of two intervals for states dual to black string geometries can be generalized to states dual to black branes, i.e. the $(d+1)$-dimensional analogue of black strings, [13]

$$ds_{BB}^2 = \frac{L^2}{z^2} \left(-\frac{z_h^d - z^d}{z_h^d} dt^2 + \frac{z_h^d}{z_h^d - z^d} dz^2 + d\vec{x}_{d-1}^2 \right) . \tag{6.66}$$

Just as for black strings, the radial coordinate z runs from $z = 0$, where the conformal boundary is located, to z_h, which is the position of the black brane horizon. Moreover, $t \in \mathbb{R}$ and $\vec{x} \in \mathbb{R}^{d-1}$ with the corresponding Euclidean metric $d\vec{x}_{d-1}^2$. These geometries are the duals of thermal states on d-dimensional Minkowski space.

We use the energy density (see e.g. [219])

$$\lambda = \frac{(d-1)L^{d-1}}{16\pi G_{d+1} z_h^d} , \tag{6.67}$$

to parametrize these states and choose A_σ to be an annulus of inner radius σ and outer radius R. The parameter σ is assumed to be sufficiently small so that for all λ we consider, the RT surface γ_{A_σ} is the union of the RT surface of the inner ball with radius σ and the outer ball with radius R. [14] We depict this setup in Figure 6.8. The reference state is taken to be the vacuum, i.e. $\lambda_0 = 0$.

We can show that $\Delta \langle K_0 \rangle (A_\sigma, \lambda)$ is in general not linear in $\tilde{\lambda}$ in the following way. We choose B_σ to be the ball of radius σ circumvented by A_σ (see Figure 6.8). By construction A_σ and B_σ form an entanglement plateau and $\Sigma = A_\sigma B_\sigma$ is

---

[12]We emphasize that the observation that the modular Hamiltonian for multiple intervals is not given by a local integral is not a new result (see e.g. [74, 76] for related work). The purpose of the discussion we present here is only to demonstrate how my result for modular Hamiltonians may be applied to show this.

[13]The black brane geometry we present here is a planar AdS$_{d+1}$ black hole. It may be seen as a generalization of the geometry (2.139) for $d = 4$ derived from black $D3$-branes (see e.g. [219]).

[14]This setup was also studied in [115].
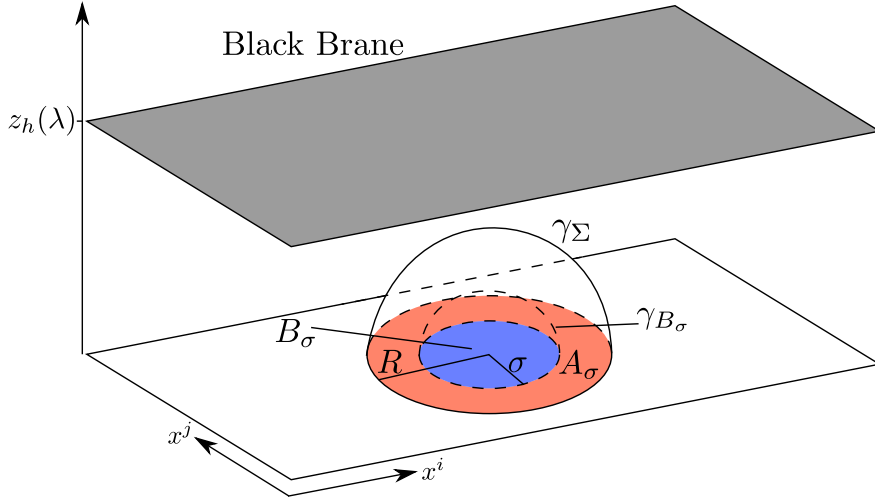
Figure 6.8: A family of annulus-shaped entangling regions A_σ for states dual to black brane geometries (6.66). We depict a constant time slice of a black brane geometry. The black brane horizon is located at $z = z_h(\lambda)$. The conformal boundary – on which the dual CFT is defined – sits at $z = 0$. We consider the entangling region A_σ to be an annulus of outer radius R and inner radius σ. If we choose σ to be sufficiently small, the RT surface γ_{A_σ} is the union of γ_{B_σ} and γ_Σ, where $\Sigma = A_\sigma B_\sigma$ and B_σ is the ball of radius σ surrounded by A_σ.

invariant under changes of σ. The entanglement entropy $S(B_\sigma, \lambda)$ is given by the area of the RT surface [115],

$$S(B_\sigma, \lambda) = \frac{L^{d-1}\Omega_{d-2}}{4G_{d+1}} \int_0^\sigma d\rho \frac{\rho^{d-2}}{z(\rho)^{d-1}} \sqrt{1 + \frac{(\partial_\rho z(\rho))^2 z_h^d}{z_h^d - z(\rho)^d}} , \qquad (6.68)$$

where the function $z(\rho)$ minimizes the integral on the r.h.s. of (6.68). We are not aware of the existence of an analytic, integral free expression for $S(B_\sigma, \lambda)$ for generic d. However, the following expansion in $\alpha\,\sigma^d\lambda$ for $\Delta S(B_\sigma, \lambda)$ is presented in [115],

$$\Delta S(B_\sigma, \lambda) = \frac{\Omega_{d-2}L^{d-1}}{4G_{d+1}} \left(\frac{d\,\alpha\,\sigma^d\lambda}{2(d^2-1)} - \frac{d^3\sqrt{\pi}\,\Gamma(d-1)\alpha^2\sigma^{2d}\lambda^2}{2^{d+4}(d+1)\Gamma\left(d+\frac{3}{2}\right)} + \mathcal{O}((\alpha\sigma^d\lambda)^3) \right) , \tag{6.69}$$

where $\alpha = 16\pi G_{d+1}L^{1-d}/d$ and $\Omega_{d-2} = 2\pi^{(d-1)/2}/\Gamma((d-1)/2)$ is the volume of the unit $(d-2)$-sphere.[15]

Since $\partial_\lambda^2\Delta S = \partial_\lambda^2 S$, we deduce from (6.69) that $\partial_\lambda^2 S(B_\sigma, \lambda)$ is not constant in σ. Moreover, $\Delta\langle K_0\rangle(B_\sigma, \lambda)$ is known to be linear in $\tilde\lambda$ for all σ [115],

$$\Delta\langle K_0\rangle(B_\sigma, \lambda) = \frac{2\pi\Omega_{d-2}}{d^2-1}\sigma^d\tilde\lambda . \tag{6.70}$$

---

[15]In [196] it was pointed out that there appears to be a typo in equation (3.55) of [115]: The term L^{d-1}/ℓ_p^{d-1} needs to be replaced by its inverse.

So we conclude, in an analogous way as for the black string geometries, that $\Delta \langle K_0 \rangle (A_\sigma, \lambda)$ is linear in $\tilde{\lambda}$ only for single values of σ. [16] Moreover, just as in the black string case, we are able to show that there is only one such value of σ. Since $\Delta \langle K_0 \rangle (B_\sigma, \lambda)$ is linear in $\tilde{\lambda}$ we conclude $D_{rel}(B_\sigma, \lambda) = S_{rel}(B_\sigma, \lambda)$ from the first law of entanglement (6.22). By inserting (6.69) and (6.70) into (6.19) it is easy to see that $S_{rel}(B_\sigma, \lambda)$ is not constant in σ on any interval. The monotonicity of the relative entropy (6.25) then implies that $S_{rel}(B_\sigma, \lambda)$ – or equivalently $D_{rel}(B_\sigma, \lambda)$ – grows strictly monotonically with σ. The discussion at the beginning of this section then allows us to conclude that $\Delta \langle K_0 \rangle (A_\sigma, \lambda)$ is non-linear in $\tilde{\lambda}$ for all σ except possibly one. As in the case of the black strings we find this special value of σ to be 0, i.e. the situation when B_σ vanishes and A_σ becomes a ball of radius R, for which $\Delta \langle K_0 \rangle$ is known to be linear in $\tilde{\lambda}$ (6.70).

6.4.3 Large Intervals on BTZ Geometries

A further application of the strategy presented at the beginning of this section are sufficiently large entangling intervals for thermal states dual to BTZ black holes (6.9). As parametrization for these states we use the square of their temperature

$$\lambda = T^2 \,, \tag{6.71}$$

which is proportional to the mass M of the black hole (2.149) (2.151),

$$LM = \frac{\pi^2 \ell_{CFT}^2 c}{3} \lambda \,, \tag{6.72}$$

and related to the horizon via (2.151)

$$\tilde{r}_h = 2\pi L \ell_{CFT} \sqrt{\lambda} \,. \tag{6.73}$$

Here $c = 3L/2G_3$ (2.117) is the central charge and ℓ_{CFT} the radius of the circle the CFT is defined on. The reference state corresponds to an arbitrary value λ_0 of the parameter λ. We define A_σ to be an entangling interval of angular size $2(\pi - \sigma)$. As pointed out in Section 6.1.2, if A_σ is sufficiently large, i.e. if σ is sufficiently small, the RT surface γ_{A_σ} is the union of the RT surface of A_σ^c and the horizon, leading to (3.49)

$$S(A_\sigma, \lambda) = \frac{c}{3} 2\pi^2 \sqrt{\lambda} \ell_{CFT} + \frac{c}{3} \log \left(\frac{1}{\pi \sqrt{\lambda} \epsilon} \sinh \left(2\pi \ell_{CFT} \sqrt{\lambda} \sigma \right) \right) \,, \tag{6.74}$$

where ϵ is a UV cut-off.[17] The first term corresponds to the horizon and gives the thermal entropy of the state. The second term gives the entanglement entropy of

---

[16]This conclusion is based on my result as presented in Section 6.3.1. By applying it we implicitly assume that the first law of entanglent (6.22) holds for A_σ and B_σ. Since the reference state corresponds to a boundary value of the parameter λ, i.e. $\lambda_0 = 0$, we have no guarantee for that, as already pointed out in [115] and Section 6.3.3. In order to proof the first law we would need to consider negative values for λ – which is unphysical. In this section we assume the first law to hold for A_σ. For B_σ it can be explicitly verified from (6.69) and (6.70).

[17]Note that in (3.49) we consider an entangling interval of angular size 2σ, while in this section A_σ has the angular size $2(\pi - \sigma)$.

A_σ^c. We depict this setup in Figure 6.3. By setting $B_\sigma = A_\sigma^c$ we find that A_σ and B_σ form an entanglement plateau.

In this setup neither $\Delta \langle K_0 \rangle (A_\sigma, \lambda)$ nor $\Delta \langle K_0 \rangle (B_\sigma, \lambda)$ are known. However, it is still possible to apply my result presented in Section 6.3.1 to conclude that there are only singular values of σ where both $\Delta \langle K_0 \rangle (A_\sigma, \lambda)$ and $\Delta \langle K_0 \rangle (B_\sigma, \lambda)$ are linear in $\tilde{\lambda}$, since $\partial_\lambda^2 S(A_\sigma, \lambda)$ is not constant in σ on any interval. This is easy to verify from (6.74). Moreover, we find

$$D_{rel}(B_\sigma, \lambda) = \frac{c}{3}\Big(\frac{1}{2}(1 - \tilde{b}^2)\big(1 - \tilde{a}\coth(\tilde{a})\big) + \log\Big(\tilde{b}\,\frac{\sinh(\tilde{a})}{\sinh(\tilde{b}\,\tilde{a})}\Big)\Big), \qquad (6.75)$$

where $\tilde{a} = 2\pi\ell_{CFT}\sqrt{\lambda_0}\sigma$ and $\tilde{b} = \sqrt{\lambda/\lambda_0}$. We have used the fact that the second term in (6.74) is $S(B_\sigma, \lambda)$ in order to derive (6.75). We see that the structure of $D_{rel}(B_\sigma, \lambda)$ is identical to the one of the corresponding quantity (6.32) for a single interval in the black string geometry. In an analogous way as for the black string setup we conclude that $D_{rel}(B_\sigma, \lambda)$ grows strictly monotonically with σ. Therefore – following the arguments made at the beginning of this section – we conclude that there is at most one value for σ where $\Delta \langle K_0 \rangle (A_\sigma, \lambda)$ is linear in $\tilde{\lambda}$.

6.4.4 Families of Pure States: Primary Excitations in CFTs

Consider an arbitrary family of pure states $|\lambda\rangle$ and an arbitrary family of entangling regions A_σ with $A_{\sigma_2} \subset A_{\sigma_1}$ for $\sigma_1 < \sigma_2$. In this setup

$$S(A_\sigma, \lambda) = S(A_\sigma^c, \lambda) \qquad (6.76)$$

and $S(A_\sigma A_\sigma^c, \lambda) = 0$ hold. Therefore we find that A_σ and $B_\sigma = A_\sigma^c$ form an entanglement plateau for which $\Sigma = A_\sigma B_\sigma$ is independent of σ. My result presented in Section 6.3.1 allows us to conclude that if $\partial_\lambda^2 S(A_\sigma, \lambda)$ is not constant in σ on any interval, there are only isolated values of σ where $\Delta \langle K_0 \rangle$ is linear in $\tilde{\lambda}$ for both A_σ and B_σ.

As an explicit example we discuss the following family of pure states.[18] We consider a two-dimensional CFT with large central charge c defined on a circle with radius ℓ_{CFT} and choose $|\lambda\rangle$ to be a spinless primary excitation with conformal dimension

$$(h_\lambda, \bar{h}_\lambda) = \Big(\frac{c\lambda}{24}, \frac{c\lambda}{24}\Big), \qquad (6.77)$$

where we have introduced the factor $c/24$ to simplify the formulae in this paragraph. The parameter λ is assumed to be smaller than one, $\lambda < 1$ and the corresponding state $|\lambda\rangle$ is considered to correspond to a heavy operator, i.e. $\Delta_\lambda = h_\lambda + \bar{h}_\lambda = \mathcal{O}(c)$. Moreover, the spectrum of light operators, i.e. operators with $\Delta = h + \bar{h} \ll c$, is taken to be sparse.

The reference value λ_0 can be chosen arbitrarily. The entangling region A_σ is defined to be an interval with angular size $2(\pi - \sigma) > \pi$ and B_σ is chosen to be

---

[18]This family of pure states was studied in [222].

the complementary interval of size $2\sigma < \pi$. Consequently, Σ is the whole circle. The entanglement entropy of B_σ is given by [222]

$$S(B_\sigma, \lambda) = \frac{c}{3} \log \left(\frac{2\ell_{CFT}}{\sqrt{1-\lambda}\,\epsilon} \sin\left(\sqrt{1-\lambda}\,\sigma\right) \right) = S(A_\sigma, \lambda), \qquad (6.78)$$

where ϵ is a UV cut-off. The second equality follows from the fact that $|\lambda\rangle$ is pure.[19] Evidently, $\partial_\lambda^2 S(B_\sigma, \lambda)$ is not constant in σ on any interval and therefore we conclude that there are only single values of σ where both $\Delta \langle K_0 \rangle (A_\sigma, \lambda)$ and $\Delta \langle K_0 \rangle (B_\sigma, \lambda)$ are linear in $\tilde{\lambda}$.

The quantity $D_{rel}(B_\sigma, \lambda)$ is given by

$$D_{rel}(B_\sigma, \lambda) = \frac{c}{3} \left(\frac{1}{2}(1 - \hat{b}^2)(1 - \hat{a}\cot(\hat{a})) + \log\left(\hat{b}\frac{\sin(\hat{a})}{\sin(\hat{b}\,\hat{a})} \right) \right), \qquad (6.79)$$

where $\hat{a} = \sqrt{1-\lambda_0}\,\sigma$ and $\hat{b} = \sqrt{1-\lambda}/\sqrt{1-\lambda_0}$. Analogous to the case of black strings discussed in Section 6.3.2 we find that $D_{rel}(B_\sigma, \lambda)$ grows strictly monotonically with σ and therefore conclude that there is at most one value for σ where $\Delta \langle K_0 \rangle (A_\sigma, \lambda)$ is linear in $\tilde{\lambda}$.

6.4.5 Ground States for CFTs on a Circle

As a comment to my result presented in Section 6.3.1 we discuss it for conformal field theories defined on a circle with radius ℓ_{CFT}. We present a situation where both $\Delta \langle K_0 \rangle (A_\sigma, \lambda)$ and $\Delta \langle K_0 \rangle (B_\sigma, \lambda)$ are linear in $\tilde{\lambda}$. So one might be tempted to use my result to conclude that $\partial_\lambda^2 S(A_\sigma, \lambda)$ and $\partial_\lambda^2 S(A_\sigma, \lambda)$ are constant in σ. However, the prerequisites of my result turn out not to be satisfied and thus this conclusion cannot be made.

We consider the same setup as in Section 6.4.4: A_σ is an interval with angular size $2(\pi - \sigma)$ and B_σ its complement. The family of primary states $|\lambda\rangle$ is parametrized by the conformal dimension (6.77). However, unlike as in Section 6.4.4 we do not impose any restrictions regarding the spectrum or the central charge. Moreover, the size of the interval A_σ may be chosen arbitrarily. The reference state is set to be the vacuum, i.e. $\lambda_0 = 0$.

For this setup both $\Delta \langle K_0 \rangle (A_\sigma, \lambda)$ and $\Delta \langle K_0 \rangle (B_\sigma, \lambda)$ are known to be linear in $\tilde{\lambda}$ as we now show. The modular Hamiltonian $K_0([-\varsigma, \varsigma])$ for an interval $[-\varsigma, \varsigma]$ of angular size 2ς has the form [64, 115]

$$K_0([-\varsigma, \varsigma]) = 2\pi\ell_{CFT}^2 \int_{-\varsigma}^{\varsigma} d\phi \frac{\cos(\phi) - \cos(\varsigma)}{\sin(\varsigma)} T_{00} \qquad (6.80)$$

in any CFT defined on a circle. By applying the CFT result[20]

$$\langle \lambda | T_{00} | \lambda \rangle - \langle 0 | T_{00} | 0 \rangle = \frac{c\tilde{\lambda}}{24\pi\ell_{CFT}^2}, \qquad (6.81)$$

---

[19]Note that the expression for the entanglement entropy presented in (6.78) is not invariant under $\sigma \longmapsto \pi - \sigma$ as the purity of $|\lambda\rangle$ seems to suggest. This is a consequence of the fact that in the derivation of (6.78) $2\sigma < \pi$ was explicitly used [222].

[20]This formula has been adopted from [195].

to (6.80) we find

$$\Delta \langle K_0 \rangle (A_\sigma, \lambda) = \frac{c}{6} \Big(1 + (\pi - \sigma) \cot(\sigma) \Big) \tilde{\lambda} \tag{6.82}$$

and

$$\Delta \langle K_0 \rangle (B_\sigma, \lambda) = \frac{c}{6} \Big(1 - \sigma \cot(\sigma) \Big) \tilde{\lambda} \tag{6.83}$$

to be linear in $\tilde{\lambda}$.

Applying my result from Section 6.3.1 to this setup requires caution since the reference parameter value $\lambda_0 = 0$ is a boundary point of the domain of λ, but my result requires λ_0 to be in the interior of the domain. As explained in Section 6.3.3 this property serves two purposes in the proof of my result: It ensures (6.39) for $S(\Sigma, \lambda_0) = 0$ and the validity of the first law of entanglement. In this specific setup (6.39) may be verified directly,[21] so this part of the proof also works here. However, it is not possible for the first law of entanglement to hold for both A_σ and B_σ. This is easily concluded from the fact that $|\lambda\rangle$ is a family of pure states: from $S(A_\sigma, \lambda) = S(B_\sigma, \lambda)$ we conclude

$$\partial_\lambda \Delta S(A_\sigma, \lambda)|_{\lambda=\lambda_0} = \partial_\lambda \Delta S(B_\sigma, \lambda)|_{\lambda=\lambda_0} . \tag{6.84}$$

If the first law of entanglement would hold for A_σ and B_σ we would conclude from (6.22) and (6.84)

$$\partial_\lambda \Delta \langle K_0 \rangle (A_\sigma, \lambda)|_{\lambda=\lambda_0} = \partial_\lambda \Delta \langle K_0 \rangle (B_\sigma, \lambda)|_{\lambda=\lambda_0} . \tag{6.85}$$

However, this is obviously not true as can be seen from (6.82) and (6.83). Therefore we see that the first law of entanglement does not hold at least for one of the regions A_σ and B_σ. Consequently my result cannot be applied to this setup.

6.5 Discussion

In this chapter, which is based on [3], we presented a result I derived for the behavior of $\Delta \langle K_0 \rangle$ on entanglement plateaux (see Section 6.1). We considered a one-parameter family of states ρ_λ reduced to two entangling regions A, B which form an entanglement plateau. This entanglement plateau was assumed to be stable under variations of the size of A for fixed $\Sigma = AB$. In order to present a precise mathematical formulation for my result, we introduced a parameter σ for the entangling regions A and B, i.e. $A \longrightarrow A_\sigma$, $B \longrightarrow B_\sigma$. This parameter allowed us to manipulate the size of the entangling regions in a systematic way. We chose the parameter dependence of A_σ in such a way that $A_{\sigma_2} \subset A_{\sigma_1}$ for $\sigma_1 < \sigma_2$ holds. This implies $B_{\sigma_1} \subset B_{\sigma_2}$, since $\Sigma = A_\sigma B_\sigma$ is considered to be constant in σ. In this setup we studied how $\Delta \langle K_0 \rangle (A_\sigma, \lambda)$ and $\Delta \langle K_0 \rangle (B_\sigma, \lambda)$ (see (6.1)) depend on $\tilde{\lambda} = \lambda - \lambda_0$, where λ_0 corresponds to a reference state ρ_{λ_0}.

My result (see Section 6.3.1) states that $\Delta \langle K_0 \rangle (A_\sigma, \lambda)$ and $\Delta \langle K_0 \rangle (B_\sigma, \lambda)$ can only both be linear in $\tilde{\lambda}$ for all σ in a given interval $[\xi, \eta]$, if $\partial_\lambda^2 S(A_\sigma, \lambda)$ and

---

[21]It is an immediate consequence of $S(A_\sigma, \lambda) = S(B_\sigma, \lambda)$ and $S(\Sigma, \lambda) = 0$ for all λ and σ.

$\partial_\lambda^2 S(B_\sigma, \lambda)$ are constant in σ on $[\xi, \eta]$. The proof of this statement was presented in Section 6.3.2, first for the special case of thermal states dual to black string geometries and subsequently for generic entanglement plateaux. The proof is a simple application of the first law of entanglement (6.22) and the monotonicity of the relative entropy S_{rel} (6.25).

Since $\Delta \langle K_0 \rangle$ plays a major role in the relative entropy (6.19), my result provides valuable insight to the behavior of S_{rel} on entanglement plateaux. In particular, it implies that it is in general to be expected that either $S_{rel}(A_\sigma, \lambda)$, $S_{rel}(B_\sigma, \lambda)$ or both contain higher order contributions of $\tilde{\lambda}$ from $\Delta \langle K_0 \rangle (A_\sigma, \lambda)$ or $\Delta \langle K_0 \rangle (B_\sigma, \lambda)$, respectively. In situations where these contributions are not present, the first law of entanglement (6.22) implies that $\Delta \langle K_0 \rangle$ and therefore S_{rel} (6.19) are completely determined by entanglement entropies. My result shows that on entanglement plateaux stable under variations of σ such a simple form of S_{rel} cannot be expected at least for one of the two regions A_σ, B_σ.

In AdS/CFT entanglement plateaux are a very common phenomenon due to the RT formula (3.32) (see Section 6.1.2). Therefore, AdS/CFT provides us with many examples where my result from Section 6.3.1 may be applied. We studied several of them in Section 6.4. For instance, we considered A_σ to be the union of two sufficiently close intervals for thermal states dual to black strings in Section 6.4.1. By defining λ to be the energy density of the states, we concluded that $\Delta \langle K_0 \rangle (A_\sigma, \lambda)$ is not linear in $\tilde{\lambda}$ for all σ with possibly one exception. We later generalized this result to an arbitrary number of entangling intervals.

Furthermore, we also considered thermal states dual to black branes (see Section 6.4.2). Here we showed a result analogous to the one for black strings for annuli A_σ with sufficiently small inner radius σ. Here the reference state was taken to be the ground state.

As a final holographic example we studied thermal CFT_2 states on a circle which are dual to BTZ black holes in Section 6.4.3. The entangling region A_σ was taken to be an entangling interval with sufficiently large angular size. The parameter λ was chosen to be the square of the temperature. By choosing B_σ to be the complement of A_σ we managed to show that $\Delta \langle K_0 \rangle (A_\sigma, \lambda)$ is linear in $\tilde{\lambda}$ for at most one particular value of σ.

We need to emphasize that in the holographic examples studied in Section 6.4 the appearing entanglement plateaux are a large N effect. We used the RT formula (3.32) to establish that the Araki-Lieb inequality (3.10) is saturated in the corresponding setups. This implies by definition that the considered entangling regions form entanglement plateaux. However, the RT formula only applies in the large N limit. For finite N bulk quantum effects lead to corrections of the RT formula which cause the Araki-Lieb inequality to be no longer saturated [172]. Thus, my result only shows that the corresponding $\Delta \langle K_0 \rangle$ are non-linear in $\tilde{\lambda}$ for the considered holographic examples in the large N limit. We expect however, by continuity, that the non-linearity is also true for finite N.

We stress that even though the examples presented above all are based on AdS/CFT, my result of Section 6.3.1 applies to any quantum system, not just AdS/CFT. In Section 6.4.4 we also apply my result to primary excitations for a two-dimensional CFT. In this setup we do not require a holographic dual.

One intriguing observation that is provided by my result of Section 6.3.1 is the fact that the non-linearity of $\Delta \langle K_0 \rangle$ in $\tilde{\lambda}$ found in the examples in Section 6.4 has the same origin for all of them. All these examples consider states on entanglement plateaux. This property allowed us to apply my result and show the non-linearity of the respective $\Delta \langle K_0 \rangle$. We emphasize that it is remarkable that even though all the considered examples are very different form each other and very little is known about the respective modular Hamiltonians, it is still possible to deduce the non-linearity of $\Delta \langle K_0 \rangle$ for all of them from the same principle.

Furthermore, we demonstrated how my result of Section 6.3.1 may be used to show that the modular Hamiltonian for certain configurations A_σ of entangling intervals is not a local integral over the energy momentum tensor, when the considered states are dual to black strings (see Section 6.4.1). This relates my result to [200], where a topological condition was presented under which the modular Hamiltonian of a suitable reduced CFT_2 state is such a local integral (see Section 3.3.1).

As we discussed in Section 3.3.3, the relative entropy is a powerful tool for studying modular Hamiltonians that provided many non-trivial results for them. My result is a further such application of S_{rel}. It establishes a relation between higher order terms of $\Delta \langle K_0 \rangle$ in $\tilde{\lambda}$ and entanglement entropies. Possible future projects could focus on making this relation more concrete. My result as stated in Section 6.3.1 only considers the existence of higher order contributions in $\tilde{\lambda}$. It is worth investigating whether entanglement entropies may be used to determine the explicit expression of these higher order terms. This could be seen as an extension of the first law of entanglement, which associates the first order term in $\tilde{\lambda}$ of $\Delta \langle K_0 \rangle$ with entanglement entropy. Studying these aspects of $\Delta \langle K_0 \rangle$ suggested by my result may provide a better understanding of modular Hamiltonians in general quantum field theories.

Chapter 7

Conclusion

In this thesis we studied the quantum information aspects of complexity and modular Hamitonians in the context of AdS/CFT. As we discussed in the introduction, quantum information in quantum field theories is currently a subject of extensive research, in particular in the AdS/CFT community. The reason for this is the close relation between quantum information on the CFT side and geometry on the AdS side (see e.g. [87–89]). On the one hand, this relation makes the bulk geometry a valuable tool for explicit computations regarding quantum information (see e.g. [82]), on the other hand, it provides an elegant way for constructing quantum information quantities via bulk objects. The main focus of this thesis was one such quantity: complexity. Even though a rigorous definition for complexity in field theories is not known, there are several geometric constructions in the bulk which are proposed to be the holographic dual of complexity [56–59, 63]. In Chapter 4 we discussed such a proposal, which my collaborators and I presented in [1], topological complexity. Moreover, we derived a field theory expression for holographic subregion complexity [63] in Chapter 5, which was published in [1, 2] by my collaborators and me.

Furthermore, we analyzed the behavior of modular Hamiltonians for one-parameter families of states on regions which form entanglement plateaux [114] in Chapter 6. The corresponding results were published in [3]. Even though these results are not restricted to field theories with holographic duals, AdS/CFT provides many examples where they can be applied.

7.1   Summary and Discussion

In preparation of the presentation and discussion of our findings, we reviewed the AdS/CFT correspondence in Chapter 2 and the aspects of quantum information relevant for this thesis in Chapter 3.

Chapter 4 was devoted to the concept of topological complexity my collaborators and I introduced in [1]. For a given entangling region A on a constant time slice of the CFT, topological complexity (4.1) is given by the integral over the Ricci scalar over the bulk region $\mathcal{B}_A$ enclosed by A and the respective RT surface. We focused on AdS_3/CFT_2 for our examination of topological complexity. The

Gauss-Bonnet theorem allowed us in Section 4.1 to derive very general expressions for topological complexity, which we applied to examples involving global AdS$_3$, BTZ black holes and conical defects in Section 4.2. Our computations of topological complexity for states dual to global AdS$_3$ (vacuum) and BTZ black holes (thermal) show that the part c_T^0 of topological complexity independent of the considered radial cut-off (4.4) is completely determined by the topology of $\mathcal{B}_A$ and A. This led us to the conclusion that c_T^0 performs a discrete jump when the RT surface undergoes a phase transition. In particular, the temperature dependence of topological complexity for thermal states manifests itself only by such a discrete jump.[1] For primary states dual to conical defect geometries c_T^0 no longer only depends on topological aspects of the setup but also the particular type of excitation. We visualized these findings for vacuum, thermal and primary excited states in Figure 4.4.

For the examples we considered, topological complexity agrees with HSRC up to a constant proportionality factor. Therefore, the observations we made for topological complexity also apply to HSRC. In particular, we saw a clear relation between the topologies of $\mathcal{B}_A$ and A and the cut-off independent part of HSRC. As this part is proposed to be universal [63], this is of particular interest for the field theory interpretation of HSRC. We summarized and discussed our findings in Section 4.3.

In Chapter 5 we presented the main result of this thesis, which was published in [1] and [2]. We constructed an explicit field theory expression for the HSRC of an entangling interval A for CFT$_2$ vacuum states dual to global AdS$_3$ and the $(2+1)$-dimensional Poincaré patch. This construction was based the concept of Kinematic space $\mathcal{K}$ [95, 96], which is the space of all boundary anchored bulk geodesics on a constant time slice. We reviewed kinematic space in Section 5.1. In Section 5.2 we presented and proved a formula which expresses the volume of an arbitrary codimension one bulk region $\mathcal{Q}$ on a constant time slice as an integral over $\mathcal{K}$. This "volume formula" in combination with the RT formula allows to express the volume of any $\mathcal{Q}$ as an integral over entanglement entropies. It may therefore be seen as a natural extension of the formalisms discussed in [94–96, 209, 210] which provide similar expressions for the lengths of bulk curves. We applied the volume formula to $\mathcal{B}_A$ in Section 5.3, which provided us with an expression for HSRC in terms of entanglement entropies. As this expression can be derived from the CFT side, it may be seen as the field theory dual of HSRC. We introduced a cut-off scheme for our formula for HSRC and applied it to compute HSRC for several explicit examples. In Section 5.4 we extended our formula to BTZ black holes and conical defect geometries. In these situations we found that HSRC is no longer only determined by entanglement entropy but also contributions related to entwinement [146] are present. Entwinement corresponds to the length of non-minimal bulk geodesics and is proposed to encode the entanglement of inner degrees of freedom on the field theory side [146]. Moreover, for BTZ black holes we found a further type of contribution to HSRC which is related to bulk geodesics running from the conformal boundary to the black hole horizon. We

---

[1]This was also observed in [188].

denoted them as *thermal contributions* due to their relation to the horizon. The appearance of additional contributions to HSRC which cannot be interpreted in terms of entanglement entropies may be seen as a motivation to further study the field theory interpretation of the corresponding bulk geodesics.

In Section 5.5 we studied our results regarding HSRC under the assumption that HSRC is indeed a bulk description of subregion complexity. We found that in this context the reference state may be seen as a field theory version of a product state. Moreover, our formulae for HSRC indicate that a concept of complexity for reduced states based on HSRC takes into account that the considered reduced state is part of a larger system. This separates HSRC from the complexity constructions for mixed states presented in [179] (see Section 3.2.1), which ignore this fact. Our results for HSRC together with their implications for possible future projects were discussed in Section 5.6.

The focus of Chapter 6 were the results regarding modular Hamiltonians published in [3]. Given a family of states ρ_λ depending on a continuous parameter λ, we studied the dependence of $\Delta \langle K_0 \rangle (A, \lambda)$ (6.1) on λ. Here $K_0(A)$ is the modular Hamiltonian of a reduced reference state $\rho_{\lambda_0}^A$ on the entangling region A. The object $\Delta \langle K_0 \rangle$ is of great importance for the computation of the relative entropy (6.19), which was the reason for our investigations. Given two entangling regions A and B, forming an entanglement plateau, we examined when $\Delta \langle K_0 \rangle (A, \lambda)$ or $\Delta \langle K_0 \rangle (B, \lambda)$ are not linear in $\lambda - \lambda_0$. The result we obtained goes as follows. Consider an entanglement plateau stable under variations of the size of A and B that keep AB invariant. Then $\Delta \langle K_0 \rangle$ may only be linear in $\lambda - \lambda_0$ for A, B and variations of their size if $\partial_\lambda^2 S$ is constant under variations of the size of A and B. Here S is the entanglement entropy. We reviewed the concept of entanglement plateaux in Section 6.1 and explained the setup and motivation for our studies in Section 6.2. In Section 6.3 we presented the exact mathematical statement of our result which we subsequently proved by a simple argument based on the first law of entanglement (6.22) and the monotonicity of the relative entropy (6.25). Moreover, we discussed various aspects of our result, including the role of the prerequisites in its proof and its generalization to n-parameter families of states.

We applied our result of Section 6.3 to several examples in Section 6.4. As we pointed out in Section 6.1, entanglement plateaux are easily constructed in AdS/CFT. This allowed us to study several holographic examples, including unions of disconnected intervals for thermal CFT_2 states dual to black string geometries. For this case, our result provided a way to show that the modular Hamiltonian may not be written as a local integral over the energy momentum tensor. This observation reveals the importance of our result in the context of [200]. Here a topological condition was constructed under which the modular Hamiltonian may be written as a local integral over the energy momentum tensor. The above example demonstrates that our result may be used to show when such an integral form does not exist. Furthermore, we applied our result to states dual to black brane geometries and BTZ black holes.

We emphasize that even though most of the examples we considered in this chapter are based on AdS/CFT, our result not only applies to field theories with

holographic duals but to any QFT. It reveals a non-trivial relation between entanglement entropy and higher order contributions in $\lambda - \lambda_0$ to $\Delta \langle K_0 \rangle$. Therefore, it may be seen as an extension of the first law of entanglement, which provides such a relation for the first order terms in $\lambda - \lambda_0$. We concluded Chapter 6 with some final remarks and discussions in Section 6.5.

The results of this thesis further clarify the close relation between bulk geometry and quantum information on the boundary (see Section 1.2). For instance, in Chapter 4 we saw that the cut-off independent term of topological complexity performs discrete jumps when the phase of the corresponding RT surface changes. Under which circumstances such transitions occur is encoded in the bulk geometry. Moreover, in Chapter 5 we demonstrated how volumes of codimension one bulk regions on a constant time slice may be expressed in terms of entanglement entropies for global AdS$_3$ and the Poincaré patch. For BTZ black holes and conical defects we observed additional contributions related to entwinement and the thermality of the states dual to BTZ black holes. In addition, the examples we studied in Chapter 6 reveal a connection between geometry and $\Delta \langle K_0 \rangle$. We argued that for a one-parameter family of states on a stable entanglement plateau $\Delta \langle K_0 \rangle$ is usually expected to contain second and higher order contributions in the parameter.[2] For the holographic examples we applied this statement to, a particular phase of the RT surface is required in order to provide an entanglement plateau (see Section 6.4). The phases of the RT surface are determined by the bulk geometry. Therefore, we see that the bulk geometry has a non-trivial influence on the behavior of $\Delta \langle K_0 \rangle$. [3]

7.2   Outlook

Future projects may further investigate and develop our findings. In addition to the possible projects we discussed in Sections 4.3, 5.6 and 6.5 we consider the comparison of our results for topological complexity (see Chapter 4) with the field theory expression for HSRC we presented in Chapter 5 of particular interest. We note that for the examples we considered in this thesis, topological complexity differs from HSRC only by a constant prefactor. Therefore, our results regarding the discrete jumps of topological complexity also hold for HSRC. These jumps may be studied in the context of our field theory expression for HSRC. For instance, it is easy to see that the expression (5.53) we derived for one entangling interval on the boundary of global AdS$_3$ can be generalized to an arbitrary number of entangling intervals. For this setup, the results of Chapter 4 imply that HSRC jumps by multiples of 2π when the position of the intervals relative to each other is changed. The study of the contributions to our field theory expression corresponding to these jumps may provide a physical interpretation for this phenomenon. The physical interpretation of these jumps may also improve our understanding of the behavior of $\Delta \langle K_0 \rangle$ on entanglement plateaux. In AdS/CFT these plateaux are usually re-

---

[2]For the exact formulation of this result we refer to Section 6.3.

[3]The behavior of the modular Hamiltonian under phase transitions of the RT surface was also discussed in e.g. [115]. We refer to [157] for related work.

lated to a particular phase of the RT surface (see Section 6.4). Since transitions of this phase cause the jumps in HSRC (see Section 4.2), an interpretation of them in the context of HSRC may provide deeper insight into the behavior of $\Delta \langle K_0 \rangle$ on entanglement plateaux.

The above discussion shows that the three projects presented in Chapters 4, 5 and 6 are related by a common theme: the phases of the RT surface. We see that these phases may be studied from several very different perspectives, providing further insight into the close relation between quantum information on the field theory side and geometry on the gravity side. The results we presented in this thesis may be seen as a starting point for future projects expanding our understanding of the role of the bulk geometry in quantum information on the boundary.

Acknowledgments

The people who granted me their support during my studies are too numerous to acknowledge them all individually. In particular, I state my gratitude to my supervisor Prof. Dr. Johanna K. Erdmenger for introducing me to the exciting field of AdS/CFT and the many opportunities for international exchange and collaboration she provided. I also highly appreciate her many helpful comments which allowed me to improve the results of my projects.

Moreover, I thank all my collaborators and colleges, including Prof. Dr. Haye Hinrichsen, Dr. René Meyer, Dr. Charles M. Melby-Thompson, Dr. Ignacio A. Reyes, Christian Northe, Marius Gerbershagen, Nina Miekley, Pascal Fries and Yiqiang Du, for their advise, enthusiasm and hard work. The working environment they created was essential for the evolution of my understanding of the field of AdS/CFT.

I also would like to acknowledge Prof. Dr. Thorsten Ohl, whose guidance during my master project as well as his lectures about algebraic quantum field theory and theoretical particle physics substantially shaped the way I approach questions in physics.

Finally, I am very grateful to my parents Christine and Karlheinz Abt. Without their constant support, understanding and patience the conclusion of my studies would not have been possible.

Appendix A

Notation and Conventions

Throughout this thesis we use the following notations and conventions.

Synonyms for the AdS Side. In AdS/CFT we refer to the theory of gravity on AdS as AdS side, AdS, gravity side, gravity dual, gravitational dual, bulk (dual) or holographic (dual). Moreover, we use analogous terms for objects in the bulk, in particular when we consider them in the context of their dual description on the CFT side.

Synonyms for the CFT Side. We use the terms field theory side, field theory dual, CFT (side), CFT dual or boundary for references regarding the conformal field theory in AdS/CFT. Moreover, we use analogous terms to refer to objects on the CFT side. In particular when we discuss them in the context of their duals on the AdS side.

Ryu-Takayanagi Surface for AdS$_3$/CFT$_2$. In AdS$_{d+1}$/CFT$_d$ the Ryu-Takayanagi (RT) surface is a $(d-1)$-dimensional hypersurface in the bulk (see Section 3.1.6). Most of the examples discussed in this thesis consider AdS$_3$/CFT$_2$. Here the RT surface is one-dimensional, i.e. a curve. In order to maintain a consistent notation throughout this thesis we still refer to this curve as the RT "surface" and to its length as "area".

Static Space-Times. In all the examples we consider in this thesis, we work with static asymptotic AdS spaces. The feature of these spaces that we frequently use is location of the RT surface on the same constant time slice as the corresponding entangling region on the boundary.

Signature of the Metric. For the space-time metrics we consider in this thesis we use the signature $(-++\cdots+)$.

Einstein's Sum Convention. We make use of Einstein's sum convention, i.e. indices appearing twice in a given term are summed over.

Natural Units. We use units where the speed of light, the reduced Planck constant and the Boltzmann constant are set to one.

Abbreviation for Symmetric Tensor Products. Throughout this thesis we discuss several metric tensors. In order to avoid cluttering we use

$$dxdy = \frac{1}{2}\big(dx \otimes dy + dy \otimes dx\big) \tag{A.1}$$

as an abbreviation for the symmetric tensor product of two one-forms dx, dy.

Abbreviation for Entangling Regions. For two entangling regions (or subsystems) A, B we use

$$AB = A \cup B \,, \tag{A.2}$$

as an abbreviation.

Newton's Constant. We refer to Newton's constant in $(d+1)$ dimensions as G_{d+1}.

Gamma Function. The Gamma function is denoted by Γ.

Bibliography

[1] R. Abt, J. Erdmenger, H. Hinrichsen, C. M. Melby-Thompson, R. Meyer, C. Northe and I. A. Reyes, *Topological Complexity in AdS3/CFT2*, *Fortschr. Phys.* **66** (2018) 1800034, [`arXiv:1710.01327`].

[2] R. Abt, J. Erdmenger, M. Gerbershagen, C. M. Melby-Thompson and C. Northe, *Holographic Subregion Complexity from Kinematic Space*, *JHEP* **01** (2019) 012, [`arXiv:1805.10298`].

[3] R. Abt and J. Erdmenger, *Properties of Modular Hamiltonians on Entanglement Plateaux*, *JHEP* **11** (2018) 002, [`arXiv:1809.03516`].

[4] F. Englert and R. Brout, *Broken Symmetry and the Mass of Gauge Vector Mesons*, *Phys. Rev. Lett.* **13** (1964) 321–323.

[5] P. W. Higgs, *Broken symmetries, massless particles and gauge fields*, *Phys. Lett.* **12** (1964) 132–133.

[6] P. W. Higgs, *Broken Symmetries and the Masses of Gauge Bosons*, *Phys. Rev. Lett.* **13** (1964) 508–509.

[7] ATLAS collaboration, G. Aad et al., *Observation of a new particle in the search for the Standard Model Higgs boson with the ATLAS detector at the LHC*, *Phys. Lett.* **B716** (2012) 1–29, [`arXiv:1207.7214`].

[8] CMS collaboration, S. Chatrchyan et al., *Observation of a new boson at a mass of 125 GeV with the CMS experiment at the LHC*, *Phys. Lett.* **B716** (2012) 30–61, [`arXiv:1207.7235`].

[9] A. Einstein, *Die Feldgleichungen der Gravitation*, *Sitzungsberichte der Königlich Preussischen Akademie der Wissenschaften zu Berlin* (1915) 844–847.

[10] A. Einstein, *Näherungsweise Integration der Feldgleichungen der Gravitation*, *Sitzungsberichte der Königlich Preussischen Akademie der Wissenschaften zu Berlin* (1916) 688–696.

[11] A. Einstein, *Über Gravitationswellen*, *Sitzungsberichte der Königlich Preussischen Akademie der Wissenschaften zu Berlin* (1918) 154–167.

[12] LIGO Scientific, Virgo collaboration, B. P. Abbott et al., *Observation of Gravitational Waves from a Binary Black Hole Merger*, *Phys. Rev. Lett.* **116** (2016) 061102, [`arXiv:1602.03837`].

[13] LIGO Scientific, Virgo collaboration, B. P. Abbott et al., *GW151226: Observation of Gravitational Waves from a 22-Solar-Mass Binary Black Hole Coalescence*, *Phys. Rev. Lett.* **116** (2016) 241103, [`arXiv:1606.04855`].

[14] P. Amaro-Seoane, H. Audley, S. Babak, J. Baker, E. Barausse, P. Bender et al., *Laser Interferometer Space Antenna*, *arXiv e-prints* (2017) , [`arXiv:1702.00786`].

[15] B. Iyer et al., *LIGO-India Technical Report No. LIGO-M1100296*, `https://dcc.ligo.org/LIGO-M1100296/public/main` (2011) .

[16] Event Horizon Telescope collaboration, K. Akiyama et al., *First M87 Event Horizon Telescope Results. I. The Shadow of the Supermassive Black Hole*, *Astrophys. J.* **875** (2019) L1.

[17] Event Horizon Telescope collaboration, K. Akiyama et al., *First M87 Event Horizon Telescope Results. II. Array and Instrumentation*, *Astrophys. J.* **875** (2019) L2.

[18] Event Horizon Telescope collaboration, K. Akiyama et al., *First M87 Event Horizon Telescope Results. III. Data Processing and Calibration*, *Astrophys. J.* **875** (2019) L3.

[19] Event Horizon Telescope collaboration, K. Akiyama et al., *First M87 Event Horizon Telescope Results. IV. Imaging the Central Supermassive Black Hole*, *Astrophys. J.* **875** (2019) L4.

[20] Event Horizon Telescope collaboration, K. Akiyama et al., *First M87 Event Horizon Telescope Results. V. Physical Origin of the Asymmetric Ring*, *Astrophys. J.* **875** (2019) L5.

[21] Event Horizon Telescope collaboration, K. Akiyama et al., *First M87 Event Horizon Telescope Results. VI. The Shadow and Mass of the Central Black Hole*, *Astrophys. J.* **875** (2019) L6.

[22] J. M. Maldacena, *The Large N limit of superconformal field theories and supergravity*, *Int. J. Theor. Phys.* **38** (1999) 1113–1133, [`arXiv:hep-th/9711200`].

[23] S. Lee, S. Minwalla, M. Rangamani and N. Seiberg, *Three point functions of chiral operators in D = 4, N=4 SYM at large N*, *Adv. Theor. Math. Phys.* **2** (1998) 697–718, [`arXiv:hep-th/9806074`].

[24] M. Henningson and K. Skenderis, *The Holographic Weyl anomaly*, *JHEP* **07** (1998) 023, [`arXiv:hep-th/9806087`].

[25] A. Einstein, B. Podolsky and N. Rosen, *Can quantum-mechanical description of physical reality be considered complete?*, *Phys. Rev.* **47** (May, 1935) 777–780.

[26] B. Hensen et al., *Loophole-free Bell inequality violation using electron spins separated by 1.3 kilometres*, *Nature* **526** (2015) 682–686, [`arXiv:1508.05949`].

[27] M. A. Nielsen and I. L. Chuang, *Quantum Computation and Quantum Information (676 pages).* Cambridge University Press, Cambridge, UK, 2000.

[28] M. M. Wilde, *Quantum Information Theory, Second Edition (757 pages).* Cambridge University Press, Cambridge, UK, 2017.

[29] E. Desurvire, *Classical and Quantum Information Theory: An Introduction for the Telecom Scientist (691 pages).* Cambridge University Press, Cambridge, UK, 2009.

[30] T. Nishioka, *Entanglement entropy: holography and renormalization group*, *Rev. Mod. Phys.* **90** (2018) 035007, [`arXiv:1801.10352`].

[31] V. Vedral, *The role of relative entropy in quantum information theory*, *Rev. Mod. Phys.* **74** (Mar, 2002) 197–234.

[32] R. Horodecki, P. Horodecki, M. Horodecki and K. Horodecki, *Quantum entanglement*, *Rev. Mod. Phys.* **81** (2009) 865–942, [`arXiv:quant-ph/0702225`].

[33] M. Rangamani and T. Takayanagi, *Holographic Entanglement Entropy*, *Lect. Notes Phys.* **931** (2017) pp.–, [`arXiv:1609.01287`].

[34] H. Araki, *Relative Entropy of States of Von Neumann Algebras*, *Publ. Res. Inst. Math. Sci. Kyoto* **1976** (1976) 809–833.

[35] E. Witten, *APS Medal for Exceptional Achievement in Research: Invited article on entanglement properties of quantum field theory*, *Rev. Mod. Phys.* **90** (2018) 045003, [`arXiv:1803.04993`].

[36] D. Petz, *Quantum Information Theory and Quantum Statistics (214 pages).* Springer, Berlin Heidelberg, GER, 2008.

[37] C. M. Papadimitriou, *Computational Complexity (523 pages).* Addison-Wesley, Reading, US, 1994.

[38] S. Aaronson, *The Complexity of Quantum States and Transformations: From Quantum Money to Black Holes*, 2016, `arXiv:1607.05256`.

[39] A. Almheiri, X. Dong and D. Harlow, *Bulk Locality and Quantum Error Correction in AdS/CFT*, *JHEP* **04** (2015) 163, [`arXiv:1411.7041`].

[40] N. Lashkari and M. Van Raamsdonk, *Canonical Energy is Quantum Fisher Information*, *JHEP* **04** (2016) 153, [`arXiv:1508.00897`].

[41] T. Ugajin, *Mutual information of excited states and relative entropy of two disjoint subsystems in CFT*, *JHEP* **10** (2017) 184, [`arXiv:1611.03163`].

[42] P. Fries and I. A. Reyes, *The entanglement and relative entropy of a chiral fermion on the torus*, `arXiv:1906.02207`.

[43] H. Reeh and S. Schlieder, *Bemerkungen zur unitäräquivalenz von lorentzinvarianten feldern*, *Il Nuovo Cimento (1955-1965)* **22** (Dec, 1961) 1051–1068.

[44] W. Israel, *Thermo field dynamics of black holes*, *Phys. Lett.* **A57** (1976) 107–110.

[45] R. Laflamme, *Geometry and Thermofields*, *Nucl. Phys.* **B324** (1989) 233–252.

[46] W. G. Unruh, *Notes on black hole evaporation*, *Phys. Rev.* **D14** (1976) 870.

[47] W. Rindler, *Kruskal Space and the Uniformly Accelerated Frame*, *Am. J. Phys.* **34** (1966) 1174.

[48] S. Chapman, M. P. Heller, H. Marrochio and F. Pastawski, *Toward a Definition of Complexity for Quantum Field Theory States*, *Phys. Rev. Lett.* **120** (2018) 121602, [`arXiv:1707.08582`].

[49] R. Jefferson and R. C. Myers, *Circuit complexity in quantum field theory*, *JHEP* **10** (2017) 107, [`arXiv:1707.08570`].

[50] L. Hackl and R. C. Myers, *Circuit complexity for free fermions*, *JHEP* **07** (2018) 139, [`arXiv:1803.10638`].

[51] R.-Q. Yang, Y.-S. An, C. Niu, C.-Y. Zhang and K.-Y. Kim, *Principles and symmetries of complexity in quantum field theory*, *Eur. Phys. J.* **C79** (2019) 109, [`arXiv:1803.01797`].

[52] D. Carmi, R. C. Myers and P. Rath, *Comments on Holographic Complexity*, *JHEP* **03** (2017) 118, [`arXiv:1612.00433`].

[53] P. Roy and T. Sarkar, *Note on subregion holographic complexity*, *Phys. Rev.* **D96** (2017) 026022, [`arXiv:1701.05489`].

[54] B. Chen, W.-M. Li, R.-Q. Yang, C.-Y. Zhang and S.-J. Zhang, *Holographic subregion complexity under a thermal quench*, *JHEP* **07** (2018) 034, [`arXiv:1803.06680`].

[55] M. Flory and N. Miekley, *Complexity change under conformal transformations in AdS_3/CFT_2*, *JHEP* **05** (2019) 003, [`arXiv:1806.08376`].

[56] L. Susskind, *Butterflies on the Stretched Horizon*, `arXiv:1311.7379`.

[57] D. Stanford and L. Susskind, *Complexity and Shock Wave Geometries*, *Phys. Rev.* **D90** (2014) 126007, [`arXiv:1406.2678`].

[58] L. Susskind, *Computational Complexity and Black Hole Horizons*, *Fortsch. Phys.* **64** (2016) 24–43, [`arXiv:1402.5674`].

[59] A. R. Brown, D. A. Roberts, L. Susskind, B. Swingle and Y. Zhao, *Holographic Complexity Equals Bulk Action?*, *Phys. Rev. Lett.* **116** (2016) 191301, [`arXiv:1509.07876`].

[60] W. Israel, *Thermo-field dynamics of black holes*, *Physics Letters A* **57** (1976) 107 – 110.

[61] J. M. Maldacena, *Eternal black holes in anti-de Sitter*, *JHEP* **04** (2003) 021, [`arXiv:hep-th/0106112`].

[62] T. Hartman and J. Maldacena, *Time Evolution of Entanglement Entropy from Black Hole Interiors*, *JHEP* **05** (2013) 014, [`arXiv:1303.1080`].

[63] M. Alishahiha, *Holographic Complexity*, *Phys. Rev.* **D92** (2015) 126009, [`arXiv:1509.06614`].

[64] G. Wong, I. Klich, L. A. Pando Zayas and D. Vaman, *Entanglement Temperature and Entanglement Entropy of Excited States*, *JHEP* **12** (2013) 020, [`arXiv:1305.3291`].

[65] D. L. Jafferis and S. J. Suh, *The Gravity Duals of Modular Hamiltonians*, *JHEP* **09** (2016) 068, [`arXiv:1412.8465`].

[66] N. Lashkari, *Modular Hamiltonian for Excited States in Conformal Field Theory*, *Phys. Rev. Lett.* **117** (2016) 041601, [`arXiv:1508.03506`].

[67] T. Faulkner, R. G. Leigh, O. Parrikar and H. Wang, *Modular Hamiltonians for Deformed Half-Spaces and the Averaged Null Energy Condition*, *JHEP* **09** (2016) 038, [`arXiv:1605.08072`].

[68] R. Arias, D. Blanco, H. Casini and M. Huerta, *Local temperatures and local terms in modular Hamiltonians*, *Phys. Rev.* **D95** (2017) 065005, [`arXiv:1611.08517`].

[69] J. Koeller, S. Leichenauer, A. Levine and A. Shahbazi-Moghaddam, *Local Modular Hamiltonians from the Quantum Null Energy Condition*, *Phys. Rev.* **D97** (2018) 065011, [`arXiv:1702.00412`].

[70] H. Casini, E. Teste and G. Torroba, *Modular Hamiltonians on the null plane and the Markov property of the vacuum state*, *J. Phys.* **A50** (2017) 364001, [`arXiv:1703.10656`].

[71] G. Sárosi and T. Ugajin, *Modular Hamiltonians of excited states, OPE blocks and emergent bulk fields*, *JHEP* **01** (2018) 012, [`arXiv:1705.01486`].

[72] R. Arias, H. Casini, M. Huerta and D. Pontello, *Anisotropic Unruh temperatures*, *Phys. Rev.* **D96** (2017) 105019, [`arXiv:1707.05375`].

[73] R. Haag, *Local Quantum Physics: Fields, Particles, Algebras (356 pages)*. Springer, Berlin Heidelberg, GER, 1992.

[74] H. Casini and M. Huerta, *Reduced density matrix and internal dynamics for multicomponent regions*, *Class. Quant. Grav.* **26** (2009) 185005, [arXiv:0903.5284].

[75] I. Klich, D. Vaman and G. Wong, *Entanglement Hamiltonians for chiral fermions with zero modes*, *Phys. Rev. Lett.* **119** (2017) 120401, [arXiv:1501.00482].

[76] R. E. Arias, H. Casini, M. Huerta and D. Pontello, *Entropy and modular Hamiltonian for a free chiral scalar in two intervals*, *Phys. Rev.* **D98** (2018) 125008, [arXiv:1809.00026].

[77] P. Fries and I. A. Reyes, *The entanglement spectrum of chiral fermions on the torus*, arXiv:1905.05768.

[78] D. Blanco and G. Pérez-Nadal, *Modular Hamiltonian of a chiral fermion on the torus*, *Phys. Rev.* **D100** (2019) 025003, [arXiv:1905.05210].

[79] G. 't Hooft, *Dimensional reduction in quantum gravity*, *Conf. Proc.* **C930308** (1993) 284–296, [arXiv:gr-qc/9310026].

[80] L. Susskind, *The World as a hologram*, *J. Math. Phys.* **36** (1995) 6377–6396, [arXiv:hep-th/9409089].

[81] L. Susskind and E. Witten, *The Holographic bound in anti-de Sitter space*, arXiv:hep-th/9805114.

[82] S. Ryu and T. Takayanagi, *Holographic derivation of entanglement entropy from AdS/CFT*, *Phys. Rev. Lett.* **96** (2006) 181602, [arXiv:hep-th/0603001].

[83] M. Headrick and T. Takayanagi, *A Holographic proof of the strong subadditivity of entanglement entropy*, *Phys. Rev.* **D76** (2007) 106013, [arXiv:0704.3719].

[84] V. E. Hubeny, M. Rangamani and T. Takayanagi, *A Covariant holographic entanglement entropy proposal*, *JHEP* **07** (2007) 062, [arXiv:0705.0016].

[85] P. Hayden, M. Headrick and A. Maloney, *Holographic Mutual Information is Monogamous*, *Phys. Rev.* **D87** (2013) 046003, [arXiv:1107.2940].

[86] A. Lewkowycz and J. Maldacena, *Generalized gravitational entropy*, *JHEP* **08** (2013) 090, [arXiv:1304.4926].

[87] M. Van Raamsdonk, *Comments on quantum gravity and entanglement*, arXiv:0907.2939.

[88] M. Van Raamsdonk, *Building up spacetime with quantum entanglement*, *Gen. Rel. Grav.* **42** (2010) 2323–2329, [arXiv:1005.3035].

[89] N. Lashkari, M. B. McDermott and M. Van Raamsdonk, *Gravitational dynamics from entanglement 'thermodynamics'*, *JHEP* **04** (2014) 195, [`arXiv:1308.3716`].

[90] F. Pastawski, B. Yoshida, D. Harlow and J. Preskill, *Holographic quantum error-correcting codes: Toy models for the bulk/boundary correspondence*, *JHEP* **06** (2015) 149, [`arXiv:1503.06237`].

[91] F. Pastawski and J. Preskill, *Code properties from holographic geometries*, *Phys. Rev.* **X7** (2017) 021022, [`arXiv:1612.00017`].

[92] B. Swingle, *Entanglement Renormalization and Holography*, *Phys. Rev.* **D86** (2012) 065007, [`arXiv:0905.1317`].

[93] B. Swingle, *Constructing holographic spacetimes using entanglement renormalization*, `arXiv:1209.3304`.

[94] V. Balasubramanian, B. D. Chowdhury, B. Czech, J. de Boer and M. P. Heller, *Bulk curves from boundary data in holography*, *Phys. Rev.* **D89** (2014) 086004, [`arXiv:1310.4204`].

[95] B. Czech and L. Lamprou, *Holographic definition of points and distances*, *Phys. Rev.* **D90** (2014) 106005, [`arXiv:1409.4473`].

[96] B. Czech, L. Lamprou, S. McCandlish and J. Sully, *Integral Geometry and Holography*, *JHEP* **10** (2015) 175, [`arXiv:1505.05515`].

[97] B. Czech, L. Lamprou, S. McCandlish and J. Sully, *Tensor Networks from Kinematic Space*, *JHEP* **07** (2016) 100, [`arXiv:1512.01548`].

[98] E. Witten, *A Mini-Introduction To Information Theory*, `arXiv:1805.11965`.

[99] S. Weinberg, *The Quantum Theory of Fields: Volume I, Foundations (609 pages)*. Cambridge University Press, Cambridge, UK, 1995.

[100] M. E. Peskin and D. V. Schroeder, *An Introduction to Quantum Field Theory (842 pages)*. Westview Press, Boulder, US, 1995.

[101] L. H. Ryder, *Quantum Field Theory. Second Edition (487 pages)*. Cambridge University Press, Cambridge, UK, 1996.

[102] S. W. Hawking and G. F. R. Ellis, *The Large Scale Structure of Space-Time (391 pages)*. Cambridge University Press, Cambridge, UK, 1973.

[103] H. Brauner, *Differentialgeometrie (424 pages)*. Vieweg, Braunschweig, GER, 1981.

[104] S. Carroll, *Spacetime and Geometry: An Introduction to General Relativity (513 pages)*. Addison-Wesley, San Francisco, US, 2004.

[105] C. W. Misner, K. S. Thorne and J. A. Wheeler, *Gravitation (1279 pages)*. Princeton University Press, Princeton, US, 2017.

[106] B. Zwiebach, *A First Course in String Theory. Second Edition (673 pages)*. Cambridge University Press, Cambridge, UK, 2009.

[107] J. Polchinski, *String Theory: Volume II, Superstring Theory and Beyond (531 pages)*. Cambridge University Press, Cambridge, UK, 1998.

[108] K. Becker, M. Becker and J. H. Schwarz, *String Theory and M-Theory: A Modern Introduction (739 pages)*. Cambridge University Press, Cambridge, UK, 2007.

[109] M. Ammon and J. Erdmenger, *Gauge/Gravity Duality: Foundations and Applications (533 pages)*. Cambridge University Press, Cambridge, UK, 2015.

[110] O. Aharony, S. S. Gubser, J. M. Maldacena, H. Ooguri and Y. Oz, *Large N field theories, string theory and gravity*, *Phys. Rept.* **323** (2000) 183–386, [`arXiv:hep-th/9905111`].

[111] C. V. Johnson, *D-brane primer*, in *Strings, branes and gravity. Proceedings, Theoretical Advanced Study Institute, TASI'99, Boulder, USA, May 31-June 25, 1999*, pp. 129–350, 2000, `arXiv:hep-th/0007170`.

[112] D. Tong, *String Theory*, `arXiv:0908.0333`.

[113] H. Araki and E. H. Lieb, *Entropy inequalities*, *Communications in Mathematical Physics* **18** (Jun, 1970) 160–170.

[114] V. E. Hubeny, H. Maxfield, M. Rangamani and E. Tonni, *Holographic entanglement plateaux*, *JHEP* **08** (2013) 092, [`arXiv:1306.4004`].

[115] D. D. Blanco, H. Casini, L.-Y. Hung and R. C. Myers, *Relative Entropy and Holography*, *JHEP* **08** (2013) 060, [`arXiv:1305.3182`].

[116] A. V. Ramallo, *Introduction to the AdS/CFT correspondence*, *Springer Proc. Phys.* **161** (2015) 411–474, [`arXiv:1310.4319`].

[117] J. Penedones, *TASI lectures on AdS/CFT*, in *Proceedings, Theoretical Advanced Study Institute in Elementary Particle Physics: New Frontiers in Fields and Strings (TASI 2015): Boulder, CO, USA, June 1-26, 2015*, pp. 75–136, 2017, `arXiv:1608.04948`.

[118] V. E. Hubeny, *The AdS/CFT Correspondence*, *Class. Quant. Grav.* **32** (2015) 124010, [`arXiv:1501.00007`].

[119] J. Erdmenger, *Introduction to Gauge/Gravity Duality*, *PoS* **TASI2017** (2018) 001, [`arXiv:1807.09872`].

[120] P. Di Francesco, P. Mathieu and D. Sénéchal, *Conformal Field Theory (890 pages)*. Springer, New York, US, 1997, 10.1007/978-1-4612-2256-9.

[121] R. Blumenhagen and E. Plauschinn, *Introduction to Conformal Field Theory: With Applications to String Theory. Lect. Notes Phys. 779 (265 pages)*. Springer, Berlin Heidelberg, GER, 2009, 10.1007/978-3-642-00450-6.

[122] P. H. Ginsparg, *Applied Conformal Field Theory*, in *Les Houches Summer School in Theoretical Physics: Fields, Strings, Critical Phenomena Les Houches, France, June 28-August 5, 1988*, pp. 1–168, 1988, `arXiv:hep-th/9108028`.

[123] E. D'Hoker and D. Z. Freedman, *Supersymmetric gauge theories and the AdS / CFT correspondence*, in *Strings, Branes and Extra Dimensions: TASI 2001: Proceedings*, pp. 3–158, 2002, `arXiv:hep-th/0201253`.

[124] G. 't Hooft, *A Planar Diagram Theory for Strong Interactions*, *Nucl. Phys.* **B72** (1974) 461.

[125] G. W. Gibbons and K.-i. Maeda, *Black Holes and Membranes in Higher Dimensional Theories with Dilaton Fields*, *Nucl. Phys.* **B298** (1988) 741–775.

[126] D. Garfinkle, G. T. Horowitz and A. Strominger, *Charged black holes in string theory*, *Phys. Rev.* **D43** (1991) 3140.

[127] G. T. Horowitz and A. Strominger, *Black strings and P-branes*, *Nucl. Phys.* **B360** (1991) 197–209.

[128] J. R. David, G. Mandal and S. R. Wadia, *Microscopic formulation of black holes in string theory*, *Phys. Rept.* **369** (2002) 549–686, [`arXiv:hep-th/0203048`].

[129] P. Kraus, *Lectures on black holes and the AdS(3) / CFT(2) correspondence*, *Lect. Notes Phys.* **755** (2008) 193–247, [`arXiv:hep-th/0609074`].

[130] J. de Boer, *Six-dimensional supergravity on S**3 x AdS(3) and 2-D conformal field theory*, *Nucl. Phys.* **B548** (1999) 139–166, [`arXiv:hep-th/9806104`].

[131] J. M. Maldacena and L. Maoz, *Desingularization by rotation*, *JHEP* **12** (2002) 055, [`arXiv:hep-th/0012025`].

[132] J. D. Brown and M. Henneaux, *Central Charges in the Canonical Realization of Asymptotic Symmetries: An Example from Three-Dimensional Gravity*, *Commun. Math. Phys.* **104** (1986) 207–226.

[133] S. S. Gubser, I. R. Klebanov and A. M. Polyakov, *Gauge theory correlators from noncritical string theory*, *Phys. Lett.* **B428** (1998) 105–114, [`arXiv:hep-th/9802109`].

[134] E. Witten, *Anti-de Sitter space and holography*, *Adv. Theor. Math. Phys.* **2** (1998) 253–291, [`arXiv:hep-th/9802150`].

[135] T. Kaluza, *Zum Unitätsproblem der Physik*, *Sitzungsber. Preuss. Akad. Wiss. Berlin (Math. Phys.)* **1921** (1921) 966–972, [`arXiv:1803.08616`].

[136] E. Witten, *Anti-de Sitter space, thermal phase transition, and confinement in gauge theories*, *Adv. Theor. Math. Phys.* **2** (1998) 505–532, [`arXiv:hep-th/9803131`].

[137] J. M. Maldacena and A. Strominger, *AdS(3) black holes and a stringy exclusion principle*, *JHEP* **12** (1998) 005, [`arXiv:hep-th/9804085`].

[138] G. Policastro, D. T. Son and A. O. Starinets, *From AdS / CFT correspondence to hydrodynamics*, *JHEP* **09** (2002) 043, [`arXiv:hep-th/0205052`].

[139] S. W. Hawking and D. N. Page, *Thermodynamics of Black Holes in anti-De Sitter Space*, *Commun. Math. Phys.* **87** (1983) 577.

[140] S. S. Gubser, I. R. Klebanov and A. W. Peet, *Entropy and temperature of black 3-branes*, *Phys. Rev.* **D54** (1996) 3915–3919, [`arXiv:hep-th/9602135`].

[141] M. Banados, C. Teitelboim and J. Zanelli, *The Black hole in three-dimensional space-time*, *Phys. Rev. Lett.* **69** (1992) 1849–1851, [`arXiv:hep-th/9204099`].

[142] M. Banados, M. Henneaux, C. Teitelboim and J. Zanelli, *Geometry of the (2+1) black hole*, *Phys. Rev.* **D48** (1993) 1506–1525, [`arXiv:gr-qc/9302012`].

[143] S. Deser, R. Jackiw and G. 't Hooft, *Three-Dimensional Einstein Gravity: Dynamics of Flat Space*, *Annals Phys.* **152** (1984) 220.

[144] S. Deser and R. Jackiw, *Three-Dimensional Cosmological Gravity: Dynamics of Constant Curvature*, *Annals Phys.* **153** (1984) 405–416.

[145] V. Balasubramanian, J. de Boer, E. Keski-Vakkuri and S. F. Ross, *Supersymmetric conical defects: Towards a string theoretic description of black hole formation*, *Phys. Rev.* **D64** (2001) 064011, [`arXiv:hep-th/0011217`].

[146] V. Balasubramanian, B. D. Chowdhury, B. Czech and J. de Boer, *Entwinement and the emergence of spacetime*, *JHEP* **01** (2015) 048, [`arXiv:1406.5859`].

[147] J. C. Cresswell and A. W. Peet, *Kinematic space for conical defects*, *JHEP* **11** (2017) 155, [`arXiv:1708.09838`].

[148] V. Balasubramanian, P. Kraus and M. Shigemori, *Massless black holes and black rings as effective geometries of the D1-D5 system*, *Class. Quant. Grav.* **22** (2005) 4803–4838, [`arXiv:hep-th/0508110`].

[149] M. Casals, A. Fabbri, C. Martínez and J. Zanelli, *Quantum dress for a naked singularity*, *Phys. Lett.* **B760** (2016) 244–248, [arXiv:1605.06078].

[150] J. R. David, G. Mandal, S. Vaidya and S. R. Wadia, *Point mass geometries, spectral flow and AdS(3) - CFT(2) correspondence*, *Nucl. Phys.* **B564** (2000) 128–141, [arXiv:hep-th/9906112].

[151] T. Takayanagi and K. Umemoto, *Entanglement of purification through holographic duality*, *Nature Phys.* **14** (2018) 573–577, [arXiv:1708.09393].

[152] P. Nguyen, T. Devakul, M. G. Halbasch, M. P. Zaletel and B. Swingle, *Entanglement of purification: from spin chains to holography*, *JHEP* **01** (2018) 098, [arXiv:1709.07424].

[153] S. Banerjee, J. Erdmenger and D. Sarkar, *Connecting Fisher information to bulk entanglement in holography*, *JHEP* **08** (2018) 001, [arXiv:1701.02319].

[154] M. Alishahiha and A. Faraji Astaneh, *Holographic Fidelity Susceptibility*, *Phys. Rev.* **D96** (2017) 086004, [arXiv:1705.01834].

[155] W.-C. Gan and F.-W. Shu, *Holographic complexity: A tool to probe the property of reduced fidelity susceptibility*, *Phys. Rev.* **D96** (2017) 026008, [arXiv:1702.07471].

[156] M. Flory, *A complexity/fidelity susceptibility g-theorem for $AdS_3/BCFT_2$*, *JHEP* **06** (2017) 131, [arXiv:1702.06386].

[157] M. Headrick, *General properties of holographic entanglement entropy*, *JHEP* **03** (2014) 085, [arXiv:1312.6717].

[158] E. H. Lieb and M. B. Ruskai, *Proof of the strong subadditivity of quantum-mechanical entropy*, *Journal of Mathematical Physics* **14** (1973) 1938–1941.

[159] E. H. Lieb and M. B. Ruskai, *A fundamental property of quantum-mechanical entropy*, *Phys. Rev. Lett.* **30** (Mar, 1973) 434–436.

[160] I. Devetak and J. Yard, *Exact cost of redistributing multipartite quantum states*, *Phys. Rev. Lett.* **100** (Jun, 2008) 230501.

[161] P. Calabrese and J. L. Cardy, *Entanglement entropy and quantum field theory*, *J. Stat. Mech.* **0406** (2004) P06002, [arXiv:hep-th/0405152].

[162] P. Calabrese and J. L. Cardy, *Entanglement entropy and quantum field theory: A Non-technical introduction*, *Int. J. Quant. Inf.* **4** (2006) 429, [arXiv:quant-ph/0505193].

[163] P. Calabrese and J. Cardy, *Entanglement entropy and conformal field theory*, *J. Phys.* **A42** (2009) 504005, [arXiv:0905.4013].

[164] H. Casini and M. Huerta, *Entanglement entropy in free quantum field theory*, *J. Phys.* **A42** (2009) 504007, [`arXiv:0905.2562`].

[165] M. Srednicki, *Entropy and area*, *Phys. Rev. Lett.* **71** (1993) 666–669, [`arXiv:hep-th/9303048`].

[166] J. L. Cardy, O. A. Castro-Alvaredo and B. Doyon, *Form factors of branch-point twist fields in quantum integrable models and entanglement entropy*, *J. Statist. Phys.* **130** (2008) 129–168, [`arXiv:0706.3384`].

[167] W. Donnelly, *Entanglement entropy and nonabelian gauge symmetry*, *Class. Quant. Grav.* **31** (2014) 214003, [`arXiv:1406.7304`].

[168] P. V. Buividovich and M. I. Polikarpov, *Entanglement entropy in gauge theories and the holographic principle for electric strings*, *Phys. Lett.* **B670** (2008) 141–145, [`arXiv:0806.3376`].

[169] W. Donnelly, *Decomposition of entanglement entropy in lattice gauge theory*, *Phys. Rev.* **D85** (2012) 085004, [`arXiv:1109.0036`].

[170] H. Casini, M. Huerta and J. A. Rosabal, *Remarks on entanglement entropy for gauge fields*, *Phys. Rev.* **D89** (2014) 085012, [`arXiv:1312.1183`].

[171] S. Ryu and T. Takayanagi, *Aspects of Holographic Entanglement Entropy*, *JHEP* **08** (2006) 045, [`arXiv:hep-th/0605073`].

[172] T. Faulkner, A. Lewkowycz and J. Maldacena, *Quantum corrections to holographic entanglement entropy*, *JHEP* **11** (2013) 074, [`arXiv:1307.2892`].

[173] X. Dong, A. Lewkowycz and M. Rangamani, *Deriving covariant holographic entanglement*, *JHEP* **11** (2016) 028, [`arXiv:1607.07506`].

[174] C. Holzhey, F. Larsen and F. Wilczek, *Geometric and renormalized entropy in conformal field theory*, *Nucl. Phys.* **B424** (1994) 443–467, [`arXiv:hep-th/9403108`].

[175] T. Azeyanagi, T. Nishioka and T. Takayanagi, *Near Extremal Black Hole Entropy as Entanglement Entropy via AdS(2)/CFT(1)*, *Phys. Rev.* **D77** (2008) 064005, [`arXiv:0710.2956`].

[176] M. Headrick, *Entanglement Renyi entropies in holographic theories*, *Phys. Rev.* **D82** (2010) 126010, [`arXiv:1006.0047`].

[177] T. Hartman, *Entanglement Entropy at Large Central Charge*, `arXiv:1303.6955`.

[178] T. Faulkner, *The Entanglement Renyi Entropies of Disjoint Intervals in AdS/CFT*, `arXiv:1303.7221`.

[179] C. A. Agón, M. Headrick and B. Swingle, *Subsystem Complexity and Holography*, *JHEP* **02** (2019) 145, [`arXiv:1804.01561`].

[180] D. Aharonov, A. Kitaev and N. Nisan, *Quantum circuits with mixed states*, `arXiv:quant-ph/9806029`.

[181] M. A. Nielsen, *A geometric approach to quantum circuit lower bounds*, *Quantum Information and Computation* **6** (May, 2006) 213–262, [`arXiv:quant-ph/0502070`].

[182] M. A. Nielsen, M. R. Dowling, M. Gu and A. C. Doherty, *Quantum computation as geometry*, *Science* **311** (2006) 1133–1135, [`arXiv:quant-ph/0603161`].

[183] R. Khan, C. Krishnan and S. Sharma, *Circuit Complexity in Fermionic Field Theory*, *Phys. Rev.* **D98** (2018) 126001, [`arXiv:1801.07620`].

[184] L. Susskind, *Entanglement is not enough*, *Fortsch. Phys.* **64** (2016) 49–71, [`arXiv:1411.0690`].

[185] L. Susskind and Y. Zhao, *Switchbacks and the Bridge to Nowhere*, `arXiv:1408.2823`.

[186] D. Harlow and P. Hayden, *Quantum Computation vs. Firewalls*, *JHEP* **06** (2013) 085, [`arXiv:1301.4504`].

[187] A. R. Brown, D. A. Roberts, L. Susskind, B. Swingle and Y. Zhao, *Complexity, action, and black holes*, *Phys. Rev.* **D93** (2016) 086006, [`arXiv:1512.04993`].

[188] O. Ben-Ami and D. Carmi, *On Volumes of Subregions in Holography and Complexity*, *JHEP* **11** (2016) 129, [`arXiv:1609.02514`].

[189] E. Bakhshaei, A. Mollabashi and A. Shirzad, *Holographic Subregion Complexity for Singular Surfaces*, *Eur. Phys. J.* **C77** (2017) 665, [`arXiv:1703.03469`].

[190] P. Roy and T. Sarkar, *Subregion holographic complexity and renormalization group flows*, *Phys. Rev.* **D97** (2018) 086018, [`arXiv:1708.05313`].

[191] D. Carmi, *More on Holographic Volumes, Entanglement, and Complexity*, `arXiv:1709.10463`.

[192] B. Czech, J. L. Karczmarek, F. Nogueira and M. Van Raamsdonk, *The Gravity Dual of a Density Matrix*, *Class. Quant. Grav.* **29** (2012) 155009, [`arXiv:1204.1330`].

[193] M. Headrick, V. E. Hubeny, A. Lawrence and M. Rangamani, *Causality & holographic entanglement entropy*, *JHEP* **12** (2014) 162, [`arXiv:1408.6300`].

[194] D. L. Jafferis, A. Lewkowycz, J. Maldacena and S. J. Suh, *Relative entropy equals bulk relative entropy*, *JHEP* **06** (2016) 004, [`arXiv:1512.06431`].

[195] G. Sárosi and T. Ugajin, *Relative entropy of excited states in two dimensional conformal field theories*, *JHEP* **07** (2016) 114, [arXiv:1603.03057].

[196] G. Sárosi and T. Ugajin, *Relative entropy of excited states in conformal field theories of arbitrary dimensions*, *JHEP* **02** (2017) 060, [arXiv:1611.02959].

[197] H. Casini, *Relative entropy and the Bekenstein bound*, *Class. Quant. Grav.* **25** (2008) 205021, [arXiv:0804.2182].

[198] D. D. Blanco and H. Casini, *Localization of Negative Energy and the Bekenstein Bound*, *Phys. Rev. Lett.* **111** (2013) 221601, [arXiv:1309.1121].

[199] H. Casini, M. Huerta and R. C. Myers, *Towards a derivation of holographic entanglement entropy*, *JHEP* **05** (2011) 036, [arXiv:1102.0440].

[200] J. Cardy and E. Tonni, *Entanglement Hamiltonians in two-dimensional conformal field theory*, *J. Stat. Mech.* **1612** (2016) 123103, [arXiv:1608.01283].

[201] J. J. Bisognano and E. H. Wichmann, *On the Duality Condition for a Hermitian Scalar Field*, *J. Math. Phys.* **16** (1975) 985–1007.

[202] J. J. Bisognano and E. H. Wichmann, *On the Duality Condition for Quantum Fields*, *J. Math. Phys.* **17** (1976) 303–321.

[203] P. D. Hislop and R. Longo, *Modular Structure of the Local Algebras Associated With the Free Massless Scalar Field Theory*, *Commun. Math. Phys.* **84** (1982) 71.

[204] D. Blanco, H. Casini, M. Leston and F. Rosso, *Modular energy inequalities from relative entropy*, *JHEP* **01** (2018) 154, [arXiv:1711.04816].

[205] A. Uhlmann, *Relative entropy and the Wigner-Yanase-Dyson-Lieb concavity in an interpolation theory*, *Communications in Mathematical Physics* **54** (Feb, 1977) 21–32.

[206] B. Czech, L. Lamprou, S. McCandlish, B. Mosk and J. Sully, *A Stereoscopic Look into the Bulk*, *JHEP* **07** (2016) 129, [arXiv:1604.03110].

[207] J. de Boer, F. M. Haehl, M. P. Heller and R. C. Myers, *Entanglement, holography and causal diamonds*, *JHEP* **08** (2016) 162, [arXiv:1606.03307].

[208] B. Czech, L. Lamprou, S. Mccandlish and J. Sully, *Modular Berry Connection for Entangled Subregions in AdS/CFT*, *Phys. Rev. Lett.* **120** (2018) 091601, [arXiv:1712.07123].

[209] J. Wien, *A Holographic Approach to Spacetime Entanglement*, arXiv:1408.6005.

[210] M. Headrick, R. C. Myers and J. Wien, *Holographic Holes and Differential Entropy*, *JHEP* **10** (2014) 149, [`arXiv:1408.4770`].

[211] L. A. Santaló, *Integral Geometry and Geometric Probability (404 pages)*. Addison-Wesley, Reading, US, 1976.

[212] C. T. Asplund, N. Callebaut and C. Zukowski, *Equivalence of Emergent de Sitter Spaces from Conformal Field Theory*, *JHEP* **09** (2016) 154, [`arXiv:1604.02687`].

[213] Q. Wen, *Fine structure in holographic entanglement and entanglement contour*, *Phys. Rev.* **D98** (2018) 106004, [`arXiv:1803.05552`].

[214] J. Lin, *A Toy Model of Entwinement*, `arXiv:1608.02040`.

[215] V. Balasubramanian, A. Bernamonti, B. Craps, T. De Jonckheere and F. Galli, *Entwinement in discretely gauged theories*, *JHEP* **12** (2016) 094, [`arXiv:1609.03991`].

[216] V. Balasubramanian, B. Craps, T. De Jonckheere and G. Sárosi, *Entanglement versus entwinement in symmetric product orbifolds*, *JHEP* **01** (2019) 190, [`arXiv:1806.02871`].

[217] B. Freivogel, R. Jefferson, L. Kabir, B. Mosk and I.-S. Yang, *Casting Shadows on Holographic Reconstruction*, *Phys. Rev.* **D91** (2015) 086013, [`arXiv:1412.5175`].

[218] J.-d. Zhang and B. Chen, *Kinematic Space and Wormholes*, *JHEP* **01** (2017) 092, [`arXiv:1610.07134`].

[219] G. T. Horowitz and R. C. Myers, *The AdS / CFT correspondence and a new positive energy conjecture for general relativity*, *Phys. Rev.* **D59** (1998) 026005, [`arXiv:hep-th/9808079`].

[220] N. Lashkari, C. Rabideau, P. Sabella-Garnier and M. Van Raamsdonk, *Inviolable energy conditions from entanglement inequalities*, *JHEP* **06** (2015) 067, [`arXiv:1412.3514`].

[221] D. Blanco, *Quantum information measures and their applications in quantum field theory*, Ph.D. thesis, Balseiro Inst., San Carlos de Bariloche, 2016. `arXiv:1702.07384`.

[222] C. T. Asplund, A. Bernamonti, F. Galli and T. Hartman, *Holographic Entanglement Entropy from 2d CFT: Heavy States and Local Quenches*, *JHEP* **02** (2015) 171, [`arXiv:1410.1392`].